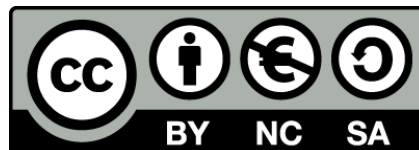




UNIVERSITAT_{DE}
BARCELONA

Epigenomic Dynamics Associated with Myeloid Cell Immune Response Remodeling

Octavio Morante Palacios

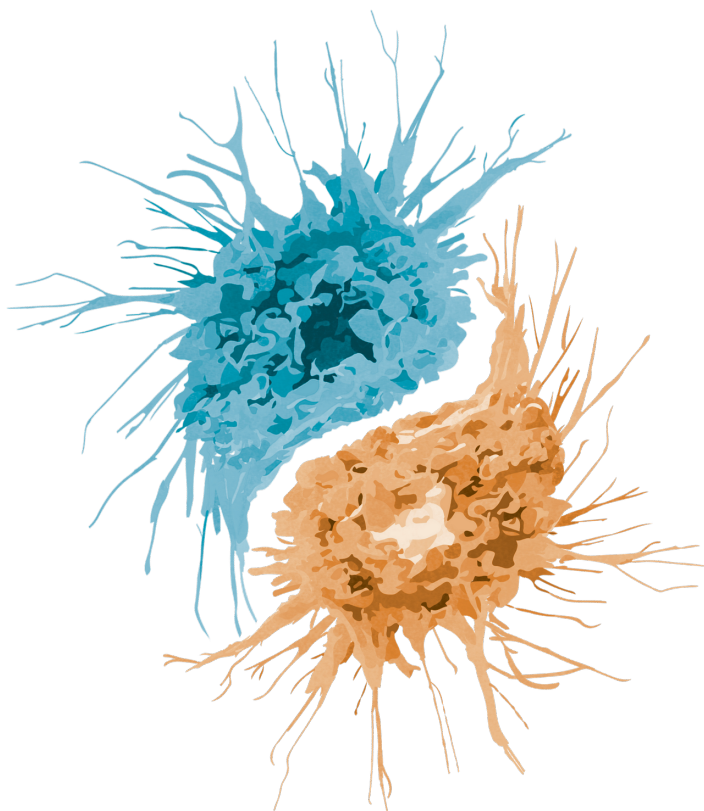


Aquesta tesi doctoral està subjecta a la llicència **Reconeixement- NoComercial – Compartir Igual 4.0. Espanya de Creative Commons.**

Esta tesis doctoral está sujeta a la licencia **Reconocimiento - NoComercial – Compartir Igual 4.0. España de Creative Commons.**

This doctoral thesis is licensed under the **Creative Commons Attribution-NonCommercial-ShareAlike 4.0. Spain License.**

EPIGENOMIC DYNAMICS
ASSOCIATED WITH MYELOID CELL
IMMUNE RESPONSE REMODELING



Octavio Morante Palacios

PhD Thesis

2022



EPIGENOMIC DYNAMICS ASSOCIATED WITH MYELOID CELL IMMUNE RESPONSE REMODELING

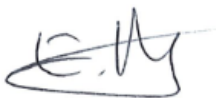
Memoria presentada por Octavio Morante Palacios para optar al grado
de Doctor por la Universidad de Barcelona

UNIVERSIDAD DE BARCELONA – FACULTAD DE
MEDICINA

PROGRAMA DE DOCTORADO EN BIOMEDICINA

Tesis realizada en el grupo de Epigenética y Enfermedad del Sistema
Inmune perteneciente al Instituto Josep Carreras bajo la dirección del
Dr. Esteban Ballestar Tarín

Dr. Esteban Ballestar
Director



Prof. Pablo Engel Rocamora
Tutor



Octavio Morante Palacios
Doctorando



Octavio Morante Palacios held an i-PFIS PhD Fellowship (grant number IFI17/00034) from Acción Estratégica en Salud 2013-2016 ISCIII, co-financed by the European Social Fund during the development of this thesis.

Figures in this Ph.D. thesis have been designed by Octavio Morante Palacios unless otherwise indicated. Resources from Servier Medical Art (smart.servier.com) licensed under CC BY 3.0 have been utilized in some figures.

Cover designed by Sonia Martí Sánchez.

INDEX

Summary.....	i
Resumen.....	iii
Resum.....	vii
Abbreviations.....	xi
1. INTRODUCTION.....	1
1.1. The immune system.....	1
1.1.1. Adaptive and innate immunity.....	1
1.1.2. The immune system: a fine-tuned balance between tolerance and immunogenesis.....	3
1.2. Monocytes and monocyte-derived cells.....	4
1.2.1. The ontogeny of monocyte subsets.....	4
1.2.2. <i>In vitro</i> differentiation of human monocytes.....	6
1.2.3. <i>In vivo</i> differentiation of human monocytes.....	7
1.2.4. Regulation of monocyte and monocyte-derived cells immunogenesis.....	9
1.3. Immunogenic and tolerogenic dendritic cells.....	14
1.3.1. Classification and biology of dendritic cells.....	14
1.3.2. <i>In vivo</i> and <i>in vitro</i> generated tolerogenic dendritic cells.....	17
1.3.3. Mechanisms of tolerogenesis.....	18
1.3.4. Clinical use of tolerogenic dendritic cells.....	21
1.3.5. Clinical use of immunogenic dendritic cells.....	22
1.4. DNA methylation dynamics in the regulation of the immune system.....	24
1.4.1. Overview.....	24
1.4.2. Vitamin C as a cofactor of TET enzymes.....	26

1.4.3. Role of DNA methylation in monocyte differentiation.....	28
2. OBJECTIVES.....	35
3. ARTICLES.....	41
Director's report.....	41
3.1. ARTICLE 1: Coordinated glucocorticoid receptor and MAFB action induces tolerogenesis and epigenome remodelling in dendritic cells.....	44
3.2. ARTICLE 2: JAK2-STAT epigenetically regulates tolerized genes in monocytes in the first encounter with gram-negative bacterial endotoxins in sepsis.....	112
3.3. ARTICLE 3: Vitamin C enhances NF- κ B-driven DNA demethylation and immunogenic properties of dendritic cells.....	168
4. GLOBAL RESULTS AND DISCUSSION.....	209
4.1. Global results.....	209
4.1.1. Coordinated glucocorticoid receptor and MAFB action induces tolerogenesis and epigenome remodeling in dendritic cells (Article 1).....	209
4.1.2. JAK2-STAT Epigenetically Regulates Tolerized Genes in Monocytes in the First Encounter With Gram-Negative Bacterial Endotoxins in Sepsis (Article 2).....	212
4.1.3. Vitamin C enhances NF- κ B-driven DNA demethylation and immunogenic properties of dendritic cells (Article 3).....	216
4.2. Global discussion.....	219
5. CONCLUSIONS.....	235
6. REFERENCES.....	243
Agradecimientos.....	267
7. APPENDIX.....	273

FIGURE INDEX

Figure 1: Overview of <i>in vitro</i> differentiation models from monocytes.....	7
Figure 2: Examples of TLR and IFN receptor signaling pathways.....	11
Figure 3: Ontogeny and differentiation of monocytes and dendritic cells across tissues.....	16
Figure 4: Mechanisms of tolerogenesis of tolerogenic dendritic cells.....	20
Figure 5: Process of immunogenic DC / tolDC generation.....	23
Figure 6: DNA demethylation cycle.....	27
Figure 7: Representation of the molecular events occurring during the differentiation of monocytes to tolDCs with glucocorticoids.....	220
Figure 8: Scheme depicting the relevance of JAK2-STAT in the regulation of tolerized genes in the first encounter of monocytes with LPS.	223
Figure 9: Representation of the monocyte to DC differentiation model in the presence of vitamin C.....	224

SUMMARY

Monocytes are highly plastic cells and possess the ability to differentiate into cell types with very different immunological properties. Depending on the external stimuli and the specific immune context, they can give rise to cells that promote immune responses or immune tolerance. These extracellular signals are recognized by specific receptors and integrated by signaling pathways which lead to the participation of transcription factors. Transcriptional remodeling promoted by these transcription factors is generally associated with epigenetic modifications such as histone modifications and DNA methylation. DNA methylation is crucial in the acquisition of immune cells' identity and function. In particular, DNA methylation changes in several human monocytes differentiation models have been previously described. In this thesis, the molecular mechanisms and epigenomic remodeling regulating the development of immunogenic or tolerogenic phenotypes of three clinically relevant monocyte-derived differentiation processes have been studied.

Firstly, we investigated the transcriptomic and epigenomic remodeling associated with glucocorticoid-mediated monocyte differentiation to tolerogenic dendritic cells (tolDCs), a cell type that constitutes a potential treatment for various autoimmune diseases. We revealed a major role of MAFB in this process, in synergy with GR. Although both GR and MAFB interact with TET2 and can drive DNA demethylation, the role of MAFB is more extensive, binding to thousands of genomic loci in tolDCs. In this regard, we demonstrated that MAFB knockdown erases the tolerogenic properties of tolDCs and reverts the specific DNA demethylation and gene upregulation. Moreover, *in vivo* monocyte-derived

cells from synovium in rheumatoid arthritis patients treated with glucocorticoids presented an expansion of ‘tolDC-like’ cells with upregulation of MAFB and MAFB target genes.

Secondly, we analyzed the effects of vitamin C treatment during monocyte to dendritic cell (DC) differentiation and their subsequent maturation. DNA demethylation has been previously reported to be crucial in that process. Vitamin C is a known cofactor of TET enzymes, which are involved in active demethylation. We outlined extensive vitamin C-mediated demethylation, together with concordant gene expression changes during DC maturation. p65 (NF- κ B) interacts with TET2 and is associated with gene upregulation and DNA demethylation produced by vitamin C treatment. Finally, vitamin C increases TNF β production and T cell stimulation capabilities of DCs.

Thirdly, we integrated the DNA methylation and gene expression remodeling following *in vitro* exposure of human monocytes to lipopolysaccharide (LPS), a process that generates endotoxin tolerance, a state of hyporesponsiveness to further immune stimuli. In addition, we described phosphorylation of STAT1, STAT3, and STAT5, factors of the JAK2 pathway, after LPS treatment of monocytes. We identified TET2-mediated demethylation and gene upregulation during the first encounter with LPS associated with the JAK2-STAT signaling pathway. In addition, we found that JAK2 inhibition accentuates the tolerant phenotype of monocytes and reduces the expression of tolerized genes. Finally, monocytes from gram-negative septic patients showed lower levels of STAT1 phosphorylation after a second LPS challenge, indicating a reduced JAK2 activity.

RESUMEN

Los monocitos son células plásticas con capacidad de diferenciación a tipos celulares con propiedades inmunológicas muy diferentes. Dependiendo de los estímulos externos y del contexto inmunológico, pueden dar lugar a células que promuevan una respuesta inmunitaria o tolerancia. Estas señales extracelulares son reconocidas por receptores específicos e integradas por vías de señalización que conducen a la participación de factores de transcripción. La remodelación transcripcional promovida por estos factores de transcripción se asocia generalmente con cambios epigenéticos como modificaciones de histonas o la metilación del DNA. La metilación del DNA es crucial en la adquisición de la identidad y la función de las células inmunitarias. En particular, se han descrito cambios en la metilación del DNA en varios modelos de diferenciación de monocitos humanos. En esta tesis, hemos estudiado los mecanismos moleculares y la remodelación epigenómica que regulan el desarrollo de fenotipos inmunogénicos o tolerogénicos de tres procesos de diferenciación de monocitos clínicamente relevantes.

En primer lugar, hemos investigado la remodelación transcriptómica y epigenómica asociada a la diferenciación de monocitos a células dendríticas tolerogénicas (tolDC) con glucocorticoides, un tipo celular que constituye un tratamiento potencial para varias enfermedades autoinmunes. MAFB tiene un papel fundamental en este proceso, en sinergia con GR. Aunque tanto GR como MAFB interactúan con TET2 y pueden promover la desmetilación del DNA, el papel de MAFB es más amplio, ya que se une a miles de loci en el genoma de las tolDC. En este sentido, hemos demostrado que la eliminación de MAFB borra las

propiedades tolerogénicas de las tolDC y revierte la desmetilación específica del DNA y la regulación de los genes. Además, las células derivadas de monocitos *in vivo*, obtenidas de membrana sinovial de pacientes con artritis reumatoide tratados con glucocorticoides presentaron una expansión de células similares a las tolDC con una alta expresión tanto de *MAFB* como de sus genes diana.

En segundo lugar, hemos analizado los efectos del tratamiento con vitamina C durante la diferenciación de monocitos a células dendríticas (DC) y su posterior maduración. La desmetilación del DNA ha sido previamente descrita como crucial en ese proceso. La vitamina C es un cofactor conocido de las enzimas TET, que participan en la desmetilación activa. En este sentido, hemos descrito una amplia desmetilación mediada por la vitamina C, junto con cambios concordantes en la expresión génica durante la maduración de las DC. p65 (NF- κ B) interactúa con TET2 y se asocia con la inducción de genes y la desmetilación del DNA producida por el tratamiento con vitamina C. Por último, la vitamina C aumenta la producción de TNF β y la capacidad de estimulación de células T de las DC.

En tercer lugar, hemos integrado la metilación del DNA y la remodelación de la expresión génica tras la exposición *in vitro* de monocitos humanos a lipopolisacárido (LPS), un proceso que genera un tipo de memoria inmune innata denominado tolerancia a endotoxinas, el cual constituye un estado hiporesponsivo a nuevos estímulos inmunitarios. Además, hemos descrito la fosforilación de STAT1, STAT3 y STAT5, factores asociados con JAK2, tras el tratamiento de los monocitos con LPS. Durante la primera exposición de los monocitos a LPS, encontramos desmetilación mediada por TET2 e inducción de genes

asociados a JAK2-STAT. Adicionalmente, encontramos que la inhibición de JAK2 acentúa la tolerancia en los monocitos y reduce la expresión de los genes tolerizados. Por último, monocitos de pacientes sépticos gram-negativos mostraron menores niveles de fosforilación de STAT1 tras un segundo tratamiento con LPS, lo cual indica que presentan una menor actividad de JAK2.

RESUM

Els monòcits són cèl·lules plàstiques amb capacitat de diferenciació a tipus cel·lulars amb propietats immunològiques molt diferents. Depenent dels estímuls externs i del context immunològic, poden donar lloc a cèl·lules que promoguen una resposta immunitària o tolerància. Aquests senyals extracel·lulars són reconeguts per receptors específics i integrats per vies de senyalització que condueixen a la participació de factors de transcripció. La remodelació transcripcional promoguda per aquests factors de transcripció s'associa generalment amb canvis epigenètics com a modificacions d'histones o la metilació del DNA. La metilació del DNA és crucial en l'adquisició de la identitat i la funció de les cèl·lules immunitàries. En particular, s'han descrit canvis en la metilació del DNA en diversos models de diferenciació de monòcits humans. En aquesta tesi, hem estudiat els mecanismes moleculars i la remodelació epigenètica que regulen el desenvolupament de fenotips immunogènics o tolerogènics de tres processos de diferenciació de monòcits clínicament rellevants.

En primer lloc, hem investigat la remodelació transcriptòmica i epigenètica associada a la diferenciació de monòcits a cèl·lules dendrítiques tolerogèniques (tolDC) amb glucocorticoides, un tipus cel·lular que constitueix un tractament potencial per a diverses malalties autoimmunes. MAFB té un paper fonamental en aquest procés, en sinergia amb GR. Encara que tant GR com MAFB interactuen amb TET2 i poden promoure la desmetilació del DNA, el paper de MAFB és més ampli, ja que s'uneix a milers de loci en el genoma de les tolDC. En aquest sentit, hem demostrat que l'eliminació de MAFB reverteix les propietats tolerogèniques de les tolDC, la desmetilació específica del

DNA i la regulació dels gens. A més, les cèl·lules derivades de monòcits *in vivo* obtingudes de membrana sinovial de pacients amb artritis reumatoide tractats amb glucocorticoides van presentar una expansió de cèl·lules similars a les tolDC amb una alta expressió tant de MAFB com dels seus gens diana.

En segon lloc, hem analitzat els efectes del tractament amb vitamina C durant la diferenciació de monòcits a cèl·lules dendrítiques (DC) i la seua posterior maduració. La desmetilació del DNA ha sigut prèviament descrita com a crucial en aquest procés. La vitamina C és un cofactor conegut dels enzims TET, que participen en la desmetilació activa. En aquest sentit, hem descrit una àmplia desmetilació mediada per la vitamina C, juntament amb canvis concordants en l'expressió gènica durant la maduració de les DCs. p65 (NF- κ B) interactua amb TET2 i s'associa amb la inducció de gens i la desmetilació del DNA produïda pel tractament amb vitamina C. Finalment, la vitamina C augmenta la producció de TNF β i la capacitat d'estimulació de cèl·lules T de les DC.

En tercer lloc, hem integrat la metilació del DNA i la remodelació de l'expressió gènica després de l'exposició *in vitro* de monòcits humans a lipopolisacàrid (LPS), un procés que genera un tipus de memòria immunitària innata denominat tolerància a endotoxines, el qual constitueix un estat hiporesponsiu a nous estímuls immunitaris. A més, hem descrit la fosforilació de STAT1, STAT3 i STAT5, elements associats amb JAK2, després del tractament dels monòcits amb LPS. Durant la primera exposició dels monòcits a LPS, hem trobat desmetilació mediada per TET2 i inducció de gens associats a JAK2-STAT. Addicionalment, hem descrit que la inhibició de JAK2 accentua la tolerància en els monòcits i redueix l'expressió dels gens toleritzats. Finalment, monòcits de pacients

sèptics infectats amb bacteris gramnegatius van mostrar menors nivells de fosforilació de STAT1 després d'un segon tractament amb LPS, indicant que presenten una menor activitat de JAK2.

ABBREVIATIONS

5caC: 5-carboxylcytosine

5fC: 5-formylcytosine

5hmC: 5-hydroxymethylcytosine

5mC: 5-methylcytosine

AHR: Aryl hydrocarbon receptor

ALR: AIM2-like receptor

BCR: B cell receptor

cDC: Classical dendritic cell

ChIP: Chromatin immunoprecipitation

CLR: C-type lectin receptor

CpG: Cytosine-followed-by-guanine

CTLA-4: Cytotoxic T-lymphocyte-associated protein 4

CXXC: Cysteine-X-X-cysteine

DAMP: Damage-associated molecular pattern

DC: Dendritic cell

DMP: Differentially methylated position

DNMT: DNA methyltransferase

DoRothEA: Discriminant Regulon Expression Analysis

EGR2: Early growth response 2

ELISA: Enzyme-linked immunosorbent assay

GM-CSF: Granulocyte-macrophage colony-stimulating factor

GMP: granulocyte-monocyte progenitor

GRE: Glucocorticoid Response Elements
HSC: Hematopoietic stem cell
iDC: Immature dendritic cell
IDO: Indoleamine 2,3-dioxygenase
IFN: Interferon
IKK: I κ B kinase
IL: Interleukin
IRF: Interferon regulatory factor
JAK: Janus kinase
LPS: Lipopolysaccharide
LT: Lymphotoxin
M-CSF: Macrophage colony-stimulating factor
MAPK: Mitogen-activated protein kinase
MARE: Maf Recognition elements
mDC: Mature dendritic cell
MDP: Monocyte and dendritic cell progenitor
mo-tolDC: Monocyte-derived tolerogenic dendritic cell
moDC: Monocyte-derived dendritic cell
moMAC: Monocyte-derived macrophage
mTEC: Medullary thymic epithelial cell
MyD88: Myeloid differentiation primary response gene 88
NLR: Nucleotide-binding leucine-rich repeat receptor
PAMP: Pathogen-associated molecular pattern
PBMC: Peripheral mononuclear cell

PD-L: Programmed death-ligand
pDC: Plasmacytoid dendritic cell
PRR: Pattern-recognition receptor
RLR: RIG-I-like receptor
SIGIRR: Single immunoglobulin interleukin-1-related receptor
SOCS: Suppressor of cytokine signaling
STAT: Signal transducer and activator of transcription
TCR: T cell receptor
TDG: Thymine DNA glycosylase
TET: Ten-eleven translocation methylecytosine dioxygenase
TGF: Transforming growth factor
TIRAP: TIR Domain-Containing Adaptor Protein
TLR: Toll-like receptor
TNF: Tumor necrosis factor
TNFAIP3: TNF α -induced protein 3
tolDC: Tolerogenic dendritic cell
TRAF6: TNF receptor-associated factor 6
TRAIL: Tumor necrosis factor-related apoptosis-inducing ligand
TRAM: TRIF-related Adaptor Molecule
Treg: Regulatory T cell
TRIF: TIR-domain-containing adaptor inducing interferon- β
VDJ: Variable, diversity and joining gene segments

INTRODUCTION

INTRODUCTION

1. INTRODUCTION

1.1. The immune system

1.1.1. Adaptive and innate immunity

The immune system is extraordinarily complex and diverse. All its different cell types act cooperatively in an intricate network of interactions deeply linked.

In brief, immune cells are produced hierarchically from hematopoietic stem cells (HSCs), which are the only cell type within the hematopoietic system with self-renewal and multi-potency capabilities¹. Subsequently, HSCs produce common myeloid and lymphoid progenitors, precursors of all myeloid (monocytes, neutrophils, eosinophils, basophils, and dendritic cells, DCs), and lymphoid cells (B, T, and NK cells).

Immune system responses have been classically classified into two categories: innate and adaptive. On the one hand, innate immune responses detect general pathogen-associated molecular patterns (PAMPs) and damage-associated molecular patterns (DAMPs). These patterns are recognized by pattern-recognition receptors (PRRs), expressed in myeloid cells, B cells, and NK lymphocytes. On the other hand, adaptive immune responses are specific to unique molecules². This type of response is mediated by B and T lymphocytes. Each B and T cell can recognize a specific antigen determined by its B cell receptor (BCR) or T cell receptor (TCR), respectively. Somatic recombination of variable (V), diversity (D), and joining (J) gene segments provide the variability for the recognition of any potential antigen³.

Since the molecules triggering innate system responses are persistently expressed on a large number of pathogens, this system is fast and

Introduction

constitutes the first defense barrier against infections. In contrast, the adaptive system is formed by a plethora of cells with specificity for any individual antigen, therefore the responding cells have to proliferate, and the reaction is slow.

A cardinal feature of the adaptive immune system, in contrast with the innate immune system, is the immunological memory, defined as the capacity to respond quickly and specifically to an antigen to which the system has already been exposed. Memory B and T lymphocytes, generated in the first encounter with an antigen, are key in the process of immunological memory. These cells can persist for life, providing a rapid response in the case of successive exposures to the antigen^{4,5}.

However, in the last few years, this paradigm has been questioned. Emerging evidence has shown that innate immune cells also possess mechanisms generating immunological memory, characterized by epigenetic remodeling, that modulates the response to successive stimuli⁶. This type of memory does not involve genetic changes, persists only for weeks to months, and is not specific for a particular antigen. In addition, some evidence indicates that innate immune memory could be transmitted across generations in invertebrates⁷, and mammals⁸, although this still is a controversial issue.

The innate and adaptive branches of the immune system are highly interconnected. In this regard, the triggering of the adaptive immune system is tightly regulated by the innate immune system, which can promote or inhibit that activation, switching between tolerogenic and immunogenic responses.

1.1.2. The immune system: a fine-tuned balance between tolerance and immunogenesis

The immune system's main function is to protect the host from diseases, distinguishing and responding against external pathogenic agents and also potential internal threats such as cancer cells.

Historically, the predominant framework of the immune system was based on the “self” vs “non-self” discrimination, highlighting the ability of immune cells to distinguish between own and external molecules⁹. However, some inconsistencies of this model, such as the lack of response against external benign microorganisms, led to the development of a new framework. Polly Matzinger created a new model (“the danger model”), postulating that immune responses are triggered by danger signals, adding an additional layer to the immune system function, not only recognizing “self” vs “non-self” but also “dangerous” vs “non-dangerous”¹⁰. Several DAMPs have been identified, including histones, heat-shock proteins, DNA, and RNA, among others¹¹. These molecules can also be recognized by PRRs, promoting the immune response.

Since the adaptive immune system can potentially recognize and react against any antigen, mechanisms of tolerance should exist to avoid the immune response against internal molecules. In this regard, these mechanisms can be divided into central and peripheral tolerance.

Central tolerance is the process by which auto-reactive T lymphocyte clones are removed during their maturation in the thymus. Auto-antigens are produced by medullary thymic epithelial cells (mTECs) under the regulation of the transcription factor AIRE, promoting T cell apoptosis when a strong interaction is produced between its TCR and the auto-

Introduction

antigen¹². A similar mechanism also occurs during B cell maturation, in the bone marrow.

However, this process does not eliminate autoreactive clones completely¹³. Peripheral tolerance mechanisms help maintain immune system homeostasis, preventing reactions against autoantigens or ‘non-dangerous’ antigens. DCs have a critical role in this process, promoting clonal deletion, clonal anergy, and differentiation of regulatory T cells (Tregs)¹⁴.

Despite the stringent central tolerance selection and the peripheral tolerance, in some cases the immune system can respond against autoantigens, producing autoimmune disorders. In recent years, a new type of cell therapy using tolerogenic dendritic cells (tolDCs) has arisen as treatment of these diseases¹⁴. These cells are generally produced *in vitro* from the patient monocytes and have the capacity to promote tolerance, reducing the immune response against specific antigens.

1.2. Monocytes and monocyte-derived cells

1.2.1. The ontogeny of monocyte subsets

Monocytes are innate immune cells of the myeloid lineage that constitute around 10% of all peripheral blood mononuclear cells (PBMCs)¹⁵, with capabilities of antigen presentation, phagocytosis, cytokine secretion, and differentiation to different cell types.

All peripheral blood monocytes are produced initially in the bone marrow from two independent pathways: monocyte and dendritic cells progenitors (MDPs), and granulocyte-monocyte progenitors (GMP)¹⁶.

In humans, circulating monocytes can be divided at least into three different subsets: classical CD14^{high}CD16⁻ monocytes, intermediate

CD14⁺CD16⁺ monocytes, and non-classical CD14⁻CD16^{high} monocytes. The more abundant subtype is the classical monocytes, comprising around 85% of total monocytes¹⁷.

Strong evidence supports a sequential differentiation process from classical to intermediate and, finally, non-classical monocytes, including *in vivo* labeling experiments with 6,6-²H₂-glucose in healthy volunteers^{18,19}. Furthermore, human exposure to endotoxin promotes a reduction of circulating monocytes, with classical monocytes recovering after 4h and intermediate and non-classical monocytes recovering after 24h²⁰. In addition, a single-cell RNA-seq study of classical monocytes found a subset of cells with an expression profile closer to non-classical monocytes, suggesting that the subset could be already committed to non-classical monocyte differentiation²¹.

The different function and phenotype of monocyte subsets is still an open issue. First, classical monocytes present higher phagocytosis and migration capacities, whereas non-classical monocytes are characterized by their ability to patrol, remove cell debris and repair the endothelium^{22,23}. Intermediate monocytes, as a transient cell type, present a mixed profile.

Moreover, several immune-mediated diseases display increased levels of intermediate and non-classical monocytes²⁴, although the implications and role of this expansion have not been unraveled yet.

Human non-classical monocytes, in comparison with classical monocytes, present a lower capacity of *in vitro* differentiation and are not able to yield DCs²⁵. In contrast, non-classical monocytes have been observed to differentiate to macrophages in mice *in vivo*^{26,27}, and also in human *in vitro* experiments²⁵. However, mice lacking non-classical monocytes present normal levels of macrophages, suggesting that most

Introduction

monocyte-derived cells in peripheral tissues derive from classical monocytes²⁸.

1.2.2. *In vitro* differentiation of human monocytes

CD14⁺ monocytes are highly abundant, in comparison with rare or difficult to obtain related cell types, such as classical DCs (cDCs) or Langerhans cells. Therefore, the possibility to determine the differentiation conditions of monocytes *in vitro* to obtain different cell types is very beneficial to generate models for the study of these cells.

There are several established *in vitro* differentiation protocols from human monocytes (Figure 1). Monocytes can be differentiated into macrophages²⁹, Langerhans cells³⁰, myeloid-derived suppressor cells³¹, osteoclasts^{32,33}, microglia³⁴, DCs^{35,36}, among others. These different types of cells are generated using different cocktails of cytokines that target specific signaling pathways.

In 1994, Sallusto and Lanzavecchia established a differentiation model to generate monocyte-derived DCs (moDCs) using Granulocyte-macrophage colony-stimulating factor (GM-CSF) and interleukin(IL)-4, which has since been widely studied³⁶.

Despite the similarities of *in vitro* DCs obtained from monocytes to blood DCs, most DCs in the steady-state are independent of monocytes, and the biological relevance of such differentiation model was not clear. In the last few years, the *in vivo* differentiation of monocytes has been studied, and putative *in vivo* moDCs have been identified¹⁷.

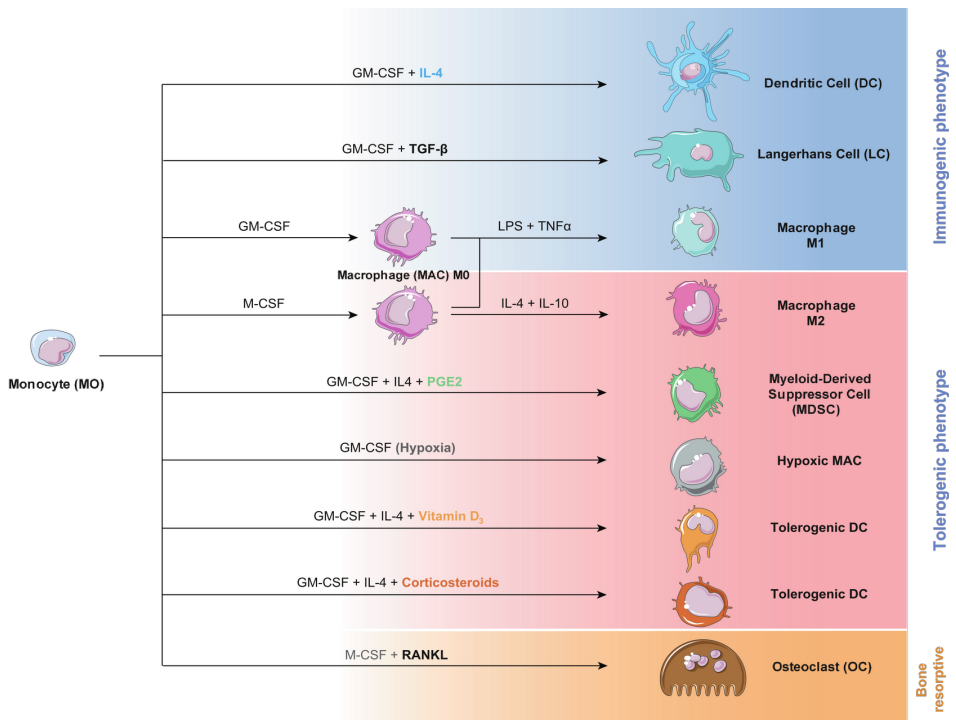


Figure 1: Overview of in vitro differentiation models from monocytes. Several protocols of differentiation are shown, with the different cytokines involved in the processes. Phenotype of the resulting cells are classified into immunogenic, tolerogenic or bone resorptive. Adapted from García-Gómez et al. 2018, Clinical Immunology.

1.2.3. In vivo differentiation of human monocytes

In humans, tracking monocyte recruitment from blood to tissues is especially challenging. One of the most common methods for phenotyping monocytes involves the characterization of surface markers by flow cytometry. However, this technique is imprecise because monocyte marker expression can potentially change across tissues. In addition to other broadly used but not totally specific markers such as CD14, CCR2, and CX3CR1, S100A8/A9 has been proposed as a specific marker for monocytes and monocyte-derived cells³⁷.

Introduction

Several lines of evidence indicate that, in humans, monocytes can be recruited to peripheral tissues. In particular, this process has been specially studied in the context of acute inflammation. CD14⁺ cell number was increased in the peritoneum of patients with peritonitis³⁸, in the bronchoalveolar lavage after lipopolysaccharide (LPS) inhalation³⁹, and in the heart of myocardial infarction patients⁴⁰. Moreover, monocytes have also been identified in tissues during chronic inflammation. For instance, injected radioactive CD14⁺ cells were detected in the intestines of patients with intestinal inflammation⁴¹ or in the joints of patients with rheumatoid arthritis⁴². In cancer, monocytes were detected in lung and breast tumors by single-cell RNA-seq^{43,44}.

Moreover, putative monocyte-derived macrophages (moMACs) and moDCs can be found in several tissues, suggesting that the corresponding *in vitro* differentiation has an equivalent process *in vivo*¹⁷. MoMACs can be distinguished from moDCs through markers. MERTK, CD68, and CD163 are markers of macrophages, whereas DCs express CD1a, CD1b, CD226, and FcεRI²¹. Furthermore, the morphology of moDCs also present distinctive features, displaying dendrites and a smaller size than moMACs⁴⁵.

The molecular determinants regulating the differentiation from monocytes to moMACs or moDCs are not completely understood, but some insights have been determined by an *in vitro* culture model resembling the simultaneous differentiation to both cell types occurring *in vivo*. MAFB was found as a critical transcription factor involved in moMAC differentiation, whereas interferon regulatory factor 4 (IRF4) controls moDC differentiation. Moreover, activation of aryl hydrocarbon receptor (AHR) promotes moDC and impairs moMAC differentiation²¹.

In addition, although both moMACs and moDCs can be found in different tissues at steady-state and inflammatory conditions¹⁷, the functional role and cytokine production of both cell types are not identical. First, both moMACs and moDCs have been reported to produce Tumor necrosis factor(TNF) α and IL1 β in several tissues⁴⁶⁻⁵⁰. Secondly, IL-12 production is specific to moDCs, whereas only moMACs produce IL-10^{46,48,51}. Furthermore, moDCs but not moMACs can stimulate CD4⁺ T cell proliferation, induce Th17 or Th1 polarization^{45,52,53}, and promote effector CD8⁺ T cell differentiation⁵¹. Altogether, these insights suggest higher immunogenic capabilities of moDCs in comparison with moMACs.

1.2.4. Regulation of monocyte and monocyte-derived cells immunogenesis

Monocytes and monocyte-derived cells are very sensitive, expressing a plethora of receptors to respond to external stimuli and orchestrate immune responses.

Several families of PRRs are expressed in monocytes, including C-type lectin receptors (CLRs), nucleotide-binding leucine-rich repeat receptors (NLRs), RIG-I-like receptors (RLRs), AIM2-like receptors (ALRs), and Toll-like receptors (TLRs)⁵⁴. First, TLRs are the best-characterized group. These receptors contain an extracellular domain with leucine-rich repeat motifs and a cytoplasmic region composed of a Toll/IL-1 receptor domain⁵⁵. There are 10 members in humans with different affinities for distinct PAMPs or DAMPs⁵⁶. For instance, TLR3 interacts with dsRNA from viruses, TLR9 binds CpG containing DNA from bacteria and TLR4 detects LPS, a component from gram-negative bacteria (Figure 2).

Introduction

TLRs lead to the activation of transcription factors from the NF- κ B, AP-1, and Interferon Regulatory Factor (IRF) families^{54,55}.

TLR4 response to LPS requires the presence of a multireceptor complex formed by LPS-binding protein (LBP), CD14, and MD-2⁵⁷. These proteins act sequentially to extract LPS from bacteria and activate signaling. This complex is extraordinarily sensitive: LPS from a single bacterium can activate TLR4 signaling on 1000 macrophages⁵⁸.

TLR4 can promote different types of signaling. First, the Myeloid Differentiation Primary Response Gene 88 (MyD88)-dependent pathway requires both MyD88 and TIR Domain-Containing Adaptor Protein (TIRAP). After TLR4 activation, MyD88 oligomerizes, also incorporating TIRAP and members of the IRAK family^{59,60}. IRAK4 is a kinase that leads to the activation of IRAK1 and IRAK2, permitting their interaction with MyD88 and TNF receptor-associated factor 6 (TRAF6)^{61,62}. Then, preassembled kinase complexes containing TAK1, TAB1, TAB2, and TAB3 are recruited. This complex controls the activation of I κ B kinase (IKK) and mitogen-activated protein kinase (MAPK) signaling to activate NF- κ B and AP-1, respectively⁶³. These transcription factors promote the production of proinflammatory cytokines. Moreover, the MyD88-independent pathway involves the recruitment of TIR-domain-containing adaptor inducing interferon- β (TRIF) and TRIF-related Adaptor Molecule (TRAM). The TRAM/TRIF complex activates IRF3, which drives the production of type 1 interferons.

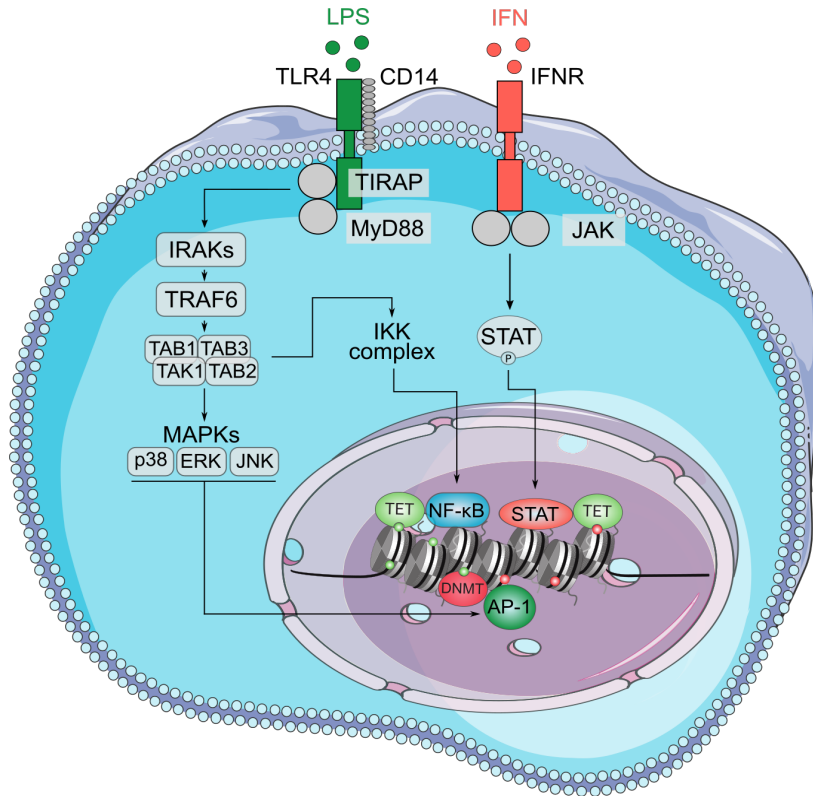


Figure 2: Examples of TLR and IFN receptor signaling pathways. The main steps in the MyD88-dependent TLR4 and IFN receptors pathway are depicted. On the one hand, LPS binds to TLR4 receptor, triggering MAPK and IKK signaling and activating AP-1 and NF- κ B transcription factors. On the other hand, IFNs such as IFN α , IFN β and IFN γ bind to their receptors, promoting JAK-mediated phosphorylation of STAT transcription factors. Phosphorylated STATs are translocated to the nucleus and bind to genomic loci. After binding to chromatin, transcription factors produce gene expression changes and can recruit epigenetic machinery such as Ten-Eleven Translocation (TET) and DNA methyltransferase (DNMT) enzymes, promoting changes in DNA methylation.

Introduction

Type I interferons such as interferon(IFN) α or IFN β , produced during TLR signaling, can signal autocrine or paracrinally through interferon receptors, which, in turn, trigger Janus kinase and signal transducer and activator of transcription (JAK/STAT) pathways⁶⁴. In mammals, there are four members of the JAK family: JAK1, JAK2, JAK3, and TYK2. When the associated receptors are activated, JAK proteins recruit and phosphorylate STAT proteins, which are translocated to the nucleus to bind specific loci in the genome to regulate gene transcription. STAT transcription factors, including STAT1, STAT2, STAT3, STAT4, STAT5A, STAT5B, and STAT6, can constitute different homodimers and heterodimers following different cytokine receptor activation⁶⁵. More than 50 cytokines and growth factors, including hormones, interferons, interleukins, and colony-stimulating factors can signal through JAK/STAT pathways⁶⁶.

These signaling pathways are tightly regulated, and several negative regulators have been identified. In the case of TLRs, some inhibitory components can diminish signaling. For instance, MyD88S is an alternative splice variant of MyD88 unable to bind IRAK4⁶⁷, IRAK-M binds the MyD88 complex and prevent the formation of IRAK-TRAF6 structures⁶⁸, TNF α -induced protein 3 (TNFAIP3) deubiquitinates and deactivates TRAF6⁶⁹ and single immunoglobulin interleukin-1-related receptor (SIGIRR) sequesters IRAK1 and TRAF6, downstream targets of MyD88⁷⁰. Furthermore, members of the suppressors of cytokine signaling (SOCS) family are involved in the inhibition of the JAK/STAT and TLR cascades⁷¹.

In addition, external stimuli can also modulate the immune response in monocytes and monocyte-derived cells. IL-10 signaling through its

membrane receptor can inhibit the production of cytokines such as GM-CSF, IL-6, TNF α , IL-1 β , or IL-12 and the induction of Th1 and Th2 responses^{72,73}. Moreover, it also promotes the production of anti-inflammatory molecules such as interleukin-1 receptor antagonist (IL-1RA) and soluble p55 and p75 TNFR^{72,74}. Additionally, hormones such as vitamin D3 or glucocorticoids can modulate differentiation and maturation of monocytes to an anti-inflammatory phenotype⁷⁵⁻⁷⁷.

Furthermore, epigenetic modifications caused by stimulation of monocytes can impact the response to further stimuli, in a process called innate immune memory, increasing or attenuating the immune response. Two examples of these innate immune memory in monocytes are represented by trained immunity and endotoxin tolerance⁷⁸.

First, trained immunity is defined as an enhanced immune response in a second insult, after the priming of monocytes or macrophages by an initial challenge⁷⁹. Exposure of monocytes to β -glucan, a paradigmatic example of trained immunity molecule, is associated with changes in H3K4me3 at the promoters of immune-related genes, such as TNF, IL6, and IL18⁸⁰. Moreover, in macrophages, β -glucan produces gains in H3K27ac in promoters and enhancers⁸¹.

Conversely, endotoxin tolerance is a type of innate memory in which initial stimulation with LPS impairs pro-inflammatory response in front of further TLR4 stimulation⁷⁸. Tolerant cells show an altered cytokine production, characterized by lower production of TNF α and higher production of IL-10⁸². This process is also associated with epigenetic alterations in H3K4me3, H3K27ac, H3K4me1, and DNA accessibility⁸¹. For instance, LPS-treated human monocytes display lower levels of H3K27ac and H3K4me1 at promoters and enhancers of phagocytic and

Introduction

lipid metabolism-related genes⁸³. This process is relevant for diseases such as sepsis, in which blood monocytes are in contact with bacterial compounds^{84,85}.

Innate immune memory can be maintained in myeloid cells for several years⁸⁶. However, monocytes and DCs present an average half-life of 5-14 days^{18,87}. Recent works have conciliated both facts, differentiating between peripheral and central trained immunity⁸⁸. Peripheral trained immunity occurs in differentiated cells, such as monocytes and DCs, whereas central trained immunity takes place in myeloid progenitors^{89,90}.

1.3. Immunogenic and tolerogenic dendritic cells

1.3.1. Classification and biology of dendritic cells

DCs are a heterogeneous group of innate immune cells, not only critical in the response to threats, orchestrating immune responses, but also in the regulation of inflammatory responses and the induction of immune tolerance. Blood DCs can be classified into plasmacytoid DCs (pDCs) and conventional DCs (cDCs). In humans, DCs comprise around 1% of PBMCs⁹¹. Both types derive from common DC progenitors (CDPs)⁸⁷ (Figure 3).

cDCs are made up of two main subsets (cDC1 and cDC2), initially characterized by the expression of CD141 (BDCA3) and CD1c (BDCA1), respectively^{92,93}. Human cDC1 cells express TLR3 and TLR10, recognize viral and intracellular antigens, and produce type III IFN⁹³⁻⁹⁵. Human cDC2s express TLR2, TLR4, TLR5, TLR6, and TLR8⁹⁶. Human cDC1 and cDC2 can cross-present antigens to CD8⁺ T cells^{97,98}. However, whereas human cDC1 seems to be specialized in cross-presenting dead cell antigens and inducing a Th2 response, cDC2 cells more potently

induce the Th1 response^{99,100}. On the other hand, pDCs secrete large amounts of type I IFNs in response to viruses, can cross-present antigens¹⁰¹ and are morphologically similar to antibody-producing plasma cells^{102,103}.

The expression profiles and surface markers of different DC groups can differ not only between species but also in distinct tissues from the same organism^{104,105}. Single-cell technologies have recently allowed the identification of additional DC subsets and redefining of existing ones. In this regard, a single-cell RNA-seq analysis of human peripheral blood has enabled the identification of six clusters of DCs: DC1, corresponding to cDC1; DC2 and DC3, corresponding to a new subdivision of cDC2; DC4, corresponding to CD11c+CD141-CD1c-CD16+ DCs; DC5, a previously uncharacterized group; and DC6, which corresponds to pDCs⁹⁶. Another study also provided evidence of the higher heterogeneity of the cDC2/DC3 population in comparison to cDC1¹⁰⁶. DC3 cells^{107,108}, despite sharing surface markers with cDC2 and monocytes, present a specific precursor (pre-DC3). DC3s stimulate naïve T cells with similar efficiency to cDC2s, but their specific function remains to be unraveled.

An additional group of DCs is represented by moDCs, the differentiation of which takes place in tissues, from monocytes extravasated from peripheral blood, both in mice and humans¹⁷. In humans, populations of moDCs have been detected in different tissues, in the steady-state and, especially, under inflammatory conditions (see section 1.2.1).

Introduction

Following differentiation, immature DCs (iDCs) can extravasate to peripheral tissues in steady-state conditions. iDCs present low antigen presentation capabilities and co-stimulatory molecules expression, which confer them tolerogenic features and a key role in peripheral tolerance¹⁰⁹.

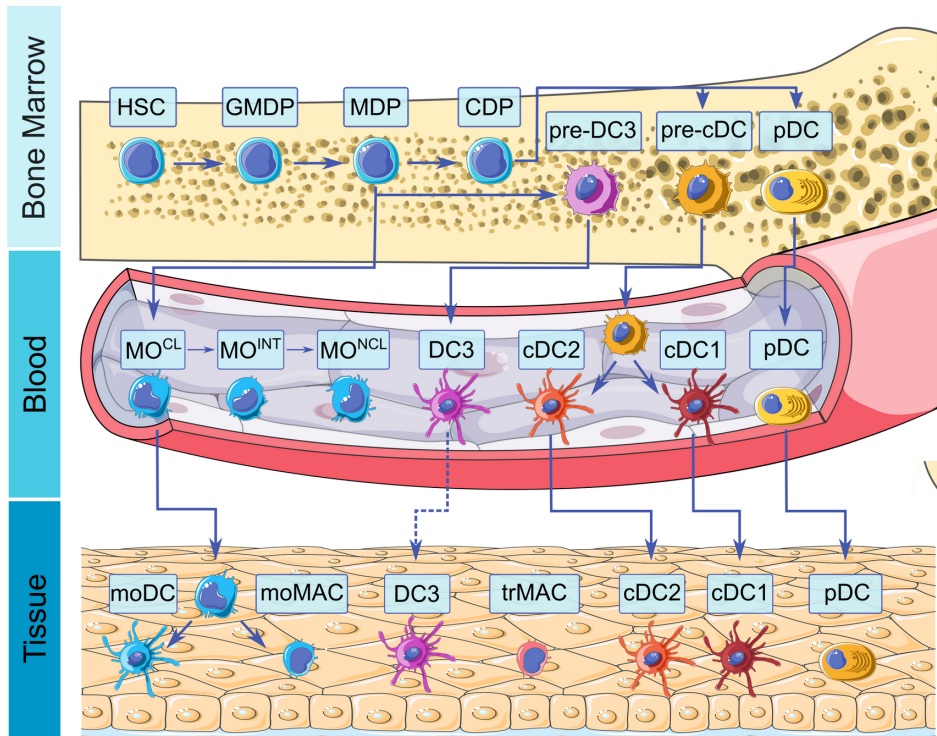


Figure 3: Ontogeny and differentiation of monocytes and dendritic cells across tissues. The hierarchical steps of differentiation from hematopoietic stem cells (HSCs) in the bone marrow, to terminal cells in the blood and tissues are depicted. GMDP: granulocyte, monocyte, and DC progenitors MDP: monocyte and DC progenitors CDP: Common dendritic cell progenitors, pre-cDC: Common dendritic cell progenitor, pDC: plasmacytoid dendritic cell, MO: Monocytes, MO^{CL}: Classical MOs, MO^{INT}: Intermediate MOs, MO^{NCL}: Non-classical MOs, cDC1: classical DC 1, cDC2: classical DC 2, moDC: inflammatory DCs, moMAC: monocyte-derived macrophages. Tissue-resident macrophages (trMAC) are generated during embryonic hematopoiesis and self-maintain independently of bone marrow contributions during adulthood. Adapted from Morante-Palacios et al. 2021, Trends in Immunology.

However, when iDCs interact with PAMPs or DAMPs through their PRRs in tissues, these cells are activated, yielding mature DCs (mDCs)¹¹⁰. This process is characterized by an increase in the expression of MHC class II, co-stimulatory molecules, cytokines, and the chemokine receptor CCR7¹¹¹.

Although iDCs and mDCs are commonly associated with a tolerogenic or immunogenic phenotype, respectively, DC maturation is not always linked to the acquisition of immunogenicity, as the final phenotype of these cells may be influenced by different stimuli. In this regard, *in vivo* steady-state maturation of iDCs into mDC with tolerogenic characteristics has been reported¹¹².

1.3.2. *In vivo* and *in vitro* generated tolerogenic dendritic cells

Generally, DCs with a stable, semi-mature phenotype and tolerogenic attributes are referred to as tolDCs¹⁴. First, a human DC subset with tolerogenic properties (DC-10) was identified in peripheral blood and spleen¹¹³. These cells are characterized by the production of IL-10 and the suppression of allogenic CD4⁺ T cells response¹¹³.

However, given the difficulty of isolating rare human subpopulations of DCs with tolerogenic phenotypes, many protocols have been designed to generate tolDCs *in vitro*, generally derived from human monocytes (mo-tolDCs). These protocols are grounded in the modulation of the monocyte to DC differentiation with the addition of different molecules such as cytokines (IL-10, Transforming growth factor (TGF) β) glucocorticoids, vitamin D3, rapamycin, minocycline, or ethyl pyruvate, among others^{114,115}. The resulting cells are able to produce anti-inflammatory cytokines and inhibit T cell growth through several mechanisms.

Introduction

1.3.3. Mechanisms of tolerogenesis

In contrast with the antigen presentation and immune response initiation of immunogenic DCs, several mechanisms have been described from tolDCs to induce tolerance. First, when T cells recognize an antigen presented by tolDCs, without co-stimulation (binding of CD28 with CD80/CD86), T cells cannot proliferate¹¹⁶ (Figure 4A).

Secondly, the expression of co-inhibitory molecules in tolDCs also inhibits T cell proliferation. For instance, programmed death-ligand 1 (PD-L1) is an inhibitory surface receptor, expression of which by DCs is involved in tolerance induction, for example, during cancer¹¹⁷ and autoimmunity. Many tolDCs express PD-L1 and PD-L2, which bind to programmed cell death protein 1 (PD-1), expressed by T cells¹¹⁸, triggering the recruitment of phosphatases SHP-1 and SHP-2, which target the TCR and CD28 signaling pathway, subsequently promoting tolerance via induction of clonal anergy and Treg differentiation^{119,120} (Figure 4A).

Moreover, cytotoxic T-lymphocyte-associated protein 4 (CTLA-4), a receptor expressed by activated T cells and Tregs, can bind CD80 and CD86 molecules expressed on DCs and mediate their transendocytosis and degradation¹²¹. Hence, CTLA-4 can regulate co-stimulatory molecules expressed by DCs, impairing the priming of naïve T cells¹²² (Figure 4A). Furthermore, tolDCs can induce CD4⁺ and CD8⁺ T cells with high CTLA-4 expression and antigen-specific suppressor activity^{123,124}.

In addition to cell-cell contact-dependent mechanisms, tolDCs can produce several tolerogenic cytokines and metabolites (Figure 4B). Various tolDC types produce IL-10^{113,125} and can induce anergy *in vitro* in both effector and memory CD4⁺ T cells and differentiation of IL-10-, interferon (IFN)- γ -, and TGF- β -secreting Tregs in both mice and

humans^{124,126} (Figure 4C). TGF- β and IL-27 are other pleiotropic cytokines secreted by several tolDCs, which promote the generation of Tregs and stimulate IL-10 secretion^{127,128}. Moreover, in a mouse model of multiple sclerosis, IL-27 was described to induce CD39 in cDCs, limiting the generation of T helper (Th)1 and Th17 effector T cells, as well as PD-L1 expression in pDCs^{128,129} to limit disease development. Also, in the same model, retinoic acid, a metabolite of vitamin A1 secreted by some DCs, promoted TGF- β -driven generation of Tregs *in vitro* and inhibited polarization of Th17 cells, which are highly inflammatory^{130,131}.

Furthermore, tolDCs can express indoleamine 2,3-dioxygenase (IDO) (an enzyme that catabolizes tryptophan to several metabolites) that, in addition to depleting tryptophan, can block the T lymphocyte cell cycle and induce apoptosis both in mice and humans^{132,133}. Moreover, kynurenine, a tryptophan catabolite, is a natural ligand of AHR which, in this context, promotes differentiation of Tregs in mice¹³⁴. A recent study also noted that human mo-tolDCs delayed graft-versus-host disease and induced a reduced T cell proliferative capacity via metabolic modulation, achieved through lactate secretion¹³⁵.

Introduction

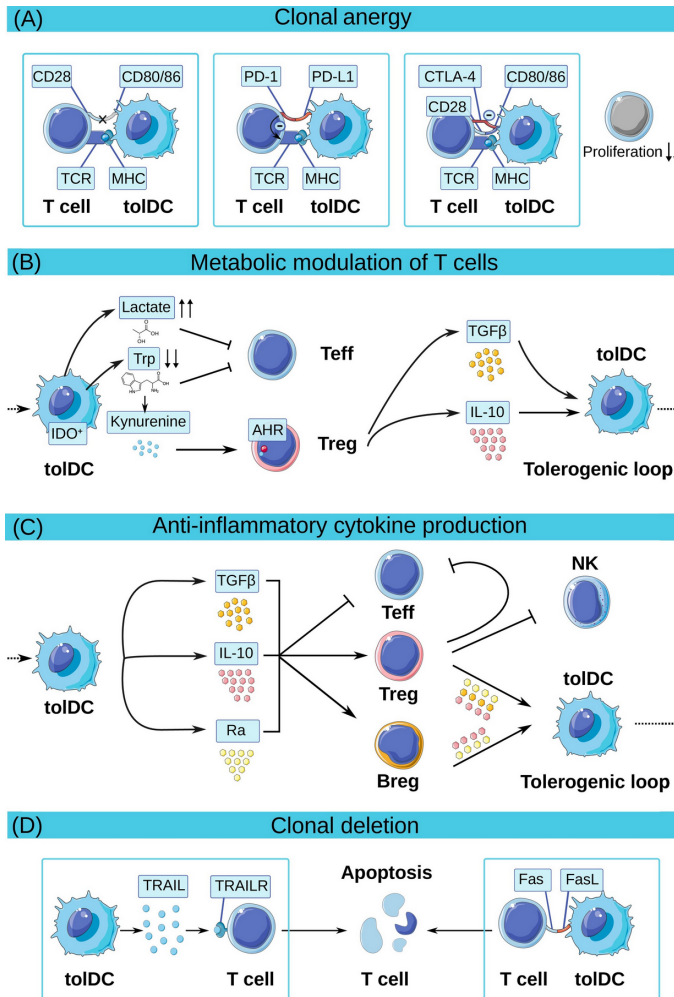


Figure 4: Mechanisms of tolerogenesis of tolerogenic dendritic cells. (A) After binding of the T cell receptor to MHC molecules expressed by toIDCs, clonal anergy can occur if co-stimulatory signal is low, or in the presence of co-inhibitory signals. (B) toIDCs can promote tryptophan-low microenvironments generating kynurenine and suppressing effector T cell activity. (C) toIDCs can suppress T cell proliferation with the secretion of cytokines and metabolites with a tolerogenic activity, such as IL-10, TGFβ and retinoic acid (Ra). (D) Surface proteins interactions between toIDCs and T cells can lead to T cell clonal deletion, including TRAIL/TRAIRL and Fas/FasL interactions.

Finally, tolDCs can directly eliminate T cells via clonal deletion. For instance, the interaction between tumor necrosis factor (TNF)-related apoptosis-inducing ligand (TRAIL) of human DCs and death receptors of T cells can promote their apoptosis by activating the caspase pathway¹³⁶. In the same way, Fas, which is upregulated in T cells during their activation, can bind to FasL in tolDCs and promote T cell apoptosis in mice¹³⁷ (Figure 4D).

In brief, tolDCs present a major effect in suppressing immune responses through different mechanisms involving cell-cell contact and the production of metabolites and cytokines.

1.3.4. Clinical use of tolerogenic dendritic cells

Chronic inflammatory diseases are characterized by the disruption of immune homeostasis and long-term inflammatory responses triggered by specific endogenous or exogenous antigens. Several drugs exist to treat some of these diseases, including small molecules and monoclonal antibodies^{138,139}. While these agents can improve the outcomes of autoimmune and inflammatory diseases, they are nonspecific drugs that require life-long administration and are associated with toxicity and increased risk of secondary infections or cancer development¹⁴⁰.

In this context, therapies based on autologous mo-tolDCs represent a promising alternative (Figure 5). Mo-tolDCs can be loaded with specific antigens and drive the immune system toward homeostasis by abrogating pathological autoimmune or inflammatory responses, without interfering with protective immunity¹⁴¹.

Several preclinical studies have indicated the potential therapeutic efficacy of tolDCs in mouse models for rheumatoid arthritis¹⁴², type I diabetes¹⁴³, multiple sclerosis^{144,145}, organ transplantation¹⁴⁶, among others.

Introduction

Moreover, phase I and phase I/II clinical trials have been completed for these diseases, with promising results^{14,147-151}. However, the existence of very diverse protocols to generate tolDCs, with different phenotypes and tolerogenicities, poses a big challenge, requiring robust quality control indicators to assess the phenotype, potency, and safety of each cell product. Moreover, evidence of *in vivo* tolDC mechanisms of action is still lacking. In this regard, the standardization of immunomonitoring protocols, functional assays, and cellular phenotyping will be key to the incorporation of mo-tolDCs into clinical practice.

1.3.5. Clinical use of immunogenic dendritic cells

Given the relevance of DCs in the development of immune responses, many efforts have been focused on the generation of cell therapies to trigger immunity against diseases, based on these cells.

First, the use of DC vaccines for cancer has been extensively investigated, with more than 200 completed clinical trials to date¹⁵². This strategy generally involves the isolation of autologous monocytes or CD34⁺ progenitors from the patient to be differentiated *in vitro* to DCs, followed by the manipulation and reinfusion into patients (Figure 5).

Several trials have been developed with autologous moDCs obtained from blood monocytes or CD34⁺ progenitors. In this regard, phase III clinical trials with moDCs are ongoing in castration-resistant prostate cancer (NCT02111577), uveal melanoma (NCT01983748), metastatic colorectal cancer (NCT02503150), and glioblastoma (NCT00045968)¹⁵³.

Since blood DCs possess greater antigen-presentation capabilities, with higher MHC molecule expression, their use has been proposed as the basis for next-generation DC vaccines for cancer treatment, despite their limited number compared to monocytes¹⁵⁴. Moreover, the improvement of moDC differentiation and maturation protocols could also increase treatment efficacy. In this respect, the study and modulation of the

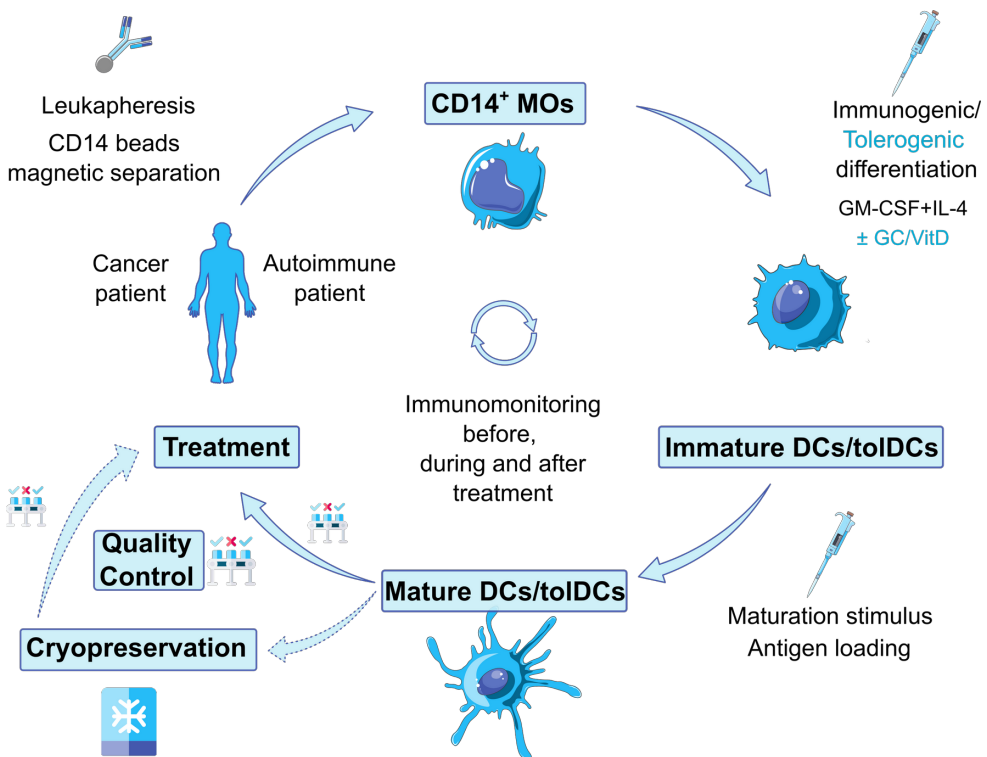


Figure 5: Process of immunogenic DC / tolDC generation. Patient leukocytes are collected from blood and monocytes are isolated via magnetic cell separation and cultured with cytokines (generally GM-CSF/IL-4) and a tolerogenic agent such as glucocorticoids (GC) or vitamin D3 (vitD), in the case of tolDCs. Then, DCs are matured and a specific antigen is loaded. Mature DC/tolDCs are analyzed for quality control and administered to the patients. After administration, tolDCs may induce tolerance to autoreactive T cells in autoimmune patients and immunogenic DCs may promote specific immune responses targeted to cancer cells.

Introduction

transcriptional determinants and epigenomic changes that take place during moDC differentiation could be a valuable step in this direction.

1.4. DNA methylation dynamics in the regulation of the immune system

1.4.1. Overview

DNA methylation is defined as the addition of methyl groups to DNA molecules. DNA methylation, particularly cytosine methylation, is the most-studied epigenetic modification¹. In mammals, DNA methylation is mostly found in carbon 5 (5mC) of CpG (cytosine-followed-by-guanine) dinucleotides.

Originally, DNA methylation was studied in CpG-rich regions (CpG islands), which are generally found in gene promoters¹⁵⁵. In that context, DNA methylation is associated with gene repression, and is also relevant for the X-chromosome inactivation and long-term gene silencing. However, more recent works have elucidated a new role of DNA methylation in the regulation of dynamic biological processes, highlighting the role of DNA methylation in enhancers, gene bodies, and partially-methylated domains^{156,157}.

DNA methylation kinetics is controlled by specific enzymes. First, the addition of methyl groups to DNA is mediated by DNA methyltransferases (DNMTs). On the one hand, DNMT1 is responsible for maintaining DNA methylation following replication through cell division. On the other hand, DNMT3A and DNMT3B mainly catalyze *de novo* DNA methylation¹⁵⁸.

DNA demethylation, the removal of methyl groups from DNA molecules, can be classified as active or passive. Passive DNA demethylation can occur after consecutive cell divisions when the function of DNMT1 is suboptimal¹⁵⁹. Active demethylation is mediated by members of the Ten-Eleven Translocation (TET) family, including TET1, TET2, and TET3¹⁶⁰. TET1 and TET3 have cysteine-X-X-cysteine (CXXC) domains which allow them to bind directly to CpGs in the genome, whereas TET2 lacks that domain¹⁶¹⁻¹⁶³. These oxygen-dependent enzymes catalyze the oxidation of 5mC to 5-hydroxymethylcytosine (5hmC), 5-formylcytosine (5fC), and 5-carboxylcytosine (5caC). 5fC- and 5caC-modified positions are bound and excised by the thymidine-DNA glycosylase (TDG) enzyme, yielding an abasic site that is replaced with an unmethylated cytosine by base-excision repair (BER) (Figure 6)¹⁶⁴.

Moreover, demethylation intermediates such as 5hmC have been proposed as *bona fide* epigenetic marks, with potential effects in genome regulation^{165,166}.

DNA methylation or demethylation in dynamic biological processes usually co-localize with transcription factor binding sites, posing that specific transcription factors, triggered by upstream signaling pathways, can recruit methylation-related enzymes to specific regulatory loci in the genome, such as enhancers¹⁶⁷. In this regard, a subset of transcription factors (pioneer transcription factors) can bind directly condensed chromatin and rearrange the epigenome¹⁶⁸. In addition, some of them can alter the DNA methylation status of their target regions¹⁶⁹. Furthermore, the binding capabilities of many transcription factors can be affected by the methylation status of their binding sites^{170,171}. The study of that bidirectional interplay enables us to describe genome-environment

Introduction

interactions at the molecular level in a variety of human biological contexts.

DNA methylation can be modulated with drugs. First, nucleoside analogues such as azacitidine, decitabine and zebularine inhibit DNMT action. After cell replication, these molecules are integrated in the DNA and lead to DNMT degradation, promoting hypomethylation^{172,173}. These drugs are used for the treatment of hematological cancer, including acute myeloid leukemia and myelodysplastic syndromes¹⁷⁴.

Disruption of DNA methylation patterns through TET mutations is a hallmark of some hematopoietic malignancies¹⁷⁵. Therefore, drugs that increase TET function, such as vitamin C, could potentially be useful for their treatment¹⁷⁶. Moreover, a TET inhibitor has also been developed, which could be a very relevant tool to study processes involving active demethylation¹⁷⁷.

1.4.2. Vitamin C as a cofactor of TET enzymes

Vitamin C (L-ascorbic acid) is an essential nutrient with pleiotropic functions. Its deficiency is associated with a plethora of symptoms, including the malfunction of the immune system¹⁷⁸. In this regard, immune cells present high contents of vitamin C in their cytoplasm. In the case of monocytes, the concentration is around 3mM, in healthy individuals, when plasma levels are around 50µM. Several diseases affect the concentration of vitamin C in immune cells, including cancer and some conditions of active inflammation¹⁷⁹⁻¹⁸¹.

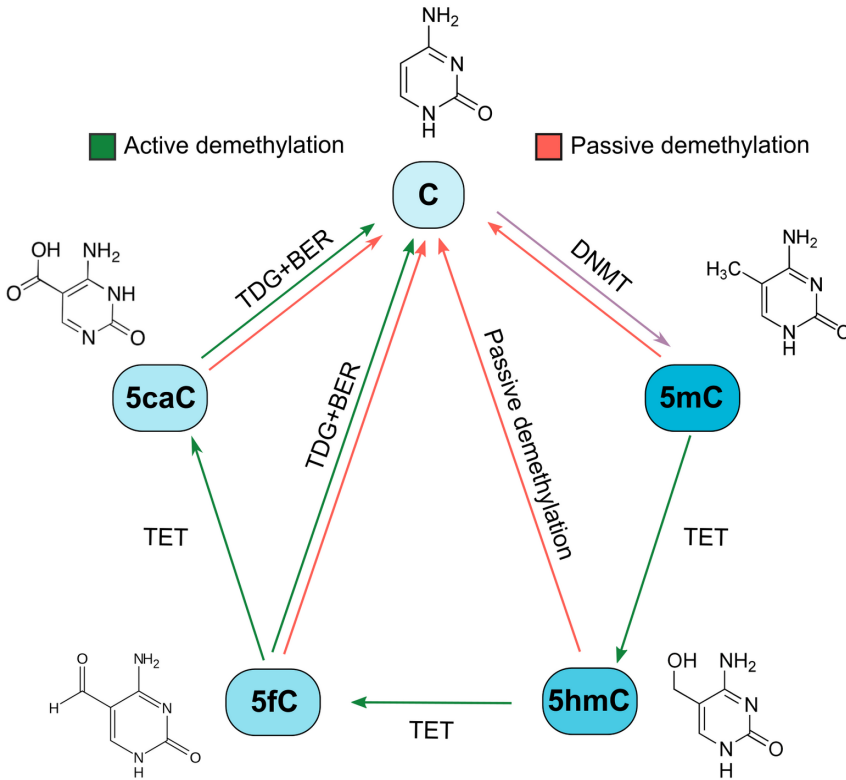


Figure 6: DNA demethylation cycle. TET enzymes can catalyze the sequential oxidation of 5mC to 5hmC, 5fC and 5caC. Active demethylation is achieved through thymine-DNA glycosylase (TDG)-mediated removal of oxidized forms of cytosines followed by base excision repair (BER). Moreover, DNA replication with inefficient maintenance of DNA methylation results in passive demethylation. In contrast, DNMT enzymes promote cytosine methylation, yielding 5mC.

It is well established that vitamin C is a cofactor for several enzymes, including dopamine beta-hydroxylase and the collagen prolyl and lysyl hydroxylases^{182,183}. Biochemically, vitamin C act as a reducing agent, recycling the Fe^{2+} active site of hydroxylases. In this regard, vitamin C can enhance TET enzymes activity through its cofactor function, promoting demethylation^{184,185}.

Introduction

Linus Pauling proposed vitamin C as a potential cancer treatment more than 40 years ago. A clinical trial published in 1976 showed promising results for the treatment of cancer with vitamin C, but the lack of appropriate controls and the negative results of further trials diminished the enthusiasm^{186,187}. Moreover, the mechanism of action by which vitamin C could act against cancer cells was not defined.

However, during the last few years, increasing interest has arisen around vitamin C as a treatment or adjuvant for several types of cancer. For instance, vitamin C intravenous treatment in mice has been shown to abrogate cancer progression through direct TET2 function restoration in cancer cells¹⁷⁶. Moreover, clinical remission following vitamin C treatment was found in a case of acute myeloid leukemia with mutations in *TET2*¹⁸⁸. Interestingly, in mice models of different types of cancer, a fully competent immune system was required to maximize the antiproliferative effects of vitamin C, suggesting that that molecule not only acts directly in the cancer cells but also through immune system modulation¹⁸⁹. Several clinical trials are trying to translate these results to clinical practice, especially in synergy with other treatments¹⁹⁰.

1.4.3. Role of DNA methylation in monocyte differentiation

DNA methylation regulation is particularly important during hematopoiesis and the subsequent regulation of terminal immune cells. In this regard, several works show how the impairment of methylation machinery can abrogate hematopoietic stem cell differentiation^{191–193}. Transcription factor networks guide the differentiation of these cells and imprint specific DNA methylation signatures along the way¹⁹⁴. In particular, monocytes are highly plastic cells, which can undergo

differentiation *in vitro* or *in vivo* under the exposure of a plethora of molecules (see sections 1.2.2 and 1.2.3).

TET2 is strongly expressed in these cells, and many studies have shown the relevance of this enzyme during *in vitro* differentiation of monocytes to macrophages. Macrophages are customarily divided into pro-inflammatory M1 and anti-inflammatory M2 phenotypes. Macrophage colony-stimulating factor (M-CSF) and GM-CSF are the primary cytokines that stimulate macrophage differentiation. GM-CSF induces differentiation to M1-like macrophages, whereas M-CSF promotes M2-like macrophage differentiation¹⁹⁵.

M-CSF stimulation of monocytes is associated with both gains and losses of DNA methylation, although most studies predominantly observe losses of DNA methylation^{35,196,197}.

On the other hand, GM-CSF produces fundamentally TET2-dependent hypomethylation, in intergenic regions and gene bodies³⁵. Regarding moDCs, generated with GM-CSF and IL-4, they also show mostly losses of DNA methylation. In this regard, the activation of the JAK3-STAT6 pathway downstream of IL-4 triggers TET2-dependent demethylation in a specific group of CpGs. Moreover, other transcription factors have been linked with demethylation in this context, such as EGR2¹⁹⁸.

Additionally, DNA methylation changes have also been found during maturation/activation of monocyte-derived cells, but generally at much lower levels than differentiation^{35,197,199}. Conversely, significant DNA methylation changes were found after the activation of immature moDCs through live bacteria exposure²⁰⁰. In this regard, the rapid transcriptomic response in contrast with DNA demethylation in this activation process

Introduction

indicates that DNA methylation changes are a consequence rather than a cause of the transcriptional changes.

OBJECTIVES

OBJECTIVES

2.OBJECTIVES

Monocytes are highly plastic cells, with the ability to differentiate into cell types with very different immunological properties. Depending on the external stimuli and the specific immune context, they can promote or diminish immune responses. These external stimuli are recognized by specific receptors and integrated by signaling pathways which lead to the participation of transcription factors. Several studies have focused on the delineation of the signaling pathways and transcription factors involved in differentiation or activation in different myeloid models. However, the epigenomic determinants associated with the action of transcription factors that may condition the immune response of monocytes and monocyte-related differentiation processes are not completely understood. The study of DNA methylation can help to infer specific transcription factors involved in different processes and also shed light on the gene expression regulation, by its role alone or linked with histone modifications or DNA accessibility. In this thesis, the molecular mechanisms that regulate the triggering of immunogenic or tolerogenic responses of three different monocyte-derived differentiation processes have been studied.

We divided this main objective into three specific points:

1. To study the transcription factors involved and the underlying epigenomic regulation of glucocorticoid-mediated differentiation of monocytes to tolDCs.

TolDCs obtained from monocytes *in vitro* with GM-CSF, IL-4 and glucocorticoids are a clinically relevant model and a potential treatment

Objectives

for autoimmune diseases such as rheumatoid arthritis. We hypothesized that the elucidation of potential glucocorticoid-mediated DNA methylation changes of tolDCs in comparison with DCs obtained from monocytes, and their integration with transcriptomic data could allow us to identify new relevant transcription factors involved in the process, conceivably providing new targets for the improvement of tolDC generation.

2. To characterize the sequence of epigenomic events occurring during the acquisition of endotoxin tolerance in human monocytes.

Microbial challenges can induce endotoxin tolerance in monocytes, both *in vivo*, in some pathological conditions such as sepsis, and *in vitro*. This process is defined as a reduced immune response against successive stimuli. Remodeling of some epigenomic traits, including histone marks and DNA accessibility, has been associated with this process, but the participation of DNA methylation is poorly understood, as well as the involvement of signaling pathways. We proposed that the examination of an *in vitro* model of endotoxin tolerance, with LPS-treated monocytes, together with samples from septic patients may shed light on this issue.

3. To assess the transcriptomic, epigenomic and phenotypic effects of vitamin C in the monocyte to DC differentiation and maturation.

L-ascorbic acid (vitamin C) is a known cofactor of epigenetic enzymes such as TET proteins and Jumonji histone demethylases, and its presence can enhance the process of active demethylation. Vitamin C deficiency produces a disease, namely scurvy, whose symptoms include impaired

immunity. Nevertheless, the effects of vitamin C on DC differentiation and maturation have not been studied yet. We planned the analysis of the epigenomic remodeling mediated by vitamin C in the context of monocyte to DC differentiation, along with its potential impact on the transcriptome and phenotype of these cells.

ARTICLES

ARTICLES

3.ARTICLES

Director's report

I certify that the PhD student Octavio Morante-Palacios will defend his Doctoral Thesis by article publication compendium, two of which have already been published. His contribution to each article is specified below:

ARTICLE 1:

Title: Coordinated glucocorticoid receptor and MAFB action induces tolerogenesis and epigenome remodelling in dendritic cells

Octavio Morante-Palacios, Laura Ciudad, Raphael Micheroli, Carlos de la Calle-Fabregat, Tianlu Li, Gisela Barbisan, Miranda Houtman, Sam G. Edalat, Mojca Frank-Bertoncelj, Caroline Ospelt and Esteban Ballestar

Journal: **Nucleic Acids Research** (Volume 50, Issue 1, Pages 108–126)
(IF 2020: 16.971)

In this article, Octavio Morante-Palacios was the main person responsible, along with myself, for conceiving the majority of the experiments and performing them. He established the differentiation model and generated samples for gene expression and DNA methylation arrays. Moreover, he performed CD8⁺ proliferation assays, flow cytometry, ELISAs, Western Blots, Chromatin Immunoprecipitations (ChIPs), co-immunoprecipitations, and silencing of MAFB with siRNAs. He was in charge of all bioinformatics analyses performed in the paper, including raw

Articles

reads alignments, processing, and plotting of methylation, expression, and ChIP-seq data. Finally, Octavio, along with me, interpreted all the results obtained and wrote the paper.

ARTICLE 2:

Title: JAK2-STAT epigenetically regulates tolerized genes in monocytes in the first encounter with gram-negative bacterial endotoxins in sepsis

Octavio Morante-Palacios*, Clara Lorente-Sorolla*, Laura Ciudad, Josep Calafell-Segura, Antonio Garcia-Gomez, Francesc Català-Moll, Adolfo Ruiz-Sanmartín, Mónica Martínez-Gallo, Ricard Ferrer, Juan Carlos Ruiz-Rodriguez, Damiana Álvarez-Errico and Esteban Ballestar

*(Equal contribution)

Journal: **Frontiers in Immunology** (12:734652. eCollection 2021) (IF 2020: 7.561)

In this article, Clara and Octavio performed most of the experiments. Octavio was involved in the flow cytometry experiments with septic patients, as well as JAK2 inhibition to obtain methylation and expression data. He performed the bioinformatics analyses, including the processing of raw reads and downstream RNA-seq data generation, and the analysis of methylation arrays. Octavio assembled the figures together with Clara. Octavio, Clara, Damiana and I wrote and revised the manuscript.

ARTICLE 3:

Title: Vitamin C enhances NF- κ B-driven DNA demethylation and immunogenic properties of dendritic cells

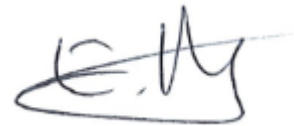
Octavio Morante-Palacios, Gerard Godoy-Tena, Josep Calafell-Segura, Laura Ciudad, Eva M. Martínez-Cáceres, José Luis Sardina and Esteban Ballestar

(In preparation)

In this paper, still in preparation, Octavio has optimized the vitamin C differentiation model, generated the samples for methylation and expression data, and performed all the bioinformatics analyses used. Finally, Octavio, along with me, interpreted all the results. He addressed all assembly figures and was involved in the writing and revision of the article.

In witness whereof, I hereby sign the present doctoral thesis,
18th February 2022, Badalona (Barcelona)

Esteban Ballestar, Ph.D.
Epigenetics and Immune Disease Group, Leader
Josep Carreras Research Institute (IJC)
Ctra de Can Ruti, Camí de les Escoles s/n
08916 Badalona, Barcelona, Spain
Tel: +34 935572800 ext. 4250
E-mail: eballestar@carrerasresearch.org



3.1. ARTICLE 1: Coordinated glucocorticoid receptor and MAFB action induces tolerogenesis and epigenome remodelling in dendritic cells

Coordinated glucocorticoid receptor and MAFB action induces tolerogenesis and epigenome remodelling in dendritic cells

Octavio Morante-Palacios^{1,2}, Laura Ciudad¹, Raphael Micheroli³, Carlos de la Calle-Fabregat¹, Tianlu Li¹, Gisela Barbisan¹, Miranda Houtman³, Sam G. Edalat³, Mojca Frank-Bertoncelj³, Caroline Ospelt³ and Esteban Ballestar^{1,2,*}

¹Epigenetics and Immune Disease Group, Josep Carreras Research Institute (IJC), 08916 Badalona, Barcelona, Spain

²Germans Trias i Pujol Research Institute (IGTP), 08916 Badalona, Barcelona, Spain

³Center of Experimental Rheumatology, Department of Rheumatology, University Hospital Zurich, University of Zurich, Zurich, Switzerland.

*Correspondence: E. Ballestar, E-mail: eballestar@carrerasresearch.org

Abstract

Glucocorticoids (GCs) exert potent anti-inflammatory effects in immune cells through the glucocorticoid receptor (GR). Dendritic cells (DCs), central actors for coordinating immune responses, acquire tolerogenic properties in response to GCs. Tolerogenic DCs (tolDCs) have emerged as a potential treatment for various inflammatory diseases. To date, the underlying cell type-specific regulatory mechanisms orchestrating GC-mediated acquisition of immunosuppressive properties remain poorly understood. In this study, we investigated the transcriptomic and epigenomic remodeling associated with differentiation to DCs in the presence of GCs. Our analysis demonstrates a major role of MAFB in this process, in synergy with GR. GR and MAFB both interact with methylcytosine dioxygenase TET2 and bind to genomic loci that undergo specific demethylation in tolDCs. We also show that the role of MAFB is more extensive, binding to thousands of genomic loci in tolDCs. Finally, MAFB knockdown erases the tolerogenic properties of tolDCs and reverts the specific DNA demethylation and gene upregulation. The preeminent role of MAFB is also demonstrated *in vivo* for myeloid cells from synovium in rheumatoid arthritis following GC treatment. Our results imply that, once directly activated by GR, MAFB plays a critical role in orchestrating the epigenomic and transcriptomic remodeling that define the tolerogenic phenotype.

Keywords: glucocorticoid receptor, MAFB, epigenetics, dendritic cells, tolerogenesis, inflammation

Introduction

Dendritic cells (DCs) are a heterogeneous group of innate immune cells with a central role not only in the response to threats, but also in the regulation of inflammatory responses and the induction of immune tolerance, which is defined as the reduced responsiveness of the immune system to molecules with the potential to produce an immune response (1). Several types of human DCs exist *in vivo*, including conventional DCs (cDCs) and plasmacytoid DCs (pDCs). Moreover, monocytes (MOs) can extravasate to tissues and differentiate to monocyte-derived macrophages (moMACs) or monocyte-derived dendritic cells (moDCs) (2, 3). MOs cultured with GM-CSF and IL-4 are a widely used *in vitro* model of DCs (4), with gene expression similarities with blood cDCs and *in vivo* moDCs (5).

Epigenetic determinants and transcription factors (TFs) critical to DC differentiation and function have been extensively studied. In particular, STAT6 (6), early growth response 2 (EGR2) (7), and interferon regulatory factor 4 (IRF4) (5) have been linked to DC fate determination and specific DNA demethylation events through recruitment of Ten-eleven translocation methylcytosine dioxygenase 2 (TET2), which is the most expressed TET enzyme in MOs (8). Moreover, AHR can act as a molecular switch that enables monocyte differentiation to moDC, via IRF4, whereas MAFB determines monocyte differentiation to moMAC (5, 9, 10).

DCs can acquire tolerogenic functions *in vivo* and *in vitro* in response to several stimuli, including interleukin (IL)-10, vitamin D₃, rapamycin, and glucocorticoids (GCs) (1). In particular, DCs differentiated from MOs *in vitro* with GM-CSF, IL-4, and GCs can suppress T cell

Articles

proliferation *in vitro*, and display a high level of production of IL-10 and low levels of TNF α and IL-12p70 (11, 12). Tolerogenic DCs (tolDCs), generated as indicated above, can be useful as a treatment for autoimmune diseases. Several clinical trials have yielded satisfactory results in diseases such as rheumatoid arthritis (13, 14), multiple sclerosis (15), and Crohn's disease (16).

GCs are a family of steroid hormones that are ligands of the Glucocorticoid Receptor (GR), a nuclear receptor expressed in most cell types that can trigger the expression of anti-inflammatory genes through direct DNA binding. Moreover, GR also represses the action of inflammatory-related TFs, such as the NF- κ B and AP-1 families, via protein–protein interactions, in a process called transrepression (17). GR has been related to chromatin remodelers, including EP300 and BRG1 (18, 19). The mechanisms underlying cell type-specific programs induced by GR upon ligand binding, as well as the participation of TFs and epigenetic enzymes, remain to be fully determined, which is particularly relevant in the case of the various innate immune cell types.

In this work, we have studied the transcriptional and epigenetic remodeling associated with tolDC differentiation, and identified a major role for MAFB in this process, in synergy with GR. We have shown that GR binds both the promoter and enhancer regions associated with MAFB, which is quickly upregulated and binds thousands of genomic sites, correlating with widespread DNA demethylation and gene upregulation. We demonstrate how MAFB is crucial for the acquisition of the transcriptomic and epigenomic remodeling that gives rise to the tolerogenic phenotype. This is achieved through a differentiation switch to macrophage-like cells with tolerogenic properties. The major role of

MAFB in activating a tolerogenic expression profile is also demonstrated in monocyte-derived cells from rheumatoid arthritis joints treated with GCs, in which an expansion of cells with a transcriptomic signature similar to MAFB-dependent tolDCs is shown.

Materials and methods

CD14⁺ monocyte purification and culture

Buffy coats were obtained from anonymous donors via the Catalan Blood and Tissue Bank (CBTB). The CBTB follows the principles of the World Medical Association (WMA) Declaration of Helsinki. Before providing blood samples, all donors received detailed oral and written information and signed a consent form at the CBTB.

PBMCs were isolated by density-gradient centrifugation using lymphocyte-isolation solution (Rafer). Pure MOs were then isolated from PBMCs by positive selection with magnetic CD14 MicroBeads (Miltenyi Biotec). Purity was verified by flow cytometry, which yielded more than 90% of CD14⁺ cells.

MOs were resuspended in Roswell Park Memorial Institute (RPMI) Medium 1640 + GlutaMAX™ (Gibco, ThermoFisher) and immediately added to cell culture plates. After 20 minutes, monocytes were attached to the cell culture plates, and the medium was changed with RPMI containing 10% fetal bovine serum (Gibco, ThermoFisher), 100 units/mL penicillin/streptomycin (Gibco, ThermoFisher), 10 ng/mL human GM-CSF (PeproTech) and 10 ng/mL human IL-4 (PeproTech). In the case of tolDCs, 100 nM dexamethasone (Sigma-Aldrich) was also added to the medium.

For cell stimulation, LPS (10 ng/mL) and IFN γ (20 ng/mL) were added to cell culture at day 5, 24h before cell collection.

CD8⁺ proliferation suppression assay

Allogenic CD8⁺ were isolated by negative selection using Dynabeads Untouched Human CD8 T Cells Kit (Invitrogen) and labeled with carboxyfluorescein succinimidyl ester (CFSE) CellTrace™ (Invitrogen), in accordance with the manufacturer's instructions.

Purified CD8⁺ cells were seeded in 96-well plates (200,000 cells per well), and monocyte-derived cells (DCs or tolDCs) were added at different cell ratios (1:2, 1:3, 1:4, and 1:8). To stimulate CD8⁺ cells, 5 μ L/mL of anti-CD3/CD28 Dynabeads (Invitrogen) were added to each well, except for the negative control.

For this experiment, cells were harvested in RPMI containing 10% fetal bovine serum (Gibco, ThermoFisher) and 100 units/mL penicillin/streptomycin (Gibco, ThermoFisher). Cells were cultured for 5 days, and the medium was changed on day 3.

Quantification of cytokine production

Cell culture supernatants were collected after 6 days and diluted appropriately. Enzyme-linked immunosorbent assays (ELISA) were performed, following the manufacturer's instructions: Human IL-10, Human IL-12p70, and Human TNF α from BioLegend, and Human IL-1 β from ThermoFisher.

Flow cytometry

To study cell-surface markers, cells were collected using Versene, a non-enzymatic dissociation buffer (ThermoFisher). Cells were resuspended in the staining buffer (PBS with 4% fetal bovine serum and 2 mM ethylenediaminetetraacetic acid (EDTA)). Cells were then incubated in ice with Fc block reagent (Miltenyi Biotec) for 10 minutes, and stained

Articles

with the viability dye LIVE/DEAD™ Fixable Violet (ThermoFisher), following the manufacturer's protocol.

Cells were stained to study the proteins of interest, using the following antibodies: CD16 (APC) (#130-113-389, Miltenyi Biotec), CD14 (APC) (#130-110-520, Miltenyi Biotec), CD163 (FITC) (#33618, BioLegend), CD1a (PE) (#300106, BioLegend), CD80 (PE)(#H12208P, eBioScience), CD83 (APC) (#130-110-504, Miltenyi Biotec), CD86 (APC) (#130-113-569, Miltenyi Biotec), HLA-DR (PE) (#12-9956-42, eBioScience).

After staining, cells were fixed with PBS + 4% paraformaldehyde (Electron Microscopy Sciences) and analyzed within 2 days using a BD FACSCanto™ II Cell Analyzer (BD Biosciences). Data were analyzed with the FlowJo v10 software.

Genomic DNA and total RNA extraction

Genomic DNA and total RNA were extracted using the Maxwell RSC Cultured Cells DNA kit (Promega) and the Maxwell RSC simplyRNA Cells kit (Promega), respectively, following the manufacturer's instructions.

Gene expression microarrays

RNA samples were processed in the Genomics Platform of the Vall d'Hebron Research Institute (Barcelona). After ensuring the RNA quality using Bioanalyzer, samples were hybridized in Clariom™ S microarrays (ThermoFisher).

Raw microarray data (CEL files) were analyzed using the oligo and limma packages of the Bioconductor project (20). First, raw data were normalized using the Robust Multichip Average algorithm (RMA), which is included as a function in the oligo package. We then performed an

independent filtering step, removing probes with fewer than 3 samples over the 75% percentile of the negative control probes. After collapsing the remaining probes by gene, using the aggregate and mean functions, we built a limma linear model using the condition and donor information, with the formula ‘~0+condition+donor’. The eBayes function in limma was then used in each pairwise comparison to obtain the FDR and logFC of each gene. Genes were considered to be differentially expressed when the FDR was less than 0.05 and the absolute logFC was greater than 0.5.

Bisulfite pyrosequencing

500 ng of genomic DNA was converted using the EZ DNA Methylation Gold kit (Zymo Research). PCR was performed using the bisulfite-converted DNA as input and primers designed for each amplicon (Supplementary Table 5). These primers were designed using the PyroMark Assay Design 2.0 software (Qiagen). PCR amplicons were pyrosequenced using the PyroMark Q48 system and analyzed with PyroMark Q48 Autoprep software.

Real-time quantitative reverse-transcribed polymerase chain reaction (qRT-PCR)

300ng of total RNA were reverse-transcribed to cDNA with Transcriptor First Strand cDNA Synthesis Kit (Roche) following manufacturer’s instructions. qRT-PCR was performed in technical triplicates for each biological replicate, using LightCycler® 480 SYBR Green Mix (Roche), and 7.5ng of cDNA per reaction. The average value from each technical replicate was obtained. Then, the standard double-delta Ct method was used to determine the relative quantities of target genes, and values were normalized against the control genes RPL38 and

Articles

HPRT1. Custom primers were designed to analyze genes of interest (Supplementary Table 5)

DNA methylation profiling

500 ng of genomic DNA was converted using the EZ DNA Methylation Gold kit (Zymo Research). Infinium MethylationEPIC BeadChip (Illumina) arrays were used to analyze DNA methylation, following the manufacturer's instructions. This platform allows around 850,000 methylation sites per sample to be interrogated at single-nucleotide resolution, covering 99% of the reference sequence (RefSeq) genes. Raw files (IDAT files) were provided for the Josep Carreras Research Institute Genomics Platform (Barcelona).

Quality control and analysis of EPIC arrays were performed using ShinyÉPICO (21), a graphical pipeline that uses minfi (22) for normalization, and limma (20) for differentially methylated positions analysis. CpH and SNP loci were removed and the Noob+Quantile normalization method was used. Donor information was used as a covariate, and Trend and Robust options were enabled for the eBayes moderated t-test analysis. CpGs were considered differentially methylated when the absolute differential of methylation was greater than 20% and the FDR was less than 0.05.

Immunofluorescence

Cells were fixed with PBS + 4% paraformaldehyde for 20 min and permeabilized with PBS + Triton X-100 0.5% for 10 min. Coverslips were washed twice with PBS and blocked with PBS + 4% BSA for 1 h. Anti-MAFB antibody HPA005653 (Sigma-Aldrich) was diluted 1:100 in PBS and incubated overnight with the samples in a humidity chamber. Then, cells were incubated with anti-rabbit Alexa Fluor 647 (ThermoFisher) in

blocking solution (PBS + BSA 4% + 0.025% Tween 20) for 1 h. After four washes with PBS, cells were stained with Alexa Fluor™ 488 Phalloidin (ThermoFisher) 1/200 and DAPI 2 µg/mL. Vectashield (Vector Laboratories) was used for the final sample preparation in slides. Images were obtained with a Leica TCS-SL confocal microscope.

Western blotting

Cytoplasmic and nuclear protein fractions were obtained using hypotonic lysis buffer (Buffer A; 10 mM Tris pH 7.9, 1.5 mM MgCl₂, 10 mM KCl supplemented with protease inhibitor cocktail (Complete, Roche) and phosphatase inhibitor cocktail (PhosSTOP, Roche) to lyse the plasma membrane. Cells were visualized under the microscope to ensure correct cell lysis. Nuclear pellets were resuspended in Laemmli IX loading buffer. For whole-cell protein extract, cell pellets were directly resuspended in Laemmli IX loading buffer.

Proteins were separated by SDS-PAGE electrophoresis. Immunoblotting was performed on polyvinylidene difluoride (PVDF) membranes following standard procedures. Membranes were blocked with 5% Difco™ Skim Milk (BD Biosciences) and blotted with primary antibodies. After overnight incubation, membranes were washed three times for 10 min with TBS-T (50 mM Tris, 150 mM NaCl, 0.1% Tween-20) and incubated for 1 h with HRP-conjugated mouse or rabbit secondary antibody solutions (Thermo Fisher) diluted in 5% milk (diluted 1/10000). Finally, proteins were detected by chemiluminescence using WesternBright™ ECL (Advansta). The following antibodies were used: Anti-MAFB (HPA005653, Sigma-Aldrich), Anti-GR (C15200010-50, Diagenode), Anti-GAPDH (2275-PC-100, Trevigen), Anti-Lamin B1 (ab229025, Abcam), Anti-TET2 (C15200179, Diagenode).

Co-immunoprecipitation (Co-IP)

Co-IP assays were performed using tolDCs differentiated from CD14⁺ monocytes for 24 h. Cell extracts were prepared in lysis buffer [50 mM Tris-HCl, pH 7.5, 1 mM EDTA, 150 mM NaCl, 1% Triton-X-100, protease inhibitor cocktail (cOmplete™, Merck)] with corresponding units of Benzonase (Sigma) and incubated at 4°C for 4 h. 100 µL of supernatant was saved as input and diluted with 2× Laemmli sample buffer (5x SDS, 20% glycerol, 1M Tris-HCl (pH 8.1)). Supernatants were first precleared with PureProteome™ Protein A/G agarose suspension (Merck Millipore) for 1 h. The lysate was then incubated overnight at 4°C with respective crosslinked primary antibodies. Cross-linking was performed in 20 mM dimethyl pimelimidate (DMP) (Pierce, ThermoFisher Scientific, MA, USA) dissolved in 0.2 M sodium borate (pH 9.0). Subsequently, the beads were quenched with 0.2M of ethanolamine (pH 8.0) and resuspended at 4°C in PBS until use. Beads were then washed three times with lysis buffer at 4°C. Samples were eluted by acidification using a buffer containing 0.2 M glycine (pH 2.3) and diluted with 2× Laemmli. Samples and inputs were denatured at 95°C in the presence of 1% β-mercaptoethanol. Anti-MAFB HPA005653 (Sigma-Aldrich), Anti-GR CI5200010-50, and Anti-TET2 antibody ab124297 (Abcam) were used for Co-IP.

Transfection of primary human monocytes

We used the #si19279 MAFB Silencer Select siRNA (Agilent, ThermoFisher) to perform knockdown experiments in MOs, using the Silencer Select Negative Control #1 (Agilent, ThermoFisher) as control. CD14⁺ MOs were cultured in 12-well plates (1 million cells/well) and transfected with siRNAs (100 nM) using Lipofectamine 3000 Reagent

(1.5 μ L/well), following the manufacturer's protocol. After 6 h, the medium was changed and DCs/tolDCs were cultured as described in "CD14⁺ monocytes purification and culture". To test transfection efficiency, siGLO Green Transfection Indicator (Horizon) was used, at the same concentration, and checked by flow cytometry 24 h after transfection.

RNA-seq

RNA-seq libraries of transfected DC/tolDCs were generated and sequenced by BGI Genomics (Hong Kong), in 100-bp paired-end, with the DNBseq platform. More than 30 million reads were obtained for each sample. Fastq files were aligned to the hg38 transcriptome using HISAT2(23) with standard options. Reads mapped in proper pair and primary alignments were selected with SAMtools (24). Reads were assigned to genes with featureCounts (25).

Differentially expressed genes were detected with DESeq2 (26). The donor was used as a covariate in the model. The Ashr shrinkage algorithm was applied and only protein-coding genes with an absolute logFC greater than 0.5 and an FDR less than 0.05 were selected as differentially expressed. For representation purposes, Variance Stabilizing Transformation (VST) values and normalized counts provided by DESeq2 were used.

Chromatin immunoprecipitation

After 4 or 24 h of cell culture, DCs and tolDCs, in biological duplicates, were fixed with Pierce™ fresh methanol-free formaldehyde (ThermoFisher) for 15 min and prepared for sonication with the truChIP Chromatin Shearing Kit (Covaris), following the manufacturer's instructions. Chromatin was sonicated for 18 min with the Covaris M220

Articles

in 1mL milliTubes (Covaris). Size distribution of the sonicated chromatin was checked by electrophoresis to ensure appropriate sonication, with a size of around 200 bp.

Magna Beads Protein A+G (Millipore) was blocked with PBS + BSA (5 mg/mL) for 1 h. Chromatin was precleared with 25 μ l of beads for 1.5 h and 10 μ g of chromatin were incubated overnight with each antibody: 10 μ l Anti-MAFB antibody HPA005653 (Sigma-Aldrich) and 5 μ l Anti-GR antibody CI5200010-50 (Diagenode), in a buffer with 1% Triton X-100 and 150 mM NaCl.

Three washes were performed with the Low Salt Wash Buffer (0.1% SDS, 1% Triton X-100, 2 mM EDTA, pH 8.0, 20 mM Tris-HCl pH 8.0, 150 mM NaCl), the High Salt Wash Buffer (0.1% SDS, 1% Triton X-100, 2 mM EDTA, pH 8.0, 20 mM Tris-HCl pH 8, 500 mM NaCl), and the LiCl Wash Buffer (0.25 M LiCl, 1% Nonidet P-40, 1% Deoxycholate, 1 mM EDTA pH 8, 10 mM Tris-HCl), followed by a final wash with TE buffer (pH 8.0, 10 mM Tris-HCl, 1 mM EDTA). Chromatin was eluted for 45 min at 65°C with 100 μ l of elution buffer (10 mM Tris-Cl, 1 mM EDTA, 1% SDS) and decrosslinked by adding 5 μ l 5M NaCl and 5 μ l 1M NaHCO₃ (2 h at 65°C). Next, 1 μ l of 10 mg/mL proteinase K (Invitrogen) was added and the samples were incubated at 37°C for 1 h. For DNA purification, iPure kit v2 (Diagenode) was used, following the manufacturer's instructions.

Chromatin immunoprecipitation sequencing (ChIP-seq) analysis

ChIP-seq inputs and immunoprecipitated DNA from biological duplicate samples were used to generate ChIP-seq libraries in the Centre for Genomic Regulation (Barcelona), using the TruSeq ChIP Library

Preparation Kit (Illumina). Quality control of the libraries was performed using 2100 Bioanalyzer (Agilent). Libraries were sequenced with an Illumina HiSeq 2500, in 50-bp single-end, yielding between 25 and 40 million reads per sample.

Potential adapter contamination was trimmed from the raw reads using Cutadapt (<https://doi.org/10.14806/ej.17.1.200>). Reads were aligned to the GRCh38 human genome assembly using the Burrows-Wheeler Alignment (BWA)-MEM algorithm (27). Aligned reads were filtered by MAPQ, removing alignments with MAPQ < 30, using SAMtools (24). Aligned reads overlapping with the ENCODE blacklist were also removed (28).

Quality control of ChIP-seq data was performed using the SPP package(29). The relative strand cross-correlation coefficient (RSC) was greater than or equal to 2 in all the immunoprecipitated samples.

Bigwig files were generated for visualization, using the bamCoverage function in the Deeptools package (30), with the bins per million mapped reads (BPM) method and ‘--binSize 20 --extendReads 150 --smoothLength 60 --centerReads’ options. Wiggletools was used to aggregate the bigwig duplicates (31).

MACS2 software with ‘--nomodel --extsize 200’ options was used for peak calling (32). Biological duplicates were aggregated using the MSPC algorithm (33) with the options ‘-r Biological -w 1E-6 -s 1E-12’. This approach allows us to obtain more robust peaks, using the information from both biological duplicates. The resulting consensus peaks were used for the downstream analysis and figure panels.

Data analysis and representation

Statistical analyses were performed in R 4.0. Gene expression and DNA methylation heatmaps were created with the heatmap.2 function of the gplots package. The findMotifsGenome.pl function of HOMER (Hypergeometric Optimization of Motif EnRichment) was used to analyze known and *de novo* motif enrichment. For ChIP-seq peaks, the parameter '-size 50' was used, whereas the parameters '-size 200 -cpg)' were used for methylation data. All EPIC array CpG coordinates were also used as background for the methylation data. GREAT software was used to calculate CpG-associated genes and gene ontology (GO) enrichment (34). Gene set enrichment analysis (GSEA) and GO enrichment of gene expression data were performed using the clusterProfiler package (35). ChIP-seq peaks files of histone marks from MO and DCs were downloaded from the BLUEprint webpage (<http://dcc.blueprint-epigenome.eu>). Consensus peaks of the different replicates were obtained with the MSPC algorithm, using the options '-r Biological -w 1E-4 -s 1E-8 -c 3'.

The chromatin state learning model for CD14⁺ monocytes was downloaded from the Roadmap Epigenomics Project webpage, and chromatin state enrichments were calculated using Fisher's exact test.

ChIP-seq overlaps and Venn diagrams were generated with the ChIPpeakAnno package (36). Genomic track plots were created with pyGenomeTracks (37). Methylated CpG set enrichment analysis (mCSEA) (38) was used to calculate CpG-set-specific DNA methylation modifications. Public GR ChIP-seq datasets were extracted from the Remap2020 database (39), excluding samples without glucocorticoid treatment. Peak intersects were calculated using bedtools (40). Public

peak-calls of histone marks were extracted from the Blueprint database(41) and replicates were aggregated using the MSPC algorithm. Public DNase-seq and ATAC-seq bigwigs were aggregated using wiggletools.

Student's paired t test

Statistical analyses involved Student's paired-samples t tests, with which the means of matched pairs of groups were compared, except where indicated otherwise. The levels of significance were: ns, $p > 0.05$; *, $p < 0.05$; **, $p < 0.01$; ***, $p < 0.001$.

Gene expression public data processing

To compare gene expression with public data, expression array matrices were downloaded from the GEO database (GSE40484, GSE117946 and GSE99056). Our expression dataset and public expression data were combined by gene symbol and batch-corrected using ComBat (42). The 1000 most variable genes were used to plot the data in a T-distributed Stochastic Neighbor Embedding (t-SNE) representation, using the Rtsne package (<https://www.jmlr.org/papers/v9/vandermaaten08a.html>).

Synovial tissue extraction and processing

Synovial biopsy and tissue analysis was approved by the Kantonal Ethic Commission Zurich, Switzerland (refs: 2019-00115 and 2016-02014). All patients signed informed consent forms. Patient's characteristics were as follows:

	Gender	Site	Diagnosis	Rheumatoid factor	Synovitis score	Histology	Therapy
28	f	MCP	RA	negative	5	lympho-myeloid	Glucocorticoids oral 10mg/d
50	f	wrist	RA	negative	8	lympho-myeloid	none

Articles

One part of the synovial biopsies was embedded in paraffin and histologically analyzed as previously described (43, 44). For scRNA-seq synovial biopsies were mechanically minced and enzymatically digested with 100 ug/ml Liberase TL (Roche) and 100 ug/ml DNaseI (Roche) in pre-warmed RPMI 1640 containing 2 mM glutamine and 25 mM HEPES Gibco for 30 min at 37°C. The digestion was stopped by adding 20 v/v % fetal calf serum (FCS) and the dissociated tissue was filtered through a 40 um cell strainer. Red blood cells were lysed with RBC lysis buffer (Milteny Biotec). Cell viability was analyzed with a LUNA-FL dual fluorescence cell counter (88% and 90%).

Single-cell RNA-seq processing and analysis

Dissociated cells were processed with the Chromium Single Cell 3' GEM, Library & Gel Bead Kit v3 or v3.1 according to the manufacturer's protocol (10x Genomics). Libraries were sequenced on the NovaSeq 6000 (Illumina). Raw sequencing data was processed with cell ranger (v6.0.0, 10x Genomics) using mkfastq and count with default settings and the provided human reference (GRCh38-2020-A).

	Targeted cell number	Estimated number of cells	Reads/cell
28	10000	4389	44396
50	6000	5760	53176

We used Seurat (4.0.3) to analyze scRNA-seq data. We first read and merge data from patients, and we filtered cells with counts lower than 200 or higher than 30000 and with RNA features lower than 100 or higher than 5000. We also filtered cells with mitochondrial or ribosomal features higher than 25%. We then integrated samples before clustering, using the standard Seurat pipeline. First, features were normalized and variable features were found for each sample, independently. Next, functions FindIntegrationAnchors and IntegrateData were used to integrate the

data. The functions `ScaleData` (using RNA counts and mitochondrial percentage as variables to regress), `RunPCA`, `FindNeighbors`, `FindClusters` and `RunUMAP` were used sequentially to perform the UMAP representation, with 30 dimensions. After selecting only monocyte-derived clusters, scaling and representation was performed again, using the same functions, with resolution 0.15 and 7 dimensions.

Results

Dexamethasone modulates dendritic cell differentiation to a tolerogenic phenotype and drives transcriptome remodeling associated with MAFB

To investigate the mechanisms underlying the glucocorticoid (GC)-mediated phenotypic remodeling of dendritic cells (DCs), as well as the involvement of myeloid-specific TFs, monocytes (MOs) isolated from peripheral blood of healthy donors were differentiated *in vitro* to DCs and tolerogenic DCs (tolDCs) for 6 days using GM-CSF and IL-4 in the absence and presence of a GR ligand (dexamethasone), respectively (Figure 1A). CD8⁺ T cell proliferation assays in co-culture with both DCs and tolDCs revealed the immunosuppressive properties of the latter (Figure 1B). ELISA assays also showed that LPS+IFN γ -stimulated tolDCs produced higher levels of IL-10 and smaller amounts of TNF α , IL-12p70, and IL-1 β than DCs (Figure 1C). Moreover, in the steady-state, higher IL-10 and lower IL-1 β levels of production were observed in tolDCs, whereas TNF α and IL-12p70 were undetectable (Supplementary Figure 1A, see at the end of the article, pages 104-111). tolDCs presented lower levels of expression of the costimulatory molecule CD86 and the maturation marker CD83 (Figure 1D). Moreover, tolDCs presented higher levels of CD14 and of the macrophage markers CD163 and CD16 (Supplementary Figure 1B).

We then profiled the transcriptome of DCs, tolDCs, and MOs. 981 genes were induced and 919 genes were repressed in tolDCs in comparison with DCs (FDR < 0.05, logFC > 0.5) (Figure 1E and Supplementary Table 1). The transcriptomes of both tolDCs and DCs were notably dissimilar to that of MOs (Supplementary Figure 1C).

The Gene Ontology (GO) over-represented categories in tolDC-upregulated genes, including terms such as ‘negative regulation of IL-12 production’, ‘regulation of complement activation’, and ‘regulation of inflammatory response’ (Figure 1F). In tolDC-downregulated genes, terms such as ‘antigen processing and presentation of endogenous antigen’, ‘adaptive immune response’, ‘positive regulation of leukocyte activation’, and ‘response to interferon-gamma’ were over-represented (Supplementary Figure 1D).

tolDCs were enriched in several gene sets, including: ‘mo-MAC signature’ (genes upregulated in mo-MACs in comparison with mo-DCs) (5), genes upregulated in M-CSF macrophages relative to GM-CSF macrophages (45), and genes downregulated in response to GM-CSF and IL-4(46) (Supplementary Figure 1E). On the other hand, tolDCs were depleted in inflammation-related gene sets such as Interferon-alpha response, TNF α Signaling via NF- κ B genes upregulated in mo-DCs relative to mo-MACs)(5), genes downregulated in M-CSF macrophages in comparison with GM-CSF macrophages, (45) and genes upregulated in response to GM-CSF and IL-4 cytokines (46) (Supplementary Figure 1F). We also confirmed the upregulation of canonical GR targets, such as PDK4, TSC22D3, ZBTB16, and FKBP5 in tolDCs, as expected (Supplementary Figure 1G).

To predict potential additional TFs involved in tolDC transcriptome acquisition, we performed a Discriminant Regulon Expression Analysis (DoRothEA) (47). DoRothEA uses a dataset of TF regulons, a collection of TF - target genes interactions obtained from different types of evidence such as literature curated resources and ChIP-seq peaks and it calculates enrichment of these regulons in the condition of interest. This analysis

Articles

revealed that eight distinct TF regulons were enriched in tolDCs, although only two of these were associated with concomitant upregulation of their coding genes: *MAFB* and *MYC* (Figure 1G). *MYC* has been previously identified as a transcriptional regulator in tolDCs (48). To assess the possible role of *MAFB* in tolDC gene expression remodeling, we obtained a public dataset of genes downregulated after the treatment with an siRNA that targets *MAFB* (9) in M2 macrophages. These genes, positively regulated by *MAFB*, were more strongly expressed in tolDCs than in DCs, as can be observed in the GSEA (Supplementary Figure 1H). In addition, tolDCs presented a transcriptome similar to those of *in vitro* M2 macrophages and *in vivo* mo-MACs (Figure 1H). *MAFB* has previously been identified as a key mediator in the differentiation of both cell types (5, 9).

Dexamethasone mediates the acquisition of a specific DNA methylation pattern which inversely correlates with gene expression during tolDC differentiation

In parallel, we obtained genome-wide DNA methylation profiles of MOs, DCs, and tolDCs after 6 days of differentiation. Principal component analysis (PCA) of all differentially methylated CpGs between groups showed non-overlapping clustering of MOs, DCs, and tolDCs alongside principal component 1 (Supplementary Figure 2A). Demethylation occurring during MO-to-DC differentiation was broadly inhibited in tolDCs (Supplementary Figure 2B). The comparison of DCs and tolDCs ($FDR < 0.05$ and absolute $\Delta\beta > 0.2$) in relation to MOs revealed two clusters of CpG sites: a group of CpGs that underwent specific demethylation in DCs and that was blocked in tolDCs (C1, 1353 CpGs), and a second group that was specifically demethylated in tolDCs (C2, 411 CpGs) (Figure 2A and Supplementary Table 2).

Figure 1

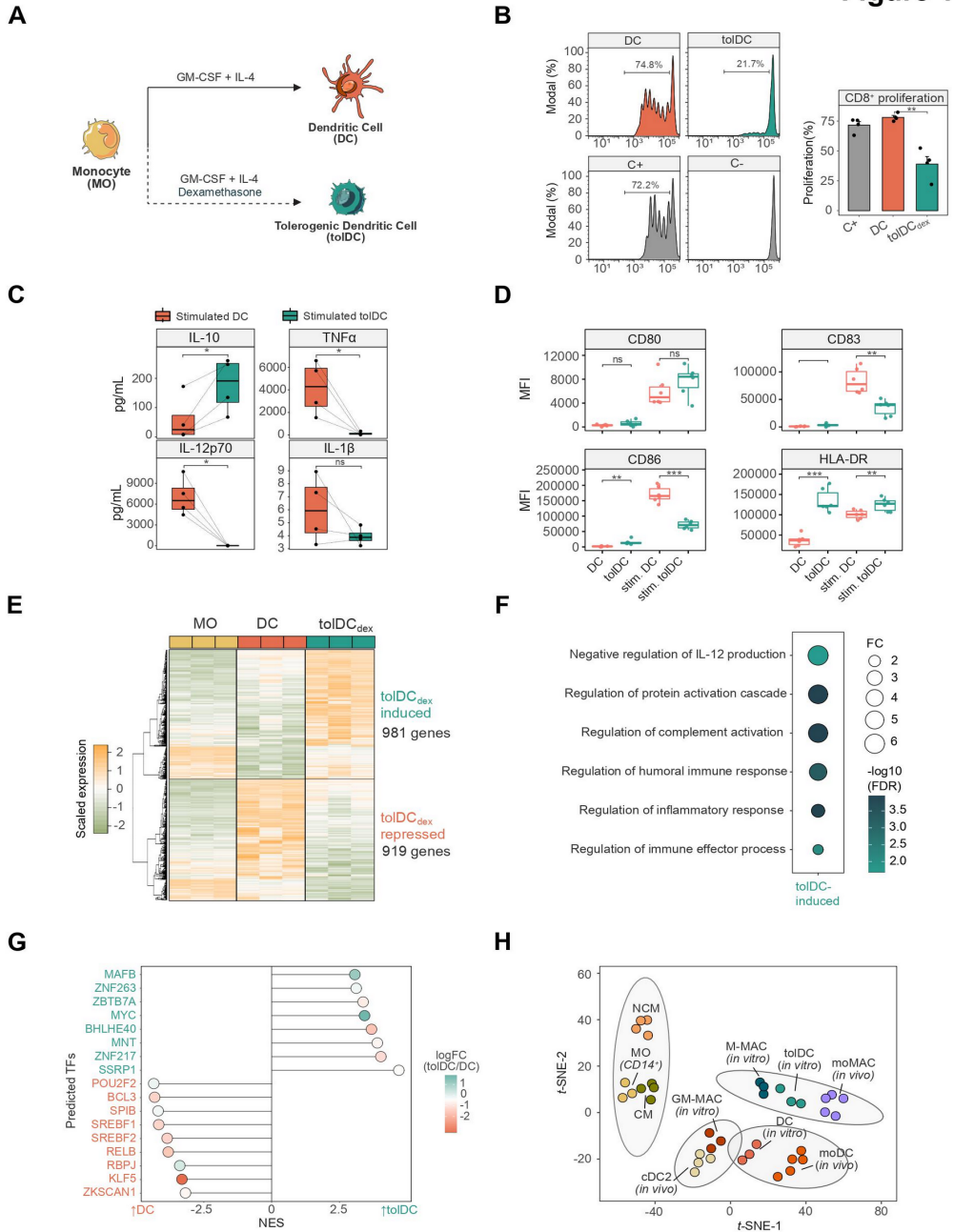


Figure 1. Phenotypic profiling of dexamethasone-mediated tolerogenic dendritic cells. (A) Schematic representation of the experimental approach, comparing dendritic cell (DC) with tolerogenic dendritic cell (tolDC) differentiation. (B) DC and tolDC were cocultured with CD8⁺ cells for 5 days. The final CFSE signal of CD8⁺ cells is shown (left panel). CD8⁺ with only CD3/CD28 T-activator beads (C⁺) or alone (C⁻) are also shown. In the right panel, the average proliferation is shown (mean \pm standard error of the mean (SEM)) (n=4). (C) IL-10, TNF α , IL-12p70 and IL1- β production of DC and tolDC, after 5 days of differentiation and 24 h of LPS (10 ng/ μ L) and IFN γ (20 ng/ μ L) stimuli. P-values of paired t-tests are shown (n=4) (ns p > 0.05, * p < 0.05). (D) Box-plots of CD80, CD83, CD86 and HLA-DR surface expression (Median Fluorescence Intensity) in DCs and tolDCs in steady-state or stimulated with LPS (10 ng/ μ L) and IFN γ (20 ng/ μ L) (n=6) (ns p > 0.05, ** p < 0.01, *** p \leq 0.001). (E) Gene expression heatmap of differentially expressed genes comparing tolDCs with DCs and also displaying the gene expression values of the precursor cell type (MO) (logFC > 0.5, FDR < 0.05). Scaled fluorescence values of expression arrays are shown, ranging from -2 (lower gene expression, green) to +2 (higher gene expression, orange) (n=3). (F) Gene ontology (GO) over-representation of GO Biological Process categories. Fold change of tolDC induced genes over background and -log₁₀(FDR) of Fisher's exact tests are shown. (G) Discriminant regulon expression analysis (DoRothEA) of tolDC compared with DC. Only transcription factors with FDR < 0.05 are shown. NES and logFC of transcription factor expression are depicted. (H) T-distributed stochastic neighbor embedding (t-SNE) plot of the aggregated and batch-corrected gene expression data from our study (MO, DC and tolDC) and two additional public datasets (GSE40484 (moMAC, moDC, cDC2, CM (Classical MOs) and NCM (Non-Classical MOs) and GSE99056 (M-MAC (M2 Macrophages) and GM-MAC (M1 Macrophages))). The 4 different groups obtained using k-means clustering are represented with grey ellipses of multivariate t-distributions.

Both CpG clusters were enriched in introns and depleted in promoters (Figure 2B). CpGs were generally located far from CpG islands (Open Sea) (Figure 2C). The two clusters were also enriched in enhancers and regions close to active transcription start sites (TSSs) (Supplementary Figure 2C). Looking at the enrichment in active enhancer histone marks (H3K4me1 and H3K27ac) in DCs and MOs, an increase in the signal of these marks was noted in MO-to-DC differentiation, especially in the C1, which became specifically demethylated in DCs (Figure 2D).

Employing the average signal of public MO DNase-seq (Blueprint database)(41) and DC ATAC-seq triplicates (49), we found that C1 and C2 CpGs had low accessibility in MOs. We also observed that C1 had greater accessibility than C2 in DCs, demonstrating an inverse correlation between chromatin accessibility and DNA demethylation (Figure 2E).

To detect potential TFs involved in the DNA methylation dynamics, we performed a TF motif enrichment analysis. As expected, C2 CpGs were enriched in Glucocorticoid Response Elements (GREs) and very closely related motifs (Androgen Receptor Elements, AREs, and Progesterone Receptor Elements, PGR). The Maf recognition element (MARE) was also enriched, including several TFs from the MAF family: MAFA, MAFB, MAFK and MAFK (Figure 2F). On the other hand, C1 CpGs were enriched in, among other binding motifs, AP-1 family, PU.1, IRF8, STAT6, and Egr1/Egr2 motifs (Supplementary Figure 2D), which are known to be associated with DC differentiation (6, 7, 50, 51).

Gene ontology (GO) analysis of C2 CpGs revealed enrichment of functional categories associated with immune system regulation, including ‘negative regulation of cytokine production involved in inflammatory response’ and ‘regulation of inflammatory response’ (Figure 2G). In

Articles

contrast, GO analysis of C1 CpGs included categories related to inflammatory processes, such as ‘positive regulation of MAPK cascade’, ‘myeloid leukocyte activation’, and ‘inflammatory response’ (Supplementary Figure 2E). Moreover, C2 CpGs are demethylated in M2 macrophages (M-CSF), whereas C1 CpGs are demethylated in M1 macrophages (GM-CSF) (Supplementary Figure 2F).

We next associated each CpG with its nearest gene and tested whether C1 and C2 associated genes were enriched in tolDC-induced or tolDC-repressed genes. We found a strong enrichment of the induced genes over the C2 associated genes (FDR = $8.88e-41$) and of the repressed genes over the C1 associated genes (FDR = $4.72e-26$) (Figure 2H). In this regard, there was a significant inverse correlation between DNA methylation and gene expression (Figure 2I), which is exemplified in some CpGs associated with genes linked to the biology of tolDCs and DCs (Figure 2J, Supplementary Figure 2G).

In relation to the potential association between MAFB and our DNA methylation and expression data, we assessed the potential upregulation of MAFB-positively regulated genes of M2 macrophages and C2-associated genes in other tolDC types. In addition to tolDCs, we found that both gene sets were upregulated in DC10 (DCs differentiated *in vitro* from MOs with GM-CSF/IL-4 and IL10), but not in rapamycin-treated or vitamin D3-treated tolDCs (Supplementary Figure 2H).

Figure 2

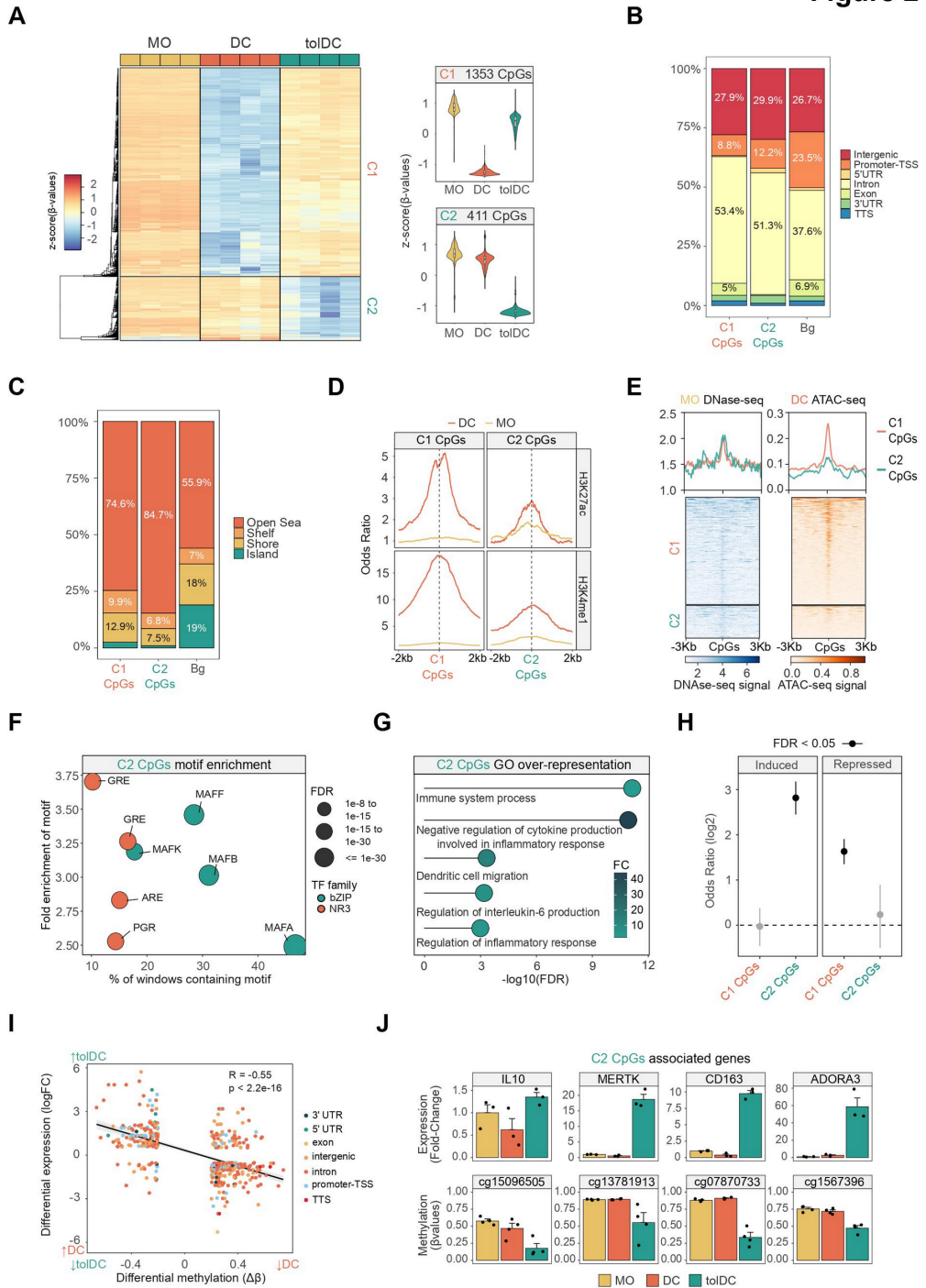


Figure 2. DNA methylation remodeling of dexamethasone-mediated tolerogenic dendritic cells. (A) DNA methylation heatmap of differentially methylated CpGs comparing DCs with tolDCs ($\Delta\beta \geq 0.2$, FDR < 0.05) and showing the DNA methylation values of the precursor cell type (MO). Scaled β -values are shown (lower and higher DNA methylation levels in blue and red, respectively) (n=4). On the right side, violin plots of Cluster 1 (C1) and Cluster 2 (C2) depict scaled DNA methylation data. (B) Bar-plot of genomic features, percentages of C1 and C2 CpGs in comparison with background CpGs (Bg). (C) Bar-plot of CpG island contexts, percentages of C1 and C2 CpGs in comparison with background CpGs. (D) Accessibility (ATAC-seq) data of C1 CpGs (red) and C2 CpGs (blue) in MOs and DCs. The average DNase-seq from an MO duplicate (BLUEprint) and ATAC-seq triplicate from DCs (GSE100374) were used in the representation. (E) ChIP-seq data of H3K27ac and H3K4me1 of CD14+ monocytes and DCs were downloaded from the BLUEPRINT database. Odds ratios of histone marks enrichment were calculated for bins of 10bp, 2000bp upstream and downstream in relation to C1 and C2 CpGs. CpGs annotated in the EPIC array were used as background. (F) Bubble scatter-plot of TF-binding motif enrichment for C2 CpGs. The x-axis shows the percentage of windows containing the motif and the y-axis shows the factor of enrichment of the motif over the EPIC background. Bubbles are colored according to the TF family. FDR is indicated by bubble size. (G) GO (Gene Ontology) over-represented categories in C2 CpGs. Fold change in comparison with background (EPIC array CpGs) and $-\log_{10}(\text{FDR})$ are shown. (H) C1 and C2 CpGs were associated with the nearest gene and the enrichment of both gene sets (C1 CpGs- and C2 CpGs- associated genes) over the tolDC-induced and tolDC-repressed genes were calculated using Fisher's exact tests. Odds ratios \pm 95% confidence intervals are shown. (I) DNA methylation of differentially methylated CpGs were correlated with gene expression of differentially expressed genes in the tolDC *vs.* DC comparison. LogFC of expression is represented in the y-axis, where a higher number represents a higher level of expression in tolDC and a lower number a higher level of expression in DC. DNA methylation is depicted on the x-axis as $\Delta\beta$, where a lower number represents a lower level of methylation in tolDC, and a higher number a lower level of methylation in DC. Points are colored according to their genomic context. A significant negative correlation between methylation and expression is observed ($R = -0.55$, $p < 2.2e-16$). (J) The fold-changes of DC and tolDC expression (with respect to MO) of some examples of C2 CpGs associated genes are shown, calculated from fluorescence values of expression arrays. Below each gene, the methylation (β -values) of an example of associated CpG is indicated. Three and four biological replicates are provided, respectively (n=3-4).

Dynamics of GR and MAFB genomic binding in tolDC differentiation

Since MAFB was predicted to be a TF of importance in the dexamethasone-specific gene expression (Figure 1H) and DNA methylation (Figure 2F) remodeling occurring in tolDCs, we investigated its role in the tolDC differentiation process and its interplay with GR.

MAFB expression was studied over time, where differences between DCs and tolDCs could be observed from 1 h of differentiation (Supplementary Figure 3A). MAFB protein levels could be detected by western blot in tolDC nuclei, at 12 and 24h, concomitant with GR translocation to the nucleus (Figure 3A). Moreover, by immunofluorescence at 24h of differentiation, MAFB was found to be localized in tolDC nuclei, whereas in DCs the level of expression was much lower (Figure 3B).

We next generated ChIP-seq data of GR and MAFB in DCs and tolDCs, at both 4h and 24h of differentiation, using biological duplicates that we consolidated to obtain the consensus peaks of each condition (see Methods). *De novo* motif discovery around GR and MAFB peaks in tolDC yielded very similar motifs to those of their respective canonical binding sites. (Supplementary Figure 3B). GR peak calling in tolDC resulted in hundreds of peaks with a strong signal (Figure 3C, Supplementary Figure 3C). By contrast, GR peak calling in DCs yielded a negligible number of significant peaks, at both 4h and 24h, with weaker signals (Figure 3C, Supplementary Figure 3C).

On the other hand, MAFB presented binding in thousands of sites in both DCs and tolDCs at 4h, with stronger signal and peak number in tolDCs (Figure 3C, Supplementary Figure 3C). Moreover, MAFB DC

Articles

peaks at 4h were highly enriched in the MAFB canonical binding site (Supplementary Figure 3D). This is consistent with the preexisting expression of MAFB in MOs, which is downregulated during the MO to DC differentiation (5). In this regard, the MAFB peak number and signal in DCs at 24h is minimal in comparison with tolDCs, concordantly to a very low MAFB expression, and no motif compatible with the canonical one was found (Figure 3C, Supplementary Figure 3C, Supplementary Figure 3D).

To distinguish potential specific features of early and late peaks of GR and MAFB, we classified the tolDC peaks as ‘4h-specific’ (present at 4h but not at 24h), ‘24h-specific’ (present at 24h but not at 4h), or ‘continuous’ (present at both times) (Figure 3D and Supplementary Table 3). In both TFs, the subset with the strongest binding was the ‘continuous’ peaks. The binding typically occurred within open chromatin in MOs, even though some GR and MAFB peaks occurred in low-accessibility regions (Supplementary Figure 3E).

Whereas GR ‘4h-specific’ and ‘continuous’ peaks were located mainly in intergenic and intronic regions and were enriched in MO enhancers and active transcription start sites (TSS), ‘24h-specific’ peaks were most frequently found in promoters, and were more enriched in active TSS but not enriched in enhancers (Figure 3E, Supplementary Figure 3D). On the other hand, no notable differences were described in the location of MAFB ‘4h-specific’, ‘24h-specific’, and ‘continuous’ peaks, all of them being found mostly in intergenic and intronic regions, where they were enriched in monocyte active TSS and enhancers (Figure 3E, Supplementary Figure 3D).

Overall, there were many more MAFB than GR peaks, at 4h and 24h. Remarkably, GR binding, which was ubiquitously expressed in most cell types, significantly overlapped with the peaks observed in a panel of 53 GR ChIP-seqs (Supplementary Figure 3G), suggesting a common role of GR across these cell types.

We also inspected overlapping GR and MAFB peaks, which involved around half of all the GR peaks (Figure 3F). These $GR \cap MAFB$ peaks can be classified into four groups, depending on their temporal association between TFs: ‘GR first’, where GR peaks at 4h, and MAFB peaks at 24h, but not at 4h; ‘MAFB first’, where MAFB peaks at 4h, and GR peaks at 24h, but not at 4h; ‘constant’, where GR and MAFB peaks at both 4 and 24h; and ‘transient’, overlapping peaks not included in any of the former groups (Figure 3G). In general, ‘GR first’, ‘constant’ and ‘transient’ peaks were enriched in GREs. In contrast, ‘MAFB first’ peaks, in which MAFB is bound before GR, are enriched in ETS family motifs, including PU.1, and AP-1 motifs, but not MAREs. (Supplementary Figure 3H). All groups were enriched in MO enhancers and TSSs, except for ‘MAFB first’ peaks, which were not enriched in enhancers (Supplementary Figure 3I).

To address the mechanism of the GC-induced upregulation of MAFB, we checked the binding of GR around the MAFB promoter. At both 4h and 24h, GR was bound in an enhancer in MOs whose closest gene was MAFB. At 24h, GR was also bound to the MAFB gene promoter. (Figure 3G). This rapid binding, together with the rapid MAFB RNA and protein upregulation (Figure 3A, Supplementary Figure 3A), suggests a direct, GR-mediated, mechanism of MAFB regulation.

Figure 3

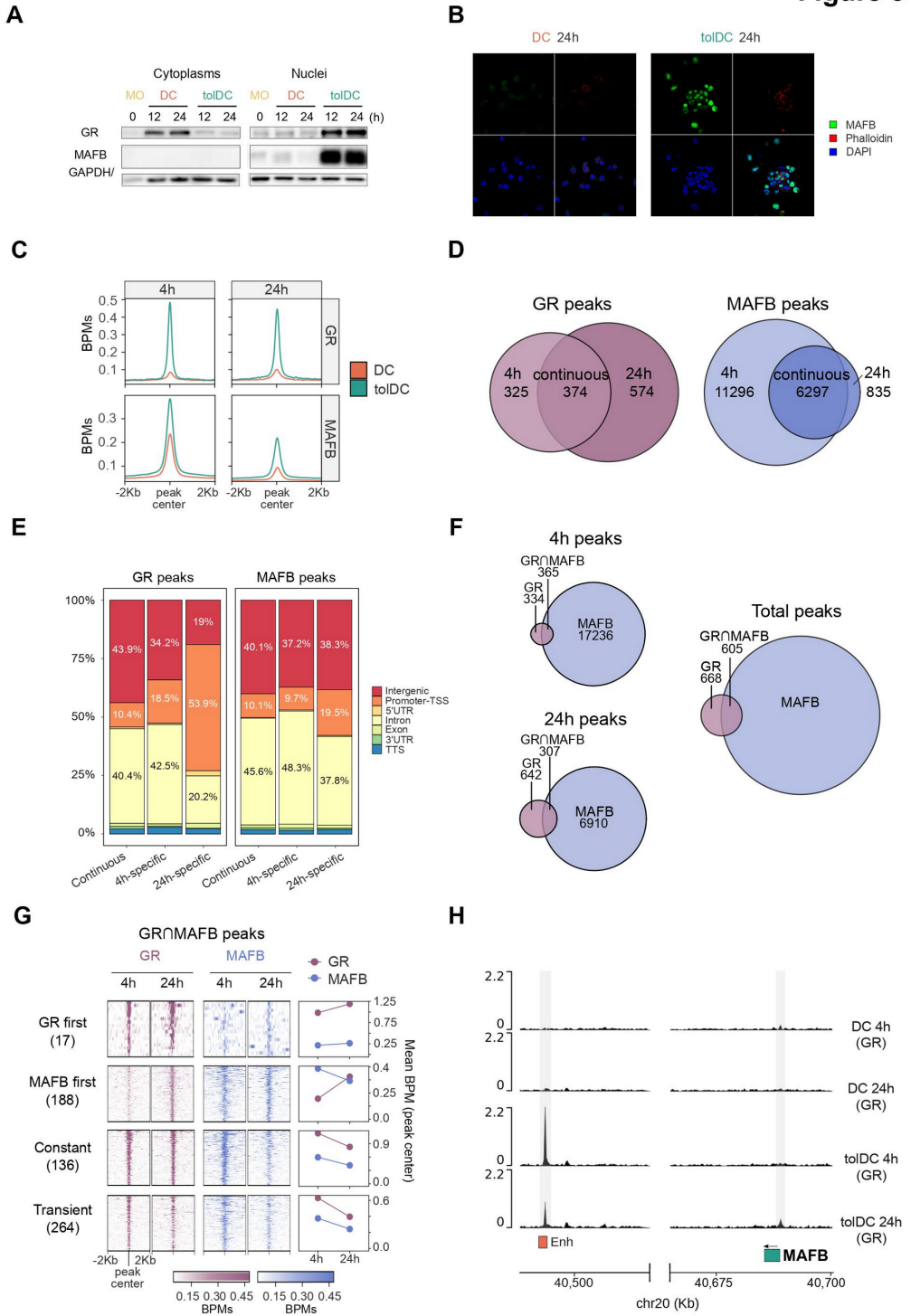


Figure 3. Delineation of GR and MAFB binding during DC and tolDC differentiation. (A) Western blot of glucocorticoid receptor (GR) and MAFB proteins in cytoplasm and nuclei of DC and tolDC. GAPDH and LaminB proteins were used as loading controls for cytoplasm and nuclei, respectively. (B) Immunofluorescence of MAFB in DC and tolDC after 24 h of differentiation. Fluorescent signal of MAFB (green), actin filaments (Phalloidin, red), nuclei (DAPI, blue) and a composite image with the sum of the three fluorescences are shown. (C) Average signal in bins per million mapped reads (BPMs) of GR and MAFB binding in DCs and tolDCs at 4 and 24 h of differentiation, after peak consolidation between two biological replicates of each condition. (D) Venn diagrams showing GR and MAFB peaks at 4h, 24h and at both times (continuous). (E) Bar-plot of genomic features percentages of ‘4 h-specific’, ‘24 h-specific’, and ‘continuous’ peaks of GR and MAFB. (F) Venn diagrams showing GR and MAFB peaks at 4 and 24 h, and the concatenation of the two (total peaks). (G) Heatmap of total peaks with GR/MAFB overlap ($GR \cap MAFB$). Peaks were classified in ‘GR first’ (GR bound at 4 h and MAFB at 24 h), ‘MAFB first’ (MAFB bound at 4 h and GR at 24 h), ‘Constant’ (GR and MAFB peaks at 4 and 24 h), and ‘Transient’ (overlapping peaks not included in any of the former groups). (H) Representation of the GR ChIP-seq signal (BPMs) close to the MAFB gene. 15-states ChromHMM of MOs in peaks are depicted in orange. Significant peaks are shown against a grey background.

GR and MAFB binding are correlated with gene upregulation and DNA demethylation in tolDCs

We measured the association between each ChIP-seq peak and its nearest gene in order to examine the link between TF binding and gene expression remodeling. Overall, both MAFB and GR ‘4h-specific’, ‘24h-specific’, and ‘continuous’ associated genes were more strongly expressed in tolDC than in DCs, indicating that both TFs may be involved in upregulating tolDC -specific genes (Figure 4A, Figure 4B). It is notable that, in both TFs, the most frequently associated subset was the ‘continuous’ associated genes.

Articles

To determine the relationship between TF binding and DNA methylation, we first profiled the initial methylation state of CpGs surrounding GR and MAFB peaks, using public whole-genome bisulfite sequencing data of CD14⁺ MOs (41). Both TFs bound methylated regions, even though they were located mainly in non-methylated regions (Supplementary Figure 4A). However, GR 24h-specific peaks were found almost exclusively in non-methylated regions, concordantly with its enrichment in MO active TSS (Supplementary Figure 3F).

We then performed co-immunoprecipitation of TET2, a key mediator of active demethylation in myeloid cells, revealing its interaction with both GR and MAFB (Figure 4C) in tolDCs. In this regard, GR ChIP-seq signal in tolDCs at both 4h and 24h was found around some CpGs specifically demethylated in tolDCs (C2 CpGs), with a strong signal around a small subset of total C2 CpGs (Figure 4D). Moreover, MAFB signal in tolDCs at both 4h and 24h was found more generally around C2 CpGs. Interestingly, MAFB signal was also present in DC at 4h, at a lower level than that of tolDCs, but was not present at 24h (Figure 4E).

C1 CpGs were associated with EGR2, among other TFs (Supplementary Figure 2D), which prompted us to use a public dataset of EGR2-FLAG ChIP-seq of DCs (7), which revealed a strong signal in C1 CpGs but not in C2 CpGs (Supplementary Figure 4B). Strikingly, the EGR2 gene was downregulated in tolDCs (Supplementary Figure 2G), which may partially explain the blockage of C1 CpG demethylation. In addition, the genes closest to the EGR2 peaks were more strongly expressed in DCs, and downregulated in tolDCs, suggesting an association between a potential loss-of-function of EGR2 in tolDCs and the specific downregulation of genes (Supplementary Figure 4C).

We also studied the temporal relation between DNA methylation and gene expression changes. We selected CpGs with GR and/or MAFB binding associated with tolDC-induced or tolDC-repressed genes (Figure 4F, Figure 4G, Supplementary Figure 4D, Supplementary Figure 4E, Supplementary Figure 4F). In some loci, DNA demethylation was concomitant with or preceded gene upregulation (Figure 4H). However, there were also examples where gene upregulation clearly anticipated DNA demethylation (Supplementary Figure 4G).

MAFB downregulation reverts dexamethasone-induced expression and DNA methylation remodeling, damping the tolerogenic phenotype of tolDCs

Given the association between MAFB binding, gene upregulation and DNA demethylation in tolDCs, we performed MAFB knockdown, using small-interfering RNAs (siRNAs) targeted against MAFB (siMAFB) or non-targeting (siCTL). Under our conditions, we achieved around 75% transfection efficiency (Supplementary Figure 5A), more than 50% RNA reduction (Supplementary Figure 5B) and a drastic decrease in MAFB protein (Supplementary Figure 5C).

Gene expression profiling of tolDCs transfected with siMAFB or siCTL was performed by RNA-seq, obtaining 222 downregulated genes and 259 upregulated genes (FDR < 0.05, logFC > 0.5) (Figure 5A and Supplementary Table 4). Among the downregulated genes, relevant tolDC-induced genes were found, including *RNASE1*, *CCL18*, *LGGMN*, *MERTK*, *IL10*, *IFIT3* and *SLCO2B1*. Moreover, the upregulated genes included tolDC-repressed genes such as *GPT*, *CDIC*, *TNF*, *EGR2*, *CSF2RB*, *CD1B* and *FLT3*.

Figure 4

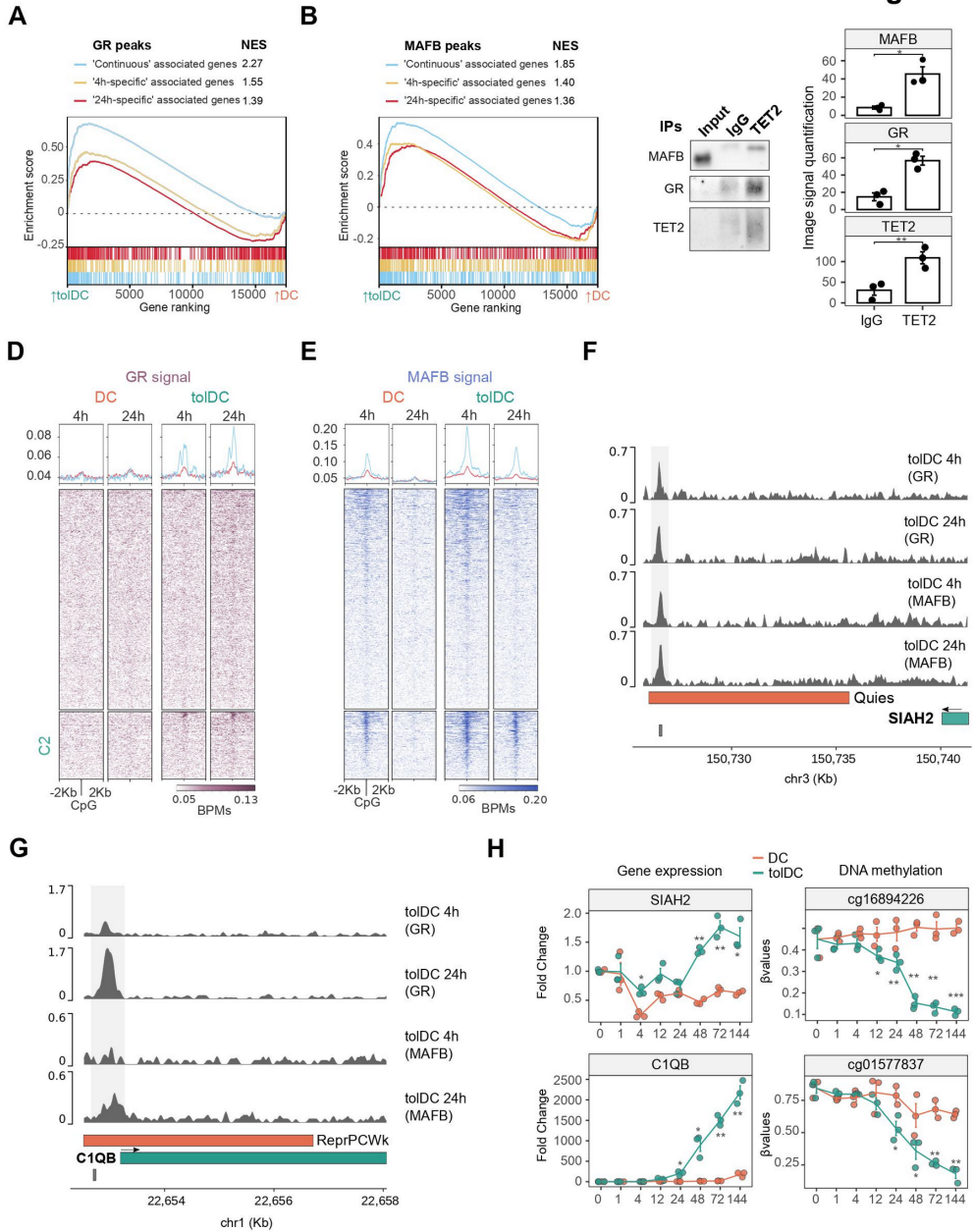


Figure 4. Integration of GR and MAFB binding with DNA methylation and gene expression changes in tolDCs. (A) Gene set enrichment analysis (GSEA) of tolDC vs. DC, with the genes closest to GR ‘continuous’, ‘4h-specific’ and ‘24h-specific’ peaks. The running enrichment score is presented with the normalized enrichment score (NES) is shown above (FDR < 0.01). (B) Gene set enrichment analysis (GSEA) of tolDC vs. DC, with the genes closest to the top500 MAFB ‘continuous’, ‘4h-specific’ and ‘24h-specific’ peaks (500 peaks with the highest joint p-value). The running enrichment score is represented in the y-axis and the normalized enrichment score (NES) is shown above (FDR < 0.01). (C) Western blot of the co-immunoprecipitation of TET2, showing the signal of MAFB, GR and TET2 proteins. On the right, the image signal quantifications of 3 independent western blots are shown for each protein. P-values of paired t-tests are shown (n=3) (* p < 0.05 ** p < 0.01) (D-E) Heatmaps of the GR and MAFB ChIP-seq signal (BPMs) around C1- and C2-CpGs in DCs and tolDCs at 4 h and 24 h of differentiation. (F-G) Representation of the GR and MAFB ChIP-seq signal (BPMs) close to the SIAH2 and CIQB genes. 15-state ChromHMM of MOs in peaks are depicted in orange. Significant peaks are shown against a grey background. (H) SIAH2 and CIQB time-course gene expression obtained from qRT-PCR (relative arbitrary units) (n=3) and DNA methylation (β -values) of associated differentially methylated CpGs obtained from pyrosequencing (n=3). P-values of paired t-tests are shown (n=3) (* p < 0.05 ** p ≤ 0.01, *** p ≤ 0.001).

GO Biological Process over-represented categories in siMAFB-downregulated genes included terms such as ‘monocyte chemotaxis’, ‘regulation of tolerance induction’ and ‘negative regulation of interferon-gamma production’ (Supplementary Figure 5D). Furthermore, among siMAFB-upregulated genes, terms such as antigen processing and presentation via MHC class Ib, positive regulation of leukocyte-mediated immunity and leukocyte differentiation were over-represented (Supplementary Figure 5E).

In this regard, tolDC-induced genes were, in general, significantly downregulated with the MAFB siRNA, whereas tolDC-repressed genes

Articles

were upregulated (Figure 5B). Moreover, genes associated with MAFB ‘continuous’ and ‘4h-specific’ ChIP-seq peaks were linked to siMAFB downregulation, whereas those GR peaks were not related to downregulation or upregulation (Supplementary Figure 5F).

We then tested the effect of MAFB downregulation on the differentially methylated CpGs. CpGs specifically demethylated in tolDCs (C2 CpGs) were more methylated in tolDC when MAFB was downregulated, confirming the role of MAFB in the tolDC demethylation process (Figure 5C). In contrast, no differences were observed in C1 CpGs, corresponding to the absence of MAREs in the cluster (Supplementary Figure 2B) and the weaker signal of MAFB in the ChIP-seq (Figure 4D). Based on their overlap with MAFB and GR ChIP-seq peaks, C2 CpGs were then divided into three groups: MAFB-specific, GR/MAFB, and GR-specific CpGs. In siMAFB-treated tolDCs, MAFB-specific and GR/MAFB CpGs were more methylated, whereas GR-specific CpGs were not affected by MAFB inhibition (Figure 5D). This suggests that both MAFB and GR can direct demethylation to C2 CpGs, consistent with their interaction with TET2.

Surface markers CD14, CD16, and CD163 were significantly reduced in tolDCs with the MAFB inhibition (Figure 5E), providing evidence of the functional role of MAFB in the tolerogenic phenotype.

Moreover, the inhibition of MAFB also reduced IL-10 production at steady-state and after stimulation of the cells with LPS. TNF α production in stimulated cells was significantly higher in siMAFB-treated tolDCs, showing that MAFB inhibition not only reduced the tolerogenic features of tolDCs but also boosted an increase in some proinflammatory traits, concordantly with RNA-seq data (Figure 5F).

Figure 5

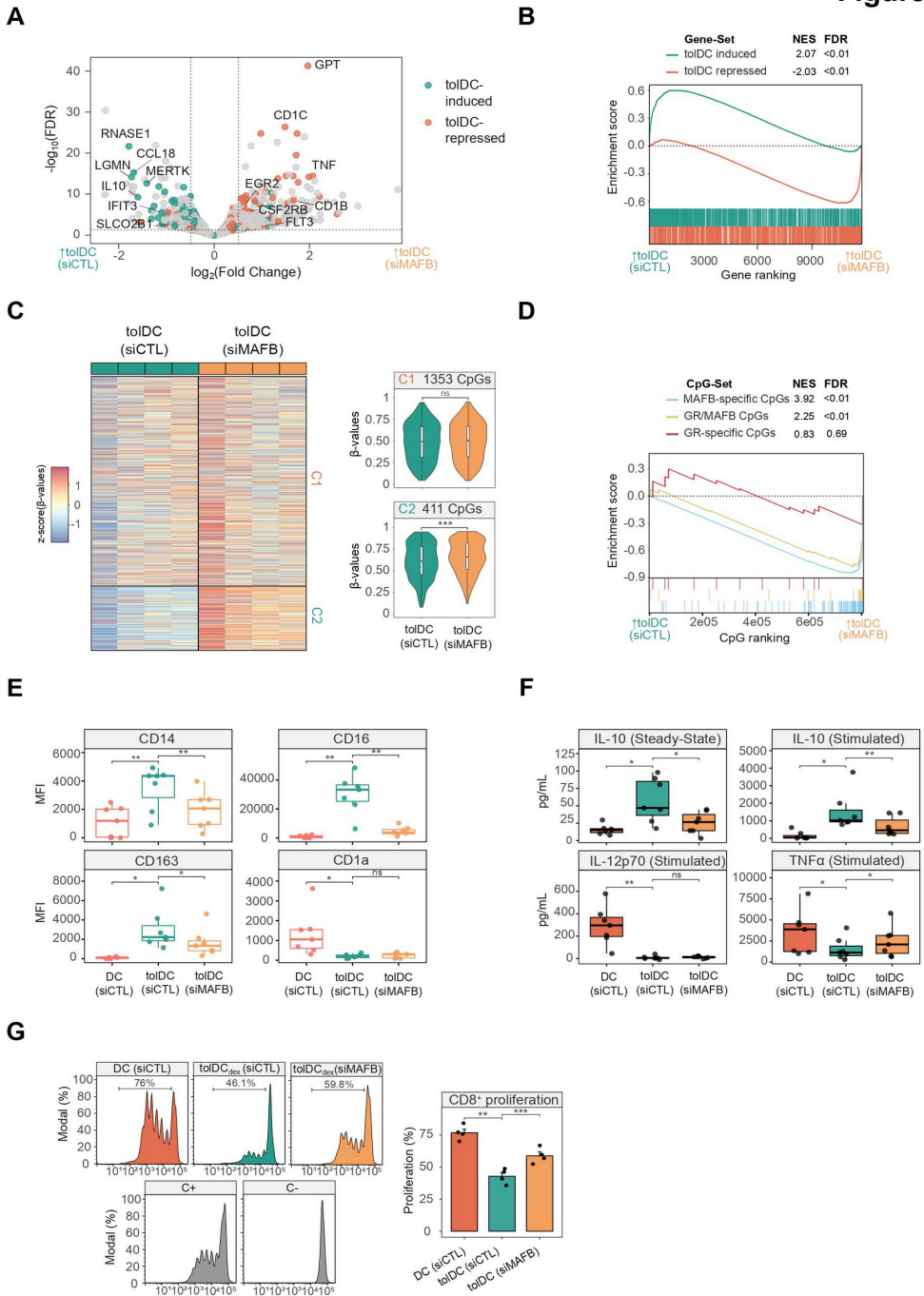


Figure 5. Effects of MAFB knockdown during tolDC differentiation. (A) Volcano plot comparing tolDCs treated with control siRNA (siCTL) and MAFB siRNA (siMAFB). Dashed lines indicate significance thresholds (FDR < 0.05, absolute logFC > 0.5) (n=4). tolDC-induced and tolDC-repressed genes are shown in blue and orange, respectively. (B) Gene set enrichment analysis (GSEA) of tolDCs (siCTL) *vs.* tolDCs (siMAFB), using tolDC-induced and tolDC-repressed gene sets. The running enrichment score is represented and the normalized enrichment score (NES) is shown above (FDR < 0.01). (C) DNA methylation heatmap of previously obtained differentially methylated CpGs (C1-CpGs and C2-CpGs) in tolDCs (siCTL) and tolDCs (siMAFB). Scaled β -values are shown (lower DNA methylation levels in blue and higher methylation levels in red). On the right side, violin plots of Cluster 1 (C1) and Cluster 2 (C2) depict β -values (n=4) (ns $p > 0.05$, *** $p \leq 0.001$). (D) Methylated CpG set enrichment analysis (mCSEA) of tolDCs (siCTL) *vs.* tolDCs (siMAFB), using MAFB-only CpGs, GR/MAFB CpGs and GR-only CpGs as CpG-sets (depending on the overlap of CpGs with GR or MAFB peaks). The running enrichment score is represented and the normalized enrichment score (NES) and FDR are shown above. (E) Box-plots of median fluorescence intensity (MFI) of CD14, CD16, CD163 and CD1a flow cytometry data from DCs (siCTL), tolDCs (siCTL) and tolDCs (siMAFB) (n = 7) (ns $p > 0.05$, * $p < 0.05$, ** $p \leq 0.01$). (F) Box-plots of supernatant concentration from DCs (siCTL), tolDCs (siCTL) and tolDCs (siMAFB) (n = 7) of IL-10 in steady-state and stimulated conditions (LPS 10 ng/ μ L and IFN γ 20 ng/ μ L) and IL-12p70 and TNF α under stimulated conditions (pg/mL). TNF α and IL-12p70 in steady state were not detected. (ns $p > 0.05$, * $p < 0.05$, ** $p \leq 0.01$) (G) DC (siCTL), tolDC (siCTL) and tolDC (siMAFB) were cocultured with CD8⁺ cells for 5 days (n = 4). The final CFSE signal of CD8⁺ cells is shown (left panel). CD8⁺ with only CD3/CD28 T-activator beads (C⁺) or alone (C⁻) are also shown. On the right panel, the average proliferation of the quadruplicate is shown (mean \pm standard error of the mean (SEM)) (** $p \leq 0.01$, *** $p \leq 0.001$).

Consequently, the suppression of CD8⁺ T cell proliferation, a main feature of tolDC, was reduced with the MAFB inhibition (Figure 5G). Overall, these data indicate that MAFB is a key player in the acquisition of tolDC tolerogenesis, and in the transcriptomic and epigenomic events driving that phenotype.

Glucocorticoids skew an MAFB-associated, monocyte-derived cell differentiation program in rheumatoid arthritis joints

In vitro tolDCs and DCs derived from MOs resembled *in vivo* cell types, moMACs and moDCs, respectively (Figure 1H). We therefore performed single-cell RNA-seq from unsorted cells of the synovium of rheumatoid arthritis (RA) joints from one patient treated with GCs and one treatment-naive patient with a similar histology type and synovitis score to further explore the *in vivo* effects of GCs in monocyte-derived cell populations.

From the total single-cell transcriptomes, we exclusively selected putative MOs and MO-derived cells, based on the expression of *CD14*, *S100A9*, and *MRC1* (2), and the absence of *THY1*, *CD248*, *CD27*, *IGHN*, *CD3G*, *CD3E*, *CD34*, *KLRD1* and *NKG7* expression (Supplementary Figure 6A-C). Clustering of these cells yielded five distinct subpopulations. We then excluded clusters containing fewer than 50 cells and annotated the three remaining clusters as M1, M2 and M3 (Figure 6A).

Looking at the gene markers with a high level of expression in each group, we found some monocytic and proinflammatory genes, such as *VCAN*, *LYZ*, *S100A8*, *S100A9* and *IL1B*, in the M1 cluster, macrophagic markers (*CIQB*, *FCGR3A*, *CD163*, *RNASE1* and *FOLR2*) in the M2 cluster, and dendritic cell-related markers (*FCER1A*, *IRF4*, *CD1C*, *CCR7* and *CCL17*) in the M3 cluster (Figure 6B).

In addition, module scores of blood *CD14*⁺MO, mo-MAC and mo-DC signatures displayed an increased signal in M1, M2 and M3 clusters, respectively (Figure 6C).

Articles

We then analyzed the relative proportions of clusters in the treatment-naïve and the GC-treated patient joints. In the GC-treated patient joints, M1 and M3 clusters were depleted, whereas the M2 cluster was increased (Figure 6D). In this regard, when M1, M2 and M3 clusters expression were analyzed in bulk, GC-upregulated genes were more expressed in *in vitro* tolDCs and downregulated with the MAFB siRNA (Figure 6E).

Moreover, *in vitro* tolDC-induced genes presented a higher level of expression in the M2 cluster, whereas tolDC-repressed genes were more strongly expressed in M3 (Figure 6F). Furthermore, the module scores of the genes associated with MAFB ‘continuous’ ChIP-seq peaks and the siMAFB-downregulated genes for each cluster showed an increased signal in the M2 cluster for both modules (Figure 6G), and *MAFB* is more expressed in the M2 than the M1 and M3 clusters (Supplementary Figure 6D), supporting the involvement of MAFB in the transcriptomic signature of the M2 cluster.

Figure 6

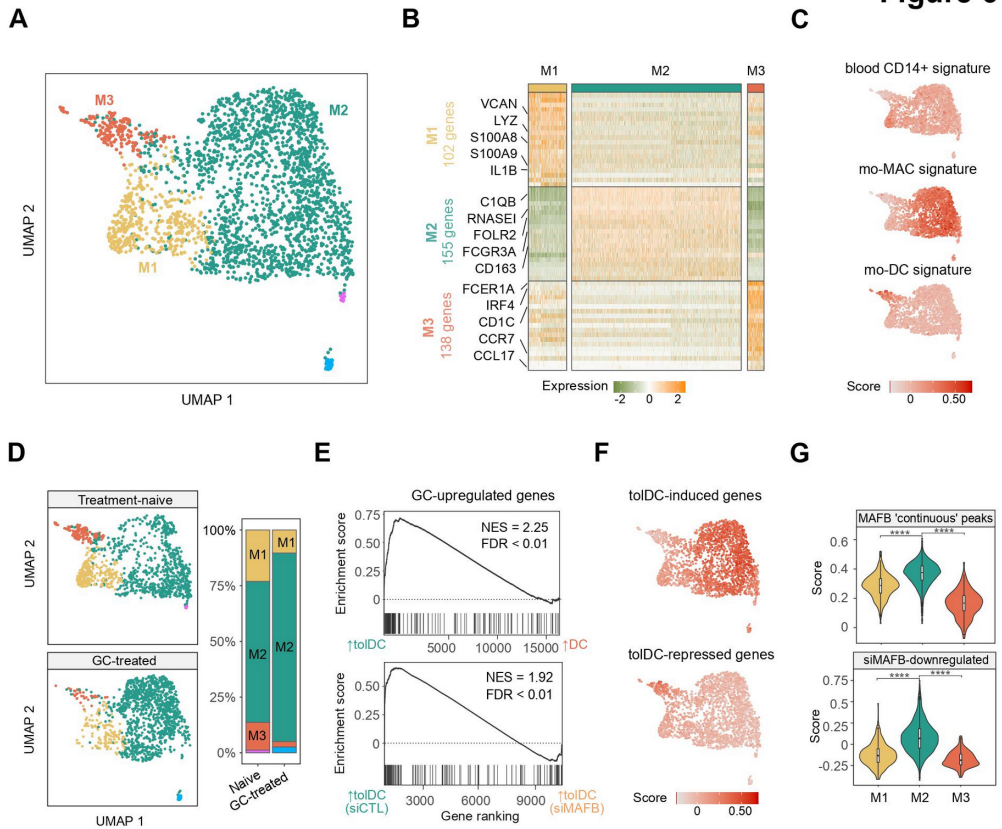


Figure 6. *In vivo* effects of glucocorticoid treatment in myeloid cells from RA synovium. (A) UMAP of putative monocyte-derived clusters from synovial tissues identified in the scRNA-seq analysis. A total of one treatment-naive and one GC-treated RA patient is shown in the UMAP. (B) Heatmap of the top 20 genes most differentially expressed from the M1, M2 and M3 clusters. Relevant cluster markers and the total number of genes identified in each cluster are shown. (C) UMAP heatmap of module scores of gene sets associated with blood CD14⁺ cells, mo-MACs and mo-DCs (67). (D) UMAP is divided depending on the treatment of RA patients (treatment-naive or GC-treated). In the right panel, proportions of each cluster in each group are shown. (E) Gene set enrichment analysis (GSEA) of tolDCs *vs.* DCs and tolDCs (siCTL) *vs.* tolDCs (siMAFB), using the genes upregulated with glucocorticoids in M1, M2 and M3 cluster cells from patients as the gene set. The

Articles

running enrichment score is represented and the normalized enrichment score (NES) is shown above (FDR < 0.01). (F) UMAP heatmap of module scores of tolDC-induced and tolDC-repressed genes. (G) Violin plots of module scores of genes associated with MAFB 'continuous' peaks and siMAFB-downregulated genes in the M1, M2 and M3 clusters (**** $p \leq 0.0001$).

Discussion

In this study, we demonstrate a fundamental role for MAFB, in combination with GR, in the acquisition of glucocorticoid-mediated tolerogenesis by tolDCs. We show a coordinated action of MAFB and GR in their binding to genomic sites, DNA methylation and gene expression changes, which lead to the establishment of a tolerogenic phenotype, in which MAFB plays a predominant role. This major role for MAFB is confirmed *in vivo*, by examining single-cell data from the synovium of rheumatoid arthritis patients treated with GC.

GR, as a ubiquitously expressed nuclear factor, is distributed fundamentally in the cytoplasm of cells, until GCs induce a conformational change and promote its translocation to the nucleus and binding to the genome in a matter of minutes(52). This, together with the previously described pioneer capacity of GR(53), suggested a direct and major role in the acquisition of the tolDC phenotype and methylome. On the other hand, MAFB has been previously linked to MO differentiation (10) and the M2 macrophage phenotype (9). Strikingly, we show that GR has an important but limited direct role in this context, given that its binding occurs in a few hundred genomic loci and is associated with a small fraction of the epigenomic and transcriptomic remodeling produced. Instead, after the glucocorticoid stimulus, GR binds to an enhancer close to *MAFB*, and the upregulation of the gene is observed after as little as 1h

of differentiation, pointing to a direct, GR-mediated regulation mechanism. MAFB, in turn, binds thousands of genomic loci in tolDCs, and is involved not only in DNA demethylation and gene upregulation, but also in the acquisition of the tolerogenic phenotype, as demonstrated by its knockdown. In this regard, MAFB acts as a surrogate to induce tolerogenesis in DCs on behalf of GR.

MAFB is a known downstream target of the IL-10/STAT3 signaling pathway(54), and additional evidence of the major role of MAFB in our model comes from the finding that *in vitro* DC-10 (tolDCs generated with IL-10) present upregulation of MAFB target genes and C2 CpG-associated genes, despite the absence of active GR.

A central question about GR biology has been how a TF that is ubiquitously expressed across most tissues can have different cell-type-specific functions(55–57). Chromatin accessibility has been described as pre-determining GR binding and shaping its differential binding across various cell types (58). Our data also indicate a preference for GR to bind preexisting open chromatin. However, we found a significant overlap of tolDC GR peaks across very different cell lines. Our findings support that, upon GC exposure, MAFB confers the cell type specificity required to acquire the tolerogenic phenotype of DCs.

DNA methylation (5mC) is generally considered a repressive epigenetic mark that is associated with gene downregulation(59). TET2, the most strongly expressed TET in MOs, has been linked to active demethylation events in these cells in several terminal myeloid differentiation models (6–8, 60). We prove that GR and MAFB both interact with TET2 in tolDCs, indicating that the demethylation process is probably triggered by MAFB- or GR-driven TET2 recruitment.

Articles

However, we cannot rule out the possibility that other TET proteins are involved.

DNA methylation changes occurring during the MO-to-tolDC differentiation is potentially both a cause and a consequence of the reshaping of gene expression. Some examples show that DNA demethylation can precede gene upregulation, or can occur at the same time (SIAH2, CIQB), whereas other genes, such as CD163 and ETS2, present a noticeable gene upregulation before DNA demethylation, as shown in other immune contexts(61). The functional role of the latter is enigmatic. Increasing evidence suggests that active demethylation intermediates, such as 5hmC, may be epigenetic marks with regulatory functions (62). DNA demethylation could also have a role later on, stabilizing the phenotype or fine-tuning the immune response after successive inflammatory stimuli. This is compatible with *IL10* gene behavior; whereby dexamethasone-mediated demethylation precedes a higher level of production of IL-10 after an inflammatory stimulus.

The transcriptome of GM-CSF/IL-4 DCs is very similar to the *in vivo* mo-DCs described in ascitic and synovial fluids (5). Intriguingly, tolDCs are more similar to *in vivo* moMACs and to *in vitro* M2 macrophages. MAFB upregulation is a hallmark of these three cell types. Several studies have produced evidence to suggest that there is a macrophagic phenotype of dexamethasone-treated monocytes, and that an increase of phagocytosis is a typical feature of tolDCs (63, 64). Here, we show that glucocorticoids skew MO-to-DC differentiation through MAFB, resembling an *in vivo* cell type. In this regard, we have shown depletion of cells with an expression pattern similar to moDCs and an increase of cells similar to moMACs in RA patients treated with GCs. Since *in vivo* moDCs are

involved in the pathogenesis of several inflammatory diseases (3, 65, 66), the GC-mediated remodeling of monocyte-derived populations in the synovium could be a significant process that modifies their proportions and modulates the inflammation produced by monocyte-derived cells in tissues. However, given the limited number of RA samples included in this study, the *in vivo* effects of GC treatment in MO differentiation should be further explored in follow up studies with a more clinical perspective.

Our results shed light on the regulatory mechanisms of GC-induced tolDC differentiation, identifying the critical role of MAFB, which takes over GR to fulfil the main roles of tolerogenesis induction. We have described a new mechanism of action of GCs in MOs, consisting of MAFB induction, overriding the MO-to-DC differentiation program, rendering macrophage-like tolerogenic cells. Moreover, in MO-derived cells from synovial tissues, we have also shown a concordant GC-mediated depletion of mo-DCs and an increase of mo-MACs. By improving the understanding of the molecular mechanisms underlying the tolDC generation mediated by GCs and the effects of GCs in MOs *in vivo*, our results can provide insights to enhance the *in vitro* generation of tolDCs and to create more specific anti-inflammatory therapies.

Data access

DNA methylation, expression, ChIP-seq data and single-cell RNAseq data for this publication have been deposited in the NCBI Gene Expression Omnibus and are accessible through GEO SuperSeries accession number GSE180542 and GSE181082.

Acknowledgements

We are very grateful to Prof. Angel Corbí and his team for useful discussions and feedback.

Funding

We thank the CERCA Programme/Generalitat de Catalunya and the Josep Carreras Foundation for institutional support. E.B. was funded by the Spanish Ministry of Science and Innovation (MICINN; grant numbers SAF2017-88086-R & PID2020-117212RB-I00; AEI/FEDER, UE). O.M.-P. holds an i-PFIS PhD Fellowship (grant number IFI17/00034) from Acción Estratégica en Salud 2013-2016 ISCIII, co-financed by Fondo Social Europeo. C.O. and M.F.-B. were supported by the Swiss National Science Foundation (project 320030_176061). M.H. was supported by the Iten-Kohaut Foundation and the MLR foundation.

Competing interests

There are no competing interests to report.

References

1. Morante-Palacios,O., Fondelli,F., Ballestar,E. and Martínez-Cáceres,E.M. (2021) Tolerogenic Dendritic Cells in Autoimmunity and Inflammatory Diseases. *Trends Immunol.*, 42, 59–75.
2. Coillard,A. and Segura,E. (2019) *in vivo* differentiation of human monocytes. *Front. Immunol.*, 10.
3. Segura,E., Touzot,M., Bohineust,A., Cappuccio,A., Chiocchia,G., Hosmalin,A., Dalod,M., Soumelis,V. and Amigorena,S. (2013) Human Inflammatory Dendritic Cells Induce Th17 Cell Differentiation. *Immunity*, 38, 336–348.
4. Sallusto,F. and Lanzavecchi,A. (1994) Efficient presentation of soluble antigen by cultured human dendritic cells is maintained by granulocyte/macrophage colony-stimulating factor plus interleukin 4 and downregulated by tumor necrosis factor α . *J. Exp. Med.*, 179, 1109–1118.
5. Goudot,C., Coillard,A., Villani,A.C., Gueguen,P., Cros,A., Sarkizova,S., Tang-Huau,T.L., Bohec,M., Baulande,S., Hacohen,N., et al. (2017) Aryl Hydrocarbon Receptor Controls Monocyte Differentiation into Dendritic Cells versus Macrophages. *Immunity*, 47, 582-596.e6.
6. Vento-Tormo,R., Company,C., Rodríguez-Ubreva,J., de la Rica,L., Urquiza,J.M., Javierre,B.M., Sabarinathan,R., Luque,A., Esteller,M., Aran,J.M., et al. (2016) IL-4 orchestrates STAT6-mediated DNA demethylation leading to dendritic cell differentiation. *Genome Biol.*, 17.
7. Mendes,K., Schmidhofer,S., Minderjahn,J., Glatz,D., Kiesewetter,C., Raithel,J., Wimmer,J., Gebhard,C. and Rehli,M. (2021) The epigenetic pioneer EGR2 initiates DNA demethylation in

Articles

differentiating monocytes at both stable and transient binding sites. *Nat. Commun.*, 12.

8. Klug, M., Schmidhofer, S., Gebhard, C., Andreesen, R. and Rehli, M. (2013) 5-Hydroxymethylcytosine is an essential intermediate of active DNA demethylation processes in primary human monocytes. *Genome Biol.*, 14.

9. Cuevas, V.D., Anta, L., Samaniego, R., Orta-Zavalza, E., Vladimir de la Rosa, J., Baujat, G., Domínguez-Soto, Á., Sánchez-Mateos, P., Escribese, M.M., Castrillo, A., et al. (2017) MAFB Determines Human Macrophage Anti-Inflammatory Polarization: Relevance for the Pathogenic Mechanisms Operating in Multicentric Carpotarsal Osteolysis. *J. Immunol.*, 198, 2070–2081.

10. Kelly, L.M., Englmeier, U., Lafon, I., Sieweke, M.H., Graf, T. (2000) MafB is an inducer of monocytic differentiation. *EMBO J.*, 19, 1987–1997.

11. García-González, P., Morales, R., Hoyos, L., Maggi, J., Campos, J., Pesce, B., Gárate, D., Larrondo, M., González, R., Soto, L., et al. (2013) A short protocol using dexamethasone and monophosphoryl lipid A generates tolerogenic dendritic cells that display a potent migratory capacity to lymphoid chemokines. *J. Transl. Med.*, 11.

12. Unger, W.W., Laban, S., Kleijwegt, F.S., van der Slik, A.R., and Roep, B.O. (2009) Induction of Treg by monocyte-derived DC modulated by vitamin D3 or dexamethasone: differential role for PD-L1. *Eur. J. Immunol.*, 39, 3147–3159.

13. Bell, G.M., Anderson, A.E., Diboll, J., Reece, R., Eltherington, O., Harry, R.A., Fouweather, T., MacDonald, C., Chadwick, T., McColl, E., et

al. (2017) Autologous tolerogenic dendritic cells for rheumatoid and inflammatory arthritis. *Ann. Rheum. Dis.*, 76, 227–234.

14. Kurochkina,Y., Tikhonova,M., Tyrinova,T., Leplina,O., Sizikov,A., Sulutian,A., Chumasova,O., Ostanin,A. and Chernykh,E. (2018) SAT0212 The safety and tolerability of intra-articular injection of tolerogenic dendritic cells in patients with rheumatoid arthritis: the preliminary results. In *Annals of the Rheumatic Diseases*. BMJ, Vol. 77, pp. 966.2-967.

15. Zubizarreta,I., Flórez-Grau,G., Vila,G., Cabezón,R., España,C., Andorra,M., Saiz,A., Llufríu,S., Sepulveda,M., Sola-Valls,N., et al. (2019) Immune tolerance in multiple sclerosis and neuromyelitis optica with peptide-loaded tolerogenic dendritic cells in a phase Ib trial. *Proc. Natl. Acad. Sci. U. S. A.*, 116, 8463–8470.

16. Jauregui-Amezaga, A., Cabezón, R., Ramírez-Morros, A., España, C., Rimola, J., Bru, C., Pinó-Donnay, S., Gallego, M., Masamunt, M.C., Ordás, I., et al. (2015) Intraperitoneal Administration of Autologous Tolerogenic Dendritic Cells for Refractory Crohn's Disease: A Phase I Study. *J. Crohns. Colitis*, 9, 1071–1078.

17. Adcock, I.M., Nasuhara, Y., Stevens, D.A., and Barnes, P.J. (1999) Ligand-induced differentiation of glucocorticoid receptor (GR) trans-repression and transactivation: preferential targetting of NF-kappaB and lack of I-kappaB involvement. *Br. J. Pharmacol.*, 127, 1003–1011.

18. McDowell, I.C., Barrera, A., D'Ippolito, A.M., Vockley, C.M., Hong, L.K., Leichter, S.M., Bartelt, L.C., Majoros, W.H., Song, L., Safi, A., et al. (2018) Glucocorticoid receptor recruits to enhancers and drives activation by motif-directed binding. *Genome Res.*, 28, 1272–1284.

Articles

19. Hoffman, J.A., Trotter, K.W., Ward, J.M., and Archer, T.K. (2018) BRG1 governs glucocorticoid receptor interactions with chromatin and pioneer factors across the genome. *Elife*, 7.

20. Carvalho, B.S. and Irizarry, R.A. (2010) A framework for oligonucleotide microarray preprocessing. *Bioinformatics*, 26, 2363–2367.

21. Morante-Palacios, O. and Ballestar, E. (2021) shinyÉPICO: A graphical pipeline to analyze Illumina DNA methylation arrays. *Bioinformatics*, 10.1093/bioinformatics/btaa1095.

22. Aryee, M.J., Jaffe, A.E., Corrada-Bravo, H., Ladd-Acosta, C., Feinberg, A.P., Hansen, K.D. and Irizarry, R.A. (2014) Minfi: A flexible and comprehensive Bioconductor package for the analysis of Infinium DNA methylation microarrays. *Bioinformatics*, 10.1093/bioinformatics/btu049.

23. Kim, D., Langmead, B. and Salzberg, S.L. (2015) HISAT: A fast spliced aligner with low memory requirements. *Nat. Methods*, 12, 357–360.

24. Li, H., Handsaker, B., Wysoker, A., Fennell, T., Ruan, J., Homer, N., Marth, G., Abecasis, G. and Durbin, R. (2009) The Sequence Alignment/Map format and SAMtools. *Bioinformatics*, 25, 2078–2079.

25. Liao, Y., Smyth, G.K. and Shi, W. (2014) FeatureCounts: An efficient general purpose program for assigning sequence reads to genomic features. *Bioinformatics*, 30, 923–930.

26. Love, M.I., Huber, W. and Anders, S. (2014) Moderated estimation of fold change and dispersion for RNA-seq data with DESeq2. *Genome Biol.*, 15.

27. Li, H. (2013) Aligning sequence reads, clone sequences and assembly contigs with BWA-MEM.
28. Amemiya, H.M., Kundaje, A., and Boyle, A.P. (2019) The ENCODE Blacklist: Identification of Problematic Regions of the Genome. *Sci. Rep.*, 9.
29. Kharchenko, P.V., Tolstorukov, M.Y., and Park, P.J. (2008) Design and analysis of ChIP-seq experiments for DNA-binding proteins. *Nat. Biotechnol.*, 26, 1351–1359.
30. Ramírez, F., Ryan, D.P., Grüning, B., Bhardwaj, V., Kilpert, F., Richter, A.S., Heyne, S., Dündar, F. and Manke, T. (2016) deepTools2: a next generation web server for deep-sequencing data analysis. *Nucleic Acids Res.*, 44, W160–W165.
31. Zerbino, D.R., Johnson, N., Juettemann, T., Wilder, S.P., and Flicek, P. (2014) WiggleTools: parallel processing of large collections of genome-wide datasets for visualization and statistical analysis. *Bioinformatics*, 30, 1008–1009.
32. Zhang, Y., Liu, T., Meyer, C.A., Eeckhoute, J., Johnson, D.S., Bernstein, B.E., Nusbaum, C., Myers, R.M., Brown, M., Li, W., et al. (2008) Model-based analysis of ChIP-Seq (MACS). *Genome Biol.*, 9.
33. Jalili, V., Matteucci, M., Masseroli, M. and Morelli, M.J. (2015) Using combined evidence from replicates to evaluate ChIP-seq peaks. *Bioinformatics*, 31, 2761–2769.
34. McLean, C.Y., Bristor, D., Hiller, M., Clarke, S.L., Schaar, B.T., Lowe, C.B., Wenger, A.M. and Bejerano, G. (2010) GREAT improves functional interpretation of cis-regulatory regions. *Nat. Biotechnol.*, 28, 495–501.

Articles

35. Yu, G., Wang, L.G., Han, Y. and He, Q.Y. (2012) ClusterProfiler: An R package for comparing biological themes among gene clusters. *Omi. A J. Integr. Biol.*, 16, 284–287.

36. Zhu, L.J., Gazin, C., Lawson, N.D., Pagès, H., Lin, S.M., Lapointe, D.S., and Green, M.R. (2010) ChIPpeakAnno: a Bioconductor package to annotate ChIP-seq and ChIP-chip data. *BMC Bioinformatics*, 11.

37. Lopez-Delisle, L., Rabbani, L., Wolff, J., Bhardwaj, V., Backofen, R., Grüning, B., Ramírez, F., and Manke, T. (2021) pyGenomeTracks: reproducible plots for multivariate genomic datasets. *Bioinformatics*, 37, 422–423.

38. Martorell-Marugán, J., González-Rumayor, V. and Carmona-Sáez, P. (2019) MCSEA: Detecting subtle differentially methylated regions. *Bioinformatics*, 35, 3257–3262.

39. Chèneby, J., Ménétrier, Z., Mestdagh, M., Rosnet, T., Douida, A., Rhalloussi, W., Bergon, A., Lopez, F., and Ballester, B. (2020) ReMap 2020: a database of regulatory regions from an integrative analysis of Human and Arabidopsis DNA-binding sequencing experiments. *Nucleic Acids Res.*, 48, D180–D188.

40. Quinlan, A.R., and Hall, I.M. (2010) BEDTools: a flexible suite of utilities for comparing genomic features. *Bioinformatics*, 26, 841–842.

41. Fernández, J.M., De La Torre, V., Richardson, D., Torrents, D., Carrillo, E., Pau, S. and Valencia, A. (2016) The BLUEPRINT Data Analysis Portal. [10.1016/j.cels.2016.10.021](https://doi.org/10.1016/j.cels.2016.10.021).

42. Leek, J.T., Johnson, W.E., Parker, H.S., Jaffe, A.E., and Storey, J.D. (2012) The sva package for removing batch effects and other

unwanted variation in high-throughput experiments. *Bioinformatics*, 28, 882–883.

43. Krenn, V., Morawietz, L., Burmester, G.R., Kinne, R.W., Mueller-Ladner, U., Muller, B., and Haupl, T. (2006) Synovitis score: discrimination between chronic low-grade and high-grade synovitis. *Histopathology*, 49, 358–364.

44. Humby, F., Lewis, M., Ramamoorthi, N., Hackney, J.A., Barnes, M.R., Bombardieri, M., Setiadi, A.F., Kelly, S., Bene, F., DiCicco, M., et al. (2019) Synovial cellular and molecular signatures stratify clinical response to csDMARD therapy and predict radiographic progression in early rheumatoid arthritis patients. *Ann. Rheum. Dis.*, 78, 761–772.

45. Sierra-Filardi, E., Puig-Kröger, A., Blanco, F.J., Nieto, C., Bragado, R., Palomero, M.I., Bernabéu, C., Vega, M.A., and Corbí, A.L. (2011) Activin A skews macrophage polarization by promoting a proinflammatory phenotype and inhibiting the acquisition of anti-inflammatory macrophage markers. *Blood*, 117, 5092–5101.

46. Rutella, S., Bonanno, G., Procoli, A., Mariotti, A., de Ritis, D.G., Curti, A., Danese, S., Pessina, G., Pandolfi, S., Natoni, F., et al. (2006) Hepatocyte growth factor favors monocyte differentiation into regulatory interleukin (IL)-10⁺⁺IL-12^{low/neg} accessory cells with dendritic-cell features. *Blood*, 108, 218–227.

47. Garcia-Alonso, L., Holland, C.H., Ibrahim, M.M., Turei, D. and Saez-Rodriguez, J. (2019) Benchmark and integration of resources for the estimation of human transcription factor activities. *Genome Res.*, 29, 1363–1375.

Articles

48. García-González, P.A., Maggi, J., Schinnerling, K., Sepúlveda-Gutiérrez, A., Soto, L., Neira, O., Mehdi, A.M., Nel, H.J., Pesce, B., Aravena, O. et al. (2019) Regulation of Tolerogenic Features on Dexamethasone-Modulated MPLA-Activated Dendritic Cells by MYC. *Front. Immunol.*, 10.

49. Johnson, J.S., Lucas, S.Y., Amon, L.M., Skelton, S., Nazitto, R., Carbonetti, S., Sather, D.N., Littman, D.R., and Aderem, A. (2018) Reshaping of the Dendritic Cell Chromatin Landscape and Interferon Pathways during HIV Infection. *Cell Host Microbe*, 23, 366-381.e9.

50. Bakri, Y., Sarrazin, S., Mayer, U.P., Tillmanns, S., Nerlov, C., Boned, A., and Sieweke, M.H. (2005) Balance of MafB and PU.1 specifies alternative macrophage or dendritic cell fate. *Blood*, 105, 2707–2716.

51. Sichien,D., Scott,C.L., Martens,L., Vanderkerken,M., Van Gassen,S., Plantinga,M., Joeris,T., De Prijck,S., Vanhoutte,L., Vanheerswyngghels,M., et al. (2016) IRF8 Transcription Factor Controls Survival and Function of Terminally Differentiated Conventional and Plasmacytoid Dendritic Cells, Respectively. *Immunity*, 45, 626–640.

52. Htun, H., Barsony, J., Renyi, I., Gould, D.L., and Hager, G.L. (1996) Visualization of glucocorticoid receptor translocation and intranuclear organization in living cells with a green fluorescent protein chimera. *Proc. Natl. Acad. Sci. U. S. A.*, 93, 4845–4850.

53. Johnson, T.A., Chereji, R.V., Stavreva, D.A., Morris, S.A., Hager, G.L., and Clark, D.J. (2018) Conventional and pioneer modes of glucocorticoid receptor interaction with enhancer chromatin *in vivo*. *Nucleic Acids Res.*, 46, 203–214.

54. Gemelli, C., Zanocco Marani, T., Bicciano, S., Mazza, E.M., Boraschi, D., Salsi, V., Zappavigna, V., Parenti, S., Selmi, T., Tagliafico, E., et al. (2014) MafB is a downstream target of the IL-10/STAT3 signaling pathway, involved in the regulation of macrophage de-activation. *Biochim. Biophys. Acta*, 1843, 955–964.
55. Evans, R.M. (1988) The steroid and thyroid hormone receptor superfamily. *Science*, 240, 889–895.
56. Franco, L.M., Gadkari, M., Howe, K.N., Sun, J., Kardava, L., Kumar, P., Kumari, S., Hu, Z., Fraser, I.D.C., Moir, S., et al. (2019) Immune regulation by glucocorticoids can be linked to cell type-dependent transcriptional responses. *J. Exp. Med.*, 216, 384–406.
57. Hardy, R.S., Raza, K., and Cooper, M.S. (2020) Therapeutic glucocorticoids: mechanisms of actions in rheumatic diseases. *Nat. Rev. Rheumatol.*, 16, 133–144.
58. John, S., Sabo, P.J., Thurman, R.E., Sung, M.H., Biddie, S.C., Johnson, T.A., and Hager, G.L., and Stamatoyannopoulos, J.A. (2011) Chromatin accessibility pre-determines glucocorticoid receptor binding patterns. *Nat. Genet.*, 43, 264–268.
59. Luo, C., Hajkova, P. and Ecker, J.R. (2018) Dynamic DNA methylation: In the right place at the right time. *Science* (80-), 361, 1336–1340.
60. de la Rica, L., Rodríguez-Ubreva, J., García, M., Islam, A.B.M.M.K., Urquiza, J.M., Hernando, H., Christensen, J., Helin, K., Gómez-Vaquero, C. and Ballestar, E. (2013) PU.1 target genes undergo Tet2-coupled demethylation and DNMT3b-mediated methylation in monocyte-to-osteoclast differentiation. *Genome Biol.*, 14.

Articles

61. Pacis,A., Mailhot-Léonard,F., Tailleux,L., Randolph,H.E., Yotova,V., Dumaine,A., Grenier,J.-C. and Barreiro,L.B. (2019) Gene activation precedes DNA demethylation in response to infection in human dendritic cells. *Proc. Natl. Acad. Sci.*, 10.1073/pnas.1814700116.

62. He, B., Zhang, C., Zhang, X., Fan, Y., Zeng, H., Liu, J., Meng, H., Bai, D., Peng, J., Zhang, Q., et al. (2021) Tissue-specific 5-hydroxymethylcytosine landscape of the human genome. *Nat. Commun.*, 12, 4249.

63. Heideveld, E., Hampton-O'Neil, L.A., Cross, S.J., van Alphen, F.P.J., van den Biggelaar, M., Toye, A.M., van den Akker, E. (2018) Glucocorticoids induce differentiation of monocytes towards macrophages that share functional and phenotypical aspects with erythroblastic island macrophages. *Haematologica*, 103, 395–405.

64. van der Goes, A., Hoekstra, K., van den Berg, T.K., and Dijkstra, C.D. (2000) Dexamethasone promotes phagocytosis and bacterial killing by human monocytes/macrophages *in vitro*. *J. Leukoc. Biol.*, 67, 801–807.

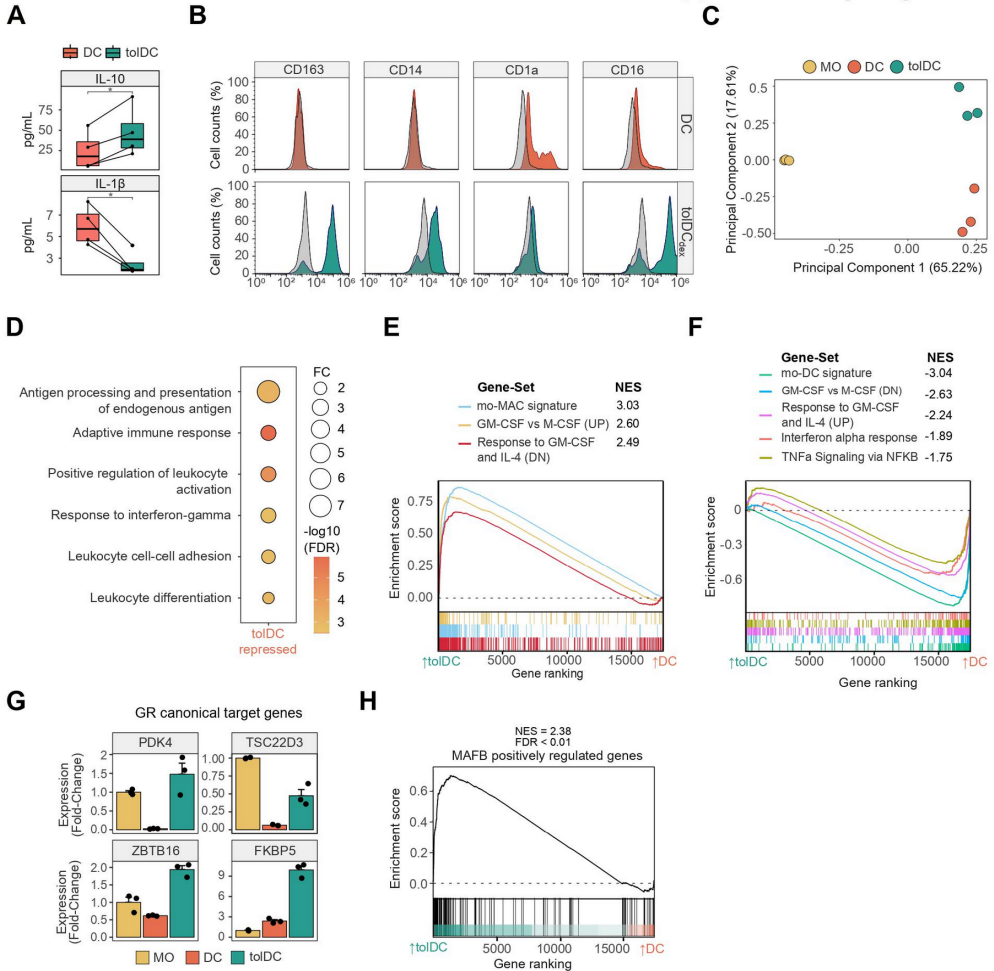
65. Kamada, N., Hisamatsu, T., Okamoto, S., Chinen, H., Kobayashi, T., Sato, T., Sakuraba, A., Kitazume, M.T., Sugita, A., Koganei, K., et al. (2008) Unique CD14 intestinal macrophages contribute to the pathogenesis of Crohn disease via IL-23/IFN-gamma axis. *J. Clin. Invest.*, 118, 2269–2280.

66. Zaba, L.C., Fuentes-Duculan, J., Eungdamrong, N.J., Abello, M.V., Novitskaya, I., Pierson, K.C., Gonzalez, J., Krueger, J.G., and Lowes, M.A. (2009) Psoriasis is characterized by accumulation of immunostimulatory and Th1/Th17 cell-polarizing myeloid dendritic cells. *J. Invest. Dermatol.*, 129, 79–88.

67. Tang-Huau,T.L., Gueguen,P., Goudot,C., Durand,M., Bohec,M., Baulande,S., Pasquier,B., Amigorena,S. and Segura,E. (2018) Human *in vivo*-generated monocyte-derived dendritic cells and macrophages cross-present antigens through a vacuolar pathway. Nat. Commun., 9.

Supplementary Figures

Supplementary Figure 1

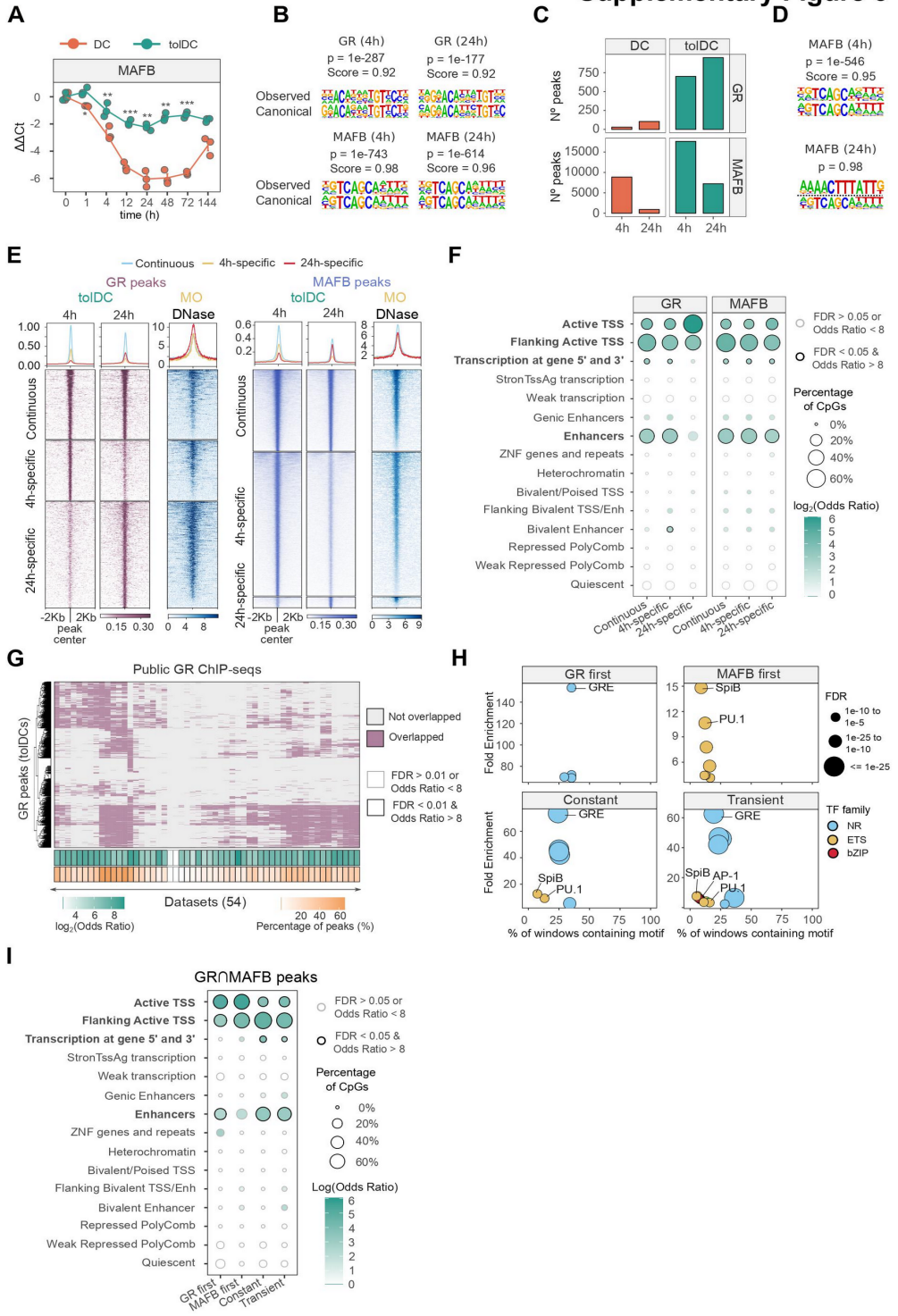


Supplementary Figure 1. (A) IL-10 and IL-1β production of DCs and tolDCs, after 6 days of differentiation. IL-12p70 and TNFα were not detected. P-values of paired-samples t-tests are shown (* p ≤ 0.05). (B) Surface markers of DCs and tolDCs. Histograms of fluorescent signals are shown. Signals of negative controls are shown in grey. (C) Principal component analysis (PCA) of gene expression. Principal component 1 and principal component 2 are represented in the x- and y-axis, respectively. (D) Gene ontology (GO) over-representation of GO Biological Process

Articles

Supplementary Figure 2. (A) Principal component analysis (PCA) of differentially methylated CpGs when comparing MOs, DCs and tolDCs. Principal components 1 and 2 are represented on the x- and y-axis, respectively. (B) DNA methylation heatmap of differentially methylated CpGs comparing MOs, DCs and tolDCs pairwise ($\Delta\beta \geq 0.2$, FDR < 0.05). Scaled β -values are shown (lower and higher DNA methylation levels in blue and red, respectively) (n=4). (C) Enrichment of C1- and C2-CpGs in ChromHMM 15-state categories of MOs (Roadmap Epigenomics Project). Odds ratio over background from Fisher's exact test and significance is shown for each category. Bubble sizes are determined by the percentage of CpGs overlapping each ChromHMM category. (D) Bubble scatter-plot of TF-binding motif enrichment for C1 CpGs. The x-axis shows the percentage of windows containing the motif and the y-axis shows the fold enrichment of the motif over the EPIC background. Bubbles are colored according to the TF family. FDR is indicated by bubble size. (E) GO (Gene Ontology) over-represented categories in C1 CpGs. The fold change in comparison with background (EPIC array CpGs) and $-\log_{10}(\text{FDR})$ are represented. (F) Violin plots of DNA methylation (β -values) of C1 and C2 CpGs in CD14⁺ MOs, M1 macrophages (GM-CSF) and M2 macrophages (M-CSF). (**** p \leq 0.0001) (G) The fold change of DC and tolDC expression (with respect to MO) of some examples of C1 CpG-associated genes are shown, calculated from fluorescence values of expression arrays (n=3). DNAmethylation (β -values) of examples of associated CpGs is represented below each gene (n=4) (H) Gene set enrichment analysis (GSEA) of mature DCs (mDCs) *vs.* mature tolDCs (mtolDCs) produced with several drugs (GSE40484, GSE117947), using C2 CpGs associated genes and MAFB positively regulated genes as gene sets. The normalized enrichment scores (NES) and significance (FDR < 0.01) are depicted for each gene set.

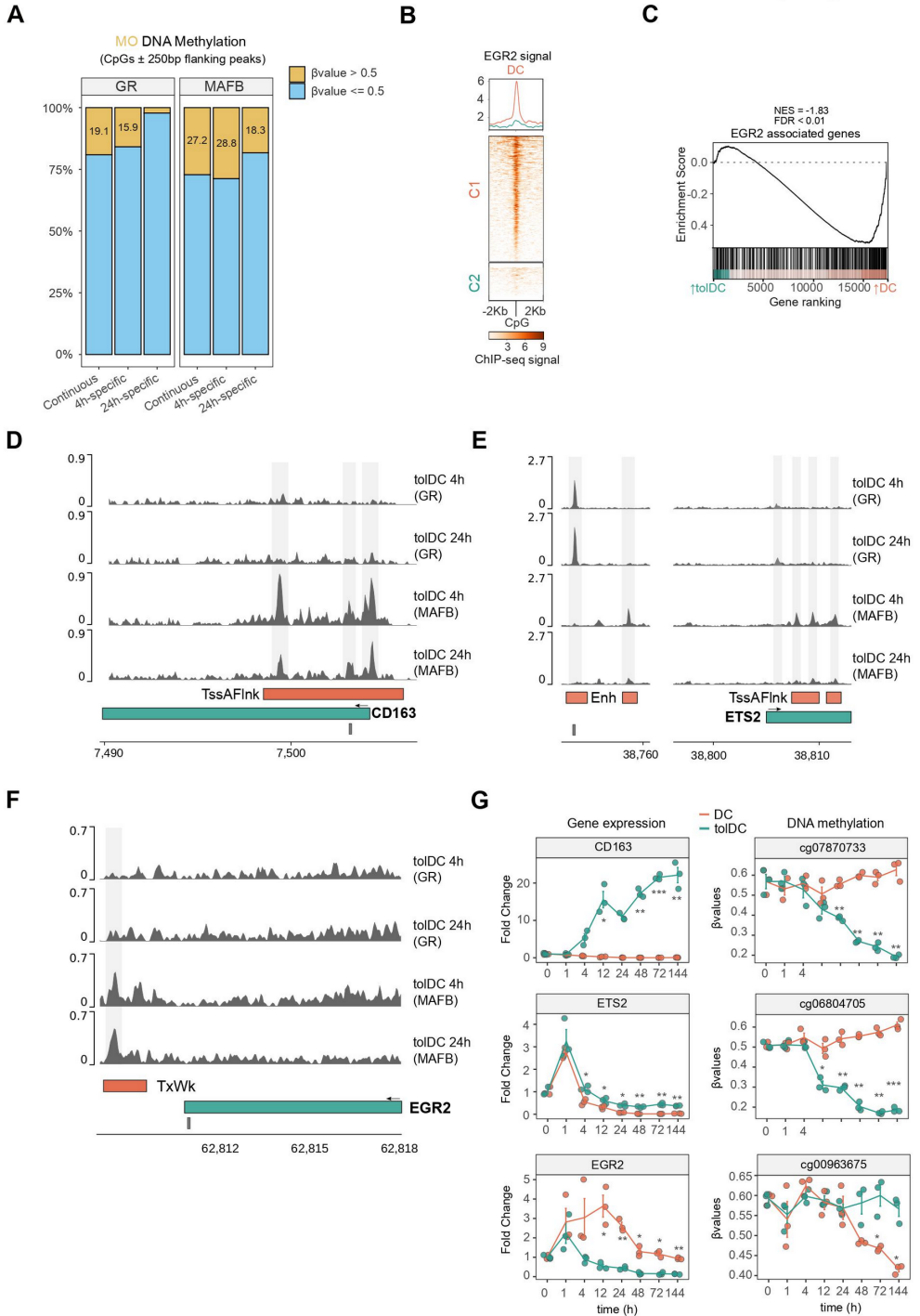
Supplementary Figure 3



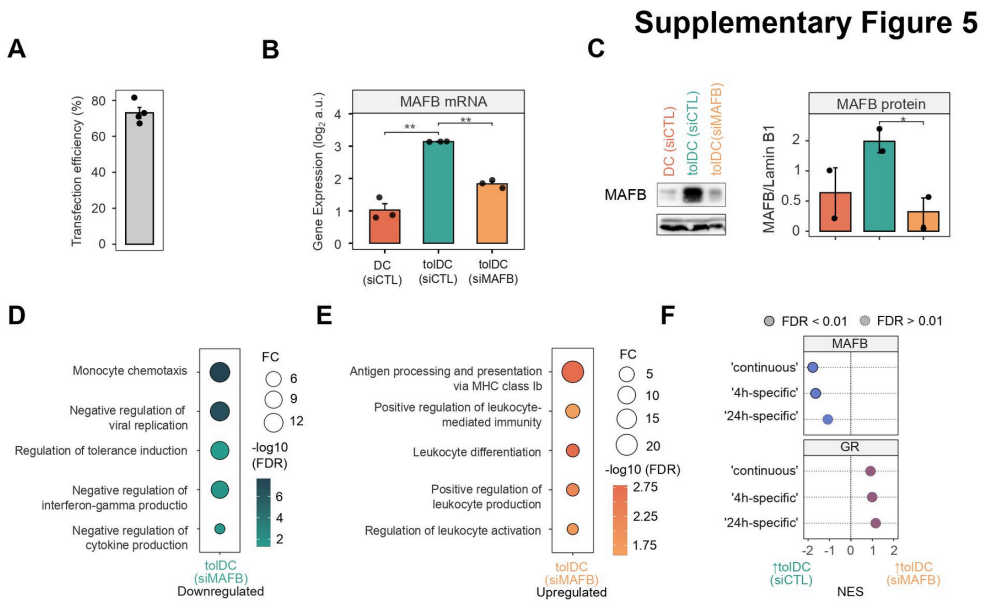
Articles

Supplementary Figure 3. (A) MAFB gene expression of DCs and tolDCs from 0 to 144 h of differentiation. $\Delta\Delta\text{Ct}$ values of real-time quantitative polymerase chain reaction (RT-qPCR) are shown (n=3) (* $p < 0.05$, ** $p \leq 0.01$, *** $p \leq 0.001$). (B) Similarity of the most frequently represented motif of tolDC GR and MAFB peaks with the respective canonical motifs. P-values and Pearson's correlation coefficients (Score) are shown. (C) Number of peaks obtained in DCs and tolDC GR and MAFB ChIP-seqs after peak-calling and consolidation of biological duplicates. (D) Similarity of the most frequently represented motif of DC MAFB peaks with the respective canonical motif. P-values and Pearson's correlation coefficients (Score) are shown. DC MAFB 24h motif is not similar to the MAFB canonical motif (p-value 0.98). (E) Heatmap of GR and MAFB 'continuous', '4h-specific' and '24h-specific' ChIP-seq peaks at 4h and 24h of differentiation. The DNase-seq signal of CD14⁺ MOs in these regions is also shown. (F) Enrichment of GR and MAFB 'continuous', '4h-specific' and '24h-specific' peaks in ChromHMM 15-state categories of MOs (Roadmap Epigenomics Project). Odds ratio over background from Fisher's exact test and significance is shown for each category. Bubble sizes are determined by the percentage of CpGs overlapping each ChromMHHM category. (G) Heatmap of the overlap of tolDC GR peaks across 54 datasets of public GR ChIP-seqs. Not-overlapped and overlapped peaks are shown in grey and purple, respectively. The overall enrichment (odds ratio) and the percentage of overlapped peaks are depicted in two different heatmaps (green and orange, respectively). (H) Bubble scatterplot of TF binding motif enrichment in the $\text{GR} \cap \text{MAFB}$ peaks, including 'GR first', 'MAFB first', 'Constant' and 'Transient' peaks. The x-axis shows the percentage of windows containing the motif and the y-axis shows the fold enrichment of the motif over the EPIC background. Bubbles are coloured according to the TF family. FDR is indicated by bubble size. (I) Enrichment of 'GR first', 'MAFB first', 'Constant' and 'Transient' peaks in ChromHMM 15-states categories of MOs (Roadmap Epigenomics Project). Odds ratio over background from Fisher's exact test and significance is shown for each category. Bubble sizes are determined by the percentage of CpGs overlapping each ChromMHHM category.

Supplementary Figure 4



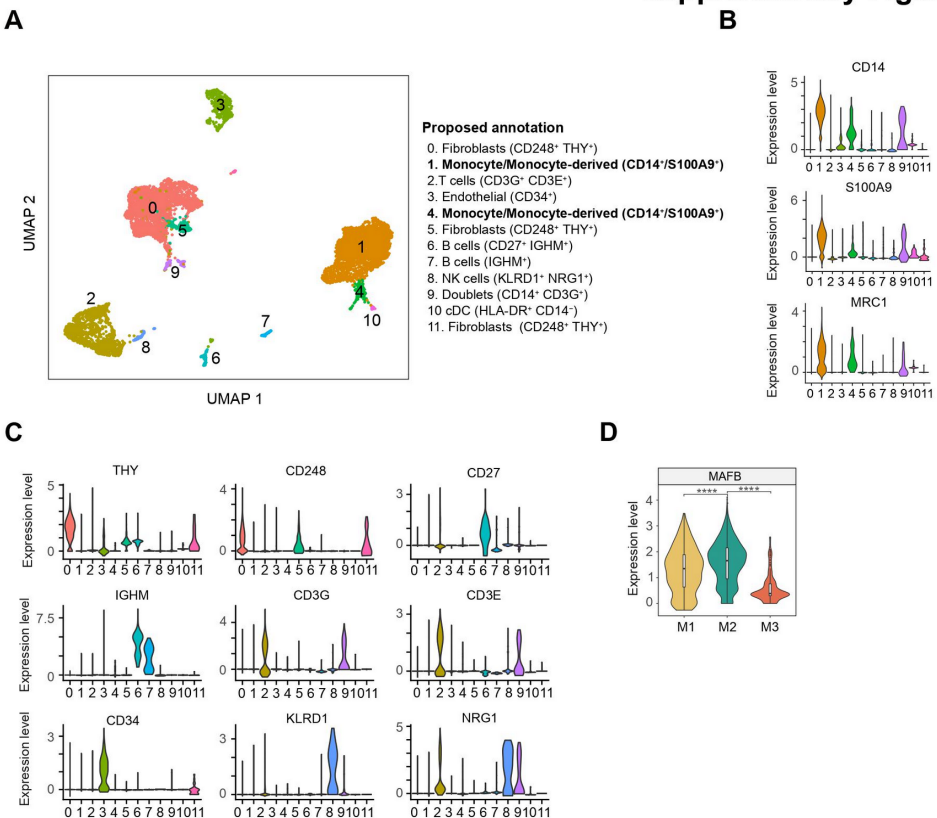
Supplementary Figure 4. (A) Proportions of DNA methylation state of GR and MAFB ‘continuous’, ‘4h-specific’ and ‘24h-specific’ peaks. Only CpGs flanking (\pm 250 bp) or overlapping ChIP-seq peaks are considered. (B) Heatmap of the EGR2 ChIP-seq signal across C1 and C2 CpGs (6). (C) Gene set enrichment analysis (GSEA) of tolDC vs. DC, with the genes closest to the top 500 EGR2 peaks (D-F) Representation of the GR and MAFB ChIP-seq signal (BPMs) close to the CD163, ETS2 and EGR2 genes. 15-state ChromHMM of MOs in peaks are depicted in orange. Significant peaks are shown against a grey background. (G) CD163, ETS2 and EGR2 time-course gene expression, obtained from qRT-PCR (relative arbitrary units) (n=3) and DNA methylation (β -values) of associated differentially methylated CpGs obtained from bisulfite pyrosequencing (n=3).



Supplementary Figure 5. (A) Bar-plot of the siRNA transfection efficiency, measured by flow cytometry with a fluorescent siRNA (n=4). (B) RT-qPCR of MAFB showing downregulation of the gene with the siRNA (n=3) (** p <= 0.01). (C) Western blot of MAFB in cells treated with siMAFB or siCTL. On the right, the image signal quantification ratios (MAFB / LamininB1) are depicted. P-values of paired t-tests are shown (n=2) (* p < 0.05) (D-E) Gene Ontology (GO) over-representation of GO Biological Process categories in tolDC (siMAFB)

downregulated and upregulated genes. Fold change of genes over background and $-\log_{10}(\text{FDR})$ of the Fisher's exact tests are shown. (F) Gene set enrichment analysis (GSEA) of tolDCs (siCTL) *vs.* tolDCs (siMAFB), using the MAFB and GR 'continuous', '4h-specific' and '24h-specific' top 500 associated genes. The normalized enrichment scores (NES) and significance ($\text{FDR} < 0.01$) are depicted for each gene set.

Supplementary Figure 6



Supplementary Figure 6. (A) UMAP of all cells from synovial tissues identified in the scRNA-seq analysis. In the right panel, the proposed annotation for each cluster is shown. (B) Violin plots of positive gene markers used to select putative monocyte/monocyte-derived cells. (C) Violin plots of negative gene markers used to select, by exclusion, monocyte/monocyte-derived cells. (D) Violin plot of MAFB mRNA expression in the M1, M2 and M3 clusters (**** $p \leq 0.0001$).

3.2. ARTICLE 2: JAK2-STAT epigenetically regulates tolerized genes in monocytes in the first encounter with gram-negative bacterial endotoxins in sepsis

JAK2-STAT epigenetically regulates tolerized genes in monocytes in the first encounter with gram-negative bacterial endotoxins in sepsis

Octavio Morante-Palacios^{1,†}, Clara Lorente-Sorolla^{1,†}, Laura Ciudad¹, Josep Calafell-Segura¹, Antonio Garcia-Gomez¹, Francesc Català-Moll¹, Adolfo Ruiz-Sanmartín², Mónica Martínez-Gallo³, Ricard Ferrer-Roca², Juan Carlos Ruiz-Rodriguez², Damiana Álvarez-Errico¹, and Esteban Ballestar¹

[†] These two authors contributed equally to the study.

¹Epigenetics and Immune Disease Group, Josep Carreras Research Institute (IJC), 08916 Badalona, Barcelona, Spain

²Intensive Care Department, Vall d'Hebron University Hospital, Shock, Organ Dysfunction and Resuscitation (SODIR) Research Group, Vall d'Hebron Research Institute (VHIR), Barcelona Hospital Campus, Universitat Autònoma de Barcelona, 08035 Barcelona, Spain

³Immunology Division, Vall d'Hebron University Hospital and Diagnostic Immunology Research Group, Vall d'Hebron Research Institute (VHIR), 08035 Barcelona, Spain

* **Correspondence:** E. Ballestar, E-mail: eballestar@carrerasresearch.org

Keywords: monocytes; lipopolysaccharide; endotoxin tolerance; sepsis; epigenetics; DNA methylation; tolerized genes; STATs; JAK2; TET2

Abstract

Microbial challenges, such as widespread bacterial infection in sepsis, induce endotoxin tolerance, a state of hyporesponsiveness to subsequent infections. The participation of DNA methylation in this process is poorly known. In this study, we perform integrated analysis of DNA methylation and transcriptional changes following *in vitro* exposure to gram-negative bacterial lipopolysaccharide, together with analysis of ex vivo monocytes from septic patients. We identify TET2-mediated demethylation and transcriptional activation of inflammation-related genes that is specific to toll-like receptor stimulation. Changes also involve phosphorylation of STAT1, STAT3 and STAT5, elements of the JAK2 pathway. JAK2 pathway inhibition impairs the activation of tolerized genes on the first encounter with lipopolysaccharide. We then confirm the implication of the JAK2-STAT pathway in the aberrant DNA methylome of patients with sepsis caused by gram-negative bacteria. Finally, JAK2 inhibition in monocytes partially recapitulates the expression changes produced in the immunosuppressive cellular state acquired by monocytes from gram-negative sepsis, as described by single cell-RNA-sequencing. Our study evidences both the crucial role the JAK2-STAT pathway in epigenetic regulation and initial response of the tolerized genes to gram-negative bacterial endotoxins and provides a pharmacological target to prevent exacerbated responses.

Introduction

Organisms are steadily exposed to threats from other species. Innate immune cells are the first line of host defense against invading pathogens. They activate the adaptive immune system to restore homeostasis and remove the infection (1). In innate immune cells, recognition of pathogen-associated molecular patterns (PAMPs) activates toll-like receptors (TLRs), triggering robust inflammatory responses (2). Different mammalian TLRs recognize distinct microbial ligands. For instance, Gram-negative bacterial lipopolysaccharide (LPS) specifically activates TLR4, while Pam3Cys-Ser-Lys4 (P3C), a synthetic analog of the triacylated N-terminal part of bacterial lipoproteins, binds TLR2.

TLR2/4 signaling, inflammatory-related transcription factors such as nuclear factor kappa-light-chain-enhancer of activated B cells (NF- κ B), activator protein 1 (AP-1) and interferon regulatory factors (IRFs) are activated (3,4). Moreover, as a consequence of the autocrine or paracrine activation of cytokine receptors such as interferon receptors, Janus kinases (JAKs) are, in turn, activated, which leads to the phosphorylation and recruitment of members of the signal transducer and activator of transcription (STAT) protein family. Phosphorylated STAT dimers are then translocated to the nucleus, where they bind to specific DNA sequences and initiate gene transcription (5). JAK/STAT activation is tightly regulated by members of the suppressors of cytokine signaling (SOCS) protein family, protein inhibitors of activated STATs (PIAS) and protein tyrosine phosphatases (PTPs) (6).

Monocytes and macrophages are highly plastic innate immune cells involved in phagocytosis and cytokine release. After stimulation, monocytes, being key mediators of the initial immune response, rapidly

Articles

migrate to tissues (7). Monocytes and macrophages develop endotoxin tolerance, a state of hyporesponsiveness following a first challenge with microbial ligands (8). Tolerant cells show an altered immune response, characterized by lower production of pro-inflammatory cytokines (TNF α , IL-6, IL-1 β , etc) and higher levels of anti-inflammatory cytokines (IL-10, TGF β , etc.) (9). Downregulation of major histocompatibility complex (MHC) class II molecules under endotoxin tolerance has also been observed (10). This immunosuppressive state can be achieved under pathological conditions, such as the state following a sepsis episode. Sepsis is characterized by a dysregulated inflammatory response driven by an infection. It is a potentially lethal disease, and, in particular, a major cause of death in intensive care units (11). Peripheral blood mononuclear cells (PBMCs) from patients with sepsis exposed *ex vivo* to LPS, express lower levels of TNF α , IL-6 and IL-1 β compared with controls (12) and upregulated levels of IL-10 (13).

Exposure to LPS and other bacterial antigens results in epigenetic remodeling. For instance, LPS-treated murine monocytes display a group of tolerized genes with reduced gene expression and active histone marks after a second stimulus in comparison with untreated monocytes (14). Moreover, LPS-treated human monocytes show reduced levels of histone H3K27ac and H3K4me1 at promoters and enhancers of phagocytic and lipid metabolism genes(15). In addition, genome-wide analyses in human macrophages showed specific epigenetic signatures in H3K4me3, H3K27Ac and H3K4me1 histone marks for LPS tolerant cells (16). Studies in human monocytic THP-1 cells also revealed that H3K9 dimethylation of the promoters of the TNF α and IL-1 β genes is responsible for their silencing during endotoxin tolerance (17). In fact, the

histone H3K9 methyltransferase G9a, combined with HP1 and DNA methylation machinery, regulates TNF α gene expression (18).

Understanding the molecular and cellular mechanisms by which TLR stimulation with bacterial endotoxins results in the acquisition of tolerance could have clinical applications in new biomarkers or promising therapies. DNA methylation is potentially relevant following TLR stimulation, given its importance in monocyte/macrophage biology(19,20) and its relative stability compared with other epigenetic marks. Recently, specific DNA methylation changes were found in monocytes from patients with sepsis associated with several clinical factors and functional features, supporting their relevance to the monocyte response to bacterial molecules and the course of the disease (21).

In this study, we integrate DNA methylation and transcriptome changes following *in vitro* exposure to bacterial LPS, which leads to endotoxin tolerance. We report a negative correlation between the two processes and a temporal sequence in relation to accessibility and active histone marks gains. Moreover, we show that JAK2-mediated pathways have a critical role in establishing the LPS-driven transcriptome and methylome remodeling, most probably due to engagement of the IFN γ R upon autocrine/paracrine IFN γ release, secondary to LPS activation, establishing a potential link with the regulation of genes that become tolerized. Our data on monocytes isolated from patients with sepsis indicate that JAK2-STAT pathway-associated methylation and expression alterations are relevant to patients infected with gram-negative bacteria, and that the pharmacological activation of this pathway could improve the regulated expression of genes that become tolerized, providing a potential target to modulate their inflammatory response.

Materials and methods

Human samples

We selected and diagnosed patients with sepsis based on the criteria of the Third International Consensus Definitions for Sepsis and Septic Shock (Sepsis-3) (22). For each patient, we calculated the Sequential [Sepsis-related] Organ Failure Assessment (SOFA) score. The study included 5 patients (1 male and 4 females) with bacterial infections with SOFA scores ranging from 2 to 8 and 6 healthy donors (2 male and 4 females). Both patients and healthy donors were obtained at the Intensive Care Unit and Immunology Service of Vall d'Hebron University Hospital. Blood samples from patients were collected within 12 h of sepsis diagnosis, which was confirmed using clinical and analytical data. The Committee for Human Subjects of Vall d'Hebron University Hospital (PR (ATR)122/2019) approved the study, which was conducted in accordance with the ethical guidelines of the 1975 Declaration of Helsinki. All samples were collected and processed in compliance with the guidelines approved by the local ethics committee. All participants (patients with sepsis and healthy controls) received oral and written information about the possibility that their blood would be used for research purposes before they gave their signed informed consent.

CD14+ monocytes purification and culture

For *in vitro* experiments, we obtained buffy coats from anonymous donors via the Catalan Blood and Tissue Bank (CBTB). The CBTB follows the principles of the World Medical Association (WMA) Declaration of Helsinki. Before providing blood samples, all donors received detailed oral and written information and signed a consent form at the CBTB. PBMCs were isolated by density-gradient centrifugation

using lymphocyte-isolation solution (Rafer, Zaragoza, Spain). Pure monocytes (MO) were then isolated from PBMCs by positive selection with magnetic CD14 MicroBeads (Miltenyi Biotec, Bergisch Gladbach, Germany). The purity was verified by flow cytometry, obtaining more than 96% of CD14⁺ cells. Purified monocytes were resuspended in Roswell Park Memorial Institute (RPMI) Medium 1640 + GlutaMAX™ (Gibco, ThermoFisher) containing 10% human pooled serum (One Lambda, ThermoFisher Scientific Brand, West Hills CA, USA), 100 units/mL penicillin, and 100 mg/mL streptomycin. Monocytes were untreated (control), or treated with lipopolysaccharide (LPS) (10 ng/ml from *E. coli* O111:B4, Sigma-Aldrich, Darmstadt, Germany), and 10 µg/ml Pam3Cys (P3C) (InvivoGen San Diego, CA, USA). After 24 hours, monocytes were washed and left to rest for 3 days in medium supplemented with human pooled serum. Cells were then re-stimulated with LPS (10 ng/ml) and after 1 day, pelleted cells and supernatants were collected and stored until use.

For JAK2 inhibition of LPS monocytes (LPS+iJAK2 monocytes), cells were grown under the same conditions as mentioned above, and in the presence of fedratinib 500 nM (formerly known as TG101348, Santa Cruz Biotechnology), unless a different concentration is indicated.

Transfection of primary human monocytes

We used ON-TARGETplus siRNAs (GE Healthcare Dharmacon) against TET2 to perform knockdown experiments in monocytes. We also used ON-TARGETplus Non-targeting Control Pool as a negative control. CD14⁺ monocytes were transfected with siRNAs (100nM) using Lipofectamine 3000 Reagent. siRNAs were added 24h before the first stimulus and then, we performed stimulation experiments as mentioned

Articles

above. Finally, the levels of the target genes were examined by qRT-PCR at day 4.

Cytokine measurements

The cytokines levels were measured from the cell culture supernatants using an enzyme-linked immunosorbent assay (ELISA), according to the manufacturer's instructions (BioLegend, San Diego, CA, USA). In addition, the Pre-defined Human Inflammatory Panel LegendPlex™ (BioLegend) was used for the simultaneous analysis of 13 cytokines (CCL2, IFN- α 2, IFN- γ , IL-1 β , IL-6, IL-8, IL-10, IL-12p70, IL-17A, IL-18, IL-23, IL-33, and TNF α) related to inflammation in the same samples, in accordance with the manufacturer's instructions.

DNA methylation profiling and pyrosequencing

Infinium MethylationEPIC BeadChip (Illumina, Inc., San Diego, CA, USA) arrays were used to analyze DNA methylation. This platform allows over 850,000 methylation sites per sample to be interrogated at single-nucleotide resolution, and covers 99% of reference sequence (RefSeq) genes. The samples were bisulfite-converted using EZ DNA Methylation-Gold™ Kit (Zymo Research, CA, USA) and were hybridized in the array following the manufacturer's instructions.

Each methylation data point was obtained from a combination of the Cy3 and Cy5 fluorescent intensities from the M (methylated) and U (unmethylated) alleles. For representation and further analysis, we used beta (β) and M values. The β value is the ratio of the methylated probe intensity to the overall intensity (the sum of the methylated and unmethylated probe intensities). The M value is calculated as the \log_2 ratio of the intensities of the methylated versus unmethylated probe. β values were used to derive heatmaps and to compare DNA methylation

percentages from bisulfite-pyrosequencing experiments. For statistical purposes, the use of M values is more appropriate, because their degree of homoscedasticity fits better with linear model assumptions.

Bisulfite pyrosequencing was used to validate CpG methylation changes. DNA was isolated using a Maxwell® RSC Cultured Cells DNA Kit (Promega). Bisulfite modification of genomic DNA isolated from monocytes was performed using an EZ DNA Methylation-Gold™ Kit (Zymo Research), following the manufacturer's protocol. Primers for PCR amplification and sequencing were designed with PyroMark® Assay Design 2.0 software (QIAGEN, Hilden, Germany). PCRs were performed with the IMMOLASE™ DNA polymerase PCR kit (Bioline), and the success of amplification was assessed by agarose gel electrophoresis. PCR products were pyrosequenced with the Pyromark Q24 system (QIAGEN).

Quality control, data normalization, and detection of differentially methylated CpGs

Methylation array data were processed with the statistical language R using methods from the Bioconductor packages minfi, and limma. Data quality was assessed using the standard pipeline from shinyepico (23) and minfi packages (24). The data were Illumina-normalized, and beta and M values were then calculated. We excluded CpGs with overlapping SNPs. M values were used to build a linear model using the limma package in R, including the donor as a covariable.

In this study, we considered a CpG to be differentially methylated when the FDR is lower than 0.05. For representation purposes, beta-values are batch-corrected with the `removeBatchEffect` function of the

Articles

limma package, using the same covariables of the linear model, when it is indicated in the figure legend.

RNA purification and RNA-seq analysis

Total RNA of uncultured monocytes, LPS monocytes, LPS+iJAK2 monocytes, and untreated monocytes were isolated using a Maxwell® RSC simplyRNA kit (Promega, Wisconsin, USA).

RNA-seq libraries were generated, selecting only mRNA with oligo-dT capture beads, and sequenced in the Genomics Unit of the Centre for Genomic Regulation (CRG) (Barcelona, Spain), with an Illumina HiSeq 2500 sequencer, in 50-bp paired-end in 50-bp paired-end. Around 100 million reads were obtained for each sample.

Fastq files were aligned to the hg38 transcriptome using HISAT2 (25) with standard options. Reads mapped in proper pair, being primary alignments were selected with samtools (26). Reads were assigned to genes with FeatureCounts (27).

Differentially expressed genes were detected with DESeq2 (28). The donor was used as a covariable in the model. The Ashr shrinkage algorithm was applied and only protein-coding genes with $\text{abs}(\log\text{FC}) > 1$ and $\text{FDR} < 0.05$ were selected as differentially expressed.

For representation purposes, Variance Stabilizing Transformation (VST) values and normalized counts provided by DESeq2 were used.

Gene ontology over-representation analysis, Gene Set Enrichment Analysis and transcription factor enrichment analysis

Gene ontology (GO) over-representation of differentially methylated CpGs was analyzed using the Genomic Regions Enrichment of Annotations Tool (GREAT, version 4.0.4) (<http://great.stanford.edu/public/html/>), adopting the standard options (29) and using EPIC array CpGs as background. Enrichment is measured as the $-\log_{10}$ binomial FDR.

Gene Set Enrichment Analysis (GSEA) was performed from the LPS versus untreated, and LPS versus LPS-iJAK2 comparisons. Genes were ranked using this formula: $-\log_{10}(\text{FDR}) * \text{sign}(\log(\text{FC}))$. As genesets collection, hallmarks (H) from the Molecular Signatures Database (MSigDB) were selected, adding the specified custom genesets. GSEA analysis and graphs were created with the ClusterProfiler (30) and enrichplot Bioconductor packages. Gene Ontology over-representation of upregulated and downregulated protein-coding genes was performed with ClusterProfiler, using all detected protein-coding genes as background.

We used the findMotifsGenome.pl command in the Hypergeometric Optimization of Motif EnRichment (HOMER) suite to look for motifs that are enriched in the target set relative to the background set (software v4.11) (31). It was used to identify enrichment of TF binding motifs in the 250bp-window upstream and downstream of the differentially methylated CpG sites. Annotated CpGs in the EPIC array were used as background.

Articles

Accessibility and histone-mark profiling of differentially methylated CpGs

Using public data sets of ATAC-seq and H3K4me1 and H3K27ac ChIP-seqs of untreated and LPS-treated monocytes at 1, 4 and 24 hours (15), the accessibility and histone mark occupancy in the differentially methylated CpG genomic positions were calculated. Moreover, data of whole-genome bisulfite sequencing (WGBS) of the same reference were also utilized.

Graphs of the ATAC-seq and WGBS data were created with the deeptools toolkit (32).

For ChIP-seq data of H3K27ac and H3K4me1, bed files were downloaded from the BLUEPRINT portal (<http://dcc.blueprint-epigenome.eu/>). A file for each histone mark, cell type, and time point was used. Enrichment of these histone marks around the CpG positions (-3kb, 3kb) was studied applying a Fisher's Exact Test to compare them with the background (EPIC array CpGs), dividing the studied region in tiles of 10 bp. The calculated odds ratio of each tile is represented.

Methylation and expression association

Hypomethylated CpGs were associated with the nearest TSS using the `annotatePeaks.pl` command in the HOMER suite (31). After removing duplicate genes, expression of that gene set was studied using a public dataset of an RNA-seq time course (15) and our RNA-seq data.

Quantitative reverse-transcription polymerase chain reaction (qRT-PCR)

Total RNA was isolated with a Maxwell® RSC simplyRNA kit (Promega, Wisconsin, USA) and reverse-transcribed using a Transcriptor First Strand cDNA Synthesis Kit (Roche, Basel, Switzerland), in accordance with the manufacturer's instructions. qRT-PCR was performed in triplicate using LightCycler® 480 SYBR Green Mix (Roche). The standard double delta Ct method was used to determine the relative quantification of target genes, and values were normalized against the expression of endogenous control genes such as *RPL38*.

Western blotting

Cytoplasmic and nuclear protein fractions were obtained using hypotonic lysis buffer (Buffer A; 10 mM Tris pH 7.9, 1.5 mM MgCl₂, 10mM KCl supplemented with protease inhibitor cocktail (Complete, Roche) and phosphatase inhibitor cocktail (PhosSTOP, Roche) to lyse the plasma membrane. Protein pellets were resuspended in Laemmli 1X loading buffer.

Proteins were separated by SDS-PAGE electrophoresis. Immunoblotting was performed on polyvinylidene difluoride (PVDF) membranes following standard procedures. Membranes were blocked with 5% bovine serum albumin (BSA) and blotted with primary antibodies. After overnight incubation, membranes were washed three times for 10 minutes with TBS-T (50 mM Tris, 150 mM NaCl, 0.1% Tween-20) and incubated for 1 hour with HPR-conjugated mouse or rabbit secondary antibody solutions (Thermo Fisher) diluted in 5% milk (diluted 1/10000). Finally, proteins were detected by chemiluminescence using WesternBright™ ECL (Advansta). The following antibodies were used:

Articles

Phospho-STAT3 (Tyr705) (D3A7), rabbit mAb (Cell Signaling Technology, ref: #9145; Phospho-STAT5b (Tyr694) (C11C5), rabbit mAb (Cell Signaling Technology, ref: #9359), Phospho-STAT1 (Tyr701) (58D6), rabbit mAb (Cell Signaling Technology, ref: #9167); Phospho-STAT6 (Tyr641) Antibody (Cell Signaling Technology, ref: #9361); STAT3 (79D7), rabbit mAb (Cell Signaling Technology, ref: #4904); STAT5B (Millipore, ref: #06-969), STAT1(42H3), rabbit mAb (Cell Signaling Technology, ref: #9175; LaminB1 (Abcam, ref: #ab65986).

pSTAT1 flow cytometry

Peripheral blood mononuclear cells (PBMCs) were purified from blood samples of septic patients and healthy donors by density gradient centrifugation using lymphocytes isolation solution (Rafer, Zaragoza, Spain). PBMCs were counted and 5 million per condition were cultured in T25 flasks in Roswell Park Memorial Institute (RPMI) Medium 1640 + GlutaMAX™ (Gibco, Life Technologies, CA, USA) containing 2% Fetal Bovine Serum (FBS), 100 units/mL penicillin, and 100 mg/mL streptomycin, for 4 hours, with or without LPS (10 ng/ml from *E. coli* O111:B4, Sigma-Aldrich, Darmstadt, Germany). Cells were collected and stained with CD14 (APC) (Miltenyi Biotec, ref: #130-091-243), CD15 (FITC), and pSTAT1 (mouse Anti-pStat1 BV421 (pY701), BD Biosciences; ref: #562985), using mouse IgG2a, κ Isotype BV421 (BD Biosciences; ref: #563464) as a control according to the BD Fixation/Permeabilization Solution Kit (#554714) and the antibodies manual.

Mann–Whitney U test and Student's paired t test

Data were analyzed with Prism version 6.0 (GraphPad). Statistical analyses consisted of non-parametric Mann–Whitney U tests, to determine differences between pairs of separate groups, and Student's paired t test, to compare the means of matched pairs of groups, except where indicated otherwise. The levels of significance were: *, $p < 0.05$; **, $p < 0.01$; ***, $p < 0.001$.

RNA-seq public data reanalysis

Counts matrix from a RNA-seq experiment (GSE133822) was downloaded from the Gene Expression Omnibus database. Only septic patients and healthy donors were used.

Differentially expressed genes were detected with DESeq2. The donor was used as a covariable in the model. The Ashr shrinkage algorithm was applied and only protein-coding genes with $\text{abs}(\log\text{FC}) > 1$ and $\text{FDR} < 0.05$ were selected as differentially expressed.

Results

TLR2/4 stimulation of monocytes yields specific DNA demethylation

To investigate the mechanisms underlying DNA methylation changes associated with the exposure to bacterial endotoxins that lead to tolerance, human CD14⁺ monocytes isolated from healthy donor blood were pre-incubated for 24 hours with lipopolysaccharide (LPS) or Pam3Cys (P3C), which signal through TLR4 and TLR2, respectively, and lead to a tolerized state. After the first stimulation, cells were washed and left to rest for 3 days in the presence of human pooled serum. Cells were then stimulated again with LPS for another 24 hours (Figure 1A). Monocytes maintained with only RPMI medium and serum for 1 + 3 days (∅; ‘untreated’) were used as negative controls. Under these conditions, we confirmed that cells pre-exposed to LPS or P3C produced much lower levels of TNF α after a second exposure to LPS (Figure 1B).

We then obtained the DNA methylation profiles using Infinium MethylationEPIC bead arrays of bisulfite-treated biological triplicates of monocytes, exposed for 24 hours to LPS or P3C, and after the 3-day resting period, with the matching untreated controls (4-days cultured monocytes; ∅; ‘untreated’) and ‘uncultured’ monocytes at day 0 (MO).

Statistical analysis of the data revealed specific DNA methylation changes between LPS-/P3C-treated, untreated monocytes and uncultured monocytes (Figure S1A, see at the end of the article, pages 160-166). Methylation changes produced with LPS and P3C are comparable (Figure S1B), suggesting that downstream events following engagement of TLR4 and TLR2 respectively (Figure S1C) converge in the acquisition of similar DNA methylome changes.

Since LPS has a more intense effect than P3C (Figure S1D), as reflected in the greater number of differentially methylated sites, but a very similar pattern (Figure S1E), we focused on the analysis of changes between LPS-treated and untreated monocytes. We found 331 hypomethylated and 29 hypermethylated CpGs, with an FDR < 0.05 and a $\Delta B > 0.2$. (Figure 1C and Supplementary Table 1). LPS-hypomethylated CpGs were located mostly in intergenic and intronic regions and were outside CpG islands (Figure 1D).

We then compared our DNA methylation data in relation to a time series (1, 4, 24 hours) of chromatin accessibility and DNA methylation datasets obtained under similar conditions (15). Interestingly, chromatin accessibility of the genomic positions bearing LPS-specific hypomethylated CpGs in LPS-treated monocytes started to increase very quickly (1 hour) and increased progressively over time (Figure 1E). In contrast, demethylation at such sites was only observed after 24 hours, indicating that accessibility precedes DNA methylation loss (Figure 1F). Similar to the changes in chromatin accessibility, histone marks characteristic of active enhancers (H3K4me1 and H3K27ac) also increased faster than DNA methylation changes (Figure 1G). No significant enrichment in other histone marks was found (Figure S1F). In summary, the genomic composition and dynamics of LPS-demethylated sites indicate that a high proportion of methylation changes occur in regulatory regions, potentially controlling gene expression of phenotype-relevant genes. Moreover, these results suggest that LPS/P3C-driven demethylation requires a pioneer factor that can access closed chromatin following TLR4/TLR2 stimulation to enable, directly or indirectly, such specific demethylation.

Figure 1

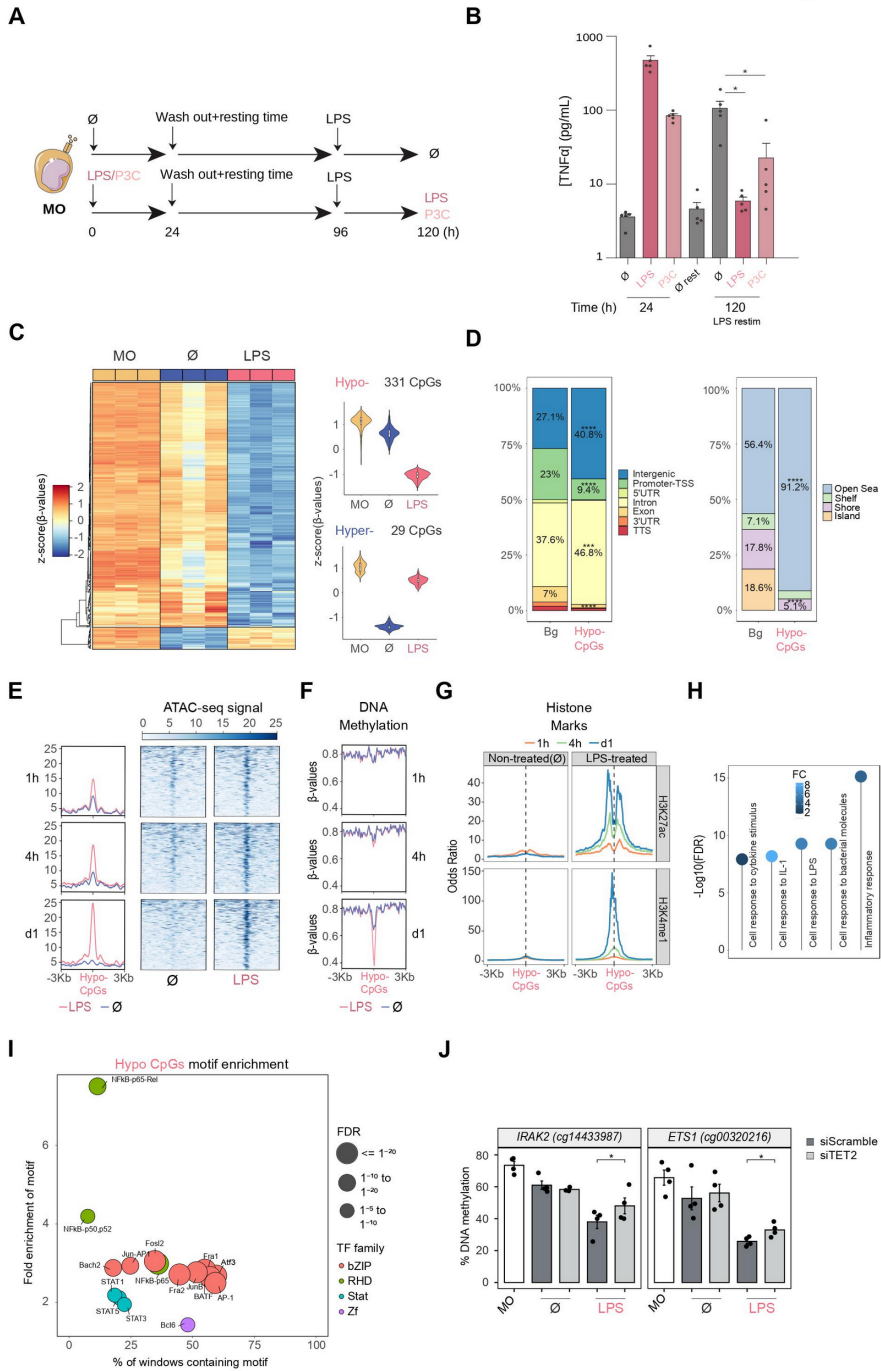


Figure 1. DNA methylation profile of LPS-treated human CD14⁺ monocytes.

(A) Schematic diagram depicting *in vitro* experiments for endotoxin tolerance models. (B) Release of TNF α from CD14⁺ monocytes isolated from healthy donor blood samples treated with LPS (10 ng/ml, 24 hours) or P3C (10 μ g/ml, 24 hours), then washed and rested (3 days) and treated again for 24 hours with LPS (10 ng/ml). These are all compared with untreated monocytes. Graphs show the mean \pm SEM of five healthy donors. (C) DNA methylation heatmap of differentially methylated CpGs comparing untreated monocytes (\emptyset) with LPS monocytes ($\Delta\beta \geq 0.2$, adjusted p (FDR) < 0.05). Scaled β -values are shown, ranging from -2 (lower DNA methylation levels, blue) to +2 (higher methylation levels, red). On the right, violin plots of hypomethylated and hypermethylated clusters depicting normalized DNA methylation data. (D) Barplot presenting the percentages of different genomic features of hypomethylated CpGs in comparison with background (Bg) CpGs (left panel), and barplot of CpG island contexts (right panel). FDRs of the Fisher's exact tests to estimate the enrichment or depletion in categories of hypomethylated CpGs in comparison with Bg are also shown (*, $p < 0.05$; **, $p < 0.01$; ***, $p < 0.001$; ****, $p < 0.0001$) (E) Accessibility (ATAC-seq) data of hypomethylated CpGs after 1, 4 and 24 hours of monocyte culture with LPS (in red) or without treatment (\emptyset) (in blue). Public ATAC-seq data were used (15) (F) Methylation of hypomethylated CpGs after 1, 4 and 24 hours of monocyte culture with LPS (in red) or without treatment (\emptyset) (in blue). Public WGBS data were used (15). (G) ChIP-seq data of H3K27ac and H3K4me1 of LPS-treated and untreated monocytes were downloaded from the Blueprint database. Odds ratios were calculated for bins of 10 bp up to ± 3000 bp around hypomethylated CpGs. CpGs annotated in the EPIC array were used as background. (H) GO (Gene Ontology) over-represented categories in the hypomethylated CpGs. The fold change relative to the background (EPIC array CpGs) and $-\log_{10}(\text{FDR})$ is shown. (I) Bubble scatterplot of TF binding motif enrichment for hypomethylated CpGs. The x-axis shows the percentage of windows containing the motif; the y-axis shows the magnitude of enrichment of the motif. Bubbles are colored according to TF family. FDR is indicated by bubble size (selected TF with $\text{FDR} \leq 1e^{-05}$). (J) DNA methylation measured by bisulfite pyrosequencing after TET2 silencing with siRNA (siTET2) in comparison with a control siRNA (siScramble). One-tailed t-test p values are depicted (*, $p < 0.05$).

Gene ontology (GO) over-representation analysis of hypomethylated CpGs in LPS-treated monocytes revealed the enrichment of functional categories associated with monocyte/macrophage cell biology and inflammation including cell response to cytokine stimulus, cell response to IL-1, cell response to bacterial molecules and inflammatory response (Figure 1H). In contrast, GO analysis of demethylated sites specific to untreated monocytes included regulatory categories such as regulation of IL-1 production, negative regulation of LPS signaling, and negative regulation of IL-12 production (Figure S1G).

To detect potential transcription factors involved in the demethylation process, we performed motif enrichment analysis. Hypomethylated CpGs of LPS-treated monocytes were enriched in transcription factor binding motifs relevant to inflammation such as NF- κ B, the AP-1 family, and some members of the STAT family (STAT1, STAT5 and STAT3) (Figure 1I). In contrast, demethylated sites specific to ‘untreated’ monocytes (4-days culture without exposure to LPS) also contained motifs for NF- κ B and AP-1, but not STAT family members (Figure S1H), suggesting a specific role for this transcription factor family in the LPS-driven demethylation process most probably due to a second wave of chromatin changes triggered by IFN release a consequence of LPS-mediated monocyte response and the subsequent activation of the IFNR/JAK2-STAT axis that can in turn activate TET2 (33).

To validate the methylation array results, we performed bisulfite pyrosequencing on a selection immune relevant genes, such as *CCL20*, *ETSI*, *HDAC9*, *IL24*, *IL2RA*, *IL36G* and *IRAK2*, from our methylation screening (Figure S1I).

Under these conditions, MOs do not proliferate. Therefore, any loss of DNA methylation is replication-independent or, in other words, resulting from an active demethylation mechanism. Ten-eleven translocation methylcytosine dioxygenases (TET) mediate active demethylation. TET2 has been implicated in catalyzing active demethylation in other monocyte-related differentiation processes (19,34). We then downregulated TET2 to determine whether this enzyme was involved in the demethylation processes observed under our conditions. Using specific siRNAs, we achieved around 50% TET2 downregulation, in both mRNA and protein levels after 3 days of treatment (Figure S1J, Figure S1K). Under these conditions, demethylation of LPS-specific hypomethylated CpG sites was partially impaired (Figure 1J), demonstrating the involvement of TET2 in this process.

LPS-driven gene expression changes are correlated with DNA methylation and are concomitant with STAT1, STAT3 and STAT5 activation

We performed RNA-seq with LPS-stimulated monocytes under the same conditions as before (3-day cultured monocytes following 24h stimulation), including ‘untreated’ and ‘uncultured’ monocytes. LPS exposure induced upregulation of 1142 genes and downregulation of 1025 genes ($\log_{2}FC > 1$, $FDR < 0.05$) in relation to ‘untreated’ monocytes (Figure 2A and Supplementary Table 2). Principal component analysis (PCA) showed that LPS-treated and ‘untreated’ monocytes were separated along the axis of PC2, and these two along the PC1 axis with respect to ‘uncultured’ monocytes (Figure S2A).

In the Gene Set Enrichment Analysis (GSEA), LPS-treated monocytes were enriched in significant inflammatory pathways such as

Articles

TNF α signaling via NF- κ B, inflammatory response, interferon gamma/alpha response, and IL6/JAK/STAT3 signaling (Figure 2B), indicating that the downstream targets of these signaling pathways had been transcriptionally activated. On the other hand, pathways depleted in LPS-treated monocytes included oxidative phosphorylation, MYC targets and fatty acid metabolism, as has also been described by others (Figure S2B) (35,36).

Similarly, GO over-represented categories in LPS-upregulated genes included terms such as cytokine secretion, response to interferon-gamma, response to LPS, and the JAK-STAT cascade (Figure 2C), with coincident categories with hypomethylated CpG GO categories (Figure 1H), whereas LPS-downregulated GO categories were related to metabolism (Figure S2C).

To identify possible transcription factors leading to gene upregulation, we performed Discriminant Regulon Expression Analysis (DoRothEA) (37), with which we identified several candidates coincident with those identified in our previous HOMER analysis of the LPS-specific DNA demethylation set: STAT (STAT1, STAT2, STAT3, STAT5B), NF- κ B (RELA, NFKB1) and AP-1 (FOS) (Figure 2D). Additionally, in the set of downregulated genes, we found enrichment of transcription factors such as FOXP1, MYC and SREBF2 (Figure S2D).

The similarities of methylation and expression GO categories and transcription factors potentially involved in the demethylation and upregulation reinforce the notion of their mutual relationship. In fact, LPS-upregulated genes are enriched in hypo-CpG-associated genes, as revealed by the GSEA analysis (Figure 2E). We also found a significant inverse correlation between DNA methylation and expression (Figure 2F).

Figure 2

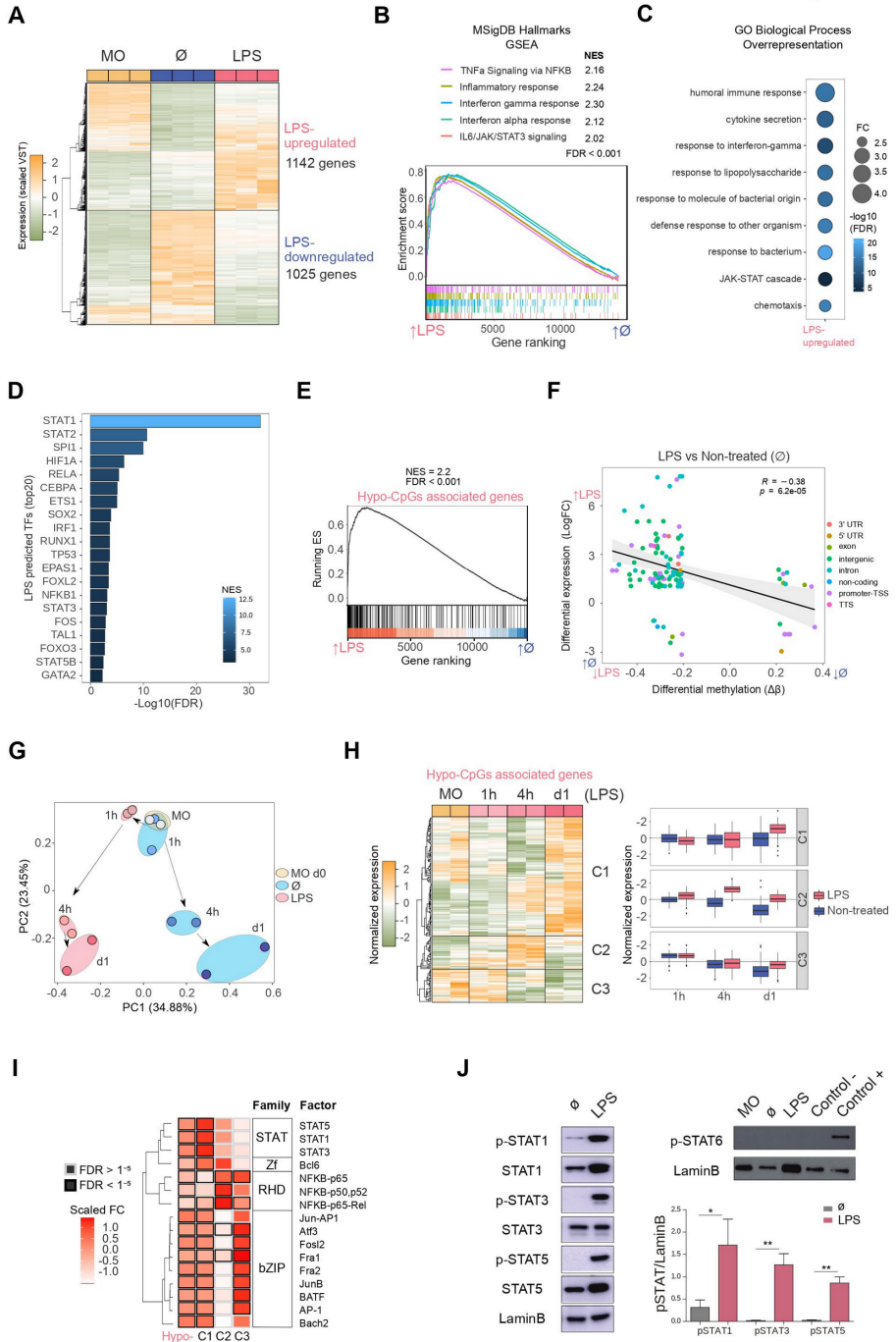


Figure 2. Gene expression, association with methylation and activation of JAK2-dependent STATs

(A) Gene expression heatmap of differentially expressed genes, comparing LPS monocytes with untreated (\emptyset) monocytes ($\text{LogFC} > 1$, $\text{FDR} < 0.05$). Scaled variance stabilizing transformation (VST) values are shown, ranging from -2 (lower gene expression level, green) to +2 (higher gene expression level, orange). (B) Gene set enrichment analysis (GSEA) of LPS versus untreated (\emptyset) monocytes, using MSigDB hallmarks (H) as gene sets. The running enrichment score and the normalized enrichment score (NES) are shown above the graph ($\text{FDR} < 0.001$). (C) Gene ontology (GO) over-representation of GO Biological Process categories. Fold change of LPS-upregulated genes relative to background and $-\log_{10}(\text{FDR})$ of the Fisher's exact tests are shown. (D) Discriminant regulon expression analysis (DoRothEA) of LPS versus untreated (\emptyset) monocytes. NES and $-\log_{10}(\text{FDR})$ of transcription factors (TFs) enriched on the LPS side are shown (20 TF with the highest NES and $\text{FDR} < 0.001$). (E) Hypomethylated CpGs were associated with the nearest gene. The resulting gene set (Hypo-CpG-associated genes) was used in the GSEA of LPS versus untreated (\emptyset) monocytes. The running enrichment score and the normalized enrichment score (NES) are shown above the graph ($\text{FDR} < 0.001$). (F) DNA methylation of differentially methylated CpGs was correlated with gene expression of differentially expressed genes in the LPS versus untreated (\emptyset) monocyte comparison. Expression is represented on the y-axis as the LogFC , where higher values indicate higher levels of expression in LPS monocytes, and lower values indicate higher levels of expression in untreated monocytes. DNA methylation is depicted on the x-axis as $\Delta\beta$, where lower numbers indicate lower levels of methylation in LPS monocytes, and higher numbers indicate lower levels of methylation in untreated monocytes. Points are colored according to their genomic context. A significant negative Pearson's correlation between methylation and expression was observed ($R = -0.38$, $p < 6.2e^{-05}$). (G) Hypo-CpG-associated gene expression was analyzed in time-course RNA-seq data from LPS-treated and untreated monocytes (15). Principal components 1 and 2 from a principal component analysis (PCA) of the expression data are shown. (H) Heatmap of Hypo-CpG-associated gene expression in a time-course RNA-seq, from LPS monocytes (left panel). The dendrogram can be considered to separate the sample into three clusters (C1, C2 and C3), depicting three distinct behaviors. Boxplot of normalized gene expression of genes in C1, C2 and C3 clusters, in LPS-treated (pink) and untreated (blue) monocytes. (I) Significant transcription factors of hypomethylated CpGs (Figure 1) were analyzed separately in the three clusters. Transcription factors are clustered by their position weight matrix differences. Scaled fold-change (FC) is represented as a color scale (a redder color indicates a greater change in relative to the background). The border of significant transcription factors ($\text{FDR} < 1e^{-5}$) are colored black; non-significant borders are shown in grey. (J) Western blot of protein phosphorylated STAT1, total STAT1, phosphorylated STAT3, total STAT3, phosphorylated STAT5 and total STAT5 (left panel) and phosphorylated-STAT6 (right panel) in LPS-treated relative to untreated (\emptyset) monocytes. LaminB was used as loading control. Signal of western blot bands was quantified for each replicate and pSTAT/LaminB signal ratio is shown ($n = 3-6$). One-tailed t-test p values are depicted (*, $p < 0.05$; **, $p < 0.01$).

Furthermore, using the expression data from the previously mentioned time-course study (1, 4 and 24 hours) in a similar model to ours (15), we monitored the expression of the LPS-hypomethylated CpGs-associated genes. Principal component analysis (PCA) revealed a divergent trajectory of LPS-treated and untreated monocytes (Figure 2G). The exposure of monocytes to LPS was sufficient to promote gene expression changes antagonistic to those in untreated monocytes, cultured without cytokines during the same period. Time-course expression analysis of LPS hypo-CpG-associated genes also revealed three main temporal clusters based on their dynamics (Figure 2H and Supplementary Table 3). The largest cluster (C1), showed an increase of gene expression at 24 hours, concomitant with DNA demethylation (Figure 2H and Figure 1F). In contrast, cluster 2 (C2) presented an increase of gene expression prior to DNA demethylation, but coincident with the accessibility and enhancer-associated histone mark gains. Finally, cluster 3 (C3) showed a reduction in gene expression over time, in untreated and LPS monocytes, although the effect was less pronounced in the latter. These data imply that DNA methylation has different relationships with gene expression changes, possibly depending on the genomic context, and that most DNA methylation changes require previous chromatin remodeling, consistent with the timing observed for those changes to appear. Whereas gene upregulation is concomitant with DNA demethylation in C1, DNA demethylation occurs after gene upregulation in C2 and C3.

C1-, C2-, and C3-associated CpGs also had distinctive genomic features (Figure S2E-2G). HOMER analysis of C1-associated CpGs (with concomitant increase of expression and demethylation) revealed specific enrichment of STAT1, STAT3 and STAT5 binding motifs, which were

Articles

not present in genes in C2 and C3 (Figure 2I), which points at the necessity of the activation of a second pathway such as IFN γ R/JAK2-STAT in response to LPS triggered events in order to promote DNA methylation changes.

Since individual and combined DNA methylation and gene expression analysis suggested a specific role for the STAT transcription factor family, we studied the protein levels and phosphorylation of STAT1, STAT3 and STAT5 (JAK2 targets) in LPS-treated and untreated monocytes. We observed an increase in the phosphorylation of these three transcription factors (Figure 2J) in LPS-treated samples. Moreover, P3C treatment also induces phosphorylation of JAK2 targets (Figure S2H). In contrast, phosphorylated-STAT6 (JAK3 target), which did not appear in our HOMER analysis, was not detected in LPS monocytes, providing further evidence of the potential specific involvement of JAK2-related pathways.

Inhibition of JAK2 partially prevents the activation of LPS-upregulated genes and tolerance-related genes

To investigate the potential role of JAK2 pathway in modulating tolerance-specific DNA methylation changes, we treated CD14⁺ monocytes with LPS (10 ng/ml) for 24 hours in the presence or absence of TG101348, a selective JAK2 inhibitor (iJAK2) (500 nM). Monocytes were washed and left to rest for 3 days (with or without iJAK2) and after that, cells were stimulated again with LPS (24 hours). Control experiments without LPS were performed in parallel. We confirmed by western blot and observed that JAK2-associated STAT phosphorylation was blocked by JAK2 inhibition, at 4 hours (left) and 96 hours (right) (Figure S3A).

To examine the effects of JAK2 inhibition on monocyte response, we measured the production of TNF α and IL-10 (Figure S3B). JAK2 inhibition resulted in decreased production of TNF α and increased IL-10 production after a second LPS stimulus (Figure S3B). This further reduction in TNF α production is consistent with the role of JAK2 in LPS-mediated inflammatory response (38).

We then performed RNA-seq of biological triplicates under the previously described cell conditions (LPS-treated monocytes, LPS+iJAK2-treated monocytes, untreated monocytes, and uncultured monocytes). JAK2 inhibition resulted in downregulation of 124 genes (iJAK2-downregulated genes), whereas only 6 genes were upregulated (LogFC > 1, FDR < 0.05) (iJAK2-upregulated genes) (Figure 3A and Supplementary Table 4).

The over-represented GO categories among the genes downregulated upon JAK2 inhibition (Figure 3B) were very similar to those found in LPS-upregulated genes (Figure 2C), including categories related to response to interferon-alpha, interferon-gamma, defense response to other organisms, etc. However, we found a generally higher magnitude change and a lower FDR in the iJAK2-downregulated genes than in the LPS-upregulated genes, suggesting specific and stronger enrichment in interferon-related genes. In this respect, the GSEA analysis revealed four hallmarks downregulated in LPS+iJAK2 cells: inflammatory response, IL6/JAK/STAT3 signaling, interferon gamma response and interferon alpha response (Figure 3C). These categories were previously associated with LPS-treated monocytes (Figure 2B).

DoRothEA analysis showed several putatively related transcription factors depleted in LPS+iJAK2 monocytes, including STAT1, STAT2,

STAT3, STAT5A and STAT5B (Figure 3D). NF- κ B was not identified by either the DoRothEA or the GSEA analysis, in contrast to the LPS-associated hallmarks and transcription factors (Figure 2B, Figure 2D).

A relationship, as suggested by previous data, was found between iJAK2-downregulated genes and LPS-upregulated genes. In a GSEA, iJAK2-downregulated genes were strongly enriched in LPS-upregulated genes side in comparison with Untreated(\emptyset) monocytes (Figure 3E).

We also found a link between iJAK2-downregulated genes and tolerized genes. Using a public dataset (15) of gene expression (\log_2 RPKM) of LPS-treated and untreated monocytes before and after a second LPS stimulus, we defined a ‘score’ of tolerization as $(\text{Untreatedreexposure} - \text{Untreated}) - (\text{LPSreexposure} - \text{LPS})$, where a positive score means that the gene is tolerized and a negative score that is non-tolerized. We then compiled a top100-tolerized gene-set comprising the 100 genes with the highest scores and a top100-non-tolerized gene-set comprising the 100 genes with the lowest scores. We performed a GSEA analysis of both gene-sets with the comparison LPS/LPS+iJAK2 and found specific significant enrichment of the tolerized genes but not of the non-tolerized genes among the iJAK2-downregulated genes (Figure 3F and Supplementary Table 5). Some examples of tolerized-gene expression are shown in Figure 3G, where the direct inhibition of their transcriptional activation by JAK2 inhibition is depicted. Notably, these genes are also involved in the IFN α or IFN γ response.

Figure 3

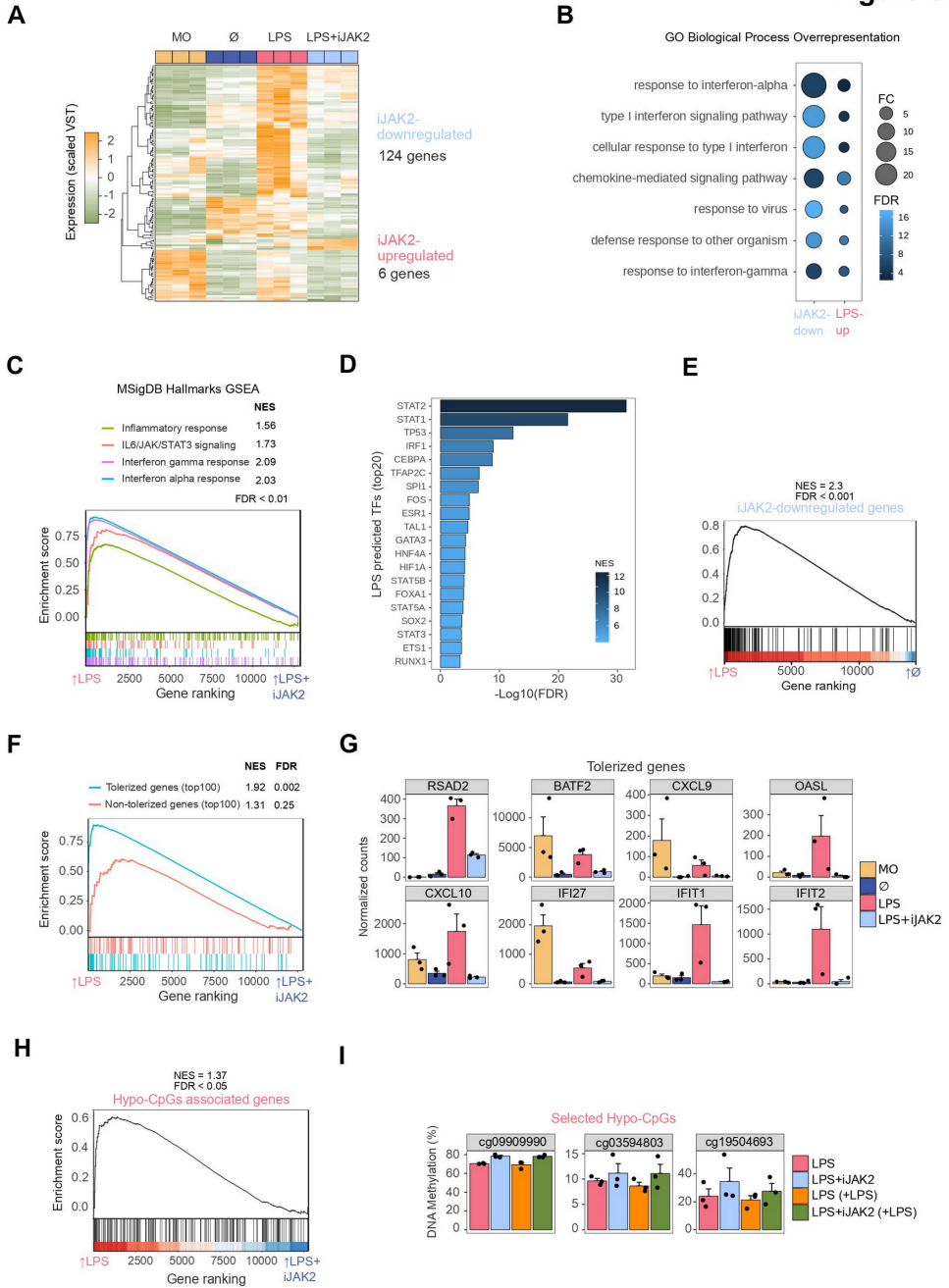


Figure 3. Role of JAK2-STAT in LPS monocytes gene expression and phenotype. (A) Gene expression heatmap of differentially expressed genes, comparing LPS with LPS+iJAK2 monocytes (LogFC > 1, FDR < 0.05). Scaled variance stabilizing transformation (VST) values are shown, ranging from -2 (lower gene expression level, green) to +2 (higher gene expression level, orange). (B) Gene ontology (GO) over-representation of GO Biological Process categories. Fold change of iJAK2-downregulated and LPS-upregulated genes relative to background and $-\log_{10}(\text{FDR})$ of the Fisher's exact tests are shown. (C) Gene set enrichment analysis (GSEA) of LPS-treated versus LPS+iJAK2-treated monocytes, using MSigDB hallmarks as gene sets. The running enrichment score and the normalized enrichment score (NES) are shown above the graph (FDR < 0.001). (D) Discriminant regulon expression analysis (DoRotheA) of LPS-treated versus LPS+iJAK2-treated monocytes. NES and $-\log_{10}(\text{FDR})$ of transcription factors (TF) enriched on the LPS side are shown (20 TF with the highest NES and FDR < 0.001). (E) GSEA of LPS-treated versus untreated (\emptyset) monocytes using the iJAK2-downregulated genes as the gene set. The running enrichment score and the normalized enrichment score (NES) are shown above the graph (FDR < 0.001). (F) Gene Set Enrichment Analysis (GSEA) of LPS vs LPS+iJAK2 monocytes using the top100 tolerized genes (blue) or the top100 non-tolerized genes (pink) as gene sets. Running enrichment score is represented and the normalized enrichment score (NES) and FDR are shown above. (G) Selected examples of iJAK2-downregulated genes (FDR < 0.05, logFC of LPS vs LPS+iJAK2 > 1). Bar plots show the mean \pm SEM (standard error of the mean) of normalized counts. (H) GSEA of LPS-treated versus LPS+iJAK2-treated monocytes using the Hypo-CpG-associated genes as the gene set. The running enrichment score and the normalized enrichment score (NES) are shown above the graph (FDR < 0.05). (I) DNA methylation percentage obtained from pyrosequencing of three selected CpGs from the hypo-CpG group in LPS monocytes, before and after a second LPS stimulus, and with or without iJAK2 treatment.

Given the correlation between our DNA methylation and expression datasets (Figure 2F), the enrichment of STAT1/3/5 in the individual and combined data, and the effects of JAK2-STAT inhibition in the regulation of some LPS-upregulated genes (Figure 3F), we studied the effects of the

inhibition of the JAK2-STAT pathway on hypomethylated CpG-associated genes. The GSEA of LPS versus LPS+iJAK2 monocytes revealed a small but significant enrichment in the LPS side, suggesting that genes related to CpGs hypomethylated with LPS are, at least partially, under the transcriptional control of the JAK2-STAT pathway (Figure 3H).

To determine whether the JAK2-STAT pathway is related to the LPS-specific DNA demethylation process we carried out pyrosequencing of three selected CpGs, with and without a second LPS stimulus (Figure 3I). A general trend of demethylation blockage was found, although only one CpG (cg09909990) had a p value < 0.05. The fact that iJAK2 did not fully inhibit the phosphorylation of STATs, and the possible redundancy of other JAK/STAT pathways could explain the heterogeneity in the triplicate.

Relevance of the JAK2-STAT pathway in monocytes from septic patients infected with gram-negative bacteria

Given the relevance of JAK2-STAT pathways secondary to LPS response in monocytes, and to the transcriptional regulation of tolerized genes, we compared the effect in DNA methylation of patients with sepsis caused by gram-negative bacteria in comparison with other patients with sepsis and patients with systemic inflammatory response syndrome (SIRS) following cardiac surgery, from our previous study (13). The comparison of healthy donors with gram-negative sepsis yielded 339 differentially methylated positions (DMPs) (FDR < 0.05), whereas only 1 DMP between healthy donors and other sepsis was found, and 0 DMPs between healthy donors and SIRS patients (Figure S4A). However, the heatmap and PCA of DMPs showed also a demethylation trend in other

sepsis, suggesting that similar upstream pathways are involved in both sepsis groups, with the highest effect in DNA methylation in patients with sepsis caused by gram-negative bacteria (Figure S4B, Figure S4C). Moreover, the gram-negative hypomethylated CpGs were enriched in STAT motifs (Figure S4D) and Gene Ontology categories related to inflammatory response and LPS stimulus (Figure S4E), showing high similarities with the motifs and Gene Ontology categories enriched in the LPS hypomethylated CpGs (Figure 1H, Figure 1I).

Interestingly, when we tested the set of hypomethylated CpGs in LPS-treated monocytes (Hypo-CpGs) with STAT1/3/5 binding motifs with the DNA methylation data of the sepsis and healthy donor's cohort, we found lower methylation levels in gram-negative sepsis patients in comparison with any of the other groups (Figure 4A), reinforcing the notion of the participation of the JAK2-STAT pathway in the first encounter with gram-negative bacteria under *in vivo* conditions.

To test whether the STAT activation was altered in patients infected with gram negative bacteria, we incubated PBMCs from patients with gram negative bacterial sepsis and healthy donors in RPMI (2% FBS) for 4 hours, in the presence of LPS (10 ng/mL) and in its absence. Since activated neutrophils can contaminate the PBMC section of Ficoll and can express CD14, we adopted a gating strategy to analyze only the intracellular pSTAT1 signal of CD14⁺ CD15⁻ cells (Q1) (Figure 4B). No differences were found between healthy donors and septic patients in the basal (unstimulated) signal of pSTAT1. However, after the LPS stimulus, pSTAT1 was increased in healthy donors, as expected, but decreased in septic patients (Figure 4C,4D).

To provide more insight into the JAK2-STAT1 pathway relevance in sepsis, we used expression data from CD14⁺ monocytes isolated from patients with sepsis and healthy age-matched (39). Interestingly, genes upregulated in septic patients are those inhibited by iJAK2 in our model, suggesting that the JAK2-STAT pathway is also involved in the transcriptomic changes after the first encounter with bacterial molecules in septic patients (Figure 4E).

Moreover, we utilized data from a single-cell study of PBMCs from septic patients (40), in which a specific monocyte subset associated with sepsis (MS1) is defined. After isolating that population from patients with sepsis caused by gram-negative bacteria and stimulating it with LPS *in vitro*, some genes (MS1 LPS-downregulated genes) were downregulated, revealing a tolerized phenotype. We performed a GSEA comparing the MS1 dataset with our LPS versus LPS+iJAK2 monocytes expression dataset revealing a downregulation of these genes, in our model, with iJAK2 treatment (Figure 4F).

This result is consistent with the decrease of STAT1 activation in monocytes from septic patients after an LPS stimulus (Figure 4B) and shows that the inhibition of JAK2 in monocytes can partially recapitulate the expression changes produced in septic monocytes after a second immune challenge.

Overall, the data suggest that the JAK2-STAT1 pathway is profoundly disturbed in patients with sepsis caused by gram-negative bacteria, producing reduced levels of pSTAT1 after a second immune challenge with LPS and potentially leading to abnormal STAT dependent gene expression patterns that could drive the dysfunctional monocyte response in septic monocytes. Our results may explain the previously reported

Articles

partial restoration of leukocytic function observed in septic patients after therapy with recombinant interferon- γ (41).

Figure 4

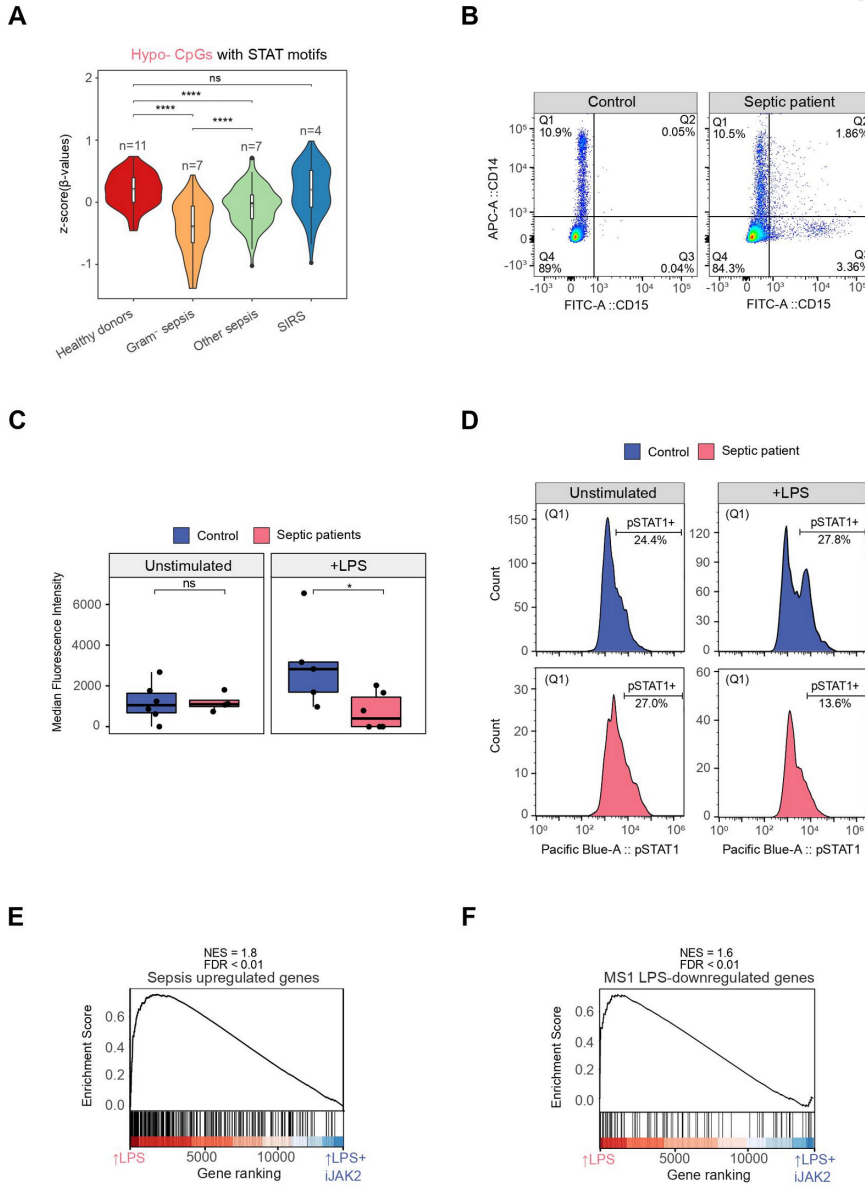


Figure 4. STAT1 phosphorylation in monocytes from healthy donors and septic patients with or without an LPS stimulus. (A) Violin plot of normalized β values of the LPS Hypomethylated CpGs associated with STAT1/STAT3/STAT5 motifs in CD14⁺ monocytes from peripheral blood of healthy donors, gram-negative sepsis, other sepsis and SIRS patients (91 CpGs). (B) Example of the strategy adopted to gate only monocytes. CD14⁺CD15⁻ (Q1) are mostly monocytes, whereas some CD15⁺ cells (neutrophils) can also express CD14 (Q2). (C) Median fluorescence intensity (pSTAT1) of monocytes (Q1) from septic patients (pink) and healthy donors (blue), with and without an LPS stimulus. Two-tailed Wilcoxon test p values are depicted (ns $p > 0.05$, * $p < 0.05$). (D) Example of a pSTAT1 signal histogram from a healthy donor (blue) and a septic patient (pink), with and without an LPS stimulus. (E) GSEA of LPS-treated versus LPS+iJAK2-treated monocytes using Sepsis upregulated genes ($\log_{FC} > 1$, FDR < 0.05). The running enrichment score and the normalized enrichment score (NES) are shown above the graph. (F) GSEA of LPS-treated versus LPS+iJAK2-treated monocytes using MSI LPS-downregulated genes (40) as gene set. The running enrichment score and the normalized enrichment score (NES) are shown above the graph.

Discussion

Our results indicate that TLR4/TLR2 stimulation induces specific TET2-dependent demethylation in monocytes, accompanying the acquisition of endotoxin tolerance. LPS (TLR4)-specific changes in DNA methylation are concomitant with upregulation of inflammatory-related genes, and these involve the JAK2-STAT pathway. Inhibition of the JAK2 pathway in this *in vitro* model of endotoxin tolerance impairs the upregulation of genes that become tolerized following a first encounter with bacterial LPS. The implication of this pathway is proven for patients with sepsis caused by gram-negative bacteria.

Many of the CpG sites that become demethylated after TLR4/TLR2 stimulation are associated with inflammatory genes. Examples include the chemokine *CCL20*, which has antimicrobial activity (42), *IL36G*,

member of the IL-1 cytokine family, and the inflammatory cytokine *IL-24* (43). Other demethylated CpGs are associated with genes encoding the transcription factor *ETSI* and the molecule *IRAK2*, an essential regulator for IL-1R and TLR signaling (44). CpGs undergoing LPS-driven demethylation, are preceded by increases in chromatin accessibility and H3K4me1/H3K27ac gains and correlate with transcriptional activation of the associated genes. This temporal uncoupling between chromatin accessibility, transcription and DNA methylation in terminally differentiated myeloid cells, has also been recently demonstrated by simultaneously assessing chromatin conformational changes and DNA methylation in a genome-wide manner on the same population of DNA molecules (ATAC-Me technique), supporting the idea of DNA methylation as a required event in during enhancer activation that underlies cell state transitions (45). Moreover, transcription factors can directly recruit DNMTs or TET enzymes and influence gene expression (46). Our analysis revealed that binding motifs of STAT1, STAT3 and STAT5, which are phosphorylated by JAK2, specifically associate with the observed LPS-specific hypomethylated CpGs and expression changes.

JAK/STAT signaling is not directly downstream of TLR4/TLR2 receptors, and its activation requires the production of other molecules, such as IFN γ or IL-6, in order to activate the pathways autocrinally or paracrinally through their receptors (6,47). This could explain why STAT factors are specifically associated with C1-associated CpGs, whose associated genes are 'late responsive' in comparison with others, upregulated prior to demethylation (C2- and C3-associated CpGs). These CpGs are enriched in NF- κ B and AP-1, directly downstream of TLR4/TLR2 signaling.

In our analysis, JAK2-STAT inhibition appeared to accentuate the tolerant phenotype of monocytes. JAK2 inhibition also reduces the expression of tolerized genes (15) following the first encounter with LPS, suggesting that these genes are under the transcriptional control of JAK2-STAT. In fact, several of these genes are also involved in the IFN α or IFN γ response. In contrast, JAK2 inhibition only partially interferes with LPS-driven DNA demethylation, supporting the existence of a complex genomic regulatory network in which JAK2-STAT plays a role in LPS-driven demethylation, but also involves the participation of additional pathways.

We can speculate whether the observed effects of this JAK2 inhibition could be countered by direct activation with, for instance, IFN γ , which could reduce the acquired endotoxin tolerance and restore the expression of some tolerized genes. In this respect, demethylation has been previously associated with the IFN γ pathway, through STAT1 stimulation, binding to TET2 and recruitment to specific sites in the genome (33). This suggests that the direct modulation of this pathway may have more widespread effects on DNA methylation and expression. In fact, a fundamental role of type 1 and type 2 interferon signaling in modulating response to endotoxin and endotoxin tolerance has been reported, including a clinical trial using IFN γ to mitigate immune paralysis in sepsis (41,48–51).

The link between tolerized genes and downregulated genes upon JAK2 inhibition indicates that JAK2-dependent signaling pathway dysfunction may contribute to the acquisition of endotoxin tolerance.

Moreover, LPS-driven demethylation of the *in vitro* model also occur in monocytes from gram-negative septic patients, and vice-versa, providing

Articles

a clinical significance of the *in vitro* model, and reinforcing the role of the JAK2-STAT pathway in septic monocytes.

Since monocytes from septic patients have been exposed to bacteria before they are extracted, they have a reduced immune response in a second immune challenge with LPS due to the endotoxin tolerance. We have shown that monocytes from septic patients exhibit a lower level of STAT1 phosphorylation after an immune challenge with LPS, compared with monocytes from healthy donors. This lower level of pSTAT1 due to a reduced activity of JAK2, could explain such a phenotype. In fact, IFN γ , whose receptor signals through JAK2, is believed to partially rescue the endotoxin tolerance phenotype in human monocytes (41), and IFN γ is sometimes used in sepsis treatment to improve immune host defense (52), perhaps activating JAK2 more intensively.

Taken together, our results demonstrate an important role of the JAK2-STAT pathway in the monocyte LPS response, both *in vitro* and *in vivo*, which contributes not only to the DNA methylation, but also to gene expression remodeling. We also show that dysfunction in this pathway can be related to the phenomenon of endotoxin tolerance, in an *in vitro* model and in *ex vivo* monocytes from septic patients.

Conflict of Interest

The authors declare that the research was conducted in the absence of any commercial or financial relationships that could be construed as a potential conflict of interest.

Author Contributions

O.M.-P., C.L.-S., L.C. and J.C.-S. conducted experiments; O.M.-P., C.L.-S., A.G.-G. and F.C.-M. performed bioinformatics analysis; A.R.S., M.M.-G., R.F.-R., J.C.R.-R. provided patient samples; O.M.-P., C.L.-S., J.C.-S., A.G.-G. A.R.S., M.M.-G., R.F.-R., J.C.R.-R., D.A.E and E.B. analyzed and interpreted the results; O. M.-P., C.L.-S., D.A.E and E.B. designed the experiments and wrote the paper.

Funding

E.B. was funded by the Spanish Ministry of Science, Innovation and Universities (grant numbers SAF2017-88086-R & PID2020-117212RB-I00), and was cofunded by FEDER funds/European Regional Development Fund (ERDF) - a way to build Europe. O.M.-P. holds an i-PFIS PhD fellowship (grant number IFI17/00034) from Acción Estratégica en Salud 2013-2016 ISCIII, cofinanced by the Fondo Social Europeo.

Acknowledgments

We thank the CERCA Programme/Generalitat de Catalunya and the Josep Carreras Foundation for institutional support.

References

1. Medzhitov R. Recognition of microorganisms and activation of the immune response. *Nature* (2007) doi:10.1038/nature06246
2. Brubaker SW, Bonham KS, Zanoni I, Kagan JC. Innate immune pattern recognition: A cell biological perspective. *Annu Rev Immunol* (2015) **33**:257–290. doi:10.1146/annurev-immunol-032414-112240
3. Akira S, Takeda K. Toll-like receptor signalling. *Nat Rev Immunol* (2004) doi:10.1038/nri1391
4. Kawai T, Akira S. Toll-like Receptors and Their Crosstalk with Other Innate Receptors in Infection and Immunity. *Immunity* (2011) doi:10.1016/j.immuni.2011.05.006
5. Leonard WJ, O’Shea JJ. JAKS AND STATS: Biological Implications. *Annu Rev Immunol* (2002) doi:10.1146/annurev.immunol.16.1.293
6. Shuai K, Liu B. Regulation of JAK-STAT signalling in the immune system. *Nat Rev Immunol* (2003) doi:10.1038/nri1226
7. Shi C, Pamer EG. Monocyte recruitment during infection and inflammation. *Nat Rev Immunol* (2011) doi:10.1038/nri3070
8. Medvedev AE, Sabroe I, Hasday JD, Vogel SN. Tolerance to microbial TLR ligands: Molecular mechanisms and relevance to disease. *J Endotoxin Res* (2006) **12**:133–150. doi:10.1179/096805106X102255
9. Biswas SK, Lopez-Collazo E. Endotoxin tolerance: new mechanisms, molecules and clinical significance. *Trends Immunol* (2009) **30**:475–487. doi:10.1016/j.it.2009.07.009

10. Wolk K, Döcke WD, von Baehr V, Volk HD, Sabat R. Impaired antigen presentation by human monocytes during endotoxin tolerance. *Blood* (2000) doi:10.1182/blood.v98.13.3800
11. Angus DC, Van Der Poll T. Severe sepsis and septic shock. *N Engl J Med* (2013) **369**:840–851. doi:10.1056/NEJMra1208623
12. Munoz C, Carlet J, Fitting C, Misset B, Blériot JP, Cavaillon JM. Dysregulation of *in vitro* cytokine production by monocytes during sepsis. *J Clin Invest* (1991) doi:10.1172/JCI115493
13. Lorente-Sorolla C, Garcia-Gomez A, Català-Moll F, Toledano V, Ciudad L, Avendaño-Ortiz J, Maroun-Eid C, Martín-Quirós A, Martínez-Gallo M, Ruiz-Sanmartín A, et al. Inflammatory cytokines and organ dysfunction associate with the aberrant DNA methylome of monocytes in sepsis. *Genome Med* (2019) **11**: doi:10.1186/s13073-019-0674-2
14. Foster SL, Hargreaves DC, Medzhitov R. Gene-specific control of inflammation by TLR-induced chromatin modifications. *Nature* (2007) doi:10.1038/nature05836
15. Novakovic B, Habibi E, Wang SY, Arts RJW, Davar R, Megchelenbrink W, Kim B, Kuznetsova T, Kox M, Zwaag J, et al. β -Glucan Reverses the Epigenetic State of LPS-Induced Immunological Tolerance. *Cell* (2016) doi:10.1016/j.cell.2016.09.034
16. Saeed S, Quintin J, Kerstens HHD, Rao NA, Aghajani-refah A, Matarese F, Cheng SC, Ratter J, Berentsem K, Van Der Ent MA, et al. Epigenetic programming of monocyte-to-macrophage differentiation and trained innate immunity. *Science (80-)* (2014) doi:10.1126/science.1251086

Articles

17. El Gazzar M, Yoza BK, Hu JYQ, Cousart SL, McCall CE. Epigenetic silencing of tumor necrosis factor?? during endotoxin tolerance. *J Biol Chem* (2007) doi:10.1074/jbc.M704584200

18. El Gazzar M, Yoza BK, Chen X, Hu J, Hawkins GA, McCall CE. G9a and HP1 couple histone and DNA methylation to TNF α transcription silencing during endotoxin tolerance. *J Biol Chem* (2008) doi:10.1074/jbc.M803446200

19. Klug M, Schmidhofer S, Gebhard C, Andreesen R, Rehli M. 5-Hydroxymethylcytosine is an essential intermediate of active DNA demethylation processes in primary human monocytes. *Genome Biol* (2013) **14**: doi:10.1186/gb-2013-14-5-r46

20. Vento-Tormo R, Company C, Rodríguez-Ubrea J, de la Rica L, Urquiza JM, Javierre BM, Sabarinathan R, Luque A, Esteller M, Aran JM, et al. IL-4 orchestrates STAT6-mediated DNA demethylation leading to dendritic cell differentiation. *Genome Biol* (2016) **17**: doi:10.1186/s13059-015-0863-2

21. Hamy F, Verwaerde P, Helbecque N, Formstecher P, Hénichart JP. Nuclear Targeting of a Viral-Cointernalized Protein by a Short Signal Sequence from Human Retinoic Acid Receptors. *Bioconjug Chem* (1991) **2**:375–378. doi:10.1021/bc00011a013

22. Singer M, Deutschman CS, Seymour C, Shankar-Hari M, Annane D, Bauer M, Bellomo R, Bernard GR, Chiche JD, Coopersmith CM, et al. The third international consensus definitions for sepsis and septic shock (sepsis-3). *JAMA - J Am Med Assoc* (2016) **315**:801–810. doi:10.1001/jama.2016.0287

23. Morante-Palacios O, Ballestar E. shinyÉPICO: A graphical pipeline to analyze Illumina DNA methylation arrays. *Bioinformatics* (2021) doi:10.1093/bioinformatics/btaa1095
24. Aryee MJ, Jaffe AE, Corrada-Bravo H, Ladd-Acosta C, Feinberg AP, Hansen KD, Irizarry RA. Minfi: A flexible and comprehensive Bioconductor package for the analysis of Infinium DNA methylation microarrays. *Bioinformatics* (2014) doi:10.1093/bioinformatics/btu049
25. Kim D, Langmead B, Salzberg SL. HISAT: A fast spliced aligner with low memory requirements. *Nat Methods* (2015) **12**:357–360. doi:10.1038/nmeth.3317
26. Li H, Handsaker B, Wysoker A, Fennell T, Ruan J, Homer N, Marth G, Abecasis G, Durbin R. The Sequence Alignment/Map format and SAMtools. *Bioinformatics* (2009) **25**:2078–2079. doi:10.1093/bioinformatics/btp352
27. Liao Y, Smyth GK, Shi W. FeatureCounts: An efficient general purpose program for assigning sequence reads to genomic features. *Bioinformatics* (2014) **30**:923–930. doi:10.1093/bioinformatics/btt656
28. Love MI, Huber W, Anders S. Moderated estimation of fold change and dispersion for RNA-seq data with DESeq2. *Genome Biol* (2014) **15**: doi:10.1186/s13059-014-0550-8
29. McLean CY, Bristor D, Hiller M, Clarke SL, Schaar BT, Lowe CB, Wenger AM, Bejerano G. GREAT improves functional interpretation of cis-regulatory regions. *Nat Biotechnol* (2010) **28**:495–501. doi:10.1038/nbt.1630

Articles

30. Yu G, Wang LG, Han Y, He QY. ClusterProfiler: An R package for comparing biological themes among gene clusters. *Omi A J Integr Biol* (2012) **16**:284–287. doi:10.1089/omi.2011.0118

31. Heinz S, Benner C, Spann N, Bertolino E, Lin YC, Laslo P, Cheng JX, Murre C, Singh H, Glass CK. Simple combinations of lineage-determining transcription factors prime cis-regulatory elements required for macrophage and B cell identities. *Mol Cell* (2010) **38**:576–89. doi:10.1016/j.molcel.2010.05.004

32. Ramírez F, Ryan DP, Grüning B, Bhardwaj V, Kilpert F, Richter AS, Heyne S, Dündar F, Manke T. deepTools2: a next generation web server for deep-sequencing data analysis. *Nucleic Acids Res* (2016) **44**:W160–W165. doi:10.1093/nar/gkw257

33. Xu YP, Lv L, Liu Y, Smith MD, Li WC, Tan XM, Cheng M, Li Z, Bovino M, Aubé J, et al. Tumor suppressor TET2 promotes cancer immunity and immunotherapy efficacy. *J Clin Invest* (2019) **129**:4316–4331. doi:10.1172/JCI129317

34. Garcia-Gomez A, Li T, Kerick M, Català-Moll F, Comet NR, Rodríguez-Ubreva J, De La Rica L, Branco MR, Martín J, Ballestar E. TET2- and TDG-mediated changes are required for the acquisition of distinct histone modifications in divergent terminal differentiation of myeloid cells. *Nucleic Acids Res* (2017) **45**:10002–10017. doi:10.1093/nar/gkx666

35. Stienstra R, Netea-Maier RT, Riksen NP, Joosten LAB, Netea MG. Specific and Complex Reprogramming of Cellular Metabolism in Myeloid Cells during Innate Immune Responses. *Cell Metab* (2017) **26**:142–156. doi:10.1016/j.cmet.2017.06.001

36. Liu L, Luc Y, Martinez J, Bi Y, Lian G, Wang T, Milasta S, Wang J, Yang M, Liu G, et al. Proinflammatory signal suppresses proliferation and shifts macrophage metabolism from Myc-dependent to HIF1 α -dependent. *Proc Natl Acad Sci U S A* (2016) **113**:1564–1569. doi:10.1073/pnas.1518000113
37. Garcia-Alonso L, Holland CH, Ibrahim MM, Turei D, Saez-Rodriguez J. Benchmark and integration of resources for the estimation of human transcription factor activities. *Genome Res* (2019) **29**:1363–1375. doi:10.1101/gr.240663.118
38. Lee JY, Sullivan KE. Gamma interferon and lipopolysaccharide interact at the level of transcription to induce tumor necrosis factor alpha expression. *Infect Immun* (2001) **69**:2847–2852. doi:10.1128/IAI.69.5.2847-2852.2001
39. Washburn ML, Wang Z, Walton AH, Goedegebuure SP, Figueroa DJ, Van Horn S, Grossman J, Remlinger K, Madsen H, Brown J, et al. T Cell- and Monocyte-Specific RNA-Sequencing Analysis in Septic and Nonseptic Critically Ill Patients and in Patients with Cancer. *J Immunol* (2019) **203**:1897–1908. doi:10.4049/jimmunol.1900560
40. Reyes M, Filbin MR, Bhattacharyya RP, Billman K, Eisenhaure T, Hung DT, Levy BD, Baron RM, Blainey PC, Goldberg MB, et al. An immune-cell signature of bacterial sepsis. *Nat Med* (2020) **26**:333–340. doi:10.1038/s41591-020-0752-4
41. Cheng SC, Scicluna BP, Arts RJW, Gresnigt MS, Lachmandas E, Giamarellos-Bourboulis EJ, Kox M, Manjeri GR, Wagenaars JAL, Cremer OL, et al. Broad defects in the energy metabolism of leukocytes underlie immunoparalysis in sepsis. *Nat Immunol* (2016) **17**:406–413. doi:10.1038/ni.3398

Articles

42. Hoover DM, Boulègue C, De Yang, Oppenheim JJ, Tucker K, Lu W, Lubkowski J. The structure of human macrophage inflammatory protein-3 α /CCL20. Linking antimicrobial and CC chemokine receptor-6-binding activities with human β -defensins. *J Biol Chem* (2002) **277**:37647–37654. doi:10.1074/jbc.M203907200

43. Persaud L, De Jesus D, Brannigan O, Richiez-Paredes M, Huaman J, Alvarado G, Riker L, Mendez G, Dejoie J, Sauane M. Mechanism of action and applications of interleukin 24 in immunotherapy. *Int J Mol Sci* (2016) doi:10.3390/ijms17060869

44. Kawai T, Akira S. The role of pattern-recognition receptors in innate immunity: Update on toll-like receptors. *Nat Immunol* (2010) doi:10.1038/ni.1863

45. Barnett KR, Decato BE, Scott TJ, Hansen TJ, Chen B, Attalla J, Smith AD, Hodges E. ATAC-Me Captures Prolonged DNA Methylation of Dynamic Chromatin Accessibility Loci during Cell Fate Transitions. *Mol Cell* (2020) **77**:1350-1364.e6. doi:10.1016/j.molcel.2020.01.004

46. Zhu H, Wang G, Qian J. Transcription factors as readers and effectors of DNA methylation. *Nat Rev Genet* (2016) doi:10.1038/nrg.2016.83

47. Yoshimura A, Naka T, Kubo M. SOCS proteins, cytokine signalling and immune regulation. *Nat Rev Immunol* (2007) **7**:454–465. doi:10.1038/nri2093

48. Chen J, Ivashkiv LB. IFN- γ abrogates endotoxin tolerance by facilitating Toll-like receptor-induced chromatin remodeling. *Proc Natl Acad Sci USA* (2010) **107**:19438–19443. doi:10.1073/pnas.1007816107

49. Leentjens J, Kox M, Koch RM, Preijers F, Joosten LAB, Van Der Hoeven JG, Netea MG, Pickkers P. Reversal of immunoparalysis in humans *in vivo*: A double-blind, placebo-controlled, randomized pilot study. *Am J Respir Crit Care Med* (2012) **186**:838–845. doi:10.1164/rccm.201204-0645OC
50. Shi L, Song L, Maurer K, Sharp J, Zhang Z, Sullivan KE. Endotoxin tolerance in monocytes can be mitigated by 2-interferon. *J Leukoc Biol* (2015) **98**:651–659. doi:10.1189/jlb.4a0914-450rr
51. Kang K, Bachu M, Park SH, Kang K, Bae S, Park-Min KH, Ivashkiv LB. IFN- γ selectively suppresses a subset of TLR4-activated genes and enhancers to potentiate macrophage activation. *Nat Commun* (2019) **10**: doi:10.1038/s41467-019-11147-3
52. Payen D, Faivre V, Miatello J, Leentjens J, Brumpt C, Tissières P, Dupuis C, Pickkers P, Lukaszewicz AC. Multicentric experience with interferon gamma therapy in sepsis induced immunosuppression. A case series. *BMC Infect Dis* (2019) **19**: doi:10.1186/s12879-019-4526-x

Supplementary Figures

Figure S1

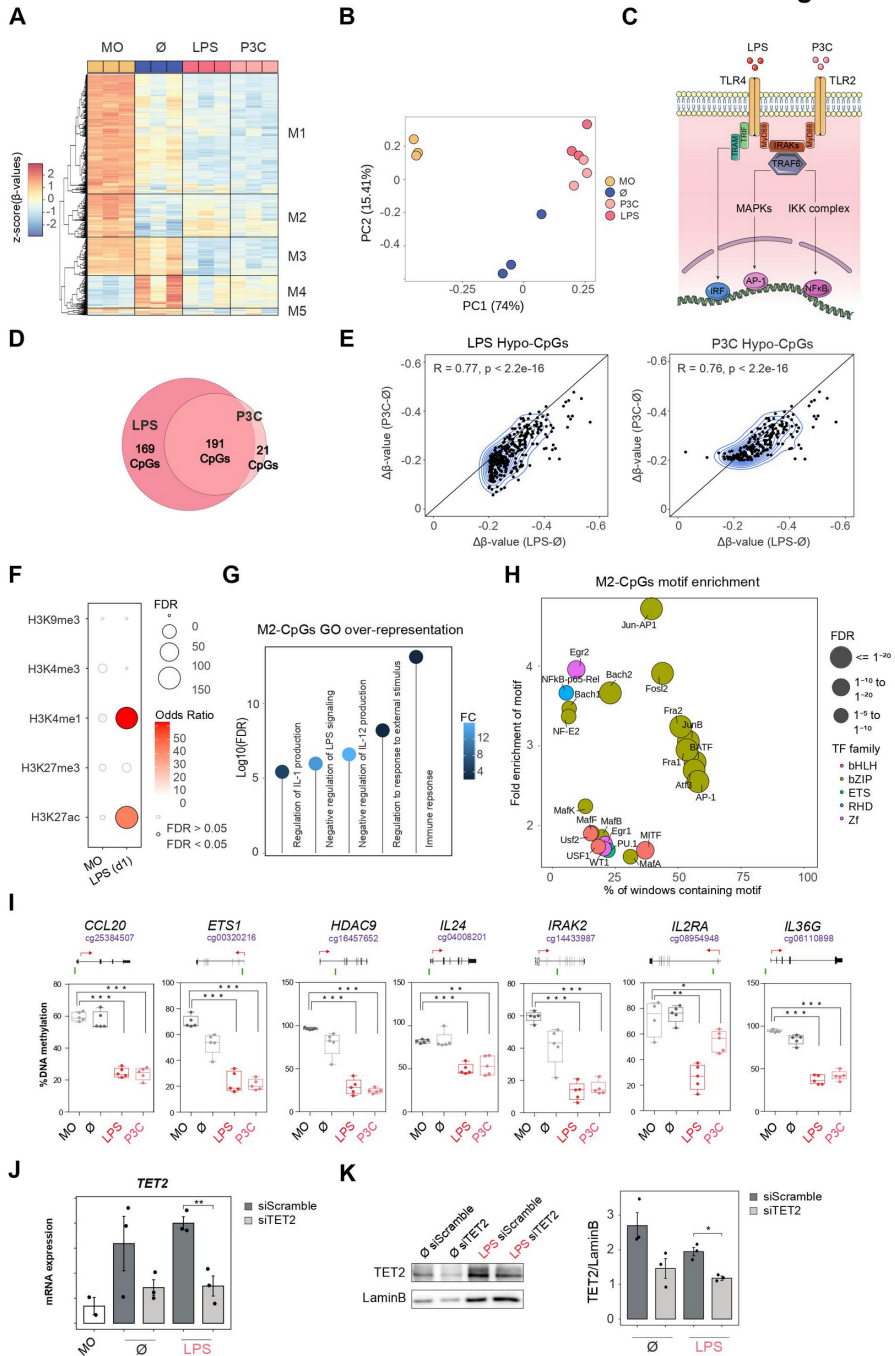
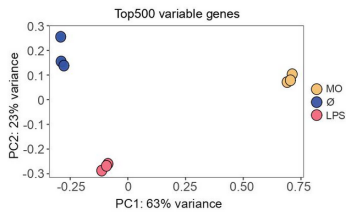


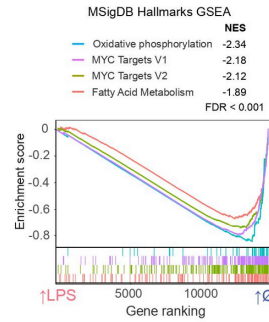
Figure S1. DNA methylation profile of P3C-treated human CD14⁺ monocytes. (A) DNA methylation heatmap of differentially methylated CpGs obtained with all the possible contrasts between the represented groups ($\Delta\beta \geq 0.2$, adjusted p (FDR) < 0.05). Scaled β -values are shown, ranging from -2 (lower DNA methylation levels, blue) to +2 (higher methylation levels, red). (B) Principal component analysis (PCA) of the CpGs shown in Supplementary Figure 1A. Principal components 1 and 2 are shown. (C) Simplified scheme of TLR4 and TLR2 signaling pathways. (D) Venn diagram of differentially methylated CpGs of LPS-treated versus untreated monocytes (LPS) and P3C-treated versus untreated monocytes (P3C). (E) Scatter plots of LPS hypomethylated and P3C hypomethylated CpGs showing differential of DNA methylation of LPS-treated versus untreated monocytes (x-axis) and P3C-treated versus untreated monocytes (y-axis). Contours in blue represent a 2D kernel density estimation. The R value and p values were obtained with Person's correlation. (F) ChIP-seq data of depicted histone marks were downloaded from the Blueprint database. Over-representation of CpGs in histone marks were calculated using the Fisher's test. Data points with FDR < 0.05 and Odds Ratio > 5 were considered significant. (G) GO (gene ontology) over-represented categories in M2 cluster CpGs. Fold change relative to background (EPIC array CpGs) and $-\log_{10}(\text{FDR})$ are shown. (H) Bubble scatterplot of TF binding motif enrichment for M2 cluster CpGs. The x-axis shows the percentage of windows containing the motif and the y-axis shows the magnitude of enrichment of the motif. Bubbles are colored according to the TF family. The FDR is indicated by the bubble size (selected TF with FDR $\leq 1e-05$). (I) Percentage methylation level of some selected LPS-hypomethylated CpGs as obtained by bisulfite pyrosequencing in the LPS and P3C samples. (J) qRT-PCR analysis to validate the downregulation of TET2 by siRNA (siScramble used as control). Data are normalized relative to the RPL38 gene. (** p < 0.01). (K) Western blot depicting TET2 protein levels in LPS-treated (LPS) and untreated (\emptyset) monocytes. Quantification of TET2/LaminB ratio is also shown (* p < 0.05).

Figure S2

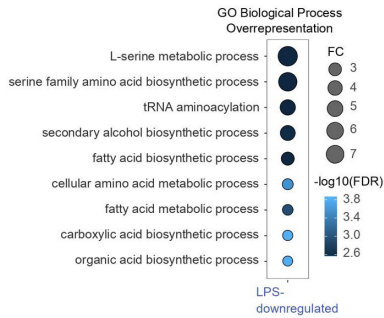
A



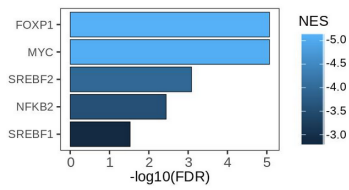
B



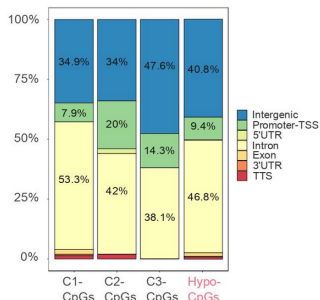
C



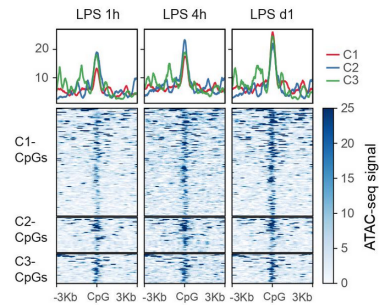
D



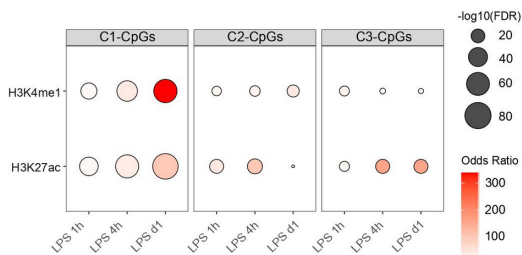
E



F



G



H

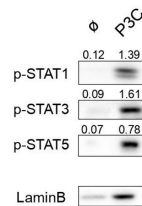


Figure S2. Additional features of differentially expressed genes and associated CpGs. (A) Principal component analysis (PCA) of the 500 most variable genes. Principal components 1 and 2 are shown. (B) Gene set enrichment analysis (GSEA) of LPS-treated versus untreated (\emptyset) monocytes, using MSigDB hallmarks (H) as gene sets. Gene sets enriched in untreated (\emptyset) monocytes are shown. The running enrichment score and the normalized enrichment score (NES) are shown above the graph (FDR < 0.001). (C) Gene ontology (GO) over-representation of GO biological process categories. Fold change of LPS-downregulated genes relative to background and $-\log_{10}(\text{FDR})$ of the Fisher's exact tests are shown. (D) Discriminant regulon expression analysis (DoRothEA) of LPS-treated versus untreated (\emptyset) monocytes. NES and $-\log_{10}(\text{FDR})$ of transcription factors (TF) enriched on the \emptyset side are shown (FDR < 0.05). (E) Barplot of genomic features as percentages of C1-, C2- and C3-associated CpGs (Figure 2H) compared with total hypo-methylated CpGs. (F) Accessibility (ATAC-seq) data of CpGs associated with C1 (in red), C2 (in blue) and C3 (in green) after 1, 4 and 24 hours of monocyte culture with LPS. Public ATAC-seq data were used [15] (G) ChIP-seq data of H3K27ac and H3K4me1 of LPS-treated monocytes were downloaded from the Blueprint database. Odds ratios were calculated with C1-, C2- and C3-associated CpGs, using EPIC array CpGs as background. Odds ratio and $-\log_{10}(\text{FDR})$ obtained from Fisher's exact tests are shown. (H) Western blot of protein phosphorylated (p)-STAT1, p-STAT3 and p-STAT5 in P3C-treated relative to untreated (\emptyset) monocytes. LaminB was used as loading control. Signal of western blot bands was quantified and the pSTAT/LaminB ratios are shown above each protein.

Figure S3

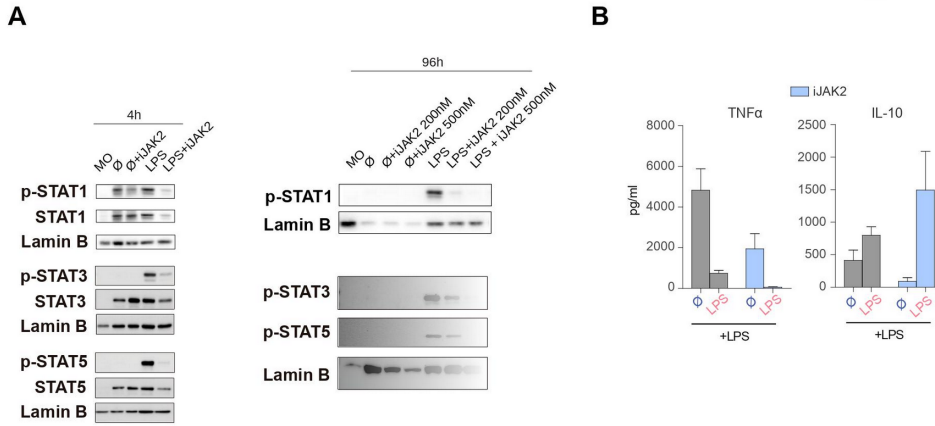


Figure S3. Additional characterization of JAK2 inhibition in LPS-treated monocytes. (A) Western blot of JAK2-dependent STAT proteins in LPS-treated and untreated (\emptyset) monocytes, with and without JAK2 inhibitor (iJAK2) after 4 hours (left) or 96 hours (right) of treatment. LaminB was used as the loading control. (B) TNF α and IL-10 levels measured in cell supernatants to assess the tolerance state after JAK2 inhibition.

Figure S4

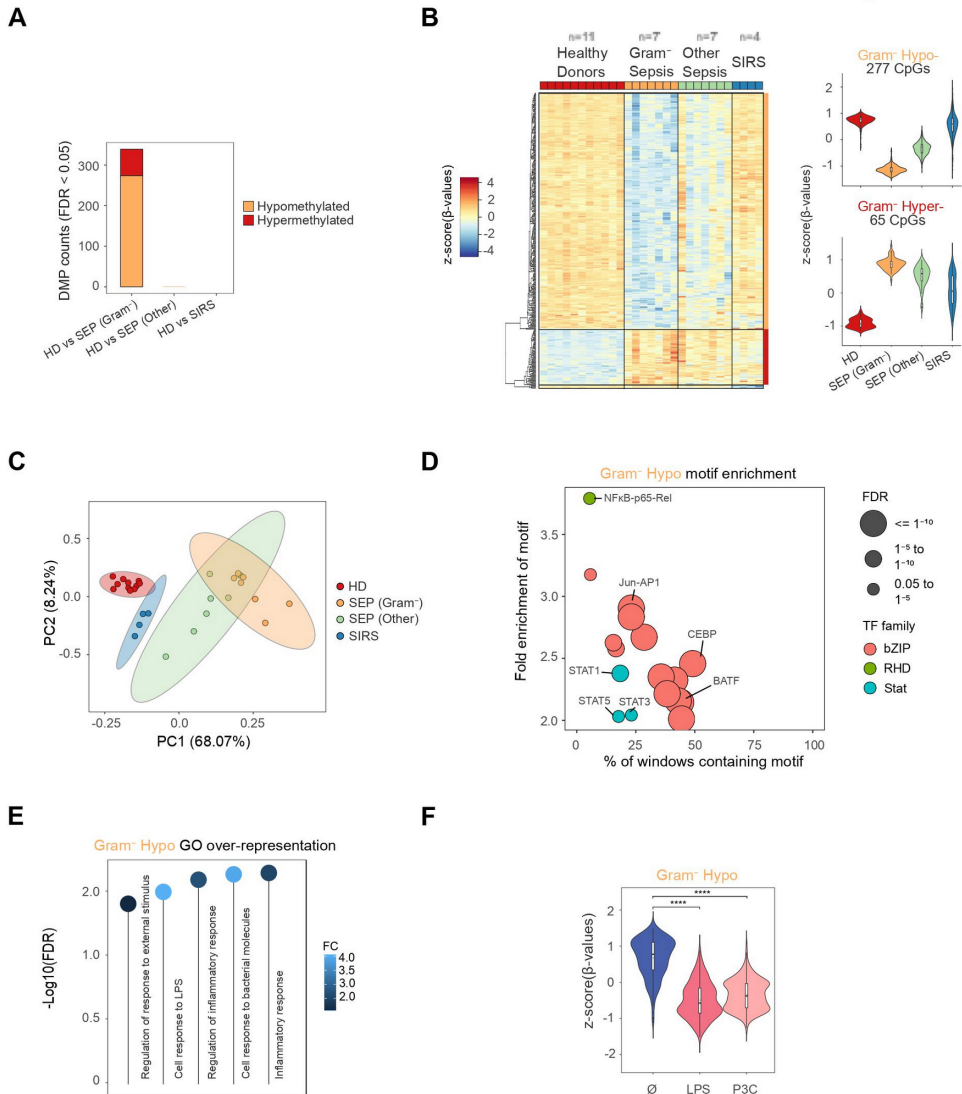


Figure S4. DNA methylation alterations in CD14⁺ monocytes from Gram-negative sepsis. (A) Differentially methylated positions (DMPs) found in the comparisons of Gram⁻ sepsis (SEP), other sepsis and SIRS patients with healthy donors (HD) (FDR < 0.05). (B) DNA methylation heatmap of differentially methylated CpGs comparing all groups shown pairwise (FDR < 0.05). Scaled and

Articles

batch-corrected β -values are shown, ranging from -4 (lower DNA methylation levels, blue) to +4 (higher methylation levels, red). On the right, violin plots of hypomethylated and hypermethylated clusters depicting normalized DNA methylation data. (C) Principal components 1 and 2 from a principal component analysis (PCA) of the DMPs from Supplementary Figure 4B are shown. (D) Bubble scatterplot of TF binding motif enrichment for Gram-negative hypomethylated CpGs. The x-axis shows the percentage of windows containing the motif; the y-axis shows the magnitude of enrichment of the motif. Bubbles are colored according to TF family. FDR is indicated by bubble size (selected TF with $FDR \leq 0.05$). (E) GO (Gene Ontology) over-represented categories in the Gram-negative hypomethylated CpGs. The fold change relative to the background (EPIC array CpGs) and $-\log_{10}(FDR)$ is shown. (F) Violin plot of normalized β values of the Gram-negative Hypomethylated CpGs in untreated monocytes (\emptyset), LPS-treated monocytes and P3C-treated monocytes (277 CpGs).

3.3. ARTICLE 3: Vitamin C enhances NF- κ B-driven DNA demethylation and immunogenic properties of dendritic cells

Vitamin C enhances NF- κ B-driven DNA demethylation and immunogenic properties of dendritic cells

Octavio Morante-Palacios^{1,2}, Gerard Godoy-Tena¹, Josep Calafell-Segura¹, Laura Ciudad¹, Eva M. Martínez-Cáceres^{3,4}, Jose Luis Sardina¹ and Esteban Ballestar^{1,2,*}

¹Epigenetics and Immune Disease Group, Josep Carreras Research Institute (IJC), 08916 Badalona, Barcelona, Spain

²Germans Trias i Pujol Research Institute (IGTP), 08916 Badalona, Barcelona, Spain

³Division of Immunology, Germans Trias i Pujol Hospital, LCMN, Germans Trias i Pujol Research Institute (IGTP), 08916 Badalona, Barcelona, Spain

⁴Department of Cell Biology, Physiology, Immunology, Autonomous University of Barcelona, 08193 Bellaterra, Barcelona, Spain

*Correspondence: E. Ballestar,

E-mail: eballestar@carrerasresearch.org

Abstract

Dendritic cells (DCs) are central in immune responses, bridging the adaptive and innate systems. The study of the *in vitro* differentiation of DCs from monocytes is relevant not only to better understand the analogous *in vivo* process but also as a potential source for cancer cell therapy. DNA demethylation has been previously reported to be crucial in that process. Vitamin C, an essential nutrient, is a known cofactor of ten-eleven translocation (TET) enzymes, that drive active demethylation. Currently, the effects of vitamin C treatment on human immune cells are poorly understood. In this study, we have analyzed the epigenomic and transcriptomic remodeling orchestrated by vitamin C in monocyte-derived DC differentiation and maturation. We have detected extensive demethylation produced by vitamin C treatment, together with concordant gene expression changes during DC maturation. p65, a component of NF- κ B, interacts with TET2 and is associated with both vitamin C-mediated gene upregulation and DNA demethylation. Finally, vitamin C increases TNF β production and T cell stimulation capabilities of DCs. This work provides a potential strategy for the improvement of cell therapies based on monocyte-derived DCs, as well as a feasible mechanism of action of intravenous high-dose vitamin C treatment in patients.

Keywords: Vitamin C, TET2, DNA demethylation, NF- κ B, dendritic cells, antigen presentation

Introduction

Dendritic cells (DCs) play a central role in the immune system, bridging innate and adaptive immune responses. As innate immune cells, they are able to recognize a plethora of pathogen-associated molecular patterns (PAMPs) and damage-associated molecular patterns (DAMPs) through pattern recognition receptors (PRRs)(1). Moreover, they are very efficient at antigen processing and presentation to T cells and are, therefore, responsible for initiating antigen-specific immune responses.

DCs are very heterogeneous, comprising plasmacytoid DCs (pDCs) and conventional DCs (cDCs). Furthermore, monocyte-derived DCs (moDCs) can be obtained *in vitro* from monocytes, with GM-CSF and IL-4(2). moDCs have been classically used as a convenient model that mimics blood DCs, especially the cDC2 subtype(3). However, increasing evidence indicates that monocytes can extravasate to peripheral tissues and give rise *in vivo* to bona fide moDCs(4).

DNA methylation is crucial for immune cell differentiation, identity, and function(5). In particular, DNA methylation changes, mostly active demethylation, have been described in several differentiation processes from monocytes, including macrophages, osteoclasts, and DCs(6–8). In general, DNA demethylation has been observed to be more extensive during monocyte differentiation than the subsequent maturation/activation of the cells(9). Additionally, maturation of moDCs with live bacteria produces DNA demethylation that follows gene activation, limiting the potential direct regulatory effects of DNA methylation in that context(10). TET2, a member of the ten-eleven translocation (TET) methylcytosine dioxygenases, and involved in multi-step active demethylation processes, is critical for terminal monocyte-

Articles

related differentiation(6, 11). Recently, TET2 has also been implicated in glucocorticoid- and vitamin D-mediated modulation of the immunogenic properties of DCs(12, 13).

Vitamin C (L-ascorbic acid) is an essential nutrient with pleiotropic functions. Its deficiency is associated with a disease, namely scurvy, characterized by a plethora of symptoms, including the malfunction of the immune system. For instance, the normal intracellular level of vitamin C in monocyte cytoplasm is ~3mM, 60 times higher than the plasma level, reflecting a specific function of the molecule in the immune cell biology. Vitamin C can act as a cofactor of Fe-containing hydroxylases such as TET enzymes and Jumonji C domain-containing histone demethylases (JHMDs), increasing their enzymatic function(14). Some studies in mice suggest that vitamin C can stimulate DC capacity to produce proinflammatory cytokines and promote differentiation of T cells(15). Moreover, vitamin C intravenous treatment in mice has been shown to abrogate cancer progression through direct TET2 function restoration in cancer cells and immune system modulation(16, 17).

The *in vivo* modulation of DC migration and function, as well as the administration of DC-based vaccines, are promising strategies to treat different types of cancer(18). In particular, the use of autologous moDCs obtained *ex vivo* from patient-derived blood monocytes have been used in several clinical trials with mixed results(19, 20). In this regard, the improvement of moDC generation *in vitro*, as well as the use of molecules to modulate monocyte differentiation *in vivo* may boost the clinical outcome of cancer patients.

In this work, we have investigated the effects of vitamin C treatment during monocyte to DC *in vitro* differentiation and maturation,

identifying extensive DNA demethylation associated with the upregulation of migration, chemotaxis, antigen presentation, and immune response-related genes. Moreover, DNA demethylation and gene upregulation during DC maturation was associated with p65, a component of the NF- κ B complex which interacts with TET2 in this context. We have shown how the modulation of DNA methylation during DC differentiation and maturation can yield functional and phenotypic changes in these cells, improving their immunogenicity.

Materials and Methods

CD14⁺ monocyte purification and culture

Buffy coats were obtained from anonymous donors via the Catalan Blood and Tissue Bank (CBTB). The CBTB follows the principles of the World Medical Association (WMA) Declaration of Helsinki. Before providing blood samples, all donors received detailed oral and written information and signed a consent form at the CBTB.

PBMCs were isolated by density-gradient centrifugation using lymphocyte-isolation solution (Rafer). Pure MOs were then isolated from PBMCs by positive selection with magnetic CD14 MicroBeads (Miltenyi Biotec). Purity was verified by flow cytometry, which yielded more than 95% of CD14⁺ cells.

MOs were resuspended in Roswell Park Memorial Institute (RPMI) Medium 1640 + GlutaMAX™ (Gibco, ThermoFisher) and immediately added to cell culture plates. After 20 minutes, monocytes were attached to the cell culture plates, and the medium was changed with RPMI containing 10% fetal bovine serum (Gibco, ThermoFisher), 100 units/mL penicillin/streptomycin (Gibco, ThermoFisher), 10 ng/mL human GM-CSF (PeproTech) and 10 ng/mL human IL-4 (PeproTech). In the case of the cells treated with vitamin C, 500 μM (+)-Sodium L-ascorbate (Sigma-Aldrich) was also added to the medium. For dendritic cell maturation, LPS (10 ng/mL) were added to cell culture at day 5.

Cells were collected at day 2 (\emptyset / \emptyset_{vitC}) and at day 7, including immature dendritic cells (iDC / iDC_{vitC}) and mature dendritic cells, with LPS stimulus (mDC / mDC_{vitC}).

Genomic DNA and total RNA extraction

Genomic DNA and total RNA were extracted using the Maxwell RSC Cultured Cells DNA kit (Promega) and the Maxwell RSC simplyRNA Cells kit (Promega), respectively, following the manufacturer's instructions.

DNA methylation profiling

500 ng of genomic DNA was converted using the EZ DNA Methylation Gold kit (Zymo Research), using 4 biological replicates for each group. Infinium MethylationEPIC BeadChip (Illumina) arrays were used to analyze DNA methylation, following the manufacturer's instructions. This platform allows around 850,000 methylation sites per sample to be interrogated at single-nucleotide resolution, covering 99% of the reference sequence (RefSeq) genes. Raw files (IDAT files) were provided for the Josep Carreras Research Institute Genomics Platform (Barcelona).

Quality control and analysis of EPIC arrays were performed using ShinyÉPICO, a graphical pipeline that uses minfi for normalization, and limma for differentially methylated positions analysis(34–36). CpH and SNP loci were removed and the Noob+Quantile normalization method was used. Donor information was used as a covariate, and Trend and Robust options were enabled for the eBayes moderated t-test analysis. CpGs were considered differentially methylated when the absolute differential of methylation was greater than 20% and the FDR was less than 0.05.

RNA-seq

RNA-seq libraries of MOs, \emptyset / \emptyset_{vitC} , iDC / iDC_{vitC}, and mDC / mDC_{vitC} were generated and sequenced by Novogene (Cambridge), in

Articles

150-bp paired-end, with the Illumina NovaSeq 6000 platform, using 3 biological replicates for each group. More than 40 million reads were obtained for each sample. Fastq files were aligned to the hg38 transcriptome using HISAT2 with standard options(37). Reads mapped in proper pair and primary alignments were selected with SAMtools(38). Reads were assigned to genes with featureCounts(39).

Differentially expressed genes were detected with DESeq2 (40). The donor was used as a covariate in the model. The Ashr shrinkage algorithm was applied and only protein-coding genes with an absolute logFC greater than 0.5 and an FDR less than 0.05 were selected as differentially expressed. For representation purposes, Variance Stabilizing Transformation (VST) values and normalized counts provided by DESeq2 were used.

Quantification of cytokine production

Cell culture supernatants were collected after 6 days and diluted appropriately. Enzyme-linked immunosorbent assays (ELISA) were performed to detect TNF β , following the manufacturer's instructions (TNF beta Human ELISA Kit, ThermoFisher).

T cell clonal expansion and proliferation assay

PBMCs from healthy donors were purified from blood by density gradient centrifugation. The PBMCs (1ml; $3 \cdot 10^6$ cells per well) were cultured in the presence of SARS-CoV-2-S (9pmol) (PepTivator) as an antigen in 24-well plate and maintained in IMDM medium (Gibco) supplemented with penicillin (100 units/mL), streptomycin (100 mg/mL) and human serum (10%) (Millipore) in the absence of IL-2 for 3 days. After 3 days, 1ml of medium with 80 U/mL of recombinant human IL-2 (PeproTech) was added to the wells, with a final concentration of $1.5 \cdot 10^6$

cell/ml and 40U/ml of IL-2. After 7-10 days of culture, T cells were expanded in the presence of 30-Gy irradiated autologous PBMCs ($3 \cdot 10^6$ cells/well) previously pulsed with 9pmol of SARS-CoV-2- S (PepTivator). Antigen-specific T cells (mix of CD4⁺ and CD8⁺ T cells) were selected by performing the same protocols two times to have a positive selection.

After 7 days of differentiation and activation, DCs were washed to remove VitC and were co-cultured with antigen-specific autologous CFSE-stained T cells at a DC: T cell ratio of 1:2 and 1:3 in 200ul of RPMI 1640 medium containing 10% FBS, penicillin (100 units/mL), streptomycin (100 mg/mL) in round bottom 96-well plates (ThermoFisher). Co-culture was performed in the presence of SARS-CoV-2- S antigen or SARS-CoV-2-N control antigen (PepTivator). T cell proliferation was analyzed by FACS and determined by considering the proliferating those where CFSE staining had decreased compared to not co-cultured T cells. T cells stimulated with anti-CD3/DC28 Dynabeads 5ug/mL (eBioscience) were used as a positive control.

Co-immunoprecipitation (Co-IP)

Co-IP assays were performed using DCs and TolDCs differentiated from CD14⁺ monocytes for 24h. Cell extracts were prepared in lysis buffer [50 mM Tris-HCl, pH 7.5, 1 mM EDTA, 150 mM NaCl, 1% Triton-X-100, protease inhibitor cocktail (cOmplete™, Merck)] with corresponding units of Benzonase (Sigma) and incubated at 4°C for 4 h. 100 µl of supernatant was saved as input and diluted with 2× Laemmli sample buffer (5x SDS, 20% glycerol, 1M Tris-HCl (pH 8.1)). Supernatants were first precleared with PureProteome™ Protein A/G agarose suspension (Merck Millipore) for 1 h. The lysate was then incubated overnight at 4°C with respective crosslinked primary antibodies. The cross-linking was

Articles

performed in 20mM dimethyl pimelimidate (DMP) (Pierce, Thermo Fisher Scientific, MA, USA) dissolved in 0.2 M sodium borate (pH 9.0). Subsequently, the beads were quenched with 0.2M of ethanolamine (pH 8.0) and resuspended at 4°C in PBS until use. Beads were then washed three times with lysis buffer at 4°C. Sample elution was done by acidification using a buffer containing 0.2 M glycine (pH 2.3) and diluted with 2× Laemmli. Samples and inputs were denatured at 95°C in the presence of 1% β-mercaptoethanol. Anti-p65 Cl5310256 (DIagenode) and control IgG Cl5410206 (Diagenode) were used for Co-IP.

Western Blotting

Cytoplasmic and nuclear protein fractions were obtained using hypotonic lysis buffer (Buffer A; 10 mM Tris pH 7.9, 1.5 mM MgCl₂, 10 mM KCl supplemented with protease inhibitor cocktail (Complete, Roche) and phosphatase inhibitor cocktail (PhosSTOP, Roche) to lyse the plasma membrane. Cells were visualized in the microscope to assure correct cell lysis. The nuclear pellets were resuspended in Laemmli 1X loading buffer. For whole-cell protein extract, cell pellets were directly resuspended in Laemmli 1X loading buffer.

Proteins were separated by SDS-PAGE electrophoresis. Immunoblotting was performed on polyvinylidene difluoride (PVDF) membranes following standard procedures. Membranes were blocked with 5% Difco™ Skim Milk (BD Biosciences) and blotted with primary antibodies. After overnight incubation, membranes were washed three times for 10 minutes with TBS-T (50 mM Tris, 150 mM NaCl, 0.1% Tween-20) and incubated for 1 hour with HRP-conjugated mouse or rabbit secondary antibody solutions (Thermo Fisher) diluted in 5% milk (diluted 1/10000). Finally, proteins were detected by chemiluminescence

using WesternBright™ ECL (Advansta). The following antibodies were used: Anti-p65 C15310256 (DIagenode), Anti-phosphorylated p65 (Ser536) 93H1 (Cell Signaling), Anti-GAPDH 2275-PC-100 (Trevigen), Anti-TET2 C15200179 (Diagenode), Anti-histone H1 ab4269 (Abcam), Anti-beta Actin ab8227 (Abcam).

Data analysis and representation

Statistical analyses were performed in R 4.0.3. Gene expression and DNA methylation heatmaps were created with the heatmap.2 function of the gplots package. The findMotifsGenome.pl function of HOMER (Hypergeometric Optimization of Motif EnRichment) was used to analyze known motif enrichment, using the parameters '-size 200 -cpg'. All EPIC array CpG coordinates were also used as background for the methylation data. GREAT software was used to calculate CpG-associated genes and gene ontology (GO) enrichment(41). GO enrichment of gene expression data was performed using the clusterProfiler package(42). ChIP-seq peaks files of histone marks from MO, iDCs, and mDCs were downloaded from the BLUEprint webpage (<http://dcc.blueprint-epigenome.eu>). Consensus peaks of the different replicates were obtained with the MSPC algorithm, using the options '-r Biological -w 1E-4 -s 1E-8 -c 3'(43).

The chromatin state learning model for CD14⁺ monocytes was downloaded from the Roadmap Epigenomics Project webpage, and chromatin state enrichments were calculated using Fisher's exact test.

Proportional Venn diagrams were generated with the Meta-Chart webpage (<https://www.meta-chart.com/>). Methylated CpG set enrichment analysis (mCSEA) (59) was used to calculate CpG-set-specific DNA methylation modifications.

Results

Vitamin C drastically enhances DNA demethylation during monocyte to dendritic cell differentiation and maturation

Monocytes (MOs) isolated from peripheral blood of healthy donors were differentiated *in vitro* to dendritic cells (DCs) for 7 days using GM-CSF and IL-4, in the presence or absence of vitamin C (vitC). Samples were collected at day 2, in the middle of the differentiation ($\emptyset / \emptyset_{\text{vitC}}$), and at day 7, including immature DCs (iDCs) (iDC / iDC_{vitC}), without further treatment, and mature DCs, exposed the last 48h to lipopolysaccharide (LPS) (mDC / mDC_{vitC}) (Figure 1A).

DNA methylation was profiled using Illumina Infinium MethyEPIC arrays, which cover around 850,000 positions in the human genome ($n = 4$). First, overall changes in DNA methylation were calculated between groups pairwise (Supplementary Figure 1A, see at the end of the article, page 204). In the differentiation process, we found mostly DNA demethylation, as previously described(7). We then compared the demethylated positions in the MO to iDC differentiation, in comparison with the MO to iDC_{vitC} differentiation, as well as the iDC to mDC maturation in comparison with the iDC_{vitC} to mDC_{vitC} maturation. As it can be observed, the positions demethylated in the differentiation and maturation processes in the presence of vitamin C include the majority of CpGs demethylated in the regular differentiation and maturation of DCs, as well as a vast number of additional CpGs (Figure 1B).

PCA analysis revealed that at day 2 most DNA methylation variance of the MO to iDC differentiation has already occurred (Figure 1C), whereas no differences with the vitamin C stimulus were found on that day. In contrast, at day 7, vast differences were observed for both iDC_{vitC}

and mDC_{vitC} , in comparison with their corresponding controls without vitamin C suggesting that the vitamin C-mediated boost in demethylation is occurring at later days, when perhaps the TET 5-mC hydroxylase activity starts to be exhausted. The variable that explains most of the variance in DNA methylation resides in the presence/absence of vitamin C during differentiation.

All differentially methylated positions (DMPs) associated with vitamin C (iDC vs iDC_{vitC} and mDC vs mDC_{vitC}) were represented together, revealing two clusters of CpG sites (M1 and M2) (Figure 1D). M1 corresponds with CpGs demethylated during differentiation in the presence of vitamin C whereas M2 are CpGs demethylated during LPS-mediated maturation in the presence of vitamin C. Both clusters were enriched in monocytic enhancers and regions flanking active transcription start sites (Figure 1E). That corresponds with predominant localization in intergenic regions, far from CpG islands (Supplementary Figure 1B, Supplementary Figure 1C). To note, M1 and M2 CpGs are located in regions with slightly increasing H3K27ac and H3K4me1 histone marks from MOs to iDC s and mDC s, respectively, suggesting priming for activation in these regions, even in the absence of vitamin C (Supplementary Figure 1D).

Gene Ontology enrichment analysis of M1 CpGs closest genes revealed categories related to positive regulation of myeloid differentiation, regulation of JAK activation, regulation of defense response to virus, and vitamin transport, among others.

Figure 1

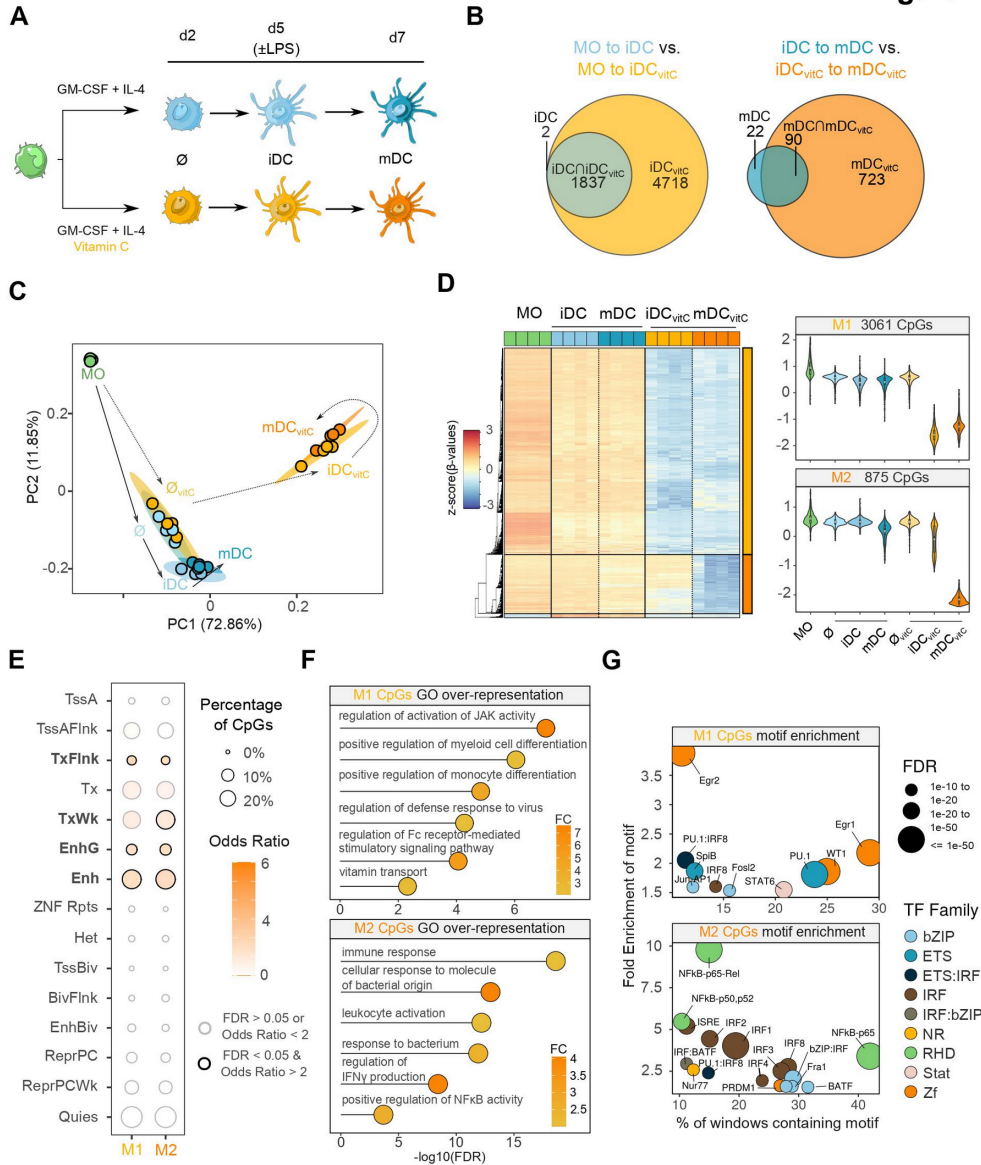


Figure 1. Vitamin C-mediated dendritic cell DNA methylome remodeling. (A) Scheme depicting the experimental setup. Monocytes (MO) were differentiated to dendritic cells (DCs) using GM-CSF and IL-4, in the presence or absence of vitamin C (vitC). Samples were collected at day 2, in the middle of the differentiation, and at

day 7, including immature DCs (iDCs) and mature DCs (mDCs), exposed the last 2 days to lipopolysaccharide (LPS). (B) Area-proportional Venn diagrams comparing the demethylated CpG sets of MO to iDC vs. MO to iDC_{vitC}, and iDC to mDC vs. iDC_{vitC} to mDC_{vitC}. (C) Principal Component Analysis (PCA) of differentially methylated CpGs comparing all groups pairwise. Principal component 1 and principal component 2 are represented in the x- and y-axis, respectively. (D) DNA methylation heatmap of differentially methylated CpGs comparing iDC to iDC_{vitC}, and mDC to mDC_{vitC} ($\Delta\beta \geq 0.3$, FDR < 0.05). Scaled β -values are shown (lower DNA methylation levels in blue and higher methylation levels in red). On the right side, violin plots of clusters M1 and M2 depict scaled β -values. (E) Enrichment of M1 and M2 CpGs in ChromHMM 15-states categories of MOs (Roadmap Epigenomics Project). Significantly enriched categories (FDR < 0.05 and odds ratio > 2) are depicted with a black stroke, including TxFlnk (Flanking Active TSS), TxWk (Weak Transcription), EnhG (Genic Enhancers), and Enh (Enhancers). (F) GO (Gene Ontology) over-represented categories in M1 and M2 CpGs. Fold Change in comparison with background (EPIC array CpGs) and $-\log_{10}(\text{FDR})$ is represented. (G) Bubble scatterplot of TF binding motif enrichment for M1 and M2 CpGs. The x-axis shows the percentage of windows containing the motif and the y-axis shows the fold enrichment of the motif over the EPIC background. Bubbles are coloured according to the TF family. FDR is indicated by bubble size.

In contrast, M2 CpGs were enriched in terms related to LPS response and immune activation such as cellular response to molecules of bacterial origin, leukocyte activation, response to bacterium, regulation of IFN γ production, and positive regulation of NF- κ B activity (Figure 1F). These functions are consistent with the respective implication of M1 and M2 clusters with the DC differentiation and maturation steps.

Active demethylation in myeloid cells is often mediated by TFs that recruit specific enzymes. In this regard, M1 CpGs were enriched in the consensus binding motifs of TFs previously related to DC differentiation, such as Egr2(21), STAT6(7), and PU.1(21), whereas M2 CpGs were

enriched in the consensus binding motifs of NF- κ B, AP-1, and IRF (Figure 1G).

Vitamin C skews gene expression of dendritic cells with upregulation of migration and antigen presentation-related genes

Given the extensive differences in DNA methylation mediated by vitamin C, we then performed RNA-seq of MOs, \emptyset , \emptyset_{vitC} , iDC, iDC $_{\text{vitC}}$, mDC and mDC $_{\text{vitC}}$ and checked for differences in their transcriptomes. In contrast with DNA methylation, transcriptome variance of principal component (PC)1 and PC2 are mainly explained by the maturation of DCs and the differentiation of MO to DC, respectively. However, differences between iDC and mDC $_{\text{vitC}}$ and mDC and mDC $_{\text{vitC}}$ can also be observed in the PCA (Figure 2A).

Since samples were obtained at day 2 (\emptyset / \emptyset_{vitC}), and at day 7, with (mDC / mDC $_{\text{vitC}}$) or without (iDC / iDC $_{\text{vitC}}$) activation, three potential comparisons of vitamin C-treated cells can be performed, in relation to their respective controls. On day 2, very few differences were found between \emptyset and \emptyset_{vitC} (63 downregulated and 75 upregulated genes). On day 7, we found 163 downregulated and 159 upregulated genes between iDC and iDC $_{\text{vitC}}$, whereas most differences were found between mDC and mDC $_{\text{vitC}}$ (185 downregulated and 772 upregulated genes) (Figure 2B). Furthermore, most differentially expressed genes (DEGs) are not common between comparisons (Figure 2C).

We then joined the differentially expressed genes of the three comparisons and divided them into six clusters (expression clusters E1-E6) with different behaviors (Figure 2D). E1, E2, and E3 clusters showed a diminished downregulation trend in the iDC $_{\text{vitC}}$ to mDC $_{\text{vitC}}$ transition, in

comparison with the iDC to mDC transition, whereas E5 genes are more upregulated in the iDC_{vitC} to mDC_{vitC} transition in comparison with the iDC to mDC transition (Figure 2E).

Gene Ontology Enriched terms were calculated for each expression cluster, obtaining distinctive categories (Figure 2F). For instance, E1 was enriched in dendritic cell migration and chemotaxis, E2 in macrophage activation and cytokine secretion, E3 in antigen processing and presentation and response to calcium ion, and E5 in type I interferon signaling pathway and defense response to virus.

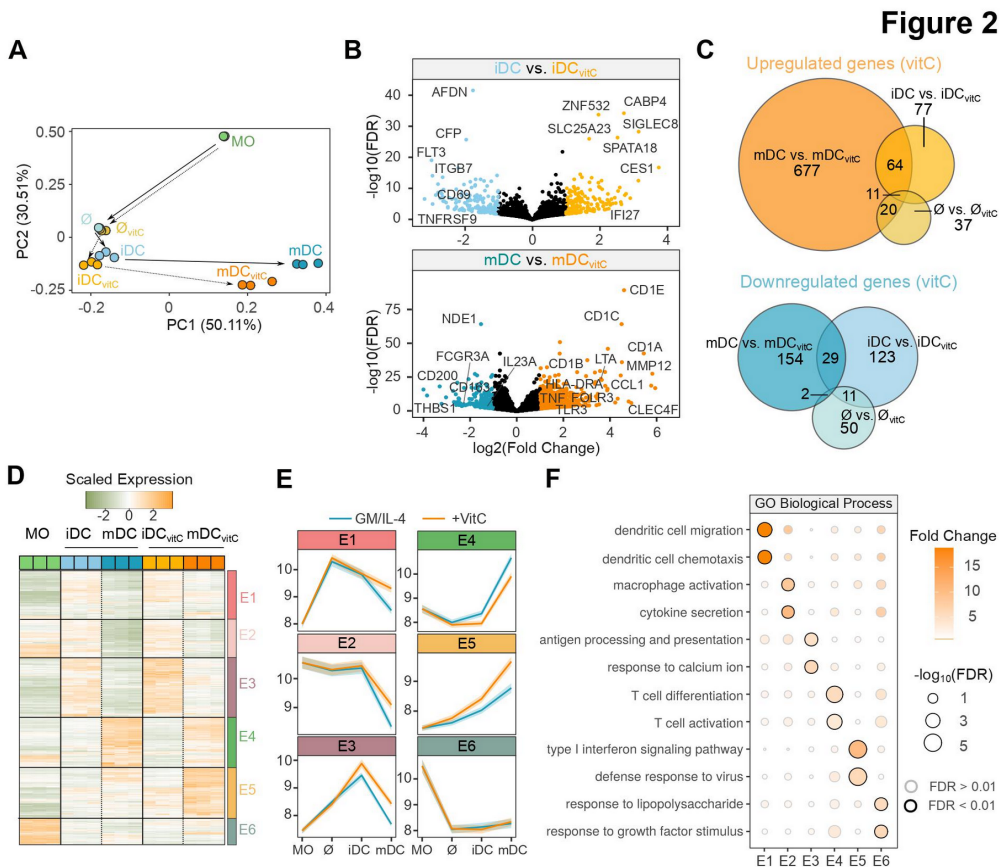


Figure 2. Shifting in gene expression of dendritic cells triggered by vitamin C. (A) Principal Component Analysis (PCA) of gene expression. Principal component 1 and principal component 2 are represented in the x- and y-axis, respectively. (B) Volcano plots of gene expression in the iDC vs. iDC_{vitC} and the mDC vs. mDC_{vitC} comparisons. The binary logarithm of the fold change is represented in the x-axis, whereas the negative decimal logarithm of the FDR is represented in the y-axis. Downregulated genes are shown in blue (FDR < 0.05, Fold Change < -2) and upregulated genes are shown in orange (FDR < 0.05, Fold Change > 2). (C) Area-proportional Venn diagrams comparing the upregulated and downregulated gene sets of the \emptyset vs. \emptyset_{vitC} , iDC vs. iDC_{vitC} and mDC vs. mDC_{vitC} comparisons. (D) Gene expression heatmap of differentially expressed genes comparing \emptyset to \emptyset_{vitC} , iDC to iDC_{vitC}, and mDC to mDC_{vitC} (absolute logFC > 1, FDR < 0.05). Scaled expression VST values are shown (lower expression levels in green and higher expression values in orange). The division of the heatmap yielded 6 different expression clusters (E1-E6). (E) Temporal progression of gene expression of the expression clusters (E1-E6) during the differentiation process with (orange) or without (blue) vitamin C. The y-axis shows VST values, where a higher value means a higher gene expression, and the line ribbons represent the 95% confidence interval. (F) Gene Ontology (GO) over-representation of GO Biological Process categories in the E1-E6 clusters. Fold Change of genes over background and $-\log_{10}(\text{FDR})$ of the Fisher's exact tests are shown. Significant categories (FDR < 0.01) are depicted with a black stroke.

Vitamin C-mediated demethylation is linked to increased gene expression during dendritic cell maturation

With the purpose of finding potential functional effects of the vitamin C-mediated demethylation, we linked each DMP with its closest gene. When the global profile of M1 and M2 associated genes intersected with differentially expressed genes of Figure 2D is represented, we found that M1 associated genes are less downregulated in mDCs with vitamin C treatment, whereas M2 associated genes are upregulated in mDCs with vitamin C treatment (Figure 3A). In this regard, E1 and E2 clusters are

enriched in M1-associated genes, and the E5 cluster is enriched in M2-associated genes (Figure 3B).

This DNA methylation/gene expression relationship can be exemplified with some DMPs and their respective associated DEGs. In the case of M1-associated genes, CIQB (complement) and CD1C (antigen presentation) show demethylation with vitamin C treatment in iDCs, conjoined with a decreased reduction in expression after activation (Figure 3C). Furthermore, M2-associated genes such as CCL1 (chemoattraction), IKBKE (NF- κ B pathway), and IRF8 (interferon regulatory transcription factor) depict a decreased methylation in mDC with vitamin C, concomitant with increased gene expression (Figure 3D).

Finally, a database of transcription factor regulation was used to infer potential transcription factors involved in the regulation of each expression cluster associated with DNA methylation changes (Figure 3E)(22). It is interesting to note that PU.1 and RELA (p65) were associated with M1/E2 and M2/E5 clusters, respectively.

To further explore the role of p65 in the transcriptomic and epigenomic changes in mDC_{vitC}, we studied the protein expression and phosphorylation by Western blot. First, we found that p65 presents similar protein levels in iDCs, mDCs, iDC_{vitC}, and mDC_{vitC}. However, phosphorylated p65 (Ser536) (p-p65) is increased in both mDCs and mDC_{vitC} (Figure 3F). Moreover, we also detected p-p65 in the nuclear fraction (NF) of mDCs and mDC_{vitC}, making possible its function as a transcription factor and the recruitment of TET enzymes in that context (Figure G).

We subsequently checked the potential interaction between p65 and TET2, a key mediator of active demethylation in myeloid cells. The co-

immunoprecipitation of p65 revealed its interaction with TET2 in both mDCs and mDC_{vitC} (Figure 3H).

Figure 3

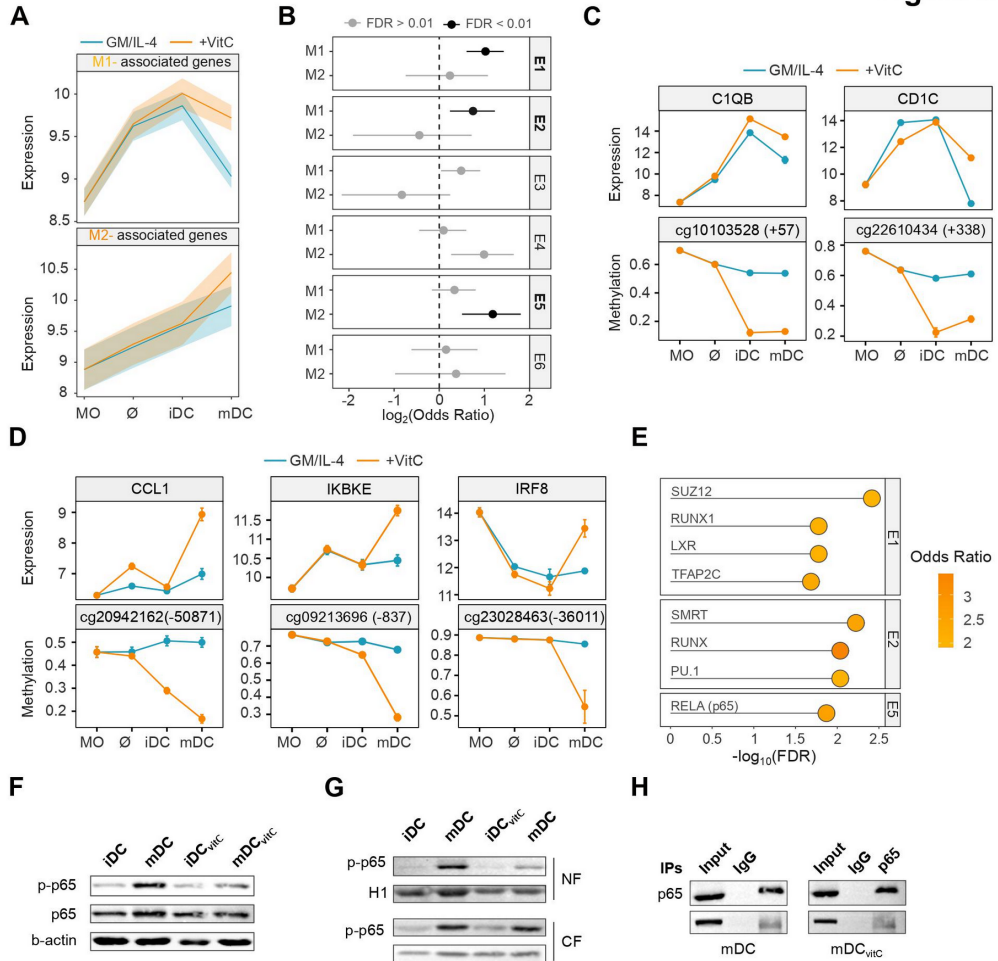


Figure 3. Integration of DNA methylation and gene expression vitamin C-mediated remodeling. (A) M1 and M2 CpGs were associated with the nearest gene. Temporal progression of gene expression of the M1- and M2-associated genes during the differentiation process with (orange) or without (blue) vitamin C. Only differentially expressed genes (Figure 2D) are used for the calculation. The y-axis shows VST values, where a higher value means a higher gene expression, and the line ribbons represent the 95% confidence interval. (B) Enrichments of M1- and M2-

associated genes over the EI-E6 expression clusters were calculated using Fisher's exact tests. Odds ratios \pm 95% confidence intervals are shown. Significant enrichments (FDR < 0.01) are shown in black. (C) Selected examples of M1 CpGs and associated genes. Temporal progression of DNA methylation (β -value) (below) and gene expression (VST) (above) during the differentiation process with (orange) or without (blue) vitamin C is depicted. (D) Selected examples of M2 CpGs and associated genes. Temporal progression of DNA methylation (β -value) (below) and gene expression (VST) (above) during the differentiation process with (orange) or without (blue) vitamin C is depicted. (E) Enrichment of clusters with gene expression / DNA methylation correlation with genesets from CheA 2016 database, containing genes putatively regulated by transcription factors. Odds ratio over background and $-\log_{10}(\text{FDR})$ of the Fisher's exact tests are shown. (F) Western blot of phosphorylated p65 (p-p65) and total p65 in whole-cell lysates. β -actin was used as a loading control. (G) Western blot of p-p65 in the nuclear (NF) and cytoplasmic fraction (CF). GAPDH and histone H1 proteins were used as loading control for cytoplasm and nuclei, respectively. (H) Western blot of the co-immunoprecipitation of p65, showing the signal of p65 and TET2 proteins.

Vitamin C produces dendritic cells with higher T cell stimulation capabilities

We then characterized the mDC_{vitC} phenotype in comparison with mDCs. First, TNF β production after LPS stimulation was studied. mDCs produced negligible amounts of TNF β whereas mDC_{vitC} supernatant contained considerably higher concentrations (Figure 4A). This increase in TNF β production is concomitant to the upregulation of its encoding gene, LTA, and demethylation of adjacent CpGs (Figure 2B).

In addition, we studied the T cell stimulation capabilities of mDC_{vitC} in contrast to mDCs. After clonal expansion of T cells with a Sars-Cov2 mix of antigens, autologous monocytes were differentiated *in vitro* to iDC_{vitC}/iDCs. After maturation with LPS and the loading of the same mix of antigens, mDC_{vitC}/mDCs were cocultured with CFSE-stained T cells.

In Figure 4B, a selected example of T cell proliferation assay is shown. The histogram of the CFSE signal of T cells alone (C^-) or cocultured with mDC/mDC_{vitC} loaded with a control antigen or with the specific set of antigens (An).

Overall, we observed a significant increase in proliferation of T cells, together with a decrease in the median intensity of fluorescence of CFSE when cocultured with mDC_{vitC} loaded with a specific set of antigens, in comparison with mDCs loaded with the same antigens (Figure 4C, Figure 4D). However, when T cells are cocultured with mDCs/mDC_{vitC} loaded with a control antigen, the differences in proliferation and MFI are not significant, indicating that specific antigen presentation is needed to the mDC_{vitC} increased T cell activation capabilities (Figure 4C, Figure 4D).

Figure 4

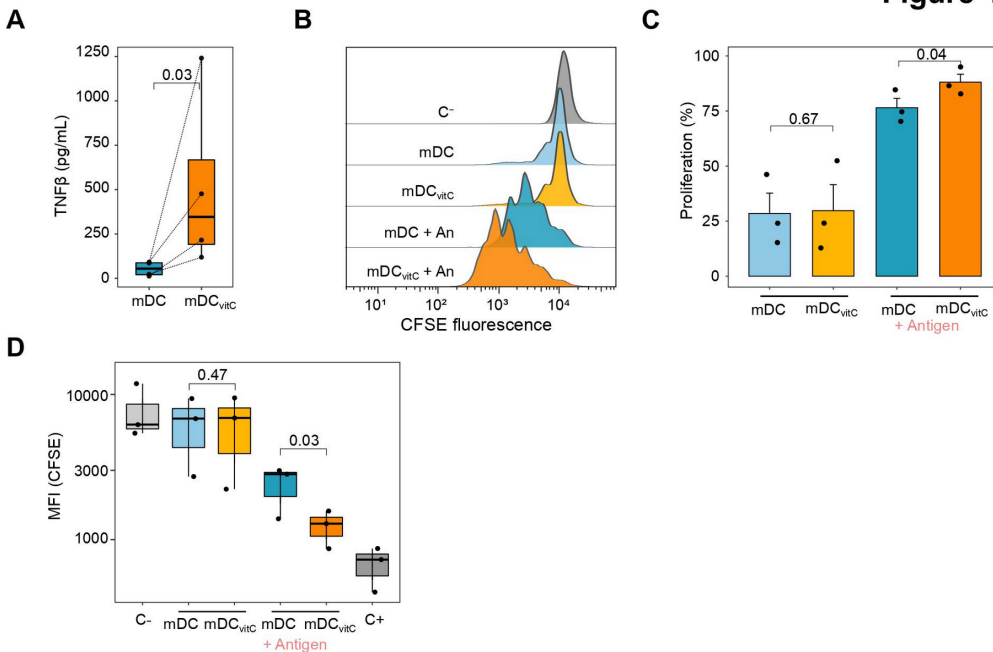


Figure 4. Functional and phenotypic alterations of vitamin C-treated dendritic cells. (A) TNF β production of mDCs and mDC_{vitC}, after 5 days of differentiation and 48h of maturation with LPS. The P-value of a Wilcoxon rank-sum test is shown. (B) Histogram of CFSE signal from T cells, alone without stimulation (C⁻) or cocultured with mDC/mDC_{vitC} treated with a control antigen or a specific set of antigens of SARS-CoV-2 (An). When T cells proliferate, the CFSE signal is diminished. (C) Proliferation of T cells cocultured with mDC/mDC_{vitC} (2:1 proportion), with or without the loading with a specific set of antigens of SARS-CoV-2. Negative control from each donor was used to calculate the proliferation percentage. P-values from two-tailed paired t-tests are shown above. (D) Median Fluorescence Intensity (MFI) of T cells alone (C⁻), cocultured with mDC/mDC_{vitC} (2:1 proportion), with or without the loading with a specific set of antigens of SARS-CoV-2, or stimulated with CD3/CD28 activation beads (C⁺). P-values from two-tailed paired t-tests are shown above.

Discussion

In this work, we have demonstrated a substantial effect of vitamin C supplementation during monocyte (MO) to dendritic cell (DC) *in vitro* differentiation. First, we show vast demethylation in DCs treated with vitamin C, consistent with its role as a TET enzyme cofactor, being the number of additional demethylated CpGs higher than the demethylation from MO to DC without vitamin C. Our analysis suggests that NF- κ B is directly implicated in the specific demethylation observed during the maturation of DCs in the presence of vitamin C. Finally, vitamin C-mediated demethylation is concomitant with an increase in the DC immunogenicity, elevated TNF β production, higher expression of proinflammatory cytokines and antigen presentation genes, and an enhanced capacity to induce the proliferation of autologous T cells with a specific antigen.

Articles

Vitamin C is a well-established cofactor of TET proteins, with the ability to catalyze the oxidation of 5-methylcytosine (5mC) into 5-hydroxymethylcytosine (5hmC) and further oxidized methylcytosine derivatives(23, 24). DNA methylation (5mC) is generally considered a repressive epigenetic mark, associated with gene downregulation(9, 25, 26). Given the absence of proliferation in the MO to DC differentiation process(12), the observed demethylation should be active, TET-mediated demethylation, which is enhanced by vitamin C. TET2, the most expressed TET enzyme in MOs, is probably driving the active demethylation process, as shown in similar contexts(7, 11, 27).

To note, the effects of vitamin C on DNA methylation occur in the last days of the differentiation process, since no DNA methylation differences were found with vitamin C treatment at day 2 of differentiation. Additionally, most variance in methylation occurring in the MO to iDC transition occurs before day 2 suggesting that, without vitamin C, the function of TET enzymes in this model is progressively diminished. Alternative reducing agents present in the culture medium such as glutathione are less efficient as TET cofactors(23, 28). Thus, the progressive oxidation of these reducing agents may explain the impairment of TET function in the absence of vitamin C.

Vitamin C-mediated demethylation occurs during the differentiation (M1 cluster) or the maturation processes of DCs (M2 cluster). Interestingly, the sets of transcription factor motifs enriched in the M1 and M2 clusters are equivalent to the transcription factors involved in the differentiation and LPS signaling, respectively. This suggests that, overall, vitamin C does not promote the recruitment of TET enzymes through new pathways but boosts the demethylation triggered by preexisting active

signaling pathways. This conception is reinforced with the fact that M1 and M2 CpGs are enriched in regions with increasing active chromatin marks (H3K27ac and H3K4me1) in the MO to iDC and the iDC to mDC transitions, respectively (Supplementary Figure 1D).

The functional relationship between DNA demethylation and gene expression has been extensively studied in several contexts(7, 9, 10, 12, 13). Genes more expressed in mDC_{vitC} than mDC, from E1 and E2 clusters are enriched in M1 CpGs closest genes. This establishes a clear temporal relation, suggesting that prior demethylation could be protecting some genes from downregulation during DC maturation. On the other hand, genes from the E5 cluster are enriched in M2 CpGs closest genes. In this case, demethylation is occurring at the same step as upregulation. Then, we cannot know if demethylation or upregulation comes first. However, since the primary mechanism of action of vitamin C through DNA and histones demethylation is well known, we hypothesize that epigenetic modifications could be mediating gene upregulation in mDC_{vitC}. This assumption starts from a different point than other works that established DNA demethylation during DC maturation as a consequence of gene upregulation because in that case, the differential stimulus is live bacteria, that can activate a plethora of signaling pathways not necessarily linked directly to DNA demethylation(10).

Moreover, transcriptome modifications caused by vitamin C are relevant but very modest, in comparison with the great amount of demethylation. This indicates that the majority of demethylation, and other potential epigenomic modifications not studied in this work, are not impacting gene expression. First, the absence of information regarding 3D chromatin structure and histone modifications simplifies the association

Articles

between gene expression and DNA methylation to the study of closest genes. This model is convenient but incomplete. Secondly, the extraordinary impact on DNA methylation of vitamin C, with more differences than the differentiation process itself, would be difficult to translate to gene expression modifications. Fundamentally, a DC treated with vitamin C is still a DC, with changes in relevant genes that can grant phenotypic alterations.

Linus Pauling proposed vitamin C as a potential cancer treatment more than 40 years ago, but the negative results of further clinical trials diminished the enthusiasm(29, 30). However, during the last few years, increasing interest has arisen around vitamin C as a treatment or adjuvant for several types of cancer. For instance, vitamin C intravenous treatment in mice has been shown to abrogate cancer progression through direct TET2 function restoration in cancer cells(16). Moreover, clinical remission following vitamin C treatment was found in a case of acute myeloid leukemia with mutations in *TET2*(31). Furthermore, in mice models of different types of cancer, a fully competent immune system was required to maximize the antiproliferative effects of vitamin C, suggesting an effect of that molecule in the modulation of the immune system(17).

On the other hand, immunotherapy with autologous DCs (DC vaccines) has been extensively investigated, with more than 200 completed clinical trials to date(18). Most efforts have been focused on cancer, but some clinical trials have also been initiated to treat infectious diseases such as COVID19 (NCT04685603, NCT05007496)(32). The use of moDCs differentiated *ex vivo* from monocytes of the same donor is a common and straightforward approach to generating DC vaccines, given the relatively high abundance of these cells in the human blood. However,

the lower antigen presentation capabilities of moDCs in comparison with blood DCs is a bottleneck for the efficacy of these treatments(33).

Here, we show that mDC_{vitC} can stimulate the proliferation of autologous T cells more efficiently than mDCs, in a mechanism dependent on loading with a specific set of antigens, in this case associated with the virus SARS-CoV-2. The improvement in the immune function is associated with epigenomic and transcriptomic remodeling mediated by vitamin C. These results can lead to the generation of new *in vitro* protocols for the generation of DC vaccines from monocytes with higher performance. Moreover, it also exposes a potential mechanistic explanation for the vitamin C antineoplastic effects, through *in vivo* modulation of DC differentiation. Further works using animal models and *in vivo* moDCs should shed light on the specific clinical implications of these insights.

Acknowledgements

We thank CERCA Programme/Generalitat de Catalunya and the Josep Carreras Foundation for institutional support. E.B. was funded by the Spanish Ministry of Science and Innovation (MICINN; grant number SAF2017-88086-R; AEI/FEDER, UE and). O.M.-P. holds an i-PFIS PhD fellowship (grant number IFI17/00034) from Acción Estratégica en Salud 2013-2016 ISCIII, co-financed by Fondo Social Europeo.

Author contributions

O.M.-P. and E.B. conceived and designed the study; O.M.-P, G.G.-T., J.C.-S. and L.C. performed experiments; O.M.-P performed the

Articles

bioinformatic analyses; O.M.-P and E.B. wrote the manuscript; all authors participated in discussions and interpreting the results.

Declaration of interests

There are no conflicts of interests.

References

1. Morante-Palacios, O., Fondelli, F., Ballestar, E. and Martínez-Cáceres, E.M. (2021) Tolerogenic Dendritic Cells in Autoimmunity and Inflammatory Diseases. *Trends Immunol.*, **42**, 59–75.
2. Sallusto, F. and Lanzavecchia, A. (1994) Efficient presentation of soluble antigen by cultured human dendritic cells is maintained by granulocyte/macrophage colony-stimulating factor plus interleukin 4 and downregulated by tumor necrosis factor alpha. *J. Exp. Med.*, **179**, 1109–18.
3. Collin, M. and Bigley, V. (2018) Human dendritic cell subsets: an update. *Immunology*, **154**, 3–20.
4. Coillard, A. and Segura, E. (2019) In vivo Differentiation of Human Monocytes. *Front. Immunol.*, **10**, 1907.
5. Álvarez-Errico, D., Vento-Tormo, R., Sieweke, M. and Ballestar, E. (2015) Epigenetic control of myeloid cell differentiation, identity and function. *Nat. Rev. Immunol.*, **15**, 7–17.
6. de la Rica, L., Rodríguez-Ubreva, J., García, M., Islam, A.B.M.M.K., Urquiza, J.M., Hernando, H., Christensen, J., Helin, K., Gómez-Vaquero, C. and Ballestar, E. (2013) PU.1 target genes undergo Tet2-coupled demethylation and DNMT3b-mediated methylation in monocyte-to-osteoclast differentiation. *Genome Biol.*, **14**, R99.
7. Vento-Tormo, R., Company, C., Rodríguez-Ubreva, J., de la Rica, L., Urquiza, J.M., Javierre, B.M., Sabarinathan, R., Luque, A., Esteller, M., Aran, J.M., *et al.* (2016) IL-4 orchestrates STAT6-mediated DNA demethylation leading to dendritic cell differentiation. *Genome Biol.*, **17**, 4.

Articles

8. Rodriguez,R.M., Suarez-Alvarez,B., Lavín,J.L., Ascensión,A.M., Gonzalez,M., Lozano,J.J., Raneros,A.B., Bulnes,P.D., Vidal-Castiñeira,J.R., Huidobro,C., *et al.* (2019) Signal Integration and Transcriptional Regulation of the Inflammatory Response Mediated by the GM-/M-CSF Signaling Axis in Human Monocytes. *Cell Rep.*, **29**, 860-872.e5.

9. de la Calle-Fabregat,C., Morante-Palacios,O. and Ballestar,E. (2020) Understanding the Relevance of DNA Methylation Changes in Immune Differentiation and Disease. *Genes (Basel)*, **11**.

10. Pacis,A., Mailhot-Léonard,F., Tailleux,L., Randolph,H.E., Yotova,V., Dumaine,A., Grenier,J.C. and Barreiro,L.B. (2019) Gene activation precedes DNA demethylation in response to infection in human dendritic cells. *Proc. Natl. Acad. Sci. U. S. A.*, **116**, 6938–6943.

11. Klug,M., Schmidhofer,S., Gebhard,C., Andreesen,R. and Rehli,M. (2013) 5-Hydroxymethylcytosine is an essential intermediate of active DNA demethylation processes in primary human monocytes. *Genome Biol.*, **14**, R46.

12. Català-Moll,F., Ferreté-Bonastre,A.G., Godoy-Tena,G., Morante-Palacios,O., Ciudad,L., Barberà,L., Fondelli,F., Martínez-Cáceres,E.M., Rodríguez-Ubreva,J., Li,T., *et al.* (2022) Vitamin D receptor, STAT3, and TET2 cooperate to establish tolerogenesis. *Cell Rep.*, **38**, 110244.

13. Morante-Palacios,O., Ciudad,L., Micheroli,R., de la Calle-Fabregat,C., Li,T., Barbisan,G., Houtman,M., Edalat,S.G., Frank-Bertoncelj,M., Ospelt,C., *et al.* (2022) Coordinated glucocorticoid receptor and MAFB action induces tolerogenesis and epigenome remodeling in dendritic cells. *Nucleic Acids Res.*, **50**, 108–126.

14. Ang,A., Pullar,J.M., Currie,M.J. and Vissers,M.C.M. (2018) Vitamin C and immune cell function in inflammation and cancer. *Biochem. Soc. Trans.*, **46**, 1147–1159.
15. Jeong,Y.-J., Kim,J.-H., Hong,J.-M., Kang,J.S., Kim,H.-R., Lee,W.J. and Hwang,Y. (2014) Vitamin C treatment of mouse bone marrow-derived dendritic cells enhanced CD8(+) memory T cell production capacity of these cells *in vivo*. *Immunobiology*, **219**, 554–64.
16. Cimmino,L., Dolgalev,I., Wang,Y., Yoshimi,A., Martin,G.H., Wang,J., Ng,V., Xia,B., Witkowski,M.T., Mitchell-Flack,M., *et al.* (2017) Restoration of TET2 Function Blocks Aberrant Self-Renewal and Leukemia Progression. *Cell*, **170**, 1079-1095.e20.
17. Magrì,A., Germano,G., Lorenzato,A., Lamba,S., Chilà,R., Montone,M., Amodio,V., Ceruti,T., Sassi,F., Arena,S., *et al.* (2020) High-dose vitamin C enhances cancer immunotherapy. *Sci. Transl. Med.*, **12**.
18. Wculek,S.K., Cueto,F.J., Mujal,A.M., Melero,I., Krummel,M.F. and Sancho,D. (2020) Dendritic cells in cancer immunology and immunotherapy. *Nat. Rev. Immunol.*, **20**, 7–24.
19. Schadendorf,D., Ugurel,S., Schuler-Thurner,B., Nestle,F.O., Enk,A., Bröcker,E.-B., Grabbe,S., Rittgen,W., Edler,L., Sucker,A., *et al.* (2006) Dacarbazine (DTIC) versus vaccination with autologous peptide-pulsed dendritic cells (DC) in first-line treatment of patients with metastatic melanoma: a randomized phase III trial of the DC study group of the DeCOG. *Ann. Oncol. Off. J. Eur. Soc. Med. Oncol.*, **17**, 563–70.
20. Liau,L.M., Ashkan,K., Tran,D.D., Campian,J.L., Trusheim,J.E., Cobbs,C.S., Heth,J.A., Salacz,M., Taylor,S., D’Andre,S.D., *et al.* (2018) First results on survival from a large Phase 3 clinical trial of an autologous

Articles

dendritic cell vaccine in newly diagnosed glioblastoma. *J. Transl. Med.*, **16**, 142.

21. Mendes,K., Schmidhofer,S., Minderjahn,J., Glatz,D., Kiesewetter,C., Raithel,J., Wimmer,J., Gebhard,C. and Rehli,M. (2021) The epigenetic pioneer EGR2 initiates DNA demethylation in differentiating monocytes at both stable and transient binding sites. *Nat. Commun.*, **12**, 1556.

22. Lachmann,A., Xu,H., Krishnan,J., Berger,S.I., Mazloom,A.R. and Ma'ayan,A. (2010) ChEA: transcription factor regulation inferred from integrating genome-wide ChIP-X experiments. *Bioinformatics*, **26**, 2438–44.

23. Minor,E.A., Court,B.L., Young,J.I. and Wang,G. (2013) Ascorbate induces ten-eleven translocation (Tet) methylcytosine dioxygenase-mediated generation of 5-hydroxymethylcytosine. *J. Biol. Chem.*, **288**, 13669–74.

24. Wu,X. and Zhang,Y. (2017) TET-mediated active DNA demethylation: mechanism, function and beyond. *Nat. Rev. Genet.*, **18**, 517–534.

25. Luo,C., Hajkova,P. and Ecker,J.R. (2018) Dynamic DNA methylation: In the right place at the right time. *Science (80-)*, **361**, 1336–1340.

26. Anastasiadi,D., Esteve-Codina,A. and Piferrer,F. (2018) Consistent inverse correlation between DNA methylation of the first intron and gene expression across tissues and species. *Epigenetics Chromatin*, **11**, 37.

27. Pacis,A., Tailleux,L., Morin,A.M., Lambourne,J., MacIsaac,J.L., Yotova,V., Dumaine,A., Danckært,A., Luca,F., Grenier,J.C., *et al.* (2015)

Bacterial infection remodels the DNA methylation landscape of human dendritic cells. *Genome Res.*, **25**, 1801–1811.

28. Blaschke,K., Ebata,K.T., Karimi,M.M., Zepeda-Martínez,J.A., Goyal,P., Mahapatra,S., Tam,A., Laird,D.J., Hirst,M., Rao,A., *et al.* (2013) Vitamin C induces Tet-dependent DNA demethylation and a blastocyst-like state in ES cells. *Nature*, **500**, 222–6.

29. Cameron,E. and Pauling,L. (1976) Supplemental ascorbate in the supportive treatment of cancer: Prolongation of survival times in terminal human cancer. *Proc. Natl. Acad. Sci. U. S. A.*, **73**, 3685–9.

30. Cabanillas,F. (2010) Vitamin C and cancer: what can we conclude–1,609 patients and 33 years later? *P. R. Health Sci. J.*, **29**, 215–7.

31. Das,A.B., Kakadia,P.M., Wojcik,D., Pemberton,L., Browett,P.J., Bohlander,S.K. and Vissers,M.C.M. (2019) Clinical remission following ascorbate treatment in a case of acute myeloid leukemia with mutations in TET2 and WT1. *Blood Cancer J.*, **9**, 82.

32. Galati,D., Zanotta,S., Capitelli,L. and Bocchino,M. (2022) A bird’s eye view on the role of dendritic cells in SARS-CoV-2 infection: Perspectives for immune-based vaccines. *Allergy*, **77**, 100–110.

33. Garg,A.D., Coulie,P.G., Van den Eynde,B.J. and Agostinis,P. (2017) Integrating Next-Generation Dendritic Cell Vaccines into the Current Cancer Immunotherapy Landscape. *Trends Immunol.*, **38**, 577–593.

34. Morante-Palacios,O. and Ballestar,E. (2021) shinyÉPICO: A graphical pipeline to analyze Illumina DNA methylation arrays. *Bioinformatics*, 10.1093/bioinformatics/btaa1095.

Articles

35. Aryee,M.J., Jaffe,A.E., Corrada-Bravo,H., Ladd-Acosta,C., Feinberg,A.P., Hansen,K.D. and Irizarry,R.A. (2014) Minfi: a flexible and comprehensive Bioconductor package for the analysis of Infinium DNA methylation microarrays. *Bioinformatics*, **30**, 1363–9.

36. Ritchie,M.E., Phipson,B., Wu,D., Hu,Y., Law,C.W., Shi,W. and Smyth,G.K. (2015) limma powers differential expression analyses for RNA-sequencing and microarray studies. *Nucleic Acids Res.*, **43**, e47.

37. Kim,D., Paggi,J.M., Park,C., Bennett,C. and Salzberg,S.L. (2019) Graph-based genome alignment and genotyping with HISAT2 and HISAT-genotype. *Nat. Biotechnol.*, **37**, 907–915.

38. Li,H., Handsaker,B., Wysoker,A., Fennell,T., Ruan,J., Homer,N., Marth,G., Abecasis,G., Durbin,R. and 1000 Genome Project Data Processing Subgroup (2009) The Sequence Alignment/Map format and SAMtools. *Bioinformatics*, **25**, 2078–9.

39. Liao,Y., Smyth,G.K. and Shi,W. (2014) featureCounts: an efficient general purpose program for assigning sequence reads to genomic features. *Bioinformatics*, **30**, 923–30.

40. Love,M.I., Huber,W. and Anders,S. (2014) Moderated estimation of fold change and dispersion for RNA-seq data with DESeq2. *Genome Biol.*, **15**, 550.

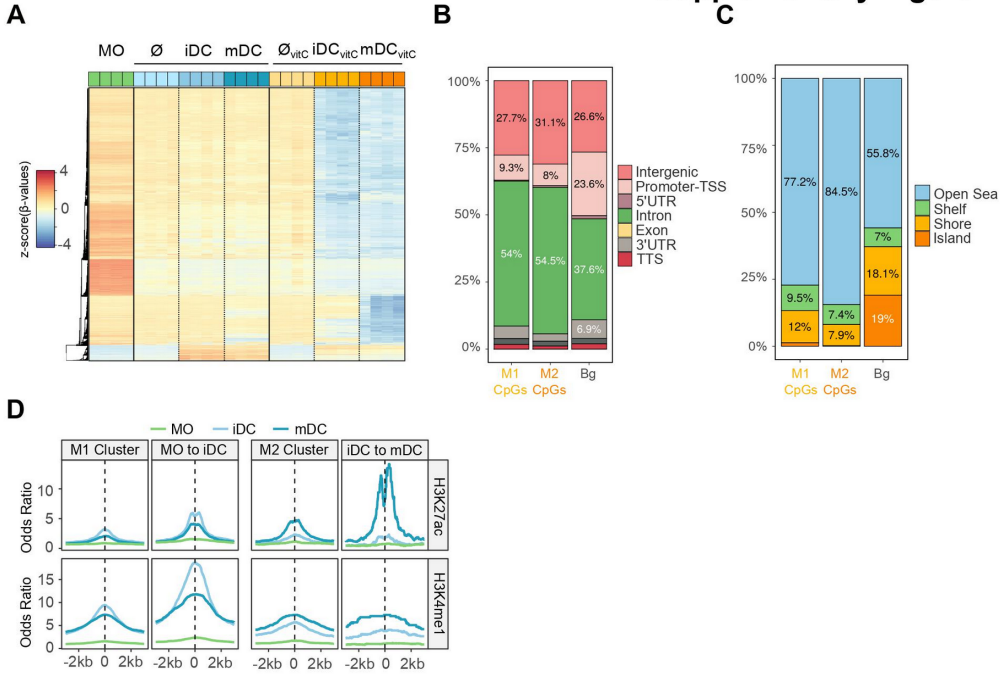
41. McLean,C.Y., Bristol,D., Hiller,M., Clarke,S.L., Schaar,B.T., Lowe,C.B., Wenger,A.M. and Bejerano,G. (2010) GREAT improves functional interpretation of cis-regulatory regions. *Nat. Biotechnol.*, **28**, 495–501.

42. Yu,G., Wang,L.-G., Han,Y. and He,Q.-Y. (2012) clusterProfiler: an R package for comparing biological themes among gene clusters. *OMICS*, **16**, 284–7.

43. Jalili,V., Matteucci,M., Masseroli,M. and Morelli,M.J. (2015) Using combined evidence from replicates to evaluate ChIP-seq peaks. *Bioinformatics*, **31**, 2761–9.

Supplementary Figures

Supplementary Figure 1



Supplementary Figure 1. (A) DNA methylation heatmap of differentially methylated CpGs between all groups, compared pairwise ($\Delta\beta \geq 0.3$, FDR < 0.05). Scaled β -values are shown (lower DNA methylation levels in blue and higher methylation levels in red). (B) Barplot of genomic features percentages of M1 and M2 CpGs in comparison with background CpGs (Bg). (C) Barplot of CpG island contexts percentages of M1 and M2 CpGs in comparison with background CpGs. (D) ChIP-seq data of H3K27ac and H3K4me1 of CD14⁺ MOs, iDCs and mDCs were downloaded from the BLUEPRINT database. Odds ratios were calculated for bins of 10 bp up to 2000 bp around M1 and M2 CpGs. CpGs annotated in the EPIC array were used as background.

GLOBAL RESULTS AND DISCUSSION

GLOBAL RESULTS AND
DISCUSSION

4. GLOBAL RESULTS AND DISCUSSION

4.1. Global results

4.1.1. Coordinated glucocorticoid receptor and MAFB action induces tolerogenesis and epigenome remodeling in dendritic cells (Article 1)

To investigate the mechanisms underlying the glucocorticoid-mediated phenotypic remodeling of DCs, monocytes isolated from peripheral blood of healthy donors were differentiated *in vitro* to DCs and tolDCs for 6 days using GM-CSF and IL-4, in the absence and presence of a GR ligand (dexamethasone), respectively.

The tolerogenic phenotype of tolDCs was confirmed with several experiments, including CD8⁺ T cell proliferation assays in co-culture with DCs and tolDCs, Enzyme-Linked ImmunoSorbent Assays (ELISAs) that revealed a higher production of IL-10 and smaller amounts of TNF α , IL-12p70 and IL-1 β in tolDCs in comparison with DCs, and flow cytometry, with high CD14, CD16, and CD163 expression and low CD86 and CD83 in tolDCs.

Transcriptomes of DCs, tolDCs, and monocytes were profiled. 981 genes were induced and 919 genes were repressed in tolDCs in comparison with DCs (FDR < 0.05, logFC > 0.5). Discriminant Regulon Expression Analysis (DoRothEA) indicated that the transcription factor MAFB was associated with the tolDC transcriptome, with concomitant upregulation of its encoding genes. Moreover, tolDCs presented a transcriptome similar to *in vitro* M2 macrophages and *in vivo* moMACs.

In parallel, we obtained genome-wide DNA methylation profiles of monocytes, DCs, and tolDCs. The comparison of DCs and tolDCs (FDR

Global results and discussion

< 0.05 and absolute $\Delta\beta > 0.2$) in relation to monocytes revealed two clusters of CpG sites: a group of CpGs that underwent specific demethylation in DCs and that was blocked in tolDCs (C1, 1353 CpGs), and a second group that was specifically demethylated in tolDCs (C2, 411 CpGs). Transcription factor motif analysis revealed that C2 CpGs were enriched in Glucocorticoid Response Elements (GREs) and Maf Recognition elements (MAREs). On the other hand, C1 CpGs were enriched in the AP-1 family, PU.1, IRF8, STAT6, and EGR1/EGR2 motifs.

We next associated each CpG with its nearest gene and tested whether C1 and C2 associated genes were enriched in tolDC-induced or tolDC-repressed genes. We found a strong enrichment of the induced genes over the C2 associated genes (FDR = $8.88e-41$) and of the repressed genes over the C1 associated genes (FDR = $4.72e-26$). In this regard, there was a significant inverse correlation between DNA methylation and gene expression ($p < 2.2e-16$).

We found increased mRNA and protein levels of MAFB in tolDCs. Then, we generated ChIP-seq data of GR and MAFB in DCs and tolDCs, at both 4 and 24h of differentiation. To distinguish potential specific features of early and late peaks of GR and MAFB, we classified the tolDC peaks as '4h-specific' (present at 4h but not at 24 h), '24h-specific' (present at 24h but not at 4h), or 'continuous' (present at both times). In both transcription factors, the subset with the strongest binding was the 'continuous' peaks.

We measured the association between each ChIP-seq peak and its nearest gene in order to examine the link between transcription factor binding and gene expression remodeling. Overall, both MAFB and GR

‘4h-specific’, ‘24 h-specific’, and ‘continuous’ associated genes were more strongly expressed in tolDCs than in DCs, indicating that both transcription factors may be involved in upregulating tolDC-specific genes. To note, for both transcription factors, the most robustly associated subset was the ‘continuous’ associated genes.

Co-immunoprecipitation of TET2, a key mediator of active demethylation in myeloid cells, revealed its interaction with both GR and MAFB. Moreover, GR ChIP-seq signal in tolDCs at both 4 and 24h was found around a small subset of CpGs specifically demethylated in tolDCs (C2 CpGs), whereas MAFB signal at both 4 and 24h was found more extensively around C2 CpGs.

Given the association between MAFB binding, gene upregulation, and DNA demethylation in tolDCs, we performed MAFB knockdown, using small-interfering RNAs (siRNAs) targeted against MAFB (siMAFB) or non-targeting (siCTL).

TolDC-induced genes were, in general, significantly downregulated with the MAFB siRNA, whereas tolDC-repressed genes were upregulated. Moreover, genes associated with MAFB ‘continuous’ and ‘4h-specific’ ChIP-seq peaks were linked to siMAFB downregulation, whereas GR peaks were neither related to downregulation nor upregulation.

We then tested the effect of MAFB downregulation on the differentially methylated CpGs. CpGs specifically demethylated in tolDCs (C2 CpGs) were more methylated in tolDC when MAFB was downregulated, confirming the role of MAFB in the tolDC demethylation process. In contrast, no differences were observed in C1 CpGs,

Global results and discussion

corresponding to the absence of MAREs in the cluster and the weaker signal of MAFB in the ChIP-seq.

The tolDC phenotype was also reverted with MAFB downregulation, including the reduction of the surface markers CD14, CD16, and CD163, the inhibition of IL-10 production, and the increase in TNF α production, as well as the impairment of the CD8⁺ T cell proliferation suppression, the main feature of tolDCs.

Finally, we analyzed by single-cell RNA-seq the synovium of rheumatoid arthritis joints from one patient treated with glucocorticoids and one treatment-naive patient. We identified three clusters of putative monocytes or monocyte-derived cells (M1, M2, and M3). The glucocorticoid-treated patient showed an expansion of the M2 cluster, which presented a moMAC signature, with high expression of MAFB and MAFB target genes, supporting the involvement of MAFB in the transcriptomic signature.

Overall, these data indicate that MAFB is a key player in the transcriptomic and epigenomic changes leading to the acquisition of the glucocorticoid-mediated tolerogenic phenotype, with also potential implications for the treatment of patients.

4.1.2. JAK2-STAT Epigenetically Regulates Tolerized Genes in Monocytes in the First Encounter With Gram-Negative Bacterial Endotoxins in Sepsis (Article 2)

To investigate the mechanisms underlying DNA methylation changes associated with the exposure to bacterial endotoxins that lead to tolerance, human CD14⁺ monocytes isolated from healthy donor blood samples were pre-incubated for 24 hours with LPS or Pam3Cys (P3C), which signal

through TLR4 and TLR2, respectively, and lead to a tolerized state. After the first stimulation, cells were washed and left to rest for 3 days in the presence of human pooled serum. Cells were then stimulated again with LPS for another 24h. Monocytes maintained with only RPMI medium and serum for 1 + 3 days (\emptyset 'untreated') were used as negative controls. We confirmed that cells pre-exposed to LPS or P3C produced much lower levels of TNF α after a second exposure to LPS.

We then obtained global DNA methylation profiles of uncultured monocytes and monocytes exposed for 24h to LPS, P3C or untreated (\emptyset), after the 3-day resting period. Methylation profiles of P3C- and LPS-treated monocytes were similar, showing mostly demethylation, but the effect of LPS was more intense. We found 331 hypomethylated and 29 hypermethylated CpGs, with an FDR < 0.05 and an absolute $\Delta\beta$ > 0.2 between LPS-treated and \emptyset monocytes. LPS-hypomethylated CpGs were located mostly in intergenic and intronic regions and were outside CpG island.

Analysis of H3K4me1 and H3K27ac ChIP-seqs, and ATAC-seq time series revealed that gains in DNA accessibility and histone marks characteristic of active enhancers precede DNA methylation changes.

To detect potential transcription factors involved in the demethylation process, we performed motif enrichment analysis. Hypomethylated CpGs of LPS-treated monocytes (Hypo-CpGs) were enriched in transcription factor binding motifs relevant to inflammation such as NF- κ B, the AP-1 family, and some members of the STAT family (STAT1, STAT5, and STAT3)

Next, we performed RNA-seq including LPS-stimulated, untreated and uncultured monocytes. LPS exposure induced upregulation of 1142

Global results and discussion

genes and downregulation of 1025 genes in relation to untreated monocytes ($\log_{2}FC > 1$, $FDR < 0.05$).

We then carried out a DoRothEA with which we identified potentially involved transcription factors coincident with those identified in our previous HOMER analysis of the LPS-specific DNA demethylation set: STAT, NF- κ B, and AP-1 families. Moreover, LPS-upregulated genes were significantly enriched in Hypo-CpG associated genes, reinforcing the notion of the mutual relationship between DNA methylation and gene expression.

Analysis of a gene expression time series of monocyte treatment with LPS (1h, 4h, and 24h) revealed a cluster of Hypo-CpG associated genes with a 'late' profile of gene upregulation, increasing its expression at 24h, concomitantly with DNA demethylation. By motif enrichment analysis, we determined that cluster as specifically enriched in STAT motifs. We then studied the protein levels of STAT1, STAT3, and STAT5 (JAK2 targets) in LPS-treated and untreated monocytes, observing an increase in the phosphorylation of these three transcription factors in LPS-treated samples.

To investigate the potential role of the JAK2 pathway in modulating tolerance-specific DNA methylation changes, we treated monocytes with LPS for 24h in the presence or absence of a selective JAK2 inhibitor (iJAK2).

First, JAK2 inhibition resulted in decreased production of TNF α and increased IL-10 production after a second LPS stimulus, indicating an accentuation of tolerance. Secondly, we performed an RNA-seq of biological triplicates under the previously described cell conditions (LPS-treated monocytes, LPS+iJAK2-treated monocytes, untreated monocytes,

and uncultured monocytes). JAK2 inhibition resulted in downregulation of 124 genes (iJAK2-downregulated genes), whereas only 6 genes were upregulated (LogFC > 1, FDR < 0.05) (iJAK2-upregulated genes).

As suggested by previous data, iJAK2-downregulated genes were associated with LPS-upregulated genes. Moreover, a link was also found between iJAK2-downregulated genes and Hypo-CpG associated genes, suggesting that some genes related to CpGs hypomethylated with LPS are under the transcriptional control of the JAK2-STAT pathway.

We then associated iJAK2-downregulated genes with tolerized genes. Using a public dataset of tolerized genes in monocytes after LPS treatment, we found that top100-tolerized genes but not non-tolerized genes were significantly enriched in iJAK2-downregulated genes.

When we tested the set of hypomethylated CpGs in LPS-treated monocytes (Hypo-CpGs) with STAT1/3/5 binding motifs with the DNA methylation data of sepsis and healthy donor's cohort (11 healthy donors, 7 Gram⁻ sepsis, 7 Other Sepsis, and 4 Systemic Inflammatory Response Syndrome), we found lower methylation levels in gram-negative sepsis patients in comparison with any of the other groups, reinforcing the notion of the participation of the JAK2-STAT pathway in the first encounter with gram-negative bacteria under *in vivo* conditions.

In this regard, we tested STAT activation in septic patients infected with Gram⁻ bacteria, incubating PBMCs from patients and healthy donors for 4h in the presence or absence of LPS. No differences were found between healthy donors and septic patients in the basal (unstimulated) signal of pSTAT1. However, after the LPS stimulus, the pSTAT1 signal was increased in healthy donors but decreased in septic patients.

Global results and discussion

Overall, the data indicate that the JAK2-STAT1 pathway is profoundly disturbed in patients with sepsis caused by Gram⁻ bacteria, producing reduced levels of pSTAT1 after a second immune challenge with LPS and potentially leading to abnormal STAT dependent gene expression patterns that could drive the dysfunctional monocyte response in septic monocytes.

4.1.3. Vitamin C enhances NF- κ B-driven DNA demethylation and immunogenic properties of dendritic cells (Article 3)

Monocytes isolated from peripheral blood of healthy donors were differentiated *in vitro* to DCs for 7 days using GM-CSF and IL-4, in the presence or absence of vitamin C (vitC). Samples were collected at day 2, in the middle of the differentiation (\emptyset / \emptyset_{vitC}), and at day 7, including immature DCs (iDCs) (iDC / iDC_{vitC}), without further treatment, and mature DCs (mDCs), exposed the last 48h to LPS (mDC / mDC_{vitC}).

All differentially methylated positions (DMPs) associated with vitamin C (iDC vs iDC_{vitC} and mDC vs mDC_{vitC}) were represented together, revealing two clusters of CpG sites (M1 and M2). M1 is composed by 3061 CpGs, whereas M2 contains 875 CpGs (FDR < 0.05 and absolute $\Delta\beta$ > 0.3). M1 corresponds with CpGs demethylated during differentiation in the presence of vitamin C whereas M2 are CpGs demethylated during LPS-mediated maturation in the presence of vitamin C. Both clusters were enriched in monocytic enhancers and regions flanking active transcription start sites.

M1 CpGs were enriched in the consensus binding motifs of transcription factors previously related to DC differentiation, such as EGR2, STAT6, and PU.1, whereas M2 CpGs were enriched in the consensus binding motifs of NF- κ B, AP-1, and IRFs.

We then performed RNA-seq of monocytes, \emptyset , \emptyset_{vitC} , iDC, iDC_{vitC}, mDC, and mDC_{vitC}, and checked for differences in their transcriptomes. Since samples were obtained at day 2 (\emptyset / \emptyset_{vitC}), and at day 7, with (mDC / mDC_{vitC}) or without (iDC / iDC_{vitC}) maturation, three potential comparisons of vitamin C-treated cells can be performed, in relation to their respective controls. On day 2, very few differences were found between \emptyset and \emptyset_{vitC} (63 downregulated and 75 upregulated genes). On day 7, we found 163 downregulated and 159 upregulated genes between iDC and iDC_{vitC}, whereas most differences were found between mDC and mDC_{vitC} (185 downregulated and 772 upregulated genes).

Next, we joined the differentially expressed genes of the three comparisons and divided them into six clusters (expression clusters E1-E6) with different behaviors. E1, E2, and E3 clusters showed a diminished downregulation trend in the iDC_{vitC} to mDC_{vitC} transition, in comparison with the iDC to mDC transition, whereas E5 genes are more upregulated in the iDC_{vitC} to mDC_{vitC} transition in comparison with the iDC to mDC transition.

Gene Ontology Enriched terms were calculated for each cluster. For instance, E1 was enriched in dendritic cell migration and chemotaxis, E2 in macrophage activation and cytokine secretion, E3 in antigen processing and presentation and response to calcium ion, and E5 in type I interferon signaling pathway and defense response to virus.

To find potential functional effects of the vitamin C-mediated demethylation, we linked each DMP with its closest gene. When the global profiles of M1 and M2 associated genes intersected with differentially expressed genes are represented, we found that M1 associated genes are less downregulated in mDCs with vitamin C

Global results and discussion

treatment, whereas M2 associated genes are upregulated in mDC_{vitC}. In this regard, E1 and E2 clusters were enriched in M1-associated genes, and the E5 cluster was enriched in M2-associated genes.

Since M2 CpGs and E5 genes were associated with NF- κ B, we decided to further investigate the expression dynamics of this factor. We found that the levels of p65 (a component of NF- κ B) do not change with vitamin C or LPS treatment. However, mDCs and mDC_{vitC} presented higher levels of phosphorylated p65 than iDC and iDC_{vitC}. Furthermore, we detected interaction between p65 and TET2 by co-immunoprecipitation, suggesting that p65 might be recruiting TET2 to specific sites in the genome, promoting demethylation.

We then characterized the mDC_{vitC} phenotype in comparison with mDCs. First, we found considerably higher concentrations of TNF β in mDC_{vitC} supernatants, concomitantly to the upregulation of its encoding gene (LTA).

In addition, we assessed T cell stimulation capabilities of both cell types. To this end, we compared the ability to stimulate T cell proliferation of mDCs/mDC_{vitC} loaded with a Sars-Cov2 mix of antigens. Overall, we observed a significant increase in the proliferation of T cells when cocultured with mDC_{vitC} loaded with a specific set of antigens, in comparison with mDCs loaded with the same antigens. However, when T cells are cocultured with mDCs/mDC_{vitC} loaded with a control antigen, the differences in proliferation are not significant.

Altogether, these results show a critical role of vitamin C modulating the epigenome of DCs during differentiation and maturation, with a relevant impact on their gene expression and immunogenic properties.

4.2. Global discussion

In the present thesis, we have studied how different stimuli can modulate the immunogenic properties and the epigenomic landscape of monocytes and moDCs. Specifically, we have used three different *in vitro* models based on monocytes to discern (a) the sequence of molecular events, transcription factors, and DNA methylation changes involved in the acquisition of glucocorticoid-mediated tolerogenicity in DCs, (b) the signaling pathways participating in the acquirement of endotoxin tolerance in monocytes, and (c) the effect in the DNA methylome, transcriptome and phenotype of a cofactor of TET enzymes, vitamin C, in the context of DC differentiation and maturation.

Firstly, the study of DNA methylation, gene expression, and GR/MAFB binding during tolDC differentiation with glucocorticoids revealed a fast GR-mediated MAFB upregulation followed by extensive MAFB-dependent DNA binding, DNA demethylation, and gene upregulation (**Article 1**) (Figure 7). Since GR is the nuclear receptor involved in recognizing and responding to glucocorticoids in a matter of minutes and possesses the ability to drive chromatin remodeling as a pioneer factor^{201,202}, we initially expected a main role of this transcription factor. In this regard, GR presented a MAFB-independent function, recruiting TET2 and directing the demethylation of some CpG. However, the direct role of GR in this biological context was limited, and its binding was associated only with a small fraction of the epigenomic and transcriptomic changes, in contrast with the high number of genomic sites directly controlled by MAFB.

Global results and discussion

MAFB is a known downstream target of the IL-10/STAT3 signaling pathway²⁰³, which has been previously associated with monocytic differentiation and myeloid cells with anti-inflammatory phenotypes, such as *in vitro* M2 macrophages and *in vivo* moMACs^{21,204,205}. To note, the

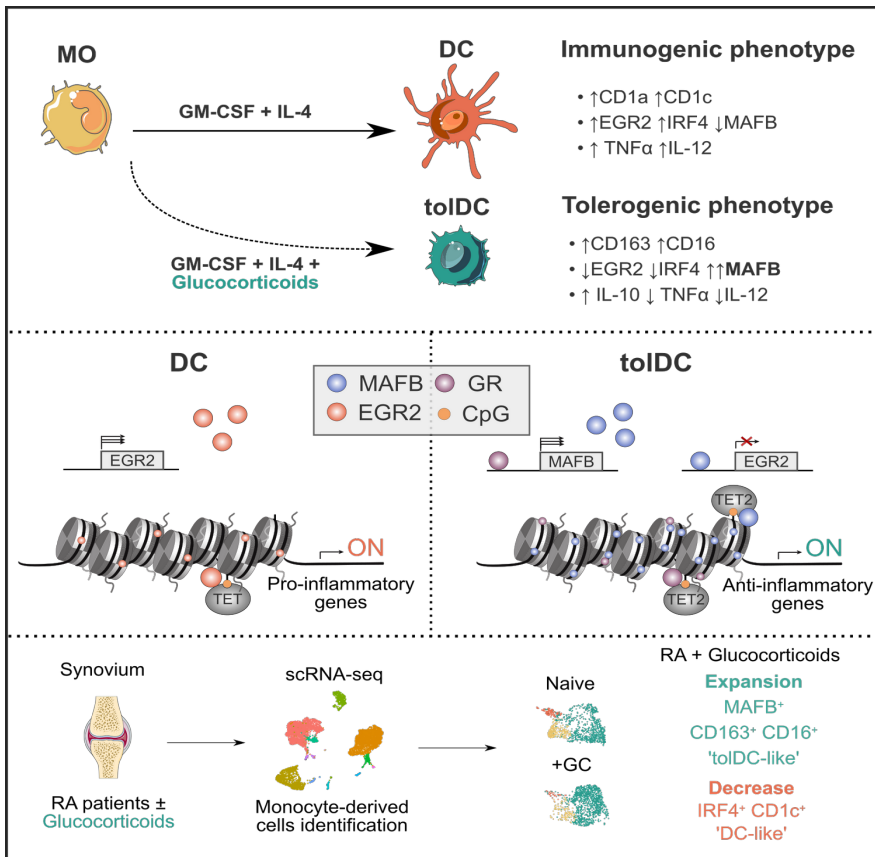


Figure 7: Representation of the molecular events occurring during the differentiation of monocytes to tolDCs with glucocorticoids. Monocytes (MO) can be differentiated to tolDCs in the presence of GM-CSF, IL-4 and glucocorticoids, developing a tolerogenic phenotype. GR binds close to the MAFB gene and promotes its upregulation. MAFB is a key transcription factor in the differentiation of tolDCs, which binds to thousands of genomic loci and promotes demethylation and upregulation of genes. An expansion of tolDC-like cells was also described in a rheumatoid arthritis (RA) patient treated with glucocorticoids.

tolDC transcriptome was very similar to those from M2 macrophages and moMACs, reinforcing the idea that the three cell types have commonalities in their transcriptional regulation. Moreover, we have also observed upregulation of MAFB target genes in anti-inflammatory DC-10 (tolDCs generated with IL-10)¹¹³. Since GR is a ubiquitously expressed transcription factor, with very different cell-type-specific functions²⁰⁶, GR-mediated upregulation of a transcription factor such as MAFB could be a way to exert these anti-inflammatory glucocorticoid-specific functions in monocyte-to-DC differentiation. Discerning the specific molecular mechanisms by which glucocorticoids exert their functions in different cells of the immune system could be a way to generate more specific drugs targeted to activate downstream processes of GR, such as other transcription factors.

Moreover, monocyte-derived cells from synovial tissue of a rheumatoid arthritis patient treated with glucocorticoids presented a depletion of a population with an expression pattern similar to moDCs, and an increase of cells similar to moMACs, in comparison with a non-treated rheumatoid arthritis patient, as studied by single-cell RNA-seq. Due to difficulties in obtaining biopsies from patients treated with glucocorticoids alone or without treatment, only one patient of each type was studied. Therefore, although this result is fully concordant with our *in vitro* model, conclusions should be drawn with caution. Hypothetically, the glucocorticoid-mediated remodeling of monocyte-derived populations in the synovium could be a significant process modulating the inflammation, given the involvement of moDCs in autoimmune pathologies, and their higher immunogenicity compared to moMACs^{45,48,207}.

Global results and discussion

In our second study, we found TET2-dependent demethylation upon TLR4 or TLR2 stimulation of human monocytes, together with the upregulation of inflammatory-related genes (**Article 2**). The JAK2 pathway was associated with both upregulation of genes and demethylation of CpGs during the first encounter with bacterial LPS (Figure 8). JAK2 activity has previously been associated with demethylation through STAT1 stimulation and TET2 recruitment²⁰⁸. Remarkably, JAK/STAT signaling is not directly downstream of TLRs. In this context, we can hypothesize that other molecules, such as IFN γ or IL-6 could activate this pathway in an autocrine or paracrine manner. In this regard, STAT factors were specifically associated with 'late responsive' genes, which upregulation started at 24h, in comparison with genes upregulated from 1h or 4h, which were more associated with AP-1 and NF- κ B transcription factors, directly downstream of TLR signaling.

Furthermore, JAK2-STAT inhibition accentuated the tolerant phenotype of monocytes and reduced the expression of tolerized genes following the first encounter with LPS, suggesting that these genes are under the transcriptional control of JAK2-STAT. In this regard, monocytes from septic patients, which were exposed to bacteria before their extraction, showed lower levels of STAT1 phosphorylation (pSTAT1) after a second immune challenge with LPS, in comparison with monocytes from healthy donors. These results suggest that the endotoxin tolerance occurring in septic monocytes may be caused in part by reduced JAK2 activity, which leads to lower pSTAT1. We can speculate whether direct stimulation of JAK2 in monocytes from septic patients might mitigate the effects of endotoxin tolerance by recovering the activity of STATs. In this regard, IFN γ , which signals through JAK2, is used to treat sepsis-induced immunosuppression²⁰⁹.

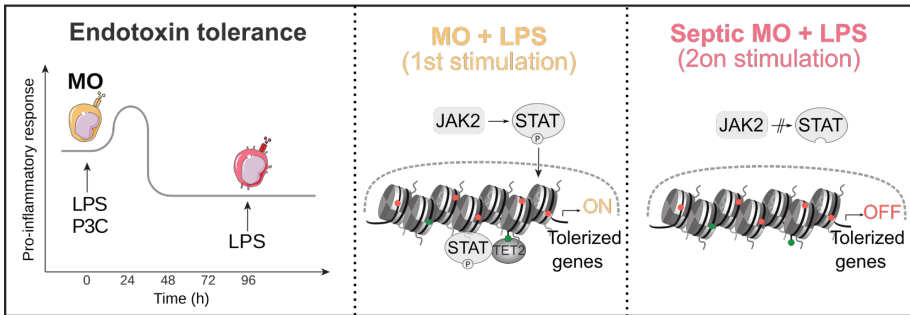


Figure 8: Scheme depicting the relevance of *JAK2-STAT* in the regulation of tolerized genes in the first encounter of monocytes with LPS. Monocytes (MO) stimulated *in vitro* with LPS or P3C develop endotoxin tolerance, a reduced immune response in a second challenge with LPS. DNA demethylation and gene upregulation during the first encounter with LPS is associated with *JAK2-STAT*. Monocytes from septic patients, which were previously exposed to gram negative bacteria *in vivo*, present reduced levels of phosphorylated *STAT1*, indicating a reduced *JAK2* activity.

In the third study, vitamin C supplementation during monocyte to DC differentiation produced widespread demethylation (Figure 9). This demethylation includes the majority of demethylated CpGs in DC differentiation without vitamin C, along with a large number of additional sites. Furthermore, during subsequent maturation with LPS, a new set of CpGs specifically demethylated with vitamin C was also produced. Considering that vitamin C is a cofactor of TET enzymes, it is not surprising that this molecule enhances active demethylation, but it is striking that the changes produced are so extensive. To note, effects of vitamin C are only noticeable in the last days of differentiation, since no changes were observed on day 2. Oxidation of the reducing agents in the culture medium could explain the progressive loss of function of TET enzymes in the absence of vitamin C. In addition, vitamin C also produced changes in the DC transcriptome, especially after maturation, including the upregulation of genes related to DC migration, cytokine

Global results and discussion

secretion, and antigen presentation. Moreover, DCs treated with vitamin C showed an improved stimulation of autologous T cells with a specific antigen and a higher production of TNF β .

TNF β , also known as lymphotoxin α (LT α), is involved in NF- κ B activation and it is related to T cell activation^{210,211}. Thus, this cytokine could act both in an autocrine and paracrine fashion to promote the activation of DCs or T cells.

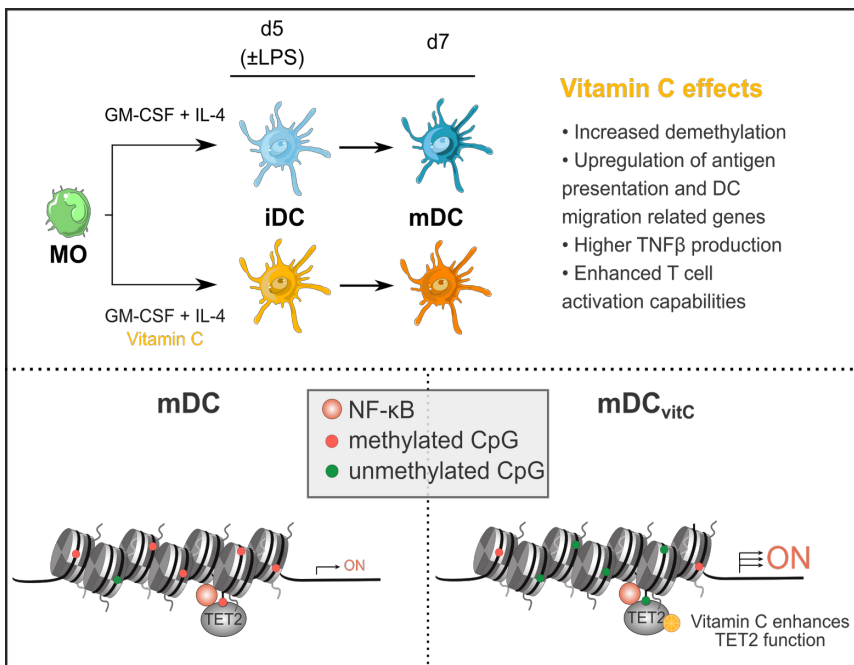


Figure 9: Representation of the monocyte to DC differentiation model in the presence of vitamin C. moDCs exposed to vitamin C during differentiation and maturation shows widespread demethylation, and enhanced immunogenic traits. NF- κ B is associated with both vitamin C-mediated gene upregulation and DNA demethylation during DC maturation. That transcription factor interact with TET2 in mDCs and mDC_{vitC}, but the vitamin C boost of TET function leads to demethylation of genes relevant to DC immunogenicity.

Increasing interest has arisen around the use of vitamin C as a treatment or adjuvant for several types of cancer. Many clinical trials have been carried out to determine the effectiveness of intravenous vitamin C as a potential treatment for cancer, independently or in combination with standard chemotherapies²¹². Moreover, vitamin C treatment in mice has been shown to abrogate cancer progression through direct TET2 function restoration in cancer cells¹⁷⁶. Additionally, another work in mice indicates that the anticancer role of vitamin C depends on the immune system¹⁸⁹. Therefore, the phenotype produced by vitamin C in our model suggests that the effects of vitamin C on cancer could be partially due to the enhancement of moDC immunogenicity through epigenetic mechanisms.

One of the common links between the three papers presented is the study of DNA methylation changes in dynamic processes, stimulating monocytes in different ways. DNA methylation remodeling during immune cell differentiation and maturation has been previously investigated¹. For instance, a recent work established the specific DNA methylation signatures of different populations of PBMCs¹⁹⁴. Moreover, specific methylome changes during *in vitro* moDC differentiation and maturation have been established³⁵. In this regard, it seems clear that the action of transcription factors can recruit methylation machinery and direct the process to specific sites in the genome. We have observed such association in **Article 1**, **Article 2**, and **Article 3**. Moreover, we have demonstrated the connection between transcription factors and DNA demethylation in **Article 1**, via MAFB silencing, and in **Article 2**, with the inhibition of JAK2. Additionally, previous studies have also shown that transcription factors drive de novo DNA methylation or active demethylation, by recruiting DNMT/TET enzymes^{1,198,213-216}.

Global results and discussion

However, the functional role of DNA methylation remodeling, in conjunction with other epigenetic changes, remains elusive. First, in **Article 1**, we have shown that glucocorticoid-mediated DNA demethylation is associated with gene upregulation. However, a detailed time-course has allowed us to determine that gene upregulation can occur before or simultaneous to DNA demethylation in several genes. Additionally, in **Article 2**, we have traced the sequence of events occurring after stimulation of monocytes with LPS, with the gain of accessibility and activation histone marks (H3K27ac and H3K4me1) preceding the loss of DNA methylation. Similarly, some genes were upregulated before DNA demethylation. These results are similar to a previous work showing LPS-mediated demethylation as a consequence of gene activation, rather than a cause²⁰⁰. Conversely, in **Article 3**, we have shown how vitamin C-mediated DNA demethylation during DC differentiation is associated with gene upregulation during maturation. This phenomenon is concordant with previous work in which DNA demethylation during monocyte to DC differentiation was linked to gene upregulation following LPS stimulation³⁵.

Although DNA demethylation is a relatively rapid process, which can occur in a matter of hours (**Article 1**)³⁵, gene expression changes triggered by nuclear receptors such as GR and signaling pathways of TLRs and cytokine receptors are generally faster and can occur in less than an hour²¹⁷. These results suggest that DNA methylation may stabilize the phenotype and have relevance in preparing the cell for response to further stimuli, but its role in the regulation of early response genes during fast signaling processes, such as those mediated upon activation of TLRs during DC maturation, appears to be more limited. However, we cannot rule out the possibility that demethylation may play a role during DC

maturation in the regulation of genes with a later response profile. Moreover, we may hypothesize that demethylation could provide a differential response to successive stimuli, as proposed by Pacis *et al.*²⁰⁰. New experiments should be performed to test whether vitamin C-mediated demethylation during LPS maturation is able to influence in any way the action of moDCs upon further stimuli.

In contrast, DNA methylation changes occurring during the first stimulus of monocytes with LPS are not clearly related to the subsequent acquisition of endotoxin tolerance upon further stimulation (**Article 2**). We described mostly demethylation of enhancers, which generally is associated with gene upregulation²¹⁸. Therefore, the potential relationship between LPS-mediated demethylation with a reduced response of the associated genes to new stimuli seems unlikely. Notably, genes associated with demethylated CpGs in monocytes treated with LPS showed a higher (1.9-fold) enrichment in non-tolerized genes than in tolerized genes, opening the possibility of a potential opposite effect, with demethylation providing some protection to gene tolerization (data not shown in the paper).

Nevertheless, our correlations between gene expression and DNA methylation have some limitations that are worth discussing. Firstly, we have associated each DMP with its closest gene. Although this approach is very convenient, because of its simplicity, it does not consider potential confounding factors such as histone mark modifications and DNA accessibility remodeling, and other relevant variables, such as the 3D structure of chromatin and the genomic context of the CpG. Furthermore, we have only studied 5mC and, therefore, we cannot discard that faster increases in 5hmC, or other demethylation intermediates, directly

Global results and discussion

influences gene expression. In this sense, 5hmC has been proposed as a bona fide epigenetic mark, and correlations between the presence of this mark and gene upregulation have been found in several contexts^{165,219,220}. Finally, the sample sizes used in our DNA methylation analysis perhaps do not allow us to detect subtle changes in methylation, potentially occurring before changes in gene expression.

Another relevant aspect of the epigenomic remodelling and underlying factors and signaling pathways in the *in vitro* models studied herein is their potential clinical relevance. On the one hand, tolDCs, produced by treating monocytes with GM-CSF, IL-4, and additional molecules, such as glucocorticoids or vitamin D, have been tested in several clinical trials to treat various diseases, including rheumatoid arthritis, multiple sclerosis, and type 1 diabetes, among others¹⁴. On the other hand, the generation of immunogenic DCs (DC vaccines) for cancer treatment is an approach with several ongoing clinical trials and one Food and Drug Administration (FDA) approved treatment¹⁵². Although tolDCs and DC vaccines are promising, their use in the treatment of patients with autoimmune diseases or cancer, respectively, is still very limited. Different aspects can be considered for the development of these therapies, including the source of the cells as well as the differentiation protocol, maturation, and antigen loading. In particular, natural populations of DCs, including cDCs and pDCs, possess greater antigenic presentation capabilities than *in vitro* moDCs²²¹. However, monocytes are much more abundant in blood than cDCs and pDCs, making them much easier to use for this type of treatment. Improving the characteristics of moDCs through modification of the *in vitro* differentiation and maturation could be key to obtaining an abundant and effective source of DCs for cell therapy.

In addition, we have observed that the extensive demethylation produced by vitamin C in the differentiation and maturation of moDCs (**Article 3**) is associated with the same set of transcription factors as the equivalent processes without vitamin C. Thus, vitamin C could be a mere booster of active demethylation, favoring the function of pre-existing signaling pathways, but without an immunogenic or tolerogenic effect per se. Modulation of the differentiation processes of tolerogenic or immunogenic moDCs can be useful to improve the properties of these cells. In this regard, vitamin C has been shown to boost several immunogenic properties in our immunogenic model, including increased production of proinflammatory cytokines and enhanced stimulation of T cells. Further experiments should be performed to better characterize these cells and to test whether DCs treated with vitamin C improve patient outcomes. Moreover, we hypothesized that vitamin C might have an effect on DNA methylation and perhaps phenotype in other differentiation or maturation processes. For instance, the tolerogenic phenotype of tolDCs produced with glucocorticoids, IL-4, and GM-CSF (**Article 1**) could be enhanced with the addition of vitamin C, paving the way for the production of better tolDCs for clinical practice.

In the three studies in this thesis, we have utilized human monocytes or moDCs. This leads to some technical limitations in the experimental procedures. For example, the difficulty in transfecting monocytes and their immune response to nucleic acids makes it difficult to use vectors or siRNAs to induce or silence genes²²². In addition, given that these are terminally differentiated, non-proliferative cells, it is not possible to create stable lines with genetic modifications. The optimization of *in vitro* mRNA transcription and transfection in monocytes and monocyte-derived cells could partially solve this problem.

Global results and discussion

On the other hand, the user of human monocytes presents some advantages over primary murine cells because the differences in the human and mouse immune systems are very extensive²²³⁻²²⁵. In addition, the analysis of monocytes from donors with a different genetic background and very different parameters provides greater variance but results that are more comparable to the general population. Furthermore, there is considerable evidence for the existence of an *in vivo* counterpart to *in vitro* moDCs¹⁷. moDC involvement in several diseases makes them very relevant, not only because of their usefulness for the development of cell therapies but also as a model for the study of the *in vivo* differentiation process and its potential modulation.

In summary, our study has shown the relevance of epigenomic dynamics in monocytes and moDCs exposed to different molecules, in relation to the signaling cascades and transcription factors that drive different immune responses to different stimuli, leading to a particular phenotype. Our results highlight how chemical modulators can skew, through epigenomic remodeling and transcription factor recruitment, the immune function of dendritic cells towards a tolerogenic or immunogenic phenotype. This knowledge is not only valuable from a basic point of view, but also could be relevant for the improvement of dendritic cell-based therapies.

CONCLUSIONS

CONCLUSIONS

5. CONCLUSIONS

The conclusions obtained during this doctoral thesis can be summarized as follows:

1. Glucocorticoids drive DNA methylation remodeling during monocyte to tolDC differentiation characterized by both extensive blockage in GM-CSF/IL-4-mediated demethylation and specific demethylation of a new cluster of CpGs.
2. DNA methylation changes of tolDCs in comparison with DCs are inversely correlated with gene expression. Gene induction can both precede or follow DNA methylation.
3. GR binds to the MAFB promoter and a close enhancer following glucocorticoid treatment, with concomitant mRNA and protein upregulation of MAFB.
4. MAFB binds to thousands of genomic loci in tolDCs associated with gene upregulation and DNA demethylation. GR binding is linked to a small subset of the transcriptome and methylome remodeling.
5. Both GR and MAFB interact with TET2 and bind to genomic regions that become demethylated in tolDCs.

Conclusions

6. MAFB knockdown erases the tolerogenic properties of tolDCs and reverts glucocorticoid-specific DNA demethylation and gene upregulation.
7. Synovial tissue from a rheumatoid arthritis patient treated with glucocorticoids displays an increase in a myeloid population characterized by a gene expression pattern similar to that from tolDCs and high expression of MAFB target genes, in comparison with a non-treated patient.
8. In monocytes exposed to bacterial LPS or P3C, the acquisition of endotoxin tolerance is accompanied by DNA demethylation close to genes that become upregulated.
9. A subset of LPS-mediated demethylation and 'late response' upregulated genes are associated with STAT transcription factors.
10. JAK2 is activated during LPS stimulation and STAT1, STAT3, and STAT5 become phosphorylated.
11. JAK2 controls the expression of genes that become tolerized in monocytes after a second challenge with LPS.

12. JAK2 inhibition during the treatment of monocytes with LPS accentuates endotoxin tolerance in a second challenge, with a decreased TNF α production and increased IL-10.
13. Monocytes from septic patients display a decrease in STAT1 phosphorylation in comparison with healthy donors, together with the acquisition of endotoxin tolerance.
14. In monocyte to DC differentiation and maturation, in the presence of vitamin C, there is extensive DNA demethylation. Demethylation in the maturation process is mainly linked to genomic sites enriched in NF- κ B motifs.
15. TET2 co-immunoprecipitates with p65 (NF- κ B) in DCs, with or without vitamin C treatment.
16. Demethylation produced by vitamin C includes CpGs of the conventional differentiation process. Additional demethylation only occurs after day 2 of differentiation.
17. p65 interacts with TET2 in mDCs with or without vitamin C and binds to genomic regions that become demethylated.

Conclusions

18. Vitamin C-mediated demethylation during differentiation and maturation is associated with increased expression of migration and antigen presentation-related genes in mDC_{vitC}.
19. Vitamin C enhances TNF β production and T cell activation capabilities of DCs.

REFERENCES

REFERENCES

6. REFERENCES

1. de la Calle-Fabregat, C., Morante-Palacios, O. & Ballestar, E. Understanding the Relevance of DNA Methylation Changes in Immune Differentiation and Disease. *Genes (Basel)*. **11**, (2020).
2. Chaplin, D. D. Overview of the immune response. *J. Allergy Clin. Immunol.* **125**, S3-23 (2010).
3. Parkin, J. & Cohen, B. An overview of the immune system. *Lancet (London, England)* **357**, 1777–89 (2001).
4. Bonilla, F. A. & Oettgen, H. C. Adaptive immunity. *J. Allergy Clin. Immunol.* **125**, S33-40 (2010).
5. Ratajczak, W., Niedźwiedzka-Rystwej, P., Tokarz-Deptuła, B. & Deptuła, W. Immunological memory cells. *Cent. J. Immunol.* **43**, 194–203 (2018).
6. Netea, M. G. *et al.* Trained immunity: A program of innate immune memory in health and disease. *Science* **352**, aaf1098 (2016).
7. Belicard, T., Jareosettasin, P. & Sarkies, P. The piRNA pathway responds to environmental signals to establish intergenerational adaptation to stress. *BMI. Zaret, K. S. Pioneer Transcr. Factors Initiat. Gene Netw. Chang. Annu. Rev. Genet.* **54**, 367–385 (2020). *C Biol.* **16**, 103 (2018).
8. Katzmarski, N. *et al.* Transmission of trained immunity and heterologous resistance to infections across generations. *Nat. Immunol.* **22**, 1382–1390 (2021).
9. Pradeu, T. & Cooper, E. L. The danger theory: 20 years later. *Front. Immunol.* **3**, 287 (2012).
10. Matzinger, P. The danger model: a renewed sense of self. *Science* **296**, 301–5 (2002).
11. Zindel, J. & Kubes, P. DAMPs, PAMPs, and LAMPs in Immunity and Sterile Inflammation. *Annu. Rev. Pathol.* **15**, 493–518 (2020).
12. Abbas, A., Lichtman, A. & Pillai, S. *Cellular and Molecular Immunology*. (2017).

References

13. Nelson, R. W. *et al.* T cell receptor cross-reactivity between similar foreign and self peptides influences naive cell population size and autoimmunity. *Immunity* **42**, 95–107 (2015).
14. Morante-Palacios, O., Fondelli, F., Ballestar, E. & Martínez-Cáceres, E. M. Tolerogenic Dendritic Cells in Autoimmunity and Inflammatory Diseases. *Trends Immunol.* **42**, 59–75 (2021).
15. Auffray, C., Sieweke, M. H. & Geissmann, F. Blood monocytes: development, heterogeneity, and relationship with dendritic cells. *Annu. Rev. Immunol.* **27**, 669–92 (2009).
16. Yáñez, A. *et al.* Granulocyte-Monocyte Progenitors and Monocyte-Dendritic Cell Progenitors Independently Produce Functionally Distinct Monocytes. *Immunity* **47**, 890-902.e4 (2017).
17. Coillard, A. & Segura, E. In vivo Differentiation of Human Monocytes. *Front. Immunol.* **10**, 1907 (2019).
18. Patel, A. A. *et al.* The fate and lifespan of human monocyte subsets in steady state and systemic inflammation. *J. Exp. Med.* **214**, 1913–1923 (2017).
19. Tak, T. *et al.* Circulatory and maturation kinetics of human monocyte subsets *in vivo*. *Blood* **130**, 1474–1477 (2017).
20. Thaler, B. *et al.* Differential *in vivo* activation of monocyte subsets during low-grade inflammation through experimental endotoxemia in humans. *Sci. Rep.* **6**, 30162 (2016).
21. Goudot, C. *et al.* Aryl Hydrocarbon Receptor Controls Monocyte Differentiation into Dendritic Cells versus Macrophages. *Immunity* **47**, 582-596.e6 (2017).
22. Auffray, C. *et al.* Monitoring of blood vessels and tissues by a population of monocytes with patrolling behavior. *Science* **317**, 666–70 (2007).
23. Wolf, A. A., Yáñez, A., Barman, P. K. & Goodridge, H. S. The Ontogeny of Monocyte Subsets. *Front. Immunol.* **10**, 1642 (2019).

24. Narasimhan, P. B., Marcovecchio, P., Hamers, A. A. J. & Hedrick, C. C. Nonclassical Monocytes in Health and Disease. *Annu. Rev. Immunol.* **37**, 439–456 (2019).
25. Boyette, L. B. *et al.* Phenotype, function, and differentiation potential of human monocyte subsets. *PLoS One* **12**, e0176460 (2017).
26. Olingy, C. E. *et al.* Non-classical monocytes are biased progenitors of wound healing macrophages during soft tissue injury. *Sci. Rep.* **7**, 447 (2017).
27. Misharin, A. V *et al.* Nonclassical Ly6C(-) monocytes drive the development of inflammatory arthritis in mice. *Cell Rep.* **9**, 591–604 (2014).
28. Hanna, R. N. *et al.* The transcription factor NR4A1 (Nur77) controls bone marrow differentiation and the survival of Ly6C- monocytes. *Nat. Immunol.* **12**, 778–85 (2011).
29. Lacey, D. C. *et al.* Defining GM-CSF- and macrophage-CSF-dependent macrophage responses by *in vitro* models. *J. Immunol.* **188**, 5752–5765 (2012).
30. Geissmann, F. *et al.* Transforming growth factor beta1, in the presence of granulocyte/macrophage colony-stimulating factor and interleukin 4, induces differentiation of human peripheral blood monocytes into dendritic Langerhans cells. *J. Exp. Med.* **187**, 961–966 (1998).
31. Rodríguez-Ubreva, J. *et al.* Prostaglandin E2 Leads to the Acquisition of DNMT3A-Dependent Tolerogenic Functions in Human Myeloid-Derived Suppressor Cells. *Cell Rep.* **21**, 154–167 (2017).
32. de la Rica, L. *et al.* PU.1 target genes undergo Tet2-coupled demethylation and DNMT3b-mediated methylation in monocyte-to-osteoclast differentiation. *Genome Biol.* **14**, R99 (2013).
33. Lacey, D. L. *et al.* Osteoprotegerin ligand is a cytokine that regulates osteoclast differentiation and activation. *Cell* **93**, 165–176 (1998).
34. Etemad, S., Zamin, R. M., Ruitenberg, M. J. & Filgueira, L. A novel *in vitro* human microglia model: characterization of human

References

- monocyte-derived microglia. *J. Neurosci. Methods* **209**, 79–89 (2012).
35. Vento-Tormo, R. *et al.* IL-4 orchestrates STAT6-mediated DNA demethylation leading to dendritic cell differentiation. *Genome Biol.* **17**, 4 (2016).
 36. Sallusto, F. & Lanzavecchia, A. Efficient presentation of soluble antigen by cultured human dendritic cells is maintained by granulocyte/macrophage colony-stimulating factor plus interleukin 4 and downregulated by tumor necrosis factor alpha. *J. Exp. Med.* **179**, 1109–18 (1994).
 37. Richter, L. *et al.* Transcriptional profiling reveals monocyte-related macrophages phenotypically resembling DC in human intestine. *Mucosal Immunol.* **11**, 1512–1523 (2018).
 38. Liao, C.-T. *et al.* Peritoneal macrophage heterogeneity is associated with different peritoneal dialysis outcomes. *Kidney Int.* **91**, 1088–1103 (2017).
 39. Jardine, L. *et al.* Lipopolysaccharide inhalation recruits monocytes and dendritic cell subsets to the alveolar airspace. *Nat. Commun.* **10**, 1999 (2019).
 40. van der Laan, A. M. *et al.* Monocyte subset accumulation in the human heart following acute myocardial infarction and the role of the spleen as monocyte reservoir. *Eur. Heart J.* **35**, 376–85 (2014).
 41. Grimm, M. C. *et al.* Direct evidence of monocyte recruitment to inflammatory bowel disease mucosa. *J. Gastroenterol. Hepatol.* **10**, 387–95.
 42. Thurlings, R. M. *et al.* Monocyte scintigraphy in rheumatoid arthritis: the dynamics of monocyte migration in immune-mediated inflammatory disease. *PLoS One* **4**, e7865 (2009).
 43. Zilionis, R. *et al.* Single-Cell Transcriptomics of Human and Mouse Lung Cancers Reveals Conserved Myeloid Populations across Individuals and Species. *Immunity* **50**, 1317-1334.e10 (2019).

44. Azizi, E. *et al.* Single-Cell Map of Diverse Immune Phenotypes in the Breast Tumor Microenvironment. *Cell* **174**, 1293-1308.e36 (2018).
45. Segura, E. *et al.* Human inflammatory dendritic cells induce Th17 cell differentiation. *Immunity* **38**, 336–48 (2013).
46. González-Domínguez, É. *et al.* CD163L1 and CLEC5A discriminate subsets of human resident and inflammatory macrophages *in vivo*. *J. Leukoc. Biol.* **98**, 453–66 (2015).
47. Bujko, A. *et al.* Transcriptional and functional profiling defines human small intestinal macrophage subsets. *J. Exp. Med.* **215**, 441–458 (2018).
48. Kamada, N. *et al.* Unique CD14 intestinal macrophages contribute to the pathogenesis of Crohn disease via IL-23/IFN-gamma axis. *J. Clin. Invest.* **118**, 2269–80 (2008).
49. Bajpai, G. *et al.* The human heart contains distinct macrophage subsets with divergent origins and functions. *Nat. Med.* **24**, 1234–1245 (2018).
50. Michea, P. *et al.* Adjustment of dendritic cells to the breast-cancer microenvironment is subset specific. *Nat. Immunol.* **19**, 885–897 (2018).
51. Tang-Huau, T.-L. *et al.* Human *in vivo*-generated monocyte-derived dendritic cells and macrophages cross-present antigens through a vacuolar pathway. *Nat. Commun.* **9**, 2570 (2018).
52. Watchmaker, P. B. *et al.* Comparative transcriptional and functional profiling defines conserved programs of intestinal DC differentiation in humans and mice. *Nat. Immunol.* **15**, 98–108 (2014).
53. Moret, F. M. *et al.* Intra-articular CD1c-expressing myeloid dendritic cells from rheumatoid arthritis patients express a unique set of T cell-attracting chemokines and spontaneously induce Th1, Th17 and Th2 cell activity. *Arthritis Res. Ther.* **15**, R155 (2013).

References

54. Brubaker, S. W., Bonham, K. S., Zanoni, I. & Kagan, J. C. Innate immune pattern recognition: a cell biological perspective. *Annu. Rev. Immunol.* **33**, 257–90 (2015).
55. Kawai, T. & Akira, S. The role of pattern-recognition receptors in innate immunity: update on Toll-like receptors. *Nat. Immunol.* **11**, 373–84 (2010).
56. Roach, J. C. *et al.* The evolution of vertebrate Toll-like receptors. *Proc. Natl. Acad. Sci. U. S. A.* **102**, 9577–82 (2005).
57. Schumann, R. R. *et al.* Structure and function of lipopolysaccharide binding protein. *Science* **249**, 1429–31 (1990).
58. Gioannini, T. L. & Weiss, J. P. Regulation of interactions of Gram-negative bacterial endotoxins with mammalian cells. *Immunol. Res.* **39**, 249–60 (2007).
59. Lin, S.-C., Lo, Y.-C. & Wu, H. Helical assembly in the MyD88-IRAK4-IRAK2 complex in TLR/IL-1R signalling. *Nature* **465**, 885–90 (2010).
60. Motshwene, P. G. *et al.* An oligomeric signaling platform formed by the Toll-like receptor signal transducers MyD88 and IRAK-4. *J. Biol. Chem.* **284**, 25404–11 (2009).
61. Kawagoe, T. *et al.* Sequential control of Toll-like receptor-dependent responses by IRAK1 and IRAK2. *Nat. Immunol.* **9**, 684–91 (2008).
62. Cao, Z., Xiong, J., Takeuchi, M., Kurama, T. & Goeddel, D. V. TRAF6 is a signal transducer for interleukin-1. *Nature* **383**, 443–6 (1996).
63. Wang, C. *et al.* TAK1 is a ubiquitin-dependent kinase of MKK and IKK. *Nature* **412**, 346–51 (2001).
64. Horvath, C. M. The Jak-STAT pathway stimulated by interferon alpha or interferon beta. *Sci. STKE* **2004**, tr10 (2004).
65. Hu, X., Li, J., Fu, M., Zhao, X. & Wang, W. The JAK/STAT signaling pathway: from bench to clinic. *Signal Transduct. Target. Ther.* **6**, 402 (2021).

66. Darnell, J. E. STATs and gene regulation. *Science* **277**, 1630–5 (1997).
67. Janssens, S., Burns, K., Vercammen, E., Tschopp, J. & Beyaert, R. MyD88S, a splice variant of MyD88, differentially modulates NF-kappaB- and AP-1-dependent gene expression. *FEBS Lett.* **548**, 103–7 (2003).
68. Kobayashi, K. *et al.* IRAK-M is a negative regulator of Toll-like receptor signaling. *Cell* **110**, 191–202 (2002).
69. Shembade, N. & Harhaj, E. W. Regulation of NF-κB signaling by the A20 deubiquitinase. *Cell. Mol. Immunol.* **9**, 123–30 (2012).
70. Wald, D. *et al.* SIGIRR, a negative regulator of Toll-like receptor-interleukin 1 receptor signaling. *Nat. Immunol.* **4**, 920–7 (2003).
71. Yoshimura, A., Naka, T. & Kubo, M. SOCS proteins, cytokine signalling and immune regulation. *Nat. Rev. Immunol.* **7**, 454–65 (2007).
72. Moore, K. W., de Waal Malefyt, R., Coffman, R. L. & O’Garra, A. Interleukin-10 and the interleukin-10 receptor. *Annu. Rev. Immunol.* **19**, 683–765 (2001).
73. Hawrylowicz, C. M. & O’Garra, A. Potential role of interleukin-10-secreting regulatory T cells in allergy and asthma. *Nat. Rev. Immunol.* **5**, 271–83 (2005).
74. Hart, P. H., Hunt, E. K., Bonder, C. S., Watson, C. J. & Finlay-Jones, J. J. Regulation of surface and soluble TNF receptor expression on human monocytes and synovial fluid macrophages by IL-4 and IL-10. *J. Immunol.* **157**, 3672–80 (1996).
75. Barragan, M., Good, M. & Kolls, J. K. Regulation of Dendritic Cell Function by Vitamin D. *Nutrients* **7**, 8127–51 (2015).
76. Zhang, Y. *et al.* Vitamin D inhibits monocyte/macrophage proinflammatory cytokine production by targeting MAPK phosphatase-1. *J. Immunol.* **188**, 2127–35 (2012).

References

77. Ehrchen, J. M., Roth, J. & Barczyk-Kahlert, K. More Than Suppression: Glucocorticoid Action on Monocytes and Macrophages. *Front. Immunol.* **10**, 2028 (2019).
78. Álvarez-Errico, D., Vento-Tormo, R., Sieweke, M. & Ballestar, E. Epigenetic control of myeloid cell differentiation, identity and function. *Nat. Rev. Immunol.* **15**, 7–17 (2015).
79. Netea, M. G., Quintin, J. & van der Meer, J. W. M. Trained immunity: a memory for innate host defense. *Cell Host Microbe* **9**, 355–61 (2011).
80. Quintin, J. *et al.* *Candida albicans* infection affords protection against reinfection via functional reprogramming of monocytes. *Cell Host Microbe* **12**, 223–32 (2012).
81. Saeed, S. *et al.* Epigenetic programming of monocyte-to-macrophage differentiation and trained innate immunity. *Science* **345**, 1251086 (2014).
82. Biswas, S. K. & Lopez-Collazo, E. Endotoxin tolerance: new mechanisms, molecules and clinical significance. *Trends Immunol.* **30**, 475–87 (2009).
83. Novakovic, B. *et al.* β -Glucan Reverses the Epigenetic State of LPS-Induced Immunological Tolerance. *Cell* **167**, 1354-1368.e14 (2016).
84. Munoz, C. *et al.* Dysregulation of *in vitro* cytokine production by monocytes during sepsis. *J. Clin. Invest.* **88**, 1747–54 (1991).
85. Cavaillon, J.-M. & Adib-Conquy, M. Bench-to-bedside review: endotoxin tolerance as a model of leukocyte reprogramming in sepsis. *Crit. Care* **10**, 233 (2006).
86. Rieckmann, A. *et al.* Vaccinations against smallpox and tuberculosis are associated with better long-term survival: a Danish case-cohort study 1971-2010. *Int. J. Epidemiol.* **46**, 695–705 (2017).
87. Merad, M., Sathe, P., Helft, J., Miller, J. & Mortha, A. The dendritic cell lineage: ontogeny and function of dendritic cells and their subsets in the steady state and the inflamed setting. *Annu. Rev. Immunol.* **31**, 563–604 (2013).

88. Netea, M. G. *et al.* Defining trained immunity and its role in health and disease. *Nat. Rev. Immunol.* **20**, 375–388 (2020).
89. Chavakis, T., Mitroulis, I. & Hajishengallis, G. Hematopoietic progenitor cells as integrative hubs for adaptation to and fine-tuning of inflammation. *Nat. Immunol.* **20**, 802–811 (2019).
90. Mitroulis, I. *et al.* Modulation of Myelopoiesis Progenitors Is an Integral Component of Trained Immunity. *Cell* **172**, 147-161.e12 (2018).
91. Haller Hasskamp, J., Zapas, J. L. & Elias, E. G. Dendritic cell counts in the peripheral blood of healthy adults. *Am. J. Hematol.* **78**, 314–5 (2005).
92. MacDonald, K. P. A. *et al.* Characterization of human blood dendritic cell subsets. *Blood* **100**, 4512–20 (2002).
93. Guilliams, M. *et al.* Dendritic cells, monocytes and macrophages: a unified nomenclature based on ontogeny. *Nat. Rev. Immunol.* **14**, 571–8 (2014).
94. Hémond, C., Neel, A., Heslan, M., Braudeau, C. & Josien, R. Human blood mDC subsets exhibit distinct TLR repertoire and responsiveness. *J. Leukoc. Biol.* **93**, 599–609 (2013).
95. Hubert, M. *et al.* IFN-III is selectively produced by cDC1 and predicts good clinical outcome in breast cancer. *Sci. Immunol.* **5**, (2020).
96. Villani, A.-C. *et al.* Single-cell RNA-seq reveals new types of human blood dendritic cells, monocytes, and progenitors. *Science* **356**, (2017).
97. Nizzoli, G. *et al.* Human CD1c⁺ dendritic cells secrete high levels of IL-12 and potently prime cytotoxic T-cell responses. *Blood* **122**, 932–42 (2013).
98. Segura, E., Durand, M. & Amigorena, S. Similar antigen cross-presentation capacity and phagocytic functions in all freshly isolated human lymphoid organ-resident dendritic cells. *J. Exp. Med.* **210**, 1035–47 (2013).

References

99. Yu, C. I. *et al.* Human CD141+ dendritic cells induce CD4+ T cells to produce type 2 cytokines. *J. Immunol.* **193**, 4335–43 (2014).
100. Jongbloed, S. L. *et al.* Human CD141+ (BDCA-3)+ dendritic cells (DCs) represent a unique myeloid DC subset that cross-presents necrotic cell antigens. *J. Exp. Med.* **207**, 1247–60 (2010).
101. Hoeffel, G. *et al.* Antigen crosspresentation by human plasmacytoid dendritic cells. *Immunity* **27**, 481–92 (2007).
102. Swiecki, M. & Colonna, M. The multifaceted biology of plasmacytoid dendritic cells. *Nat. Rev. Immunol.* **15**, 471–85 (2015).
103. Siegal, F. P. *et al.* The nature of the principal type 1 interferon-producing cells in human blood. *Science* **284**, 1835–7 (1999).
104. Guilliams, M. *et al.* Unsupervised High-Dimensional Analysis Aligns Dendritic Cells across Tissues and Species. *Immunity* **45**, 669–684 (2016).
105. Granot, T. *et al.* Dendritic Cells Display Subset and Tissue-Specific Maturation Dynamics over Human Life. *Immunity* **46**, 504–515 (2017).
106. Brown, C. C. *et al.* Transcriptional Basis of Mouse and Human Dendritic Cell Heterogeneity. *Cell* **179**, 846–863.e24 (2019).
107. Bourdely, P. *et al.* Transcriptional and Functional Analysis of CD1c+ Human Dendritic Cells Identifies a CD163+ Subset Priming CD8+CD103+ T Cells. *Immunity* **53**, 335–352.e8 (2020).
108. Villar, J. & Segura, E. Decoding the Heterogeneity of Human Dendritic Cell Subsets. *Trends Immunol.* **41**, 1062–1071 (2020).
109. Iberg, C. A., Jones, A. & Hawiger, D. Dendritic Cells As Inducers of Peripheral Tolerance. *Trends Immunol.* **38**, 793–804 (2017).
110. Dalod, M., Chelbi, R., Malissen, B. & Lawrence, T. Dendritic cell maturation: functional specialization through signaling specificity and transcriptional programming. *EMBO J.* **33**, 1104–16 (2014).
111. Sánchez-Sánchez, N., Riol-Blanco, L. & Rodríguez-Fernández, J. L. The multiple personalities of the chemokine receptor CCR7 in dendritic cells. *J. Immunol.* **176**, 5153–9 (2006).

112. Idoyaga, J. *et al.* Specialized role of migratory dendritic cells in peripheral tolerance induction. *J. Clin. Invest.* **123**, 844–54 (2013).
113. Comi, M. *et al.* Coexpression of CD163 and CD141 identifies human circulating IL-10-producing dendritic cells (DC-10). *Cell. Mol. Immunol.* **17**, 95–107 (2020).
114. Švajger, U. & Rožman, P. J. Recent discoveries in dendritic cell tolerance-inducing pharmacological molecules. *Int. Immunopharmacol.* **81**, 106275 (2020).
115. Cauwels, A. & Tavernier, J. Tolerizing Strategies for the Treatment of Autoimmune Diseases: From *ex vivo* to *in vivo* Strategies. *Front. Immunol.* **11**, 674 (2020).
116. Jenkins, M. K. & Schwartz, R. H. Antigen presentation by chemically modified splenocytes induces antigen-specific T cell unresponsiveness *in vitro* and *in vivo*. *J. Exp. Med.* **165**, 302–19 (1987).
117. Dendritic-Cell PD-L1 Mediates CD8⁺ T Cell-Dependent Antitumor Immunity. *Cancer Discov.* **10**, OF9 (2020).
118. Vander Lugt, B. *et al.* Transcriptional determinants of tolerogenic and immunogenic states during dendritic cell maturation. *J. Cell Biol.* **216**, 779–792 (2017).
119. Song, S. *et al.* Dendritic cells with an increased PD-L1 by TGF- β induce T cell anergy for the cytotoxicity of hepatocellular carcinoma cells. *Int. Immunopharmacol.* **20**, 117–23 (2014).
120. Sage, P. T. *et al.* Dendritic Cell PD-L1 Limits Autoimmunity and Follicular T Cell Differentiation and Function. *J. Immunol.* **200**, 2592–2602 (2018).
121. Qureshi, O. S. *et al.* Trans-endocytosis of CD80 and CD86: a molecular basis for the cell-extrinsic function of CTLA-4. *Science* **332**, 600–3 (2011).
122. Jain, N., Nguyen, H., Chambers, C. & Kang, J. Dual function of CTLA-4 in regulatory T cells and conventional T cells to prevent

References

- multiorgan autoimmunity. *Proc. Natl. Acad. Sci. U. S. A.* **107**, 1524–8 (2010).
123. Steinbrink, K., Graulich, E., Kubsch, S., Knop, J. & Enk, A. H. CD4(+) and CD8(+) anergic T cells induced by interleukin-10-treated human dendritic cells display antigen-specific suppressor activity. *Blood* **99**, 2468–76 (2002).
124. Pletinckx, K. *et al.* Immature dendritic cells convert anergic nonregulatory T cells into Foxp3- IL-10+ regulatory T cells by engaging CD28 and CTLA-4. *Eur. J. Immunol.* **45**, 480–91 (2015).
125. Boks, M. A. *et al.* IL-10-generated tolerogenic dendritic cells are optimal for functional regulatory T cell induction--a comparative study of human clinical-applicable DC. *Clin. Immunol.* **142**, 332–42 (2012).
126. Torres-Aguilar, H. *et al.* Tolerogenic dendritic cells generated with different immunosuppressive cytokines induce antigen-specific anergy and regulatory properties in memory CD4+ T cells. *J. Immunol.* **184**, 1765–75 (2010).
127. Awasthi, A. *et al.* A dominant function for interleukin 27 in generating interleukin 10-producing anti-inflammatory T cells. *Nat. Immunol.* **8**, 1380–9 (2007).
128. Mascanfroni, I. D. *et al.* IL-27 acts on DCs to suppress the T cell response and autoimmunity by inducing expression of the immunoregulatory molecule CD39. *Nat. Immunol.* **14**, 1054–63 (2013).
129. Karakhanova, S., Bedke, T., Enk, A. H. & Mahnke, K. IL-27 renders DC immunosuppressive by induction of B7-H1. *J. Leukoc. Biol.* **89**, 837–45 (2011).
130. Xiao, S. *et al.* Retinoic acid increases Foxp3+ regulatory T cells and inhibits development of Th17 cells by enhancing TGF-beta-driven Smad3 signaling and inhibiting IL-6 and IL-23 receptor expression. *J. Immunol.* **181**, 2277–84 (2008).

131. Mucida, D. *et al.* Retinoic acid can directly promote TGF-beta-mediated Foxp3(+) Treg cell conversion of naive T cells. *Immunity* **30**, 471–2; author reply 472–3 (2009).
132. Lee, G. K. *et al.* Tryptophan deprivation sensitizes activated T cells to apoptosis prior to cell division. *Immunology* **107**, 452–60 (2002).
133. Sundrud, M. S. *et al.* Halofuginone inhibits TH17 cell differentiation by activating the amino acid starvation response. *Science* **324**, 1334–8 (2009).
134. Mezrich, J. D. *et al.* An interaction between kynurenine and the aryl hydrocarbon receptor can generate regulatory T cells. *J. Immunol.* **185**, 3190–8 (2010).
135. Marin, E. *et al.* Human Tolerogenic Dendritic Cells Regulate Immune Responses through Lactate Synthesis. *Cell Metab.* **30**, 1075–1090.e8 (2019).
136. Fanger, N. A., Maliszewski, C. R., Schooley, K. & Griffith, T. S. Human dendritic cells mediate cellular apoptosis via tumor necrosis factor-related apoptosis-inducing ligand (TRAIL). *J. Exp. Med.* **190**, 1155–64 (1999).
137. Süss, G. & Shortman, K. A subclass of dendritic cells kills CD4 T cells via Fas/Fas-ligand-induced apoptosis. *J. Exp. Med.* **183**, 1789–96 (1996).
138. Lucas, C. J., Dimmitt, S. B. & Martin, J. H. Optimising low-dose methotrexate for rheumatoid arthritis-A review. *Br. J. Clin. Pharmacol.* **85**, 2228–2234 (2019).
139. Bigaut, K., De Seze, J. & Collongues, N. Ocrelizumab for the treatment of multiple sclerosis. *Expert Rev. Neurother.* **19**, 97–108 (2019).
140. Scottà, C. *et al.* Impact of immunosuppressive drugs on the therapeutic efficacy of ex vivo expanded human regulatory T cells. *Haematologica* **101**, 91–100 (2016).

References

141. Mansilla, M. J. *et al.* Beneficial effect of tolerogenic dendritic cells pulsed with MOG autoantigen in experimental autoimmune encephalomyelitis. *CNS Neurosci. Ther.* **21**, 222–30 (2015).
142. Jansen, M. A. A. *et al.* Matured Tolerogenic Dendritic Cells Effectively Inhibit Autoantigen Specific CD4+ T Cells in a Murine Arthritis Model. *Front. Immunol.* **10**, 2068 (2019).
143. Ferreira, G. B. *et al.* 1,25-Dihydroxyvitamin D3 promotes tolerogenic dendritic cells with functional migratory properties in NOD mice. *J. Immunol.* **192**, 4210–20 (2014).
144. Derdelinckx, J. *et al.* Clinical and immunological control of experimental autoimmune encephalomyelitis by tolerogenic dendritic cells loaded with MOG-encoding mRNA. *J. Neuroinflammation* **16**, 167 (2019).
145. Xie, Z. *et al.* 1,25-dihydroxyvitamin D3 -induced dendritic cells suppress experimental autoimmune encephalomyelitis by increasing proportions of the regulatory lymphocytes and reducing T helper type 1 and type 17 cells. *Immunology* **152**, 414–424 (2017).
146. Ochando, J., Ordikhani, F., Jordan, S., Boros, P. & Thomson, A. W. Tolerogenic dendritic cells in organ transplantation. *Transpl. Int.* **33**, 113–127 (2020).
147. Benham, H. *et al.* Citrullinated peptide dendritic cell immunotherapy in HLA risk genotype-positive rheumatoid arthritis patients. *Sci. Transl. Med.* **7**, 290ra87 (2015).
148. Bell, G. M. *et al.* Autologous tolerogenic dendritic cells for rheumatoid and inflammatory arthritis. *Ann. Rheum. Dis.* **76**, 227–234 (2017).
149. Zubizarreta, I. *et al.* Immune tolerance in multiple sclerosis and neuromyelitis optica with peptide-loaded tolerogenic dendritic cells in a phase 1b trial. *Proc. Natl. Acad. Sci. U. S. A.* **116**, 8463–8470 (2019).
150. Willekens, B. *et al.* Tolerogenic dendritic cell-based treatment for multiple sclerosis (MS): a harmonised study protocol for two phase I

- clinical trials comparing intradermal and intranodal cell administration. *BMJ Open* **9**, e030309 (2019).
151. Sawitzki, B. *et al.* Regulatory cell therapy in kidney transplantation (The ONE Study): a harmonised design and analysis of seven non-randomised, single-arm, phase 1/2A trials. *Lancet (London, England)* **395**, 1627–1639 (2020).
 152. Wculek, S. K. *et al.* Dendritic cells in cancer immunology and immunotherapy. *Nat. Rev. Immunol.* **20**, 7–24 (2020).
 153. Liao, L. M. *et al.* First results on survival from a large Phase 3 clinical trial of an autologous dendritic cell vaccine in newly diagnosed glioblastoma. *J. Transl. Med.* **16**, 142 (2018).
 154. Garg, A. D., Coulie, P. G., Van den Eynde, B. J. & Agostinis, P. Integrating Next-Generation Dendritic Cell Vaccines into the Current Cancer Immunotherapy Landscape. *Trends Immunol.* **38**, 577–593 (2017).
 155. Jones, P. A. Functions of DNA methylation: islands, start sites, gene bodies and beyond. *Nat. Rev. Genet.* **13**, 484–92 (2012).
 156. Lister, R. *et al.* Human DNA methylomes at base resolution show widespread epigenomic differences. *Nature* **462**, 315–22 (2009).
 157. Neri, F. *et al.* Intragenic DNA methylation prevents spurious transcription initiation. *Nature* **543**, 72–77 (2017).
 158. Lyko, F. The DNA methyltransferase family: a versatile toolkit for epigenetic regulation. *Nat. Rev. Genet.* **19**, 81–92 (2018).
 159. He, S. *et al.* Passive DNA demethylation preferentially up-regulates pluripotency-related genes and facilitates the generation of induced pluripotent stem cells. *J. Biol. Chem.* **292**, 18542–18555 (2017).
 160. Matuleviciute, R., Cunha, P. P., Johnson, R. S. & Foskolou, I. P. Oxygen regulation of TET enzymes. *FEBS J.* **288**, 7143–7161 (2021).
 161. Zhang, H. *et al.* TET1 is a DNA-binding protein that modulates DNA methylation and gene transcription via hydroxylation of 5-methylcytosine. *Cell Res.* **20**, 1390–3 (2010).

References

162. Xu, Y. *et al.* Tet3 CXXC domain and dioxygenase activity cooperatively regulate key genes for *Xenopus* eye and neural development. *Cell* **151**, 1200–13 (2012).
163. Ko, M. *et al.* Modulation of TET2 expression and 5-methylcytosine oxidation by the CXXC domain protein IDAX. *Nature* **497**, 122–6 (2013).
164. Kohli, R. M. & Zhang, Y. TET enzymes, TDG and the dynamics of DNA demethylation. *Nature* **502**, 472–9 (2013).
165. Branco, M. R., Ficz, G. & Reik, W. Uncovering the role of 5-hydroxymethylcytosine in the epigenome. *Nat. Rev. Genet.* **13**, 7–13 (2011).
166. Shi, D.-Q., Ali, I., Tang, J. & Yang, W.-C. New Insights into 5hmC DNA Modification: Generation, Distribution and Function. *Front. Genet.* **8**, 100 (2017).
167. Ziller, M. J. *et al.* Charting a dynamic DNA methylation landscape of the human genome. *Nature* **500**, 477–481 (2013).
168. Zaret, K. S. Pioneer Transcription Factors Initiating Gene Network Changes. *Annu. Rev. Genet.* **54**, 367–385 (2020).
169. Mayran, A. & Drouin, J. Pioneer transcription factors shape the epigenetic landscape. *J. Biol. Chem.* **293**, 13795–13804 (2018).
170. Zhu, H., Wang, G. & Qian, J. Transcription factors as readers and effectors of DNA methylation. *Nat. Rev. Genet.* **17**, 551–65 (2016).
171. Shi, J. *et al.* The concurrence of DNA methylation and demethylation is associated with transcription regulation. *Nat. Commun.* **12**, 5285 (2021).
172. Ghoshal, K. *et al.* 5-Aza-deoxycytidine induces selective degradation of DNA methyltransferase 1 by a proteasomal pathway that requires the KEN box, bromo-adjacent homology domain, and nuclear localization signal. *Mol. Cell. Biol.* **25**, 4727–41 (2005).
173. Szyf, M. Epigenetics, DNA methylation, and chromatin modifying drugs. *Annu. Rev. Pharmacol. Toxicol.* **49**, 243–63 (2009).

174. Derissen, E. J. B., Beijnen, J. H. & Schellens, J. H. M. Concise drug review: azacitidine and decitabine. *Oncologist* **18**, 619–24 (2013).
175. Rasmussen, K. D. & Helin, K. Role of TET enzymes in DNA methylation, development, and cancer. *Genes Dev.* **30**, 733–50 (2016).
176. Cimmino, L. *et al.* Restoration of TET2 Function Blocks Aberrant Self-Renewal and Leukemia Progression. *Cell* **170**, 1079-1095.e20 (2017).
177. Chua, G. N. L. *et al.* Cytosine-Based TET Enzyme Inhibitors. *ACS Med. Chem. Lett.* **10**, 180–185 (2019).
178. Ang, A., Pullar, J. M., Currie, M. J. & Vissers, M. C. M. Vitamin C and immune cell function in inflammation and cancer. *Biochem. Soc. Trans.* **46**, 1147–1159 (2018).
179. Anthony, H. M. & Schorah, C. J. Severe hypovitaminosis C in lung-cancer patients: the utilization of vitamin C in surgical repair and lymphocyte-related host resistance. *Br. J. Cancer* **46**, 354–67 (1982).
180. Mayland, C. R., Bennett, M. I. & Allan, K. Vitamin C deficiency in cancer patients. *Palliat. Med.* **19**, 17–20 (2005).
181. Bonham, M. J. *et al.* Early ascorbic acid depletion is related to the severity of acute pancreatitis. *Br. J. Surg.* **86**, 1296–301 (1999).
182. Peterkofsky, B. Ascorbate requirement for hydroxylation and secretion of procollagen: relationship to inhibition of collagen synthesis in scurvy. *Am. J. Clin. Nutr.* **54**, 1135S-1140S (1991).
183. England, S. & Seifter, S. The biochemical functions of ascorbic acid. *Annu. Rev. Nutr.* **6**, 365–406 (1986).
184. Minor, E. A., Court, B. L., Young, J. I. & Wang, G. Ascorbate induces ten-eleven translocation (Tet) methylcytosine dioxygenase-mediated generation of 5-hydroxymethylcytosine. *J. Biol. Chem.* **288**, 13669–74 (2013).
185. Bakaev, V. V & Duntau, A. P. Ascorbic acid in blood serum of patients with pulmonary tuberculosis and pneumonia. *Int. J. Tuberc. Lung Dis.* **8**, 263–6 (2004).

References

186. Cameron, E. & Pauling, L. Supplemental ascorbate in the supportive treatment of cancer: Prolongation of survival times in terminal human cancer. *Proc. Natl. Acad. Sci. U. S. A.* **73**, 3685–9 (1976).
187. Cabanillas, F. Vitamin C and cancer: what can we conclude--1,609 patients and 33 years later? *P. R. Health Sci. J.* **29**, 215–7 (2010).
188. Das, A. B. *et al.* Clinical remission following ascorbate treatment in a case of acute myeloid leukemia with mutations in TET2 and WT1. *Blood Cancer J.* **9**, 82 (2019).
189. Magri, A. *et al.* High-dose vitamin C enhances cancer immunotherapy. *Sci. Transl. Med.* **12**, (2020).
190. Böttger, F., Vallés-Martí, A., Cahn, L. & Jimenez, C. R. High-dose intravenous vitamin C, a promising multi-targeting agent in the treatment of cancer. *J. Exp. Clin. Cancer Res.* **40**, 343 (2021).
191. Challen, G. A. *et al.* Dnmt3a is essential for hematopoietic stem cell differentiation. *Nat. Genet.* **44**, 23–31 (2011).
192. Challen, G. A. *et al.* Dnmt3a and Dnmt3b have overlapping and distinct functions in hematopoietic stem cells. *Cell Stem Cell* **15**, 350–364 (2014).
193. Rasmussen, K. D. *et al.* TET2 binding to enhancers facilitates transcription factor recruitment in hematopoietic cells. *Genome Res.* **29**, 564–575 (2019).
194. Roy, R. *et al.* DNA methylation signatures reveal that distinct combinations of transcription factors specify human immune cell epigenetic identity. *Immunity* **54**, 2465-2480.e5 (2021).
195. Jaguin, M., Houlbert, N., Fardel, O. & Lecreur, V. Polarization profiles of human M-CSF-generated macrophages and comparison of M1-markers in classically activated macrophages from GM-CSF and M-CSF origin. *Cell. Immunol.* **281**, 51–61 (2013).
196. Wallner, S. *et al.* Epigenetic dynamics of monocyte-to-macrophage differentiation. *Epigenetics Chromatin* **9**, 33 (2016).
197. Dekkers, K. F., Neele, A. E., Jukema, J. W., Heijmans, B. T. & de Winther, M. P. J. Human monocyte-to-macrophage differentiation

- involves highly localized gain and loss of DNA methylation at transcription factor binding sites. *Epigenetics Chromatin* **12**, 34 (2019).
198. Mendes, K. *et al.* The epigenetic pioneer EGR2 initiates DNA demethylation in differentiating monocytes at both stable and transient binding sites. *Nat. Commun.* **12**, 1556 (2021).
199. Gerrick, K. Y. *et al.* Transcriptional profiling identifies novel regulators of macrophage polarization. *PLoS One* **13**, e0208602 (2018).
200. Pacis, A. *et al.* Gene activation precedes DNA demethylation in response to infection in human dendritic cells. *Proc. Natl. Acad. Sci. U. S. A.* **116**, 6938–6943 (2019).
201. Htun, H., Barsony, J., Renyi, I., Gould, D. L. & Hager, G. L. Visualization of glucocorticoid receptor translocation and intranuclear organization in living cells with a green fluorescent protein chimera. *Proc. Natl. Acad. Sci. U. S. A.* **93**, 4845–50 (1996).
202. Johnson, T. A. *et al.* Conventional and pioneer modes of glucocorticoid receptor interaction with enhancer chromatin *in vivo*. *Nucleic Acids Res.* **46**, 203–214 (2018).
203. Gemelli, C. *et al.* MafB is a downstream target of the IL-10/STAT3 signaling pathway, involved in the regulation of macrophage deactivation. *Biochim. Biophys. Acta* **1843**, 955–64 (2014).
204. Cuevas, V. D. *et al.* MAFB Determines Human Macrophage Anti-Inflammatory Polarization: Relevance for the Pathogenic Mechanisms Operating in Multicentric Carpotarsal Osteolysis. *J. Immunol.* **198**, 2070–2081 (2017).
205. Kelly, L. M., Englmeier, U., Lafon, I., Sieweke, M. H. & Graf, T. MafB is an inducer of monocytic differentiation. *EMBO J.* **19**, 1987–97 (2000).
206. Franco, L. M. *et al.* Immune regulation by glucocorticoids can be linked to cell type-dependent transcriptional responses. *J. Exp. Med.* **216**, 384–406 (2019).

References

207. Zaba, L. C. *et al.* Psoriasis is characterized by accumulation of immunostimulatory and Th1/Th17 cell-polarizing myeloid dendritic cells. *J. Invest. Dermatol.* **129**, 79–88 (2009).
208. Xu, Y.-P. *et al.* Tumor suppressor TET2 promotes cancer immunity and immunotherapy efficacy. *J. Clin. Invest.* **129**, 4316–4331 (2019).
209. Payen, D. *et al.* Multicentric experience with interferon gamma therapy in sepsis induced immunosuppression. A case series. *BMC Infect. Dis.* **19**, 931 (2019).
210. Müller, J. R. & Siebenlist, U. Lymphotoxin beta receptor induces sequential activation of distinct NF-kappa B factors via separate signaling pathways. *J. Biol. Chem.* **278**, 12006–12 (2003).
211. Suresh, M. *et al.* Role of lymphotoxin alpha in T-cell responses during an acute viral infection. *J. Virol.* **76**, 3943–51 (2002).
212. Nauman, G., Gray, J. C., Parkinson, R., Levine, M. & Paller, C. J. Systematic Review of Intravenous Ascorbate in Cancer Clinical Trials. *Antioxidants (Basel, Switzerland)* **7**, (2018).
213. de la Rica, L. *et al.* PU.1 target genes undergo Tet2-coupled demethylation and DNMT3b-mediated methylation in monocyte-to-osteoclast differentiation. *Genome Biol.* **14**, 1–21 (2013).
214. Sardina, J. L. *et al.* Transcription Factors Drive Tet2-Mediated Enhancer Demethylation to Reprogram Cell Fate. *Cell Stem Cell* **23**, 727-741.e9 (2018).
215. Català-Moll, F. *et al.* Vitamin D receptor, STAT3, and TET2 cooperate to establish tolerogenesis. *Cell Rep.* **38**, 110244 (2022).
216. Ichiyama, K. *et al.* The methylcytosine dioxygenase Tet2 promotes DNA demethylation and activation of cytokine gene expression in T cells. *Immunity* **42**, 613–26 (2015).
217. Reddy, T. E. *et al.* Genomic determination of the glucocorticoid response reveals unexpected mechanisms of gene regulation. *Genome Res.* **19**, 2163–71 (2009).

218. Hon, G. C. *et al.* 5mC oxidation by Tet2 modulates enhancer activity and timing of transcriptome reprogramming during differentiation. *Mol. Cell* **56**, 286–297 (2014).
219. Lin, I.-H., Chen, Y.-F. & Hsu, M.-T. Correlated 5-Hydroxymethylcytosine (5hmC) and Gene Expression Profiles Underpin Gene and Organ-Specific Epigenetic Regulation in Adult Mouse Brain and Liver. *PLoS One* **12**, e0170779 (2017).
220. Johnson, K. C. *et al.* 5-Hydroxymethylcytosine localizes to enhancer elements and is associated with survival in glioblastoma patients. *Nat. Commun.* **7**, 13177 (2016).
221. Saxena, M. & Bhardwaj, N. Re-Emergence of Dendritic Cell Vaccines for Cancer Treatment. *Trends in cancer* **4**, 119–137 (2018).
222. Moradian, H., Roch, T., Lendlein, A. & Gossen, M. mRNA Transfection-Induced Activation of Primary Human Monocytes and Macrophages: Dependence on Carrier System and Nucleotide Modification. *Sci. Rep.* **10**, 4181 (2020).
223. Mestas, J. & Hughes, C. C. W. Of mice and not men: differences between mouse and human immunology. *J. Immunol.* **172**, 2731–8 (2004).
224. Tao, L. & Reese, T. A. Making Mouse Models That Reflect Human Immune Responses. *Trends Immunol.* **38**, 181–193 (2017).
225. Masopust, D., Sivula, C. P. & Jameson, S. C. Of Mice, Dirty Mice, and Men: Using Mice To Understand Human Immunology. *J. Immunol.* **199**, 383–388 (2017).

AGRADECIMIENTOS

AGRADECIMIENTOS

AGRADECIMIENTOS

Y de repente, miras atrás y ya has andado el camino que comenzó hace ahora más de cuatro años. Resulta complicado sintetizar en unos pocos párrafos cómo me siento y lo agradecido que estoy por haber llegado hasta aquí. En esta etapa, tan corta y tan larga al mismo tiempo, ha pasado casi de todo: una mudanza a otro laboratorio, múltiples asaltos de jabalíes, bandas misteriosas en los Westerns que aparecen y desaparecen y una pandemia que ha cambiado nuestras vidas de una manera que no nos podíamos imaginar. Por supuesto, también han existido las decepciones y alegrías propias de esa montaña rusa emocional en la que consiste una tesis doctoral. Echando la vista atrás, solo puedo quedarme con lo bueno. Creo que en este tiempo he podido aprender a ser mejor profesional y mejor persona, en muchos aspectos. Por ello, me gustaría dedicar unas palabras a todos aquellos que lo han hecho posible y a los que seguirán en la brecha, trabajando en esa disciplina tan importante, tan bonita y, en ocasiones, tan ingrata e incomprendida que es la Ciencia, con la esperanza de que algún día se valore como se merece.

En primer lugar, me gustaría dar las gracias a Esteban por haberme dado la oportunidad de realizar la tesis en su laboratorio, confiar en mí desde el principio y dejarme la libertad y el espacio para pensar y desarrollar los proyectos.

También a mis compañeros de laboratorio, pasados y presentes, por habérmelo puesto todo tan fácil, apoyándome y ayudándome a encontrarme cuando estaba perdido. Javi, por estar siempre ahí para darme ideas cuando he estado bloqueado. Espero que pronto lleguen más *workshops* panarras. Laura, por su calidez y cercanía. Los días hubieran sido mucho más aburridos sin esos cafés con sus historias. Anna, con la

Agradecimientos

que comparto parte de mi (sano) espíritu nihilista ante los experimentos, por escucharme y ser mi confesora cuando me ha hecho falta. Damiana, con la que he podido coincidir en mi etapa en el IJC, por sus ideas y buen humor. También Ricardo, que vio antes que nadie la que se nos venía encima con la pandemia. Gerard, por transmitir su entusiasmo y pasión por la investigación, ¡no la pierdas! Pep, por su empuje, ganas y optimismo. Quedan pendientes más clases de ping-pong, pero mejor si no son a las nueve de la noche, entre experimento y experimento. Clara, compañera de aventuras y desventuras con Renfe, por haber estado siempre tan disponible para ayudarme, incluso desde la distancia. No olvidaré lo bien que me lo pasé grabando y montando su vídeo de tesis. Carlos, por ayudarme en mis comienzos en el laboratorio y acogermme en Barcelona cuando no conocía a nadie. No sería justo desvirtuar lo anterior por el desenlace. Tampoco puedo olvidarme de Nono que, aunque parece que ha pasado un mundo desde que se marchó, todavía recuerdo la serenidad que transmitía y su disposición a echar una mano. Tian, que, sin darle ella misma demasiada importancia a lo que hacía, es una de las personas más eficientes en el laboratorio y con la mente más rápida que he conocido. Gracias por ser mi amiga, escucharme y hacerme reír tanto.

A Sonia, autora de la portada, por ser capaz de transformar una idea vaga en mi cabeza en algo tan chulo, ayudarme con el diseño de la tesis y acompañarme en estos últimos meses.

A la Tropa de Valencia, con la que he compartido instantes, viajes y más partidas de fútbolín de las que podría contar. A mis amigos de Barcelona, especialmente Pablo, Lara y Zapi, que me han hecho la vida mucho más divertida y los malos momentos mucho más llevaderos.

Aunque parezca obvio, me gustaría agradecer también a la educación pública en general, y a los buenos profesores en particular, porque sin ellos probablemente sería imposible que hubiera llegado a este punto.

Por último, pero no menos importante, a mi familia. A mis padres, que siempre están incondicionalmente cuando los necesito y a mi hermana Carla que, desde Nueva York, siempre ha estado disponible como apoyo moral durante el desarrollo de esta tesis.

A todos,

Gracias.

APPENDIX

APPENDIX

7. APPENDIX

1. **Morante-Palacios,O.**, Ciudad,L., Micheroli,R., de la Calle-Fabregat,C., Li,T., Barbisan,G., Houtman,M., Edalat,S.G., Frank-Bertoncelj,M., Ospelt,C., *et al.* (2022) Coordinated glucocorticoid receptor and MAFB action induces tolerogenesis and epigenome remodeling in dendritic cells. *Nucleic Acids Res.*, **50**, 108–126.

2. **Morante-Palacios,O.**, Lorente-Sorolla,C., Ciudad,L., Calafell-Segura,J., Garcia-Gomez,A., Català-Moll,F., Ruiz-Sanmartín,A., Martínez-Gallo,M., Ferrer,R., Ruiz-Rodriguez,J.C., *et al.* (2021) JAK2-STAT Epigenetically Regulates Tolerized Genes in Monocytes in the First Encounter With Gram-Negative Bacterial Endotoxins in Sepsis. *Front. Immunol.*, **12**, 734652.

3. **Morante-Palacios,O.**, Fondelli,F., Ballestar,E. and Martínez-Cáceres,E.M. (2021) Tolerogenic Dendritic Cells in Autoimmunity and Inflammatory Diseases. *Trends Immunol.*, **42**, 59–75.

4. **Morante-Palacios,O.** and Ballestar,E. (2021) shinyÉPICo: A graphical pipeline to analyze Illumina DNA methylation arrays. *Bioinformatics*, 10.1093/bioinformatics/btaa1095.

Appendix

5. de la Calle-Fabregat,C., **Morante-Palacios,O.** and Ballestar,E. (2020) Understanding the Relevance of DNA Methylation Changes in Immune Differentiation and Disease. *Genes (Basel)*, **11**.

6. Li,T., Garcia-Gomez,A., **Morante-Palacios,O.**, Ciudad,L., Özkaramehmet,S., Van Dijk,E., Rodríguez-Ubreva,J., Vaquero,A. and Ballestar,E. (2020) SIRT1/2 orchestrate acquisition of DNA methylation and loss of histone H3 activating marks to prevent premature activation of inflammatory genes in macrophages. *Nucleic Acids Res.*, **48**, 665–681.

7. Rodríguez-Ubreva,J., de la Calle-Fabregat,C., Li,T., Ciudad,L., Ballestar,M.L., Català-Moll,F., **Morante-Palacios,O.**, Garcia-Gomez,A., Celis,R., Humby,F., *et al.* (2019) Inflammatory cytokines shape a changing DNA methylome in monocytes mirroring disease activity in rheumatoid arthritis. *Ann. Rheum. Dis.*, **78**, 1505–1516.

8. Català-Moll,F., Ferreté-Bonastre,A.G., Godoy-Tena,G., **Morante-Palacios,O.**, Ciudad,L., Barberà,L., Fondelli,F., Martínez-Cáceres,E.M., Rodríguez-Ubreva,J., Li,T., *et al.* (2022) Vitamin D receptor, STAT3, and TET2 cooperate to establish tolerogenesis. *Cell Rep.*, **38**, 110244.

